The Development of a Hybrid Scaffold for Use in Oesophageal Tissue Engineering

Omaer Syed BSc, MSc

Division of Biomaterials and Tissue Engineering, Eastman Dental Institute, UCL

Thesis submitted to University College London in accordance with the requirements for the degree of Doctor of Philosophy

September 2015

Primary Supervisor: Professor Jonathan Knowles

Secondary Supervisor: Dr Richard Day

eastman DENTAL INSTITUTE

Declaration

I, Omaer Syed confirm that the work presented in this thesis is my own. Where information has been derived from other sources, I confirm that this has been indicated in the thesis.

Signature

Date 18 September 2015

Abstract

The oesophagus as an organ can be affected by a number of medical conditions which may necessitate the need for extensive treatment to correct. One potential approach is to tissue engineer a suitable biomaterial-based replacement for oesophageal tissue. Small intestine submucosa (SIS) is one of a number of naturally-derived extracellular matrix (ECM) biomaterials currently in clinical use; however one of their key limitations is poor mechanical properties.

In this work it was found that SIS can be consistently and reliably processed into tubular scaffolds which impart certain potential advantages. The decellularisation of tubular SIS was carried out using four different protocols. One protocol emerged as the most suitable by the criteria mentioned, a perfusion-based method using sodium deoxycholate.

Electrospinning was used produce to polymers PLGA nanofibres which mechanically reinforced the tubular SIS. It was hypothesised that this would improve the ECM material's mechanical properties. Attachment remained an issue between the two layers but this was overcome by altering the shape of the SIS. The SIS-PLGA scaffold was produced with varying fibre alignment, a factor shown to have some influence *in vitro* and *in vivo.* The drug delivery potential of the fibres was also considered and the scaffolds had VEGF added to them. Evaluation was by physical testing, *in vitro* analysis and *in vivo* implantation.

The PLGA scaffold were found to perform well both mechanically and in terms of biocompatibility. They also performed well *in vivo* with a limited foreign body reaction. The highly aligned fibres (5000 rpm) group was chosen as the best in terms of its all-round properties including good cellular infiltration. The electrospun fibres remained intact at 4 weeks which indicates a potential lasting support role,

which was intended. The result of the VEGF incorporation was that there was an increase in the blood vessel density of the tissue surrounding the scaffolds highlighting the benefits of adding growth factors to the scaffold. Overall, it was concluded that the hybrid scaffold have potential for use in oesophageal tissue engineering.

Table of Contents

Title page……..…..…..1
Signed declaration……..……..……...2
Abstract……..……3
Table of contents……..…5
List of Figures……..……..……....8
List of Tables……..……..10
Abbreviations……..……....11
Acknowledgements……..…..……...12

Chapter 1: INTRODUCTION AND LITERATURE REVIEW…….……..……..…….....13

1.1 Introduction..…….……..……..…….....14

1.2 The Oesophagus ……...…15
1.2.1 Structure & Function..……..……...…15
1.2.2 Clinical Significance..……..……..……...…17
1.2.3 Tissue Engineering as an Approach to Treatment.……..……..…20

1.3 ECM materials…...……..……...…25
1.3.1 Background and Composition..……..……...…25
1.3.2 Advantages Over Synthetic Materials..……..……..…….....28
1.3.3 Small Intestine Submucosa……..……..……..…31
1.3.4 Decellularisation……..……..……....35

1.4 Electrospun Scaffolds.……..…44
1.4.1 Electrospinning..……..……...……44
1.4.2 Scaffold Properties..……..……..……...52
1.4.3 Drug Delivery..……..……..……..…63

1.5 Aims and Objectives.……..……..…66
1.5.1 Primary Objectives..……..……...…..66
1.5.2 Hypothesis..……..……..……...……66
1.5.3 Experimental Objectives..……..……...……..…67

Chapter 2: DECELLULARISATION AND SYNTHESIS OF TUBULAR SIS…..……..……..……..…68

2.1 Introduction..……..……..……..……..…69

2.2 Materials and Methods ……..…71
2.2.1 SIS Preparation..……..……...71
2.2.2 Decellularisation Method 1 (Perfusion/Immersion)……..……..…72
2.2.3 Decellularisation Method 2 (Immersion/Agitation)……..…74
2.2.4 Post-decellularisation Processing..……..……..…75
2.2.5 Analysis..……..……..……..……76
2.2.6 Histology..……..……..……..…77
2.2.7 Scanning electron microscopy (SEM)……..……..…77
2.2.8 DNA Quantification.……..……..……..…78
2.2.9 Mechanical Testing..……..……..……...78
2.2.10 Statistical Analysis……..……..……..……..…79

2.2.11 Cell Culture…..……..……79
2.2.12 Biocompatibility Assay..……..……..……..……..…80

2.3 Results ……..…82
2.3.1 Histology..……..……82
2.3.2 SEM..……..……83
2.3.3 Biocompatibility Assay..……..…84
2.3.4 DNA Quantification..……..……..…87
2.3.5 Mechanical Analysis..……..……..89

2.4 Discussion..……93
2.4.1 General Discussion..……..……..…93
2.4.2 Conclusion..……..……..…99

Chapter 3: ELECTROSPINNING…..……..……..……101

3.1 Introduction..……..……102

3.2 Materials and Methods……..…103
3.2.1 SIS Preparation..……..…103
3.2.2 Electrospinning……..……105
3.2.3 SEM Analysis..……..……..110
3.2.4 Alignment..……..……..……110
3.2.5 Mechanical Testing..……..……..110
3.2.6 Attachment..……..……..……111

3.3 Results ……..112
3.3.1 Series 1 (PCL)..……..……..112
3.3.2 Series 2 (PLGA)..……..……..121
3.3.3 Sample Yield..……..……..128

3.4 Discussion ……..……130
3.4.1 Series 1 (PCL)..……..……..…130
3.4.2 Series 2 (PLGA)..……..……..134
3.4.3 Conclusion..……..……..139

Chapter 4: HYBRID SCAFFOLDS…..……..……..…140

4.1 Introduction..……..……..…141

4.2 Materials and Methods……..…143
4.2.1 SIS Preparation..……..143
4.2.2 Electrospinning..……..……..144
4.2.3 Mechanical Testing..……..……..145
4.2.4 SEM Imaging……..……..146
4.2.5 Porosity..……..……..146
4.2.6 Biocompatibility..……..147
4.2.7 VEGF Incorporation ……..……..149
4.2.8 CAM Assay..……..……..…150

4.2.9 In Vivo Study……153
4.2.10 Analysis ……155

4.3 Results ……157
4.3.1 SEM Analysis……157
4.3.2 Mechanical Testing……165
4.3.3 Porosity……168
4.3.4 Smooth Muscle Actin……171
4.3.5 Biocompatibility……172
4.3.6 VEGF Assay……175
4.3.7 CAM Assay……177
4.3.8 In Vivo Study……179

4.4 Discussion……189
4.4.1 General Discussion……189
4.4.2 Conclusion……207

Chapter 5: CONCLUSIONS AND FUTURE WORK……209

5.1 Conclusions……210

5.2 Future Work……212

References……215
Appendix A……229
Appendix B……231
Appendix C……238

List of Figures

Figure 1.1	Physical features of the oesophagus……..	16
Figure 1.2	Representation of the cone-jet mode indicating the controlling forces ……..	46
Figure 1.3	Electrospraying Modes……..	47
Figure 1.4	Fibre formation by electrospinning……	48
Figure 1.5	Synthesis and structure of Poly(ε-caprolactone)……..	57
Figure 1.6	Chemical structure of glycolide and polyglycolic acid/poly(glycolide) (PGA)……	57
Figure 1.7	Chemical structure of lactide and polylactic acid/poly(lactide) (PLA)……..	58
Figure 1.8	Chemical structure of polylactic acid isomers: (a) L- PLA and (b) D-PLA……..	58
Figure 1.9	(a) Synthesis of PLGA (b) Half-life of PLA and PGA homopolymers and copolymers……	59
Figure 1.10	Structure of polylactic-co-glycolic acid and its decomposition in lactic and glycolic acid…….	60
Figure 2.1	Stages of SIS preparation……..	72
Figure 2.2	Decellularisation container arrangement……..	72
Figure 2.3	Orbital shaker arrangement for agitation decellularisation……	75
Figure 2.4	SIS processing equipment……..	76
Figure 2.5	Histological images (stained with H&E)……	82
Figure 2.6	Histological images (stained with EVG)……	83
Figure 2.7	SEM images of SIS from the protocol groups……	84
Figure 2.8	Metabolic activity of the cells (HESMC) cultured on the scaffold groups……	85
Figure 2.9	Metabolic activity of the cells (HESMC) cultured on the SDS/TX scaffolds showing the difference between the SDS/TX original protocol and an adapted protocol……..	86
Figure 2.10	(a) The average number of distinct nuclei counted per µm2 of SIS for all SIS groups. (b) DNA quantification values (ng/mg of dry weight)……	91
Figure 2.11	Tensile testing data of SIS showing (a) Elastic modulus values (MPa) (b) Yield stress values (MPa) and (c) Failure strain values (%) ……	92
Figure 2.12	Tensile testing data of SIS taken from different time points during the decellularisation process……..	85
Figure 3.1	Images showing porous polyethylene solid tubes used for SIS preparation……	104
Figure 3.2	Electrospinning arrangement used in Series 1……	105
Figure 3.3	Electrospinning arrangement used in Series 2……	107
Figure 3.4	SEM images from electrospinning PCL and onto SIS……	112
Figure 3.5	The average diameter for PCL electrospun fibres at 10%, 15% and 20%.....	113
Figure 3.6	Mechanical testing data from the tensile testing of the PCL-SIS……	115
Figure 3.7	SEM images of 20%PCL electrospun fibres on SIS under different conditions……	117
Figure 3.8	Graph of the percentage of 20% PCL fibres attached under different spin conditions……	117
Figure 3.9	SEM images of 20% PCL electrospun fibres + SIS at different mandrel rotation speeds…..	119
Figure 3.10	SEM images of 15% PLGA electrospun fibres + SIS at different mandrel rotation speeds….	121
Figure 3.11	Fibre diameter of PLGA electrospun fibres at various mandrel rotational speeds……	122
Figure 3.12	PLGA electrospun fibre orientation at the various mandrel rotation speeds……	123
Figure 3.13	Mechanical testing data from the longitudinal tensile testing of the PLGA-SIS……	124
Figure 3.14	Mechanical testing data from the circumferential tensile testing of the PLGA-SIS……	125
Figure 3.15	Images of highly extended PLGA fibres from 3000 rpm……	126
Figure 3.16	Graph comparing the percentage of attached samples from different sample sets……	127
Figure 3.17	Images of the SIS produced using two alternative methods……	128
Figure 3.18	Generalised illustration of a typical stress-strain graph for (a) SIS and (b) PLGA/SIS hybrid materials……	137
Figure 4.1	MTS calibration plate using known cells concentration values……	148
Figure 4.2	Stages of the CAM assay……..	152

Figure 4.3	Examples of test images taken from the work utilising the Angioquant software……	153
Figure 4.4	Histological image before (a) and after (b) processing to allow for nuclei (particle) counting.	155
Figure 4.5	SEM images of the PLGA electrospun fibres spun onto SIS at varying speeds……	157
Figure 4.6	Frequency histograms of fibre diameter data for the different scaffold samples produced…	160
Figure 4.7	The average fibre diameter of electrospun PLGA fibres collected on a rotating mandrel at different speeds of rotation…….	160
Figure 4.8	PLGA fibre orientation when electrospun onto SIS at the different mandrel rotation speeds	162
Figure 4.9	SEM images demonstrating a degree of HESMC orientation with the direction of the fibres..	163
Figure 4.10	The average thickness of the PLGA fibre layer produced at different rotational speeds……	164
Figure 4.11	Mechanical testing data from the longitudinal tensile testing of the PLGA-SIS…….	165
Figure 4.12	Mechanical testing data from the circumferential tensile testing of the PLGA-SIS……	166
Figure 4.13	(a) Graph representing the porosity of the hybrid scaffolds produced using mercury intrusion porometry (n = 4-6). The errors are bars are standard deviation. (b) Graph illustrating the potential trend between fibre alignment and the porosity of electrospun scaffolds…….	168
Figure 4.14	Pore size distribution for the scaffolds……..	169
Figure 4.15	Histological images of the smooth muscle actin (SMA) staining of HESMC's cultured on the PLGA-SIS scaffolds……	171
Figure 4.16	Graph representing the normalised levels of metabolic activity of HESMC's cultured on the scaffold groups……..	172
Figure 4.17	Series of confocal images (10 rpm) showing the 3D projections of a stack of confocal images for the purpose of live-dead analysis……..	173
Figure 4.18	Graph representing the percentage of live cells observed by performing a Live-Dead assay on HESMC's cultured on the scaffold groups……..	173
Figure 4.19	Confocal images demonstrating random (a) 10 rpm Day 7 and aligned cells (b) 5000 rpm Day 14……	174
Figure 4.20	(a) Graph representing the concentration of VEGF in solution following scaffold immersed at day intervals of 1, 7 and 14. (b) Graph representing the calculated quantity of VEGF present in solution at the same time intervals…….	175
Figure 4.21	The mean length of vessel complex on the CAM as identified by quantification software…..	177
Figure 4.22	The mean number junctions found per vessel complex on the CAM as identified by quantification software……	177
Figure 4.23	Histological image (3000rpm - 4 Weeks) illustrating the general observations of the in vivo samples……..	179
Figure 4.24	The cell types chosen for histological analysis……	181
Figure 4.25	Images contrasting the difference in the of density of blood vessels between the surrounding tissues for (a) non VEGF and (b) VEGF samples…….	181
Figure 4.26	Images of features observed in historical analysis……	182
Figure 4.27	Graph of the mean cellular infiltration score……	182
Figure 4.28	The average number of nuclei per mm^2 of histologically visible tissue from images of the scaffold groups……..	183
Figure 4.29	The average number of nuclei per mm^2 of histologically visible capsule surrounding tissue from images of the scaffold groups……...	183
Figure 4.30	The average number of cells per mm^2 of histologically visible capsule tissue for the following the cell types (a) Eosinophils (b) Lymphocytes (c) FBGC's (d) Monocytes……..	185
Figure 4.31	The average number of cells per mm^2 of histologically visible capsule sounding tissue for the following the cell types (a) Eosinophils (b) Lymphocytes (c) FBGC's (d) Monocytes……	186
Figure 4.32	The number of histologically visible blood vessels per mm^2 of tissue…….	187
Figure 4.33	The average cross-sectional area of the blood vessels…….	187
Figure A1	Comparison data from mechanical testing of the proximal (jejunum) and distal (ileum) submucosa……	229
Figure A2	Early perfusion rig…….	230
Figure B1	PCL fibres (20%) with salt crystals before and after washing……...	231
Figure B2	Results electrospinning onto foil with different concentrations of PLGA solution…….	237
Figure C1	Low resolution histological images (H&E) from the samples groups……...	238
Figure C2	Full size mercury intrusion porometry data charts……..	142

List of Tables

Table 1.1	A selection of commercially available SIS products……	34
Table 1.2	Table of parameters affecting fibre morphology……	50
Table 2.1	Experimental conditions for SIS production……..	75
Table 3.1	Table listing the variations in speed mandrel speeds for samples of electrospun fibres prepared with 20% PCL onto SIS……	119
Table B1	Parameters and variations of electrospun fibres produced for Chapters 3 & 4……..	232

Abbreviations

b-FGF	Basic fibroblast growth factor
CAB	sodium cacodylate buffer
DAPI	4’,6-diamidino-2-phenylindole
DN	Deoxyribonuclease I
DNA	Deoxyribonucleic acid
DNase	Deoxyribonuclease I
ECM	Extracellular matrix
EVG	Elastic Van Gieson (Verhoeff's Van Gieson)
FBGC	Foreign-body giant cells
FBS	Foetal Bovine Serum
FGF-2	Fibroblast growth factor
GAG	Glycosaminoglycans
H&E	Haematoxylin and Eosin
HESMC	Human Esophageal Smooth Muscle Cells (US spelling)
IgM	Immunoglobulin M
kU	Kilo-units (U = enzyme unit)
MTS	3-(4,5-dimethylthiazol-2-yl)-5-(3-carboxymethoxyphenyl)-2-(4-sulfophenyl)-2H-tetrazolium
N	Newton
Pa	Pascals
PBS	Phosphate buffer saline
PCL	Poly(caprolactone)
PGA	Poly(glycolic acid)
PLLA	Poly (L-lactic acid)
PLLC	Poly(L-lactide-co-caprolactone)
PMMA	Polymethylmethacrylate
PS	Polystyrene
PTFE	Polytetrafluoroethylene
rpm	Revolutions per minute
RT	Room Temperature
SD	Sodium deoxycholate
SDS	Sodium dodecyl sulphate
SEM	Scanning electron microscope
SIS	Small intestine submucosa
T/X	Triton X-100 (t-octylphenoxypolyethoxyethanol)
TCP	Tissue Culture Plastic
TGF-β1	Transforming growth factor beta
TMC	N,N,N-trimethyl chitosan chloride
TX	Triton X-100 (t-octylphenoxypolyethoxyethanol)
UBM	Urinary bladder matrix
uSIS	Untreated small intestine submucosa
VEGF	Vascular endothelial growth factor

Acknowledgements

I would sincerely like to thank Professor Knowles for all his guidance, support and encouragement throughout the entire period of my work. I would also like to thank Dr Richard Day for his support and feedback which helped shape the direction of my research.

From BTE, I would like to thank George Georgiou, Graham Palmer and Nicola Morden for all their time, technical assistance and, above all, patience. From Dankook University, I would like to thank Dr Kim Hae-Won for the opportunity to work there and Dr Kim Joong-Hyun for all his help and input into my work. Thanks also to the UCL Grand Challenge and all the staff there, for this opportunity presented to me.

I would finally like to take this opportunity to thank all my family and friend for their care and support.

1. Introduction and Literature Review

1.1 - Introduction

Oesophageal tissue engineering has a spectrum of considerations and complications, which make no current approach currently adopted as being deemed to be entirely successful. Decellularised extracellular matrix (ECM) represent a potential option for a scaffold material however they are inherently limited in their physical properties. It was hypothesised that the limitations of an ECM material could be overcome by the additional of an electrospun polymer layer and would make a hybrid scaffold better suited to the role as an oesophageal scaffold. The criteria for a successful scaffold would be determined by creating the scaffold with an application in mind. In addition to this, the question was raised and assessed whether the ECM material (small intestine submucosa) could be made in a seamless tubular form.

1.2 - The Oesophagus

1.2.1 Structure & Function

The primary role of the oesophagus is the transportation of food and liquids from the oral cavity and oropharynx down to the stomach and the on to the rest of the gastrointestinal tract. The food or liquids are transported in distinct quantities known as boli (singular: bolus), which correspond to material which is swallowed. The oesophagus performs this action by a series of peristaltic contractions which occur along the length of the organ. A lesser function is the drainage of mucus and saliva from the nasal and oral cavities respectively. Finally the oesophagus also facilitates the evacuation of stomach contents to the oral cavity when vomiting occurs.

The oesophagus is a tubular organ that descends within the thorax, alongside the trachea, and then through the diaphragm itself into the abdomen where it joins the stomach as seen in Figure 1.1(a). The oesophagus possesses two sphincters; an upper oesophageal sphincter (the pharyngoesophageal sphincter) and a lower oesophageal sphincter (the gastroesophageal sphincter) where it joins the stomach.

While the outwards appearance of the oesophagus is smooth and featureless the internal structure of the oesophagus is quite a complex one. Work carried out on the mechanical properties of the passive oesophagus describe the revised structure of the oesophagus consisting of three (two in earlier work) separate mechanically functional layers (Yang, Fung *et al.* 2007; Sokolis 2010; Stavropoulou, Dafalias *et al.* 2012). These layers being an inner mucosal-submucosa layer surrounded by a muscularis externa layer which is further divided into two distinct layers i.e. the inner circumferential muscular layer and the outer longitudinal muscle layer. While mechanically they may be intimately associated, the mucosal and submucosal layers are well known to be two distinct functional layers.

Structurally speaking, however, there are a far larger number of layers. Starting from the lumen there is the mucosa which itself is layered in structure, with the first being the epithelial layer which consists of stratified squamous non-keratinized epithelium and is commonly found on surfaces which encounter friction. Moving outwards there is the lamina propria, which is a connective tissue layer. The final mucosal layer is the muscularis mucosae which is a layer of smooth muscle consisting mainly of longitudinal muscle fibres. After the mucosa is the submucosa containing mucous secreting glands (oesophageal glands) and connective structures termed papillae. There are then the two muscular fibre layers (inner circumferential and outer longitudinal) both separated by a connective tissue layer. The oesophagus also has an outer "sheath" layer, the serosal (adventitia). Consequently it can be said that there are at least 7 layers, as seen in Figure 2.1(b) & (c).

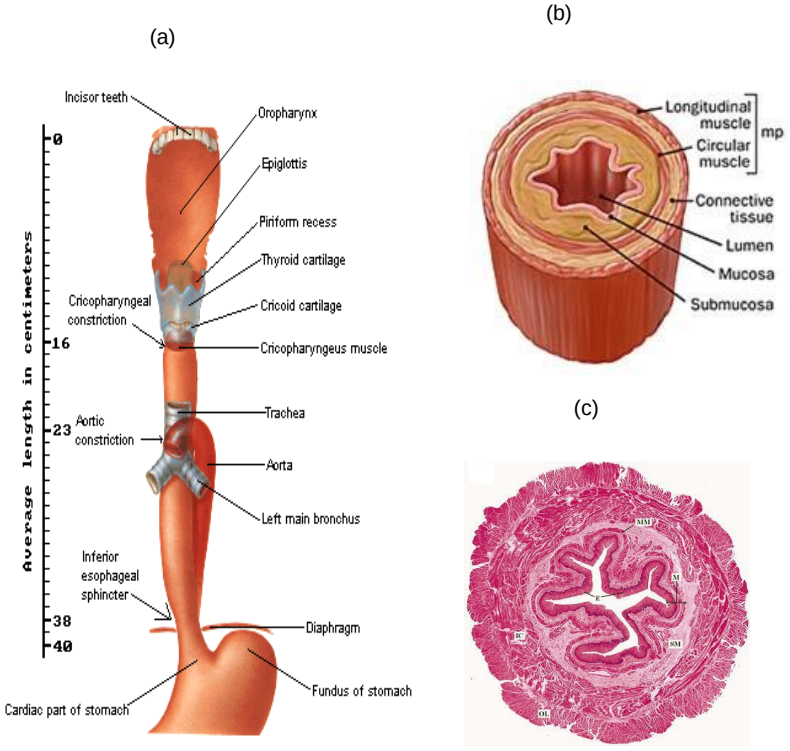

Figure 1.1 Physical features of the oesophagus. **(a)** Location and surrounding tissues. **(b)** Illustrative cross-section highlighting the layered anatomy (from www.hopkins-gi.org- John Hopkins Medicine) **(c)** Cross-section of the human oesophagus: Mucosa (M) consisting of epithelium (E) and the muscularis mucosa (MM), the submucosa (SM) and muscularis externa showing the inner circular (IC) and outer longitudinal (OL) muscle layer. (Tan, Chua *et al.* 2012)

Another structural feature of the oesophagus is that the muscularis externa varies throughout the length of the oesophagus. The upper third of the oesophagus consists of skeletal muscle and has the capacity for voluntary contraction. The middle third is a mixture of both skeletal and smooth, while the lower third is made up entirely of smooth muscle.

The mechanical structure of the oesophagus is a complex one. An investigation the mechanical properties of the oesophagus by Yang *et al.* (Yang, Fung *et al.* 2007) describes how, in the rat oesophagi studied, the mucosa/submucosa layer was much stiffer than the muscle layer in both the longitudinal and the circumferential directions, as well as in shear. Thus, the oesophagus was found to be anisotropic and non-homogeneous.

1.2.2 Clinical Significance

There are a number of widespread medical conditions which necessitate surgical treatment for damaged or missing lengths of the oesophagus usually due to surgical removal or developmental malformation. While less common oesophageal trauma might also necessitate such treatment. Some of the most common conditions which might involve treatment of this nature are listed below.

1.2.2.1 Oesophageal Atresia

This is a congenital medical condition which presents in new-born children in which the oesophagus ends in a blind-ended pouch as opposed to connecting normally with the stomach. In 85-88% of cases it also presents with associated tracheoesophageal fistula, involving one or both unconnected ends of the oesophagus forming abnormal communications with the trachea. Oesophagus atresia appears in most populations with a frequency of between 1 and 2,500 to 4,500 live births. (Holland and Fitzgerald 2010).

In the majority of cases treatment of this condition is usually in the form of primary repair where the two “free” ends of the oesophagus are surgically connected following any required fistula sectioning. In cases referred to as “long gap” this is not possible and alternative methods are required. The number of methods that can be employed is extensive and will usually be determined by the condition of the host oesophagus and the location and type of any fistula present. Methods include either delayed primary anastomosis following dilation, or a variety of surgical oesophageal lengthening techniques including the creation of flaps, spiral myotomy and gastric division (Spitz, Kiely *et al.* 1996).

The indications for actual oesophageal replacement are quite rare, though causes include intractable corrosive strictures, extended long gap situations or in cases where there have been repeated failed attempts at retaining the host oesophagus and the infants life is at risk (Spitz 2007; Arul and Parikh 2008). In current clinical practice there are currently three predominant methods used on children requiring oesophageal replacement; gastric transportation, colonic interposition and jejunal interposition (Spitz 2007). All three methods are quite pronounced in their levels of surgical invasiveness and an alternative to these methods would provide a significant improvement as no further organs would have to be compromised.

This condition represents the most likely application for oesophageal tissue engineering as here an implanted scaffold would form the basis of a treatment. The following two conditions, while undoubtedly could benefit from tissue engineered approaches, are neoplastic in origin and therefore the scaffolds use would only be reconstructive in nature following more conventional treatment forms.

1.2.2.2 Barratt’s Oesophagus

This is a pathologic change in the cells lining the lower oesophagus from normal squamous epithelial cells to metaplastic specialised columnar cells, a type found in

the intestine. The condition is highly associated with chronic gastro-oesophageal reflux disease (GORD or GERD) which has a damaging effect on the lower oesophageal cells and it is presumed that the high degree of cellular renewal and replacement creates the opportunity for columnar metaplasia (the name for this process of metaplastic replacement) (Spechler 2000). These metaplastic cells in Barrett's oesophagus are prone to develop genetic changes which then can then lead to malignancy. Indeed, both GORD and Barrett's Oesophagus are considered clinical risk factors for oesophagus adenocarcinoma. Barrett's oesophagus is diagnosed in approximately 10-15% of patients who present with reflux and have undergone an endoscopy (Vaira, Gatta *et al.* 2011).

1.2.2.3 Oesophageal Cancer

Oesophageal cancer is a highly prevalent condition and has been observed to be increasing in incidence worldwide (Hartel and Wente 2004). In 2007 oesophageal cancer accounted for an estimated 400,000 deaths annually (Smith et al., 2008) and was the sixth leading cause of cancer-related deaths worldwide (Lin and Papadopoulos, 2007) and this is currently likely to be higher. It has a higher incidence rate in the regions of India, China, Iran and Africa where it can be between 10-100 times more common than worldwide averages (Ritchie, Chian *et al.* 2006). In the United States alone, in 2011 there were 16,980 new cases and 14,710 deaths (Kuppan, Sethuraman *et al.* 2012). There are two predominant types which occur which are adenocarcinoma and squamous carcinoma. Diagnosis of this condition has not progressed to the stage where it can detected early and the 5-year survival rate amongst suffers of the oesophageal cancer is less than 5%. Oesophageal cancer is difficult to treat and this has been attributed to the poor regenerative properties of oesophageal tissue (Kuppan, Sethuraman *et al.* 2012). Squamous cell carcinoma and adenocarcinoma are both aggressive malignancies largely require surgical removal of the portion of affected oesophagus (Tan, Chua et

al. 2012). While current surgical techniques are often employed to bridge any gaps these are large relatively destructive in nature necessitating surgical relocation of intestinal segments or in extreme cases sectioning and repositioning of the stomach itself. A tissue engineered construct which was able to be used as an alternative would represent a significant step forward.

1.2.3 Tissue Engineering as an Approach to Treatment

An alternative approach to conventional surgical techniques is the repair of damaged or malformed oesophageal tissue with tissue engineered constructs. Tissue engineering approaches have been used for a variety of different applications including the regeneration of bone, skin, cardiovascular tissues , and nervous tissue to name only a few (Kuppan, Sethuraman *et al.* 2012).

1.2.3.1 Properties of an Ideal Replacement

The foundation of any tissue engineered construct is usually the scaffold. The scaffold forms the primary support for the cells grow and multiply upon and can be permanent or temporary. Principally the scaffold should have suitable levels of porosity, surface chemistry and mechanical properties to aid cell attachment. Important other *in vivo* events such as tissue organisation, matrix deposition and angiogenesis have also been shown to be influenced by scaffold characteristic such as the surface morphology, size distribution of porosity, geometry and thickness and so these factors need to be taken into consideration (Ritchie, Chian *et al.* 2006; Kuppan, Sethuraman *et al.* 2012).

In the case of the oesophagus, a cylindrical structure with a complex layered morphology, an ideal scaffold should also have a cylindrical shape and aim to replicate some of the complex functional layers which may necessitate the use of a composite material. A scaffold should be biocompatible and not cause inflammation

to any significant degree and should have a level of micromorphology present which will also facilitate cell regeneration. The composite materials should be biodegradable and the degradation rate should reflect the tissue regeneration time, and in doing so also function as an oesophagus replacement until regeneration has occurred. It should also be resistant to hot and cold temperatures associated with food and drink in addition to the reflux of gastric juices from the stomach. The scaffold should have sufficient mechanical strength to withstand abrasive forces and pressure generated by the bolus in addition to resisting the forces associated with suturing. It should have a large enough burst strength to allow for normal function without the risk of rupturing. To maintain its mechanical properties the oesophageal scaffold will have to be able to minimise a fibrosis reaction. The porosity of the scaffold will also be highly significant; outer pore sizes in the range of 50 to 200 μm are able to facilitate cell seeding, and transport of waste and nutrients, and smaller pores in the range of 35 to 70 μm are considered important in the promotion of angiogenesis (Ritchie, Chian *et al.* 2006; Poghosyan, Gaujoux *et al.* 2011; Kuppan, Sethuraman *et al.* 2012; Tan, Chua *et al.* 2012).

1.2.3.2 Past and Current Approaches

A number of different tissue engineering approaches have been investigated for oesophageal defect repair and short-segment replacement. Earlier approaches were dominated by non-resorbable materials. Some of the materials which were used for defect repair were tubular silicone, polyethylene terephthalate (Dacron) and expanded polytetraflouroethylene. These materials were not particularly biocompatible and their use resulted in chronic infection, material extrusion, anastomotic leakage, stricture and poor tissue growth (Poghosyan, Gaujoux *et al.* 2011; Kuppan, Sethuraman *et al.* 2012; Tan, Chua *et al.* 2012). These results have prompted to the move to biodegradable materials (both synthetic and natural) and ECM (extracellular matrix) materials.

Polymer scaffolds have been one of the most studied approaches for oesophageal tissue engineering. The number of approaches is growing and is covers a large range of materials. Natural materials have been used and some have shown some promising results. The use of glutaraldehyde cross-linked bovine collagen sheets was investigated in conjunction with ovine oesophagus epithelial cells and patches of oesophageal epithelium organization were observed on the luminal side and vascular ingrowths on the outer surface (Saxena, Baumgart *et al.* 2010). Collagen in graft form has also been investigated (OptiMaix®) (Kuppan, Sethuraman *et al.* 2012) and showed some smooth muscle and tissue organisation. Collagen sheets have also been cultured with multiple cell types also showed good tissue growth and promising oesophageal organisation (Hayashi *et al.* 2004). Ultimately, the limitation of natural polymers was rapid degredation, poor mechanical strength and inflammatory responses (Kuppan, Sethuraman *et al.* 2012).

Synthetic polymers represent an alternative to the natural polymers. They also have the advantage of being highly modifiable with respect to degradation rates, pore sizes and mechanical properties. Poly (L-lactic acid) (PLLA), poly (lactide-*co*-glycolide) (PGLA), poly (caprolactone) (PCL), poly(glycolic acid) PGA, poly(L-lactide-co-caprolactone) (PLLC) are all polymers that have been used in various approaches in oesophageal tissue engineering.

Electrospun PLLC fibres were used to construct a tubular scaffold with the use of a rotating mandrel modified with fibronectin, and cultured with porcine oesophageal epithelial cells (Zhu, Leong *et al.* 2007). Immunochemistry showed good oesophagus-resembling epithelial morphology particularly on the modified scaffold over the unmodified. A scaffold made from non-woven polyglycolic acid along with oesophagus organoid units of rat origin (mesenchyme surrounded by epithelial cells) were tested *in vivo*, using a rat model and histology revealed a seemingly

complete oesophagus wall. Immunostaining also confirmed smooth muscle was present by staining for α-actin. (Grikscheit, Ochoa *et al.* 2003)

Polymer scaffolds which are made without the addition of cells for oesophageal tissue engineering are not common and have not met with much success. One of the advantages of this approach, however, is that is promotes growth from the surrounding epithelium (Kuppan, Sethuraman *et al.* 2012). One of the major disadvantages is that this approach is quite slow, with epithelial regeneration taking 3 to 4 weeks (Saxena, Ainoedhofer *et al.* 2009). In studies where a section of oesophagus was replaced common complications included stricture, dilation and the lack of significant muscle growth (Doede, Bondartschuk *et al.* 2009).

An alternative to polymer scaffolds is the use of ECM (extracellular matrix) materials. ECM material will be discussed in more depth in Section 1.3. A number of different ECM materials have been applied to oesophageal tissue engineering including small intestine submucosa (SIS), urinary bladder matrix (UBM), dermal grafts, and also acellular tissues such as the oesophagus and aorta (Lopes, Cabrita *et al.* 2006; Doede, Bondartschuk *et al.* 2009; Gu and Zhang 2011; Basu, Mihalko *et al.* 2012). Patches in a rat model have shown that there was promising growth when used to repair defects using UBM (Basu, Mihalko *et al.* 2012) and SIS (Lopes, Cabrita *et al.* 2006). However, when SIS was used in a tubular form in a porcine model the results were largely unsuccessful with severe stenosis reported in several animals (Doede, Bondartschuk *et al.* 2009). The mechanical properties of the material were likely a contributing cause for this failure and the authors also indicate that a biodegradable stent which was able to function during the initial “problematic” three month period may be a possible solution to the observed failures.

1.2.3.3 Properties of an Oesophageal Scaffold

As mentioned previously, the ideal medical condition for which oesophageal tissue engineering could be applied is in oesophageal atresia. Consequently the scaffolds for this purpose would be required to have some specific properties beyond that those discussed above particularly with respect to how the scaffold will be applied *in vivo*. This will be discussed further in Section 1.5 Aims and Objectives.

1.3 - ECM materials

1.3.1 Background and Composition

The extracellular matrix is made up of a highly complex cross-linked network of various proteins and other macromolecules of which collagen is the principle structural component. The structural and functional molecules present in the ECM includes; proteins, proteoglycans, glycosaminoglycans, glycoproteins and other small molecules. The matrix aids in organising the cells in space and additionally provides attachment, environmental signals and separation between tissues. The use of extracellular matrices (ECMs) as surgical materials has become a successful and established practice for a number of years. These materials consist of the processed, and yet largely intact, ECM sourced from a variety of allogeneic or xenogeneic tissues. The increasing variety of different tissue types all individually vary in their composition and properties, consequently they are suitable for different applications. ECM materials in clinical use, have been created with the goal being to preserve as much of the composition and structure of the ECM as possible without any adverse effects to the recipient (Badylak 2004; Badylak 2005; Hodde 2006; Huber and Badylak 2011).

The function of the extracellular matrix is not only limited to functioning as a constituent of mature tissues. Additionally, the ECM plays a crucial role in embryonic development by acting to mediate biophysical stimuli, biochemical and molecular signalling and spatial organisation (Song and Ott 2011). The ECM continues to play important roles throughout development, up to and including organogenesis. A process of dynamic reciprocity occurs where the constant interchange between cells and the ECM occurs, and aiding in determining cell fate and influencing the shift from proliferation to structural formation (Bissell, Hall *et al.* 1982). The ECM continues to play a role and is also influential though to organ

maturation and even plays an active role in organ maintenance and repair (Song and Ott 2011).

ECM, as all biomaterials, have to be assessed carefully prior to application in a clinical capacity. A large number of factors can affect can affect their clinical behaviour including the tissue type and source, structure, composition, the type of processing performed, and the relative *in vivo* performance of the material at the site of application.

In clinical use extracellular matrix materials are derived entirely from mammalian sources and to date these have been human, porcine, bovine or equine in origin (Badylak, Freytes *et al.* 2009). The tissues from which ECM can be isolated from including small intestine (Badylak 1989), urinary bladder (Merguerian, Reddy *et al.* 2000), skin (Wainwright 1995), liver (Sellaro, Ravindra *et al.* 2007) , skeletal muscle (Borschel, Dennis *et al.* 2004), heart valves (Bader, Schilling *et al.* 1998) blood vessels (Conklin, Richter *et al.* 2002), nerves (Dufrane, Mourad *et al.* 2008; Huber and Badylak 2011), fascia lata (Barber and Aziz-Jacobo 2009), tendons (Omae, Zhao *et al.* 2009) and ligaments (Woods and Gratzer 2005). Given the variety of the source material it is understandable that significant differences in the structure, function and molecular characteristics of each ECM material exist. An example of this is in the comparison of the two most frequently used materials, small intestine submucosa (SIS) and urinary bladder matrix (UBM) in terms of the relative quantities of different collagen forms. ECM materials made from SIS typically contain approximately 90% collagen, which is predominately collagen type I, with smaller quantities of collagen types III, IV, V and VI (Badylak, Tullius *et al.* 1995). ECM materials made from UBM, however, have been shown to have larger amounts of collagen types III and IV, type IV being notable as it is an important epithelial basement membrane component and therefore is characteristic of the source tissue being highly epithelial (Brown, Lindberg *et al.* 2006).

An extensive amount of research has been carried out on SIS in recent years with respect to its components. In addition to the most abundant component collagen, there is also glycosaminoglycans (GAGs), including heparin, hyaluronic acid, heparin sulfate, chondroitin sulfates (Hodde, Badylak *et al.* 1996); proteoglycans such as dorcin (Badylak, Freytes *et al.* 2009); glycoproteins such as biglycan and enactin (Badylak, Freytes *et al.* 2009); in addition to a number of adhesion molecules such as fibronectin and laminin (Hodde, Record *et al.* 2002; Brown, Lindberg *et al.* 2006). A large variety of growth factors (Roberts, Gallagher *et al.* 1988) are also found including, transforming growth factor (TGF-b) (VoytikHarbin, Brightman *et al.* 1997; McDevitt, Wildey *et al.* 2003); basic fibroblast growth factor (b-FGF) (VoytikHarbin, Brightman *et al.* 1997), and vascular endothelial growth factor (VEGF) (Hodde, Record *et al.* 2001). This list is by no means exhaustive and a study carried out on decellularised UBM using high-performance liquid chromatography with an ion trap mass spectrometer identified 129 distinct proteins with a large spectrum of functional roles and with 14% native to the ECM with 39% of those being cytoplasmic in origin (Marcal, Ahmed *et al.* 2012). While the composition of ECM materials differs they all broadly share the same component macromolecules with each other and with the tissues into which they are implanted and this is likely one of their reasons for success.

The composition of ECM materials is undoubtedly important but structure also plays a significant role in the materials interaction with the surrounding cells and tissue (Brown, Barnes *et al.* 2010). Using time of flight mass spectroscopy and SEM the ultrastructure and the molecular composition of three porcine lab-prepared decellularised ECM materials were analysed; SIS, UBM and liver matrix were shown to have significant differences not only in their composition both also in their ultrastructure (Brown, Barnes *et al.* 2010). In a different study carried out using the same three matrices with *in vitro* culture using hepatic sinusoidal endothelial cells it

was found that that the liver based scaffold was better able to culture cells and for a longer duration than the two other matrices (SIS and UBM) (Sellaro, Ravindra et al. 2007). Therefore the origin of the tissue will likely have an effect on the cellular phenotype with which it interacts. Additionally it was shown (Brown, Barnes et al. 2010) that there were also ultrastructural differences in the individual UBM and SIS matrices between the two planar faces i.e. between the luminal face and the abluminal face, though obviously the liver tissue was shown not have this characteristic though the actual significance of this is currently unknown. In summary the microstructure of the ECM will likely influence cellular interaction and the behaviour of the material and is different for each ECM.

The composition and the ultrastructure of a material are not the only factors which influence cell-scaffold integration with other scaffold properties such as ligand presence and presentation (Hodde, Record *et al.* 2002; Quirk, Kellam *et al.* 2003; Beckstead, Santosa *et al.* 2006) the hydophilicity/hydrophobicity (Jansen, Sladek *et al.* 2005), mechanical properties (Rehfeldt, Engler *et al.* 2007) and surface topography (Flemming, Murphy *et al.* 1999; Henry, Burugapalli *et al.* 2009) also shown to play a role, amongst a large number of other factors .

1.3.2 Advantages over synthetic materials

The effective use of ECM materials depends largely on their post implantation *in vivo* properties at the localised site of treatment. The immune response of a host to any implantable device will always be a very important consideration. In the study of organ transplantation, it is a well-established fact that immune recognition of “foreign” antigens, whether xenogeneic or allogeneic, is followed by the production of pro-inflammatory mediators, cytotoxicity and in extreme cases, subsequent organ rejection (Brown, Valentin *et al.* 2009). This extreme rejection response has not

been observed with the use ECM materials. Work has been carried out which has shown that the macromolecules present in the ECM are quite well conserved between mammalian species and are quite well received even if xenogeneic in origin. The ECM materials are found to provoke a reaction in accordance with integration into the host tissue or degraded by non-immunogenic means (Badylak, Taylor *et al.* 2011).

Studies have shown that decellularised xenogeneic ECM grafts are found to elicit an immune response which is restricted to Th2 lymphocytes (Allman, McPherson *et al.* 2001). This response is believed to be conducive to graft acceptance, and which differs from Th1 lymphocyte-mediated immune response which is more commonly associated with xenogeneic graft rejection (Bach, Ferran *et al.* 1997). The immune response associated with ECM materials has also been identified as having an increased presence of alternatively activated M2 macrophages and also associated low levels of pro-inflammatory cytokines (Brown, Valentin *et al.* 2009; Keane, Londono *et al.* 2012).

It is believed that following the *in vivo* degradation of ECM materials there is a release of growth factors and biologically active cryptic peptides whose action can directly influence the processes of angiogenesis, mononuclear infiltration, cell proliferation, cell migration and cell differentiation (VoytikHarbin, Brightman *et al.* 1997; Valentin, Badylak *et al.* 2006). Cumulatively all these processes are important for new tissue formation which is undoubtedly one of the fundamental functional clinical benefits which ECM materials provide. The rapid degradation of the ECM materials in conjunction with the resultant release of the growth factors both contribute towards successful constructive tissue remodelling.

Generally speaking degradation does result in an initial loss with respect to mechanical strength during the early phase of *in vivo* modelling. However

subsequent newly infiltrated cells experience mechanical stress which initiates the formation of new ECM. With the development of this new site-specific tissue strength eventually increases though this process does take time (Badylak, Kokini *et al.* 2001).

To improve their properties, ECM's have been modified by cross-linking. However the effects of the *in vivo* implantation to ECM are altered when the ECM materials have been chemically cross-linked using glutaraldehyde, carbodiimide or hexamethylene-diisocyanate, or even through the use of non-chemical means. The benefits of cross-linking are quite well known in that the mechanical strength of the material is improved and the rate of scaffold degradation is reduced (Huber and Badylak 2011). However as a consequence these modification can result in the development of a chronic, pro-inflammatory, foreign-body type tissue response upon implantation and consequently a lower level of constructive remodelling. This adverse host response is observed in the higher proportion of M1 macrophages, a higher level of pro-inflammatory cytokines and the initiation of a Th-1 response which corresponds with a cell-mediated immune response (Mosser 2003) which is not dissimilar to that observed with synthetic polymers scaffolds. The negative impact on the healing and regenerative responses elicited by the material as a result of cross-linking is well researched (Brennan, Reing *et al.* 2006; Beattie, Gilbert *et al.* 2009). In addition to this, while SIS has also demonstrated the ability to delay clotting, crosslinking of the material resulted in an increase in clotting time. (Glynn, Polsin *et al.* 2014)

1.3.3 Small Intestine Submucosa (SIS)

1.3.3.1 Background

Small intestine submucosa is a material what has been the subject of research for a significant period of time. Work done as early 1966 by Matsumoto *et al.*, used various sections taken from the jejunum of the small intestine and used it as a vascular graft in a canine model. Different variations of the jejunum were grafted between ends of the vena cavae of the animals and one variation contained only the submucosa which was prepared by "*vigorous abrasion of the serosal and mucosal surface with gauze*". The method for isolating this layer seems to have been established here. The study was carried out with a large number of animals and all those with the mucosal lining facing the blood flow failed. It is important to note that the SIS used in this work was grafted in an inverted orientation. So while it was deemed to be successful its orientation was not a reason for its success (Matsumoto, Holmes *et al.* 1966; Matsumoto, Holmes *et al.* 1966).

Inverted SIS in the canine model was again investigated as a vascular graft by Lawler *et al*. The finding from this work indicated that inverted SIS was again successful as an autograft for the thoracic vena cava (though the same success was not achieved with the abdominal vena cava, and this was consistent with other work). The use of preserved homografts from donor dogs was also observed to be quite successful. The issues of rejection were not very well analysed in this work. (Lawler, Foster *et al.* 1971)

Preserved SIS homografts were observed to initially function well when applied to the thoracic aorta up to six months, prior to aneurysms developing. When these grafts were analysed with elastin stains they were observed to show *"absence of strong supporting fibers*". The fresh samples did not perform as well as the preserved ones when used as aortic grafts. In order to even prevent immediate

aneurysmal dilatation of the fresh tissue the segment were actually carefully prepared to be *"tailored to size and muscularis of the bowel wall left attached to the submucosa"*. What could be inferred here is that the turnica muscularis layer gave the SIS grafts some addition mechanical support and prevented failure. With additional thickness made of a smooth muscle it appears quite logical that these grafts would have better mechanical properties than SIS alone (Lawler, Foster *et al.* 1971).

1.2.3.2 Heterogeneity in SIS

While the commercial SIS is produced in the form of a uniform sheet there is some evidence for a degree of heterogeneity present in the tissue of origin. The organisation of the divisions of the small intestine is as follows (in bold): stomach → pyloric valve → **duodenum** → **jejunum** → **ileum** → ileocecal valve. The duodenum of the small intestine is usually discarded, so Raghavan *et al*. took SIS samples labelled proximal (from the proximal end of the jejunum) and distal (from the distal end of the ileum) and analysed these as separate samples. The distal samples were shown to be more elastic in tensile tests and also less permeable to urea. The surface structure was observed to be different (i.e. proximal being more porous) using SEM imaging however this was not quantified and there was no evidence to suggest that this difference was present throughout the thickness of the SIS (Raghavan, Kropp *et al.* 2005). This reinforces the notion that the material is intrinsically heterogeneous. In a previous canine bladder augmentation study it was demonstrated that distal SIS remarkably enhances bladder regeneration relative to proximal SIS, reduces the risk of both heavy scarring and calcification, and resulted in greater smooth muscle bundle formation (Kropp, Cheng *et al.* 2004). A more recent study has shown that in a rat model for bladder regeneration proximal and distal SIS samples were shown to have different immune cell profiles over a 56 day time period (Ashley, Roth *et al.* 2010).

While these are important considerations it should be mentioned that in all the above cases the proximal and distal samples were taken from quite extreme ends of the small intestine and any inherent differences are likely to be exaggerated as the structural changes also occur in a gradual fashion. In all these cases the application was only limited to bladder regeneration therefore these apparent differences might not manifest in other applications.

1.2.3.3 Applications of SIS

SIS is one of the most frequently used ECM materials along with urinary bladder and dermal materials. There are a significantly large number of applications for which commercially available SIS products, in their various forms and brands, are being applied with some listed in Table 1.1. SIS as a material is used in the repair of multiple types of hernia (Franklin, Gonzalez *et al.* 2004) and are also in use for the repair of the rotator cuff tendon of the shoulder joint (Derwin, Baker *et al.* 2006; Ricchetti, Aurora *et al.* 2012). It has been used extensively in urological and gynaecological surgery, including bladder repair, pelvic organ prolapse repair, stress urinary incontinence treatment and Peyronie's disease treatment amongst others. It has also been applied gastrointestinal surgery; for the use of anal fistula closure and small intestine reparative surgery. Other applications in which SIS has been used include in abdominal wall repair, general wound healing when augmentation of primary closure is required, burns treatment, ulcer treatment, localised head and neck tissue repair, post-mastectomy breast reconstruction, cardiovascular repair and as a dural replacement/graft (Misseri, Cain *et al.* 2005; Derwin, Baker *et al.* 2006; Bejjani, Zabramski *et al.* 2007; Trabuco, Klingele *et al.* 2007; Hoshiba, Lu *et al.* 2010; Huber and Badylak 2011; Stokes 2011; Caione, Boldrini *et al.* 2012). This list is by no means exhaustive and new more varied applications will undoubtedly arise.

Table 1.1 A selection of commercially available SIS products.

Product	Company	Material	Processing	Form
CuffPatch™	Arthrotek	Porcine small intestinal submucosa (SIS)	Crosslinked	Hydrated sheet
Durasis ™	SIS Cook	Porcine small intestinal submucosa (SIS)	Natural	Dry sheet
Oasis ™	Healthpoint	Porcine small intestinal submucosa (SIS)	Natural	Dry sheet
Restore ™	DePuy	Porcine small intestinal submucosa (SIS)	Natural	Dry sheet
Stratasis ™	Cook	Porcine small intestinal submucosa (SIS)	Natural	Dry sheet
Surgisis ™	Cook	Porcine small intestinal submucosa (SIS)	Natural	Dry sheet

1.3.3.4 SIS in Research

Clinical applications aside, extracellular matrix materials are currently being researched in a variety of different application in both *in vitro* and *in vivo* animal studies. SIS has been researched in numerous different potential applications, including tracheal reconstruction (Du, Kwon *et al.* 2012), oesophageal repair (Badylak, Meurling *et al.* 2000), small intestine interposition (Qin and Dunn 2011), vascular repair (Sandusky, Badylak *et al.* 1992; Fallon, Goodchild *et al.* 2012; Wang, He *et al.* 2012). SIS has also been applied for corneal reconstruction in an animal study (cats and dogs) involving 106 individual cases where materials was found to be an excellent alternative to conventional conjunctival grafts with nearly 69.8% of cases had healing with no or discrete healing scars, and the remaining cases had only mild or marked scarring. Additionally, vision was preserved in all eyes at three months post-surgery (Goulle 2012).

SIS was also compared with decellularised skeletal muscle in muscle tissue engineering, though no clear advantage of muscle ECM over the control SIS was found (Borschel, Dennis *et al.* 2004; Wolf, Daly *et al.* 2012). Additionally myocardial repair has been carried out using by SIS patch (Badylak, Obermiller *et al.* 2003; Kochupura, Azeloglu *et al.* 2005; Kelly, Rosen *et al.* 2009).

Further development will most likely be the development of new modified or hybrid materials, some early examples of which are UBM/Polyglycolic acid (Eberli, Filho *et al.* 2009) and SIS/Hyaluronic Acid (Roth, Mondalek *et al.* 2011). These developments will, of course, also compete with efforts to make entirely artificial extracellular matrices (Kim, Park *et al.* 2011).

1.3.3.5 Limitations of SIS

It is well known that the main limitation of SIS, and indeed, all ECM materials is that they do not provide any significant level of mechanical stability (Badylak, Freytes *et al.* 2009). In addition to this they are known to lose mechanical properties relatively rapidly as they are remodelled *in vivo.* Consequently there have been attempts made to improve these properties through cross-linking however, as mentioned previously, this approach negatively impacts their *in vivo* performance. Another approach has been to make the SIS in multilaminate form, which is the method used for most commercial products available.

1.3.4 Decellularisation

1.3.4.1 Background

The use of a decellularised matrix has been well described in the literature. Work done as early as 1972 isolated renal tubular basement membranes from rabbits kidneys by decellularising proximal convoluted, proximal straight, and cortical collecting tubules by a perfusion method using sodium deoxycholate (Welling and Grantham 1972). They also investigated using the same method but alternatively using Triton X-100. The result was a tubular sheath described as “transparent” which is a common observation of decellularised matrices. While the purpose of their work was carried out to study the physical properties of the matrix, and not

concerned with for example cell culture work, the method they utilised is readily identifiable in today's tissue engineering practices. They also found that sodium deoxycholate consistently yielded tubular basement membrane fragments entirely free of adherent cellular debris.

Work done by Meezan *et al.* (Meezan, Hjelle *et al.* 1975) isolated basement membranes from a variety of tissues including bovine retinal and brain blood vessels, rabbit renal tubules and rat renal glomeruli. Their method did not aim to preserve the structure of the tissue, however they did utilise 4% sodium deoxycholate, 0.1% sodium azide (which was used *to "lyse the cells and release the intracellular contents"*), and DNase (Deoxyribonuclease 1), and all of these reagents are readily identifiable in modern decellularisation protocols. The use of centrifugation stages indicates that their aim was to merely isolate, and not preserve, the basement membranes. They described their method, i.e. deoxycholate treatment, as not altering the chemical composition of the basement membrane.

This method has also been used in a more modern context. A modified version of this method was used in the decellularisation of the trachea by Conconi *et al.* (Conconi, De Coppi *et al.* 2005) . The method was used here in the form of repeated cycles which had the effect of producing a decellularised scaffold which was subsequently used in patient treatment (Macchiarini, Jungebluth *et al.* 2008). The use of this method was also then used by Totonelli *et al.* (Totonelli, Maghsoudlou *et al.* 2012) and applied to the decellularisation of the rat small intestine using a perfusion method. In summary the method described has shown a degree of effectiveness in decellularisation that has been successfully applied to a number of different tissues

The use of the detergents is quite common generally in the area of tissue engineering. Triton X-100 is a detergent which has been in use for some time. Its early use has been well described by Cortijo *et al.* (Cortijo, Dixon *et al.* 1987). This work also describes a number of tissues which have been decellularised with this agent. SDS is another detergent which has been shown to be an extremely useful for decellularisation, and described in early work as breaking down cell membranes by "generally disrupting all tertiary and quaternary structure in the formation of rod shaped protein-dodecyl sulfate complexes"[sic](Clarke 1981)

For any ECM to function *in vivo* it must be suitably decellularised as the presence of specific cell membrane epitopes and DNA, xenogeneic or allogeneic, could result in an adverse immune response upon implantation (Gilbert, Freund et al. 2009). In reviewing tissue decellularisation Crapo *et al.* proposed a potential framework of three criteria to determine satisfactory decellularisation. These criteria are; <50ng dsDNA (double stranded DNA) per mg of ECM (dry weight), a lack of visible nuclear material in tissue sections stained with 4',6-diamidino-2-phenylindole (DAPI) or Hematoxylin and Eosin (H&E), and <200bp DNA fragment length (Crapo and Gilbert 2011). It should be stated that these criteria are theoretical as no substantial work has been carried out which establishes the threshold level of cellular remnants in ECM materials that elicits a negative remodelling response.

1.3.4.2 ECM Material Production

The production of ECM materials is a biochemical, physical and mechanical multistage process which aims to remove the cellular content of the ECM. It aims to do this while preserving the mechanical integrity, the composition and the biological activity of the remaining ECM matrix. The stages involved include physical manipulation to extricate and isolate the tissues; one or more means of actual

decellularisation usually in a particular sequence, disinfection, lyophilisation and/or hydrolysation, followed by final sterilisation.

Most commercial ECM products available today are processed into sheets prior to decellularisation which also necessitates at least one further step. In the case of porcine SIS the cylindrical intestine segments are cut to produce sheets which will then undergo gentle mechanical abrasion to remove the layers of the intestinal wall either side of the submucosa (Lantz, Badylak *et al.* 1990). Porcine urinary bladder matrix is also largely produced in a similar manner (Hodde, Record *et al.* 2002).

Once isolated, the sheet-like ECM material undergoes the actual process of decellularisation and DNA removal. It is understood that any decellularisation requires a degree of disruption of the ECM to allow for adequate exposure to reagents and to provide a pathway for the removal of cellular debris (Gilbert, Sellaro *et al.* 2006). The actual process of decellularisation is achieved in a number of ways. Detergents, hypotonic or hypertonic solutions, acids, bases, solvents, alcohols and enzymes or other biological agents have all been applied for this purpose. A number of physical means have also been employed including freeze-thawing, agitation, temperature, sonication, force and pressure and also non-thermal irreversible electroporation (NTIRE) (Gilbert, Sellaro *et al.* 2006; Crapo and Gilbert 2011).

The process of decellularisation is not uniquely applied in the preparation of ECM-derived materials, the process has also been applied to a large number of intact tissues for the purposes of tissue engineering (which are not covered here and are reviewed elsewhere) (Badylak, Taylor *et al.* 2011; Song and Ott 2011).

In decellularisation the primary purpose of the process is to remove xenogeneic and allogeneic cellular antigens whose presence may result in an adverse inflammatory response or even immune-related rejection (Badylak and Gilbert 2008). However, it

has been shown that residual amounts of DNA and certain species specific immunogenic antigens will still be present in the ECM matrices, including the galactosyl-a-1,3-galactose (Gal epitope), though these fail to trigger immune mechanisms such as complement activation or the IgM antibody-mediated response. This is likely to be due to the relatively small quantities of antigens in addition to their dispersed distribution within the matrices (Raeder, Badylak *et al.* 2002; Daly, Stewart-Akers *et al.* 2009; Gilbert, Freund *et al.* 2009).

ECM materials are further processed prior to terminal sterilisation and packaging. The materials can be lyophilised (freeze-dried), vacuum pressed or subjected to both to extend the products longevity. These processes are also said to avoid the leaching of soluble factors, such as VEGF and b-FGF, which might otherwise occur. SIS has been shown to be capable of being processed into a variety of shapes including multilaminate sheets (Freytes, Badylak et al. 2004), cones (Nieponice, Gilbert et al. 2006) or tubes (Badylak, Vorp et al. 2005). That being said, the vast majority of the commercially available SIS products are in the form of sheets, in single or multilaminate forms, which aid in the handling characteristics of the materials. Variations in the number of layers and structural features (such as holes) can influence the properties of the material and so can aid in matching the properties to the most suitable applications (Freytes, Badylak et al. 2004).

SIS can also be lyophilised and crushed to produce powders (Gilbert, Stolz et al. 2005), liquids, or hydrogels (Choi, Yang et al. 2009). In these forms it can be potentially used in minimally invasive treatments or combined with sheet forms to produce hybrid materials (Huber and Badylak 2011).

The processing changes do inevitably lead to changes in the structure and composition of the ECM materials. Peracetic acid is a commonly used decellularisation agent which is used in the production of UBM and SIS (Hodde,

Record *et al.* 2002). Peracetic acid is a well-known oxidative agent (Freytes, Badylak *et al.* 2004) and when SIS that was decellularised with it was subjected to analysis it was found that the levels of VEGF had fallen by 99%, the levels of TGF-β1 had fallen to 18% of the original quantity present, while the level of FGF-2 had only fallen by 50%. Alternatively the fibronectin, sulphated GAG, and hyaluronic acid quantities were only slightly affected (Hodde, Janis *et al.* 2007).

Peracetic acid has been used as a sterilisation for a large number of tissues including dermal tissues (Huang, Dawson *et al.* 2004). With respect to SIS peracetic acid is ostensibly used in a disinfectant capacity and forms an important part of much of the initial work on ECM materials (where SIS was principally tested mechanically and its constituent components analysed) (Kropp, Eppley *et al.* 1995; Badylak, Kokini *et al.* 2001). In the initial protocols it represents the only form of chemical treatment of the materials aside from washes with PBS. Consequently as the DNA content was tested it was also found that the washing with peracetic acid also removed DNA. This was reinforced by Keane] *et al.* where it was shown that lowering the 2 h wash with peracetic acid to 1 h resulted in a higher DNA content in the SIS (Keane, Londono *et al.* 2012). It is important to note that these samples were all then terminally sterilised with ethylene oxide at the end of the process. Peracetic acid is organic peroxide that acts as an oxidising agent giving it highly biocidal properties. Oxidising agents have been known to denature proteins, disrupt cell wall permeability, and oxidize sulfhydral and sulfur bonds in proteins, enzymes, and other metabolites. Consequently it stands to reason that the cellular component of the SIS would be affected, including the DNA present, though this effect is not likely limited to the cellular component and this will be discussed later. The direct action of peracetic acid in decellularisation has not been researched in any detail.

This loss of component is not limited to a single decellularisation agent, another study carried out with porcine dermis, decellularised with two protocols using the

commonly used detergents sodium dodecylsulfate (SDS) and Triton X-100 (SDS was excluded in one protocol) along with the enzyme Trypsin (Crapo and Gilbert 2011), showed similar levels of component loss with the decellularised tissues shown to contain no detectable VEGF or TGF-β1, FGF levels at 99% or 60.1%(without SDS) lower, though an unaffected GAG content (Reing, Brown *et al.* 2010).

The effects of the loss of these components are difficult to assess. When decellularised SIS and UBM were compared with control tissue the adherence of human microvascular endothelial cells was unaffected (Freytes, Badylak *et al.* 2004) possibly indicating the preservation of adhesion molecules. In addition to this murine fibroblasts cultured on decellularised SIS have been shown to produce endogenous VEGF and thus possibly negating the need to retain certain growth factors at all (Hodde, Janis *et al.* 2007b) and also highlight that the effectiveness of ECM materials may not be limited to the growth factors retained.

Some growth factors may be lost however research had shown that there are a large number of functionally active proteins are still retained (Freytes, Badylak *et al.* 2004; Freytes, Rundell *et al.* 2005; Freytes, Tullius *et al.* 2008; Gilbert, Wognum *et al.* 2008).

1.3.4.3 Sterilisation

The final stage of production is sterilisation which is necessary if the material is to be used in any form *in vivo* application. SIS as a material has been sterilised a number of different ways and these methods have been well documented. The most commonly used methods include using E-beam irradiation, γ- irradiation and the ethylene oxide infiltration (Grimes, Pembroke *et al.* 2005). Each of these methods has certain advantages and disadvantages. Both forms of irradiation are forms of ionising radiation and work through the action of disrupting the DNA present in the

microorganisms (Grimes, Pembroke *et al.* 2005). However these can greatly affect the properties of the material particularly due to the physical damage which can occur especially in the form of collagen chain scission which results in the reduced mechanical properties. They also cause the materials to have an increased degradation rate.(Delgado, Pandit *et al.* 2014). Ethylene oxide involves the gaseous infiltration into the material and while it does also result in some increased degradation this occurs to a far lower degree than that observed with irradiation methods and have lower collagen chain scission (Grimes, Pembroke *et al.* 2005). Ethylene oxide has also been shown to and also a good retention of growth factors (Hodde, Janis *et al.* 2007; Hodde, Janis *et al.* 2007b). The method has been shown to suffer from residual gas remaining in a material which may result in cytotoxicity towards the surrounding cells and tissue after implantation however this can be mitigated by allowing for adequate time for the gas to diffuse out (Olde Damink, Dijkstra *et al.* 1995).

Sterilisation need not be limited to these methods and alternative approaches have been employed on other collagen-based materials. These methods include gas plasma, ethanol and peracetic acid. While peracetic acid has been applied to SIS extensively it is commonly applied in the initial phase of preparation. Ostensibly this is under the description of being a “disinfectant”, which given the contents of the small intestine, is understandable. The use of peracetic acid as a complete means of sterilisation is generally not carried out but has been applied to was shown to have a negative effect on the mechanical properties (Delgado, Pandit *et al.* 2014). In the case of gas plasma it has been applied to collagen sponges which caused a degree of structural degradation though this was found to be less than γ- irradiation. Ethanol has not been extensively used, though when used with pericardium though was found to affect the mechanical properties (Delgado, Pandit *et al.* 2014).

A further form of sterilisation which is largely restricted to skin is the use of glycerol immersion. While considered to be slow-acting it has effective bactericidal and antiviral properties (Mackie 1997; Ectors, Lismont *et al.* 2008). Cadaveric dermal grafts for some time have been successfully used clinically after being sterilised and stored in glycerol (Khoo, Halim *et al.* 2010; Pirayesh, Hoeksema *et al.* 2015). By immersing the grafts the antimicrobial properties of the glycerol has been shown to take effect and furthermore the graft can be then stored in the glycerol at 4°C. This method has not been used with small intestine submucosa given that the materials differ greatly in their structure and properties the effect of the method could possibly be different particularly with respect to altering the properties of the SIS.

In summary, collagen-based material can be sterilised a large number of ways but there does not appear to be a definitive method. It should also be noted that high temperature or steam related methods have not been addressed here due to the damage they would cause to these materials. What is more likely the case is that each material will have an optimum method according to the properties of the material and the application for which the material is being used.

In this work the sterilisation methods will likely be selected from the established methods which have been applied to SIS. Of these methods, ethylene oxide does appear to be the most suitable particularly due to the fact that it does the least damage to the material in question and this remains an important consideration if the material is too be used in form requiring strength. In addition to this modern ethylene oxide sterilisation units can cycle at far lower temperatures (i.e. 37°C) than that used for equipment sterilisation such as 55°C and so limit the temperature damage that might occur otherwise.

1.4 - Electrospun Scaffolds

1.4.1 Electrospinning

1.4.1.1 Background

Electrohydrodynamic processing is the term given to describe a number of related processes used to create polymer particles or fibres by applying an electrical field to polymer solutions or melts. More specifically, the term electrospinning has been used to describe the creation of micro and nano scale polymer fibres by the formation and the charge induced elongation of an electrified fluid jet (Reneker and Yarin 2008).

Over the last few decades the use of electrospinning has increased and emerged as a significant method for the production of micrometre and nanometre scale fibres for a variety of electrical, chemical and biomedical applications (Reneker and Yarin 2008; Bellan and Craighead 2011). Within biomedical research significant promising work has been carried out in the synthesis of nanofibre-based three-dimensional scaffolds for use in tissue engineering, and in the creation of nanofibre devices for controlled delivery of pharmaceuticals (Andrady 2008). Additional potential biomedical applications include the fabrication and development of microfluidic devices, printed 3D structures and patterns, and “lab on a chip” devices. As electrospinning has become more established it has become an effective method for the large scale synthesis of nanofibres which themselves can be used for textile, filter, mechanical reinforcement, sensors, optoelectronics, catalysis applications amongst others (Dersch, Graeser *et al.* 2007). A key advantage of electrospinning is the ability it gives operators to manipulate the micro-morphology of the fibres which are produced.

1.4.1.2 Theory of Electrospinning

Electrospinning is now a well-established process for the production of polymer fibres and on which an extensive amount of research has been carried out (Reneker and Chun 1996; Yarin, Koombhongse *et al.* 2001; Thompson, Chase *et al.* 2007; Yu, Branford-White *et al.* 2010). The process involves the use of an applied electrical field which interacts with the charge of the polymer solution or melt thus overcoming the surface tension of the liquid and causing an electrified jet to be produced (Reneker and Chun 1996). The process shares many similarities with electrospraying (or electrohydrodynamic (EDH) atomisation) from which atomised particles are produced as opposed to fibres.

Pioneering work was done in both these areas by Lord Rayleigh who observed that above a critical charge level, the electrical forces (electrostatic) overcome the surface tension forces of the liquid and render it unstable. He also observed that there is in fact a balance of opposing forces which affect the behaviour of a drop suspended from a capillary (Rayleigh 1882).

In further work done in this area Zeleny observed the characteristic “cone-jet” which is formed at the mouth of the nozzle of the needle when electrohydrodynamic activity is present (Zeleny 1917) and identified the “cone-jet” mode which is the basis of electrospraying and spinning. Sir Geoffrey Taylor then provided an explanation for the formation of the liquid cone based on the balance of electrostatic and capillary pressure (Taylor 1964). When EHD processes occur and the pendant drop deforms into a stable cone shape this is now referred to as a “Taylor cone” (Yarin, Koombhongse *et al.* 2001). Following Taylor, a large amount of work advancing electrohydrodynamic knowledge was performed with these works providing the basis for electrohydrodynamic theory upon which the later developments were built.

Electrospinning, as separate from electrospraying, in that if the viscosity of the polymer solution is sufficiently high then the flow that is produced does not disperse and a charged liquid stream is formed. The literature on this subject often refers to this stream as a “jet”.

The applied voltage, the polymer viscosity, and the surface tension are not the only forces involved in the process, Hartman *et al.* describes the varying forces which are at work within the cone shape and demonstrated its dependence on these forces (Hartman, Borra *et al.* 1999). The forces described are liquid pressure, liquid surface tension, gravity and electrical stresses present on the liquid surface as seen in Figure 1.2.

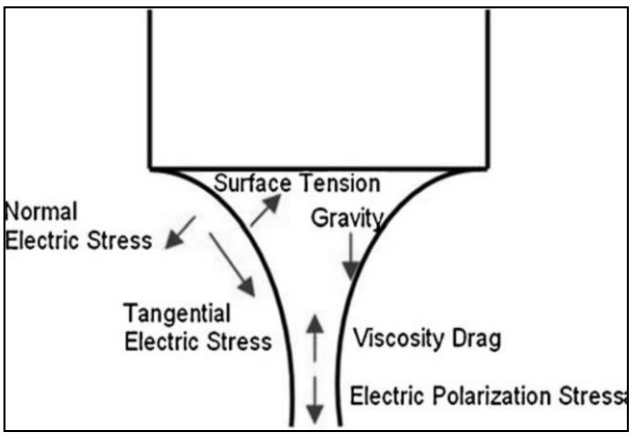

Figure 1.2: Representation of the cone–jet mode indicating the controlling forces (Hartman, Borra *et al.* 1999).

There are a number of spraying modes which have been described by various researchers (Hayati, Bailey *et al.* 1987a; Hayati, Bailey *et al.* 1987b; Enayati, Chang *et al.* 2011). These descriptions are more concerned with the process of electrohydrodynamic spraying and not on electrospinning. The different modes that have been mentioned are summarised in Figure 1.3.

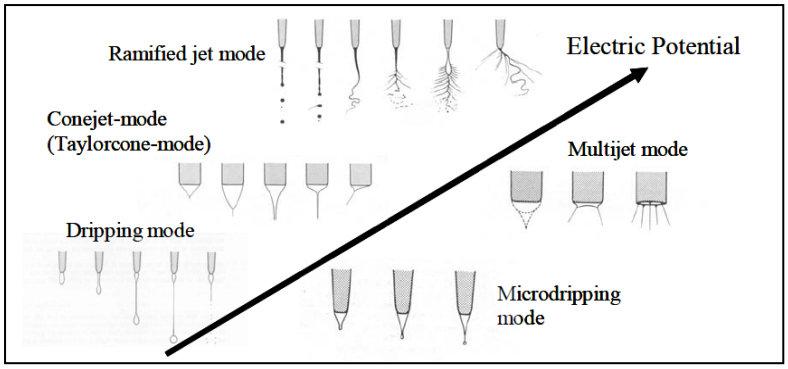

Figure 1.3: Electrospraying Modes (Wilhelm 2004).

The modes of electrohydrodynamic processing will be dependent on various factors though these are all not essential for electrospinning and are not covered here and reviewed elsewhere (Paine, Alexander *et al.* 2007). The electrospinning process may be broken down into several operational components. The actual process of electrospinning involves the several different stages to occur successfully. These basic stages can be summarised as follows:

- The formation of the cone-jet
- The movement of the jet through the electrical field and the effects of the instabilities. (Thinning also occurs.)
- The solidification of the fibres

The basic structure of the jet begins with a short straight segment where the trajectory of the polymer solution jet is parallel to the axis of the jet. Within this straight segment the diameter of the jet decreases with distance from the tip (Reneker and Yarin 2008; Hardick, Stevens *et al.* 2011). Extensive work has shown that the charged jet then begins to move in a radial manner in addition to moving along the axis of the needle. This radial movement occurs due the development of an electrical bending instability (Reneker and Yarin 2008). The jet continues to move in a radial manner and begins a coiling action. The electrical forces due to the charge carried within the jet then cause the jet to further elongate as it progresses in

its coiling action and in the process it becomes narrower in diameter. This is illustrated in the Figure 1.4.

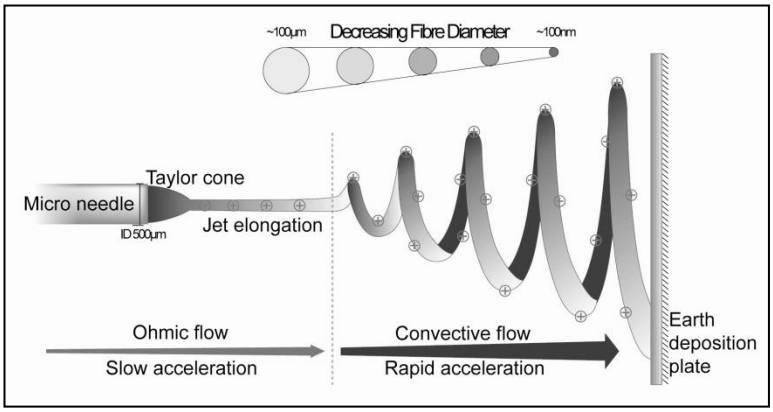

Figure 1.4: Fibre formation by electrospinning (Hardick, Stevens *et al.* 2011).

As the fibres flow through the electrical field with some tangential electrical stresses stabilising the accelerating jet, it will ultimately become unstable and a number of instabilities develop. These instabilities distort the jet as it traverses through the applied electrical field. The significance of these instabilities is considered high and they are believed to be the primary basis for electrospraying and electrospinning in addition to being the prevailing forces in determining the fibre morphology.

These modes of instability are Raleigh instability, axisymmetric instability, and bending mode (or whipping) instability (Shin, Hohman *et al.* 2001a; Shin, Hohman *et al.* 2001b). The mode of instability which occurs during the electrospinning process will largely depend on the strength of the electrical field, the polymer solution surface charge density and the surface tension (Andrady 2008).

The whipping instabilities are the significant driving forces in electrospinning (Reneker, Yarin *et al.* 2000). The movement of the jet at this point is usually referred as a “whipping action”. There have been several mathematical models which have been created to describe and explain this process and these are outlined by Hartman *et al.* (Hartman, Borra *et al.* 1999). A large amount of work been carried

out modelling the whipping jet and has described it as essentially occurring due to competition between several modes of instability (Reneker, Yarin *et al.* 2000).

For a steady jet to be produced there are two primary conditions which are important. There must be sufficient forces present which hold the jet together (i.e. viscoelastic forces) against any capillary instabilities which occur and additionally there must also be suitable relaxation time for the solution to behave in a viscoelastic manner. Reneker and Yarin (Reneker, Yarin *et al.* 2000) describe three stages in the whipping process, a straight section, the development of an array of bends and finally the bends developing into a series of spiralling loops. As the diameter of the loops increases the diameter of the fibres decreases as seen in Figure 1.4.

The radial "whipping" motion causes the process of elongation by electrostatic repulsion which occurs at small bends in the jet. The result of this elongation is an increasingly narrow jet eventually reaching the grounded collection plate at the nanometre-scale. The whipping action dramatically increases the surface area of the jet but it also rapidly lowers the surface charge density. During this process the solvent evaporates and the result is solidified polymer fibres (Hardick, Stevens *et al.* 2011). Evaporation of the solvent also contributes to the decreasing diameter in addition to elongation. Multiple polymer fibres can also be formed when the radial forces exerted by the electrical charges overcome the cohesive forces in the jet and due to mutual repulsion they separate in a phenomenon known as splaying (Reneker and Chun 1996; Natarajan and Mahavadi 2011).

1.4.1.3 Factors Affecting Electrospinning

While the influence of the instabilities in electrified fluid jet can be described in simple terms involving only a few important variables such as applied voltage and some basic properties of the polymer solution there are in fact a large number of

variables which can influence the electrospinning process and, in turn, the fibre morphology.

These factors include gravitational forces, the electrostatic force (which actually attracts and extends the jet towards the charged collection plate), Coulombic repulsion forces on the surface of the jet (which are responsible of the instabilities and therefore the whipping motion), viscoelastic forces (which working against the elongation process are also vital to the creation of continuous fibres and are dependent on the polymer molecular weight, the solvent properties and the type of polymer which is used), surface tension forces (which also could be said to work against the forces which act to elongate the electrospinning jet), and frictional forces (which act between the surface of the jet and atmospheric gas molecules through which they traverse (Fong, Chun et al. 1999; Reneker, Yarin et al. 2000). A list of some of these factors is presented in Table 1.2.

Table 1.2: Table of parameters affecting fibre morphology

Solution Properties	Operating Conditions	Ambient Conditions
Dielectric Constant	*Potential Difference*	*Temperature*
Electrical Conductivity	*Needle Diameter*	*Humidity*
Entanglement Concentration	*Solution Flow Rate*	*Pressure*
Extensional Viscosity	*Collection Distance*	
Polymer Concentration	*Collection Method*	
Polymer Molecular Weight		
Polymer Molecule Chain Length		
Shear Viscosity		
Solvent Vapour Pressure		
Surface Tension		
Temperature		

In addition to the aforementioned factors there are a number of more subtle factors that can also be considered. These include the diameter of the flowing jet near its

origin, the relaxation time, the elongation velocity and the partial pressure of the solvent vapour which is surrounding the jet (Reneker, Yarin *et al.* 2007; Reneker and Yarin 2008). While all these factors have important influences the key ones which have been described as have dominating the onset of the transformation from electrospraying to electrospinning and therefore the synthesis of fibres, and the also having a key influence on the morphology on the aforementioned fibres are the feed rate of the polymer solution, the applied voltage and the properties of the solution, such as concentration, viscosity and surface tension (Deitzel, Kleinmeyer *et al.* 2001; Luo, Nangrejo *et al.* 2010). Consequently the feed rate of the polymer solution and the applied voltage were decided on to be the variables which would be investigated in this work, as it was already decided to keep the polymer solution properties constant.

One further consideration that can be made for the influence of the variables is the geometrical dimension of the needle used (Frenot 2003). In general terms work has been done which indicates that smaller diameter needles yield fibres which are smaller in diameter. Having said that, there is a limited practicality to pumping a viscous liquid through very small diameter tubes. It should also be noted that the diameter of the jet will have a similar effect and this is influenced by the applied electrical field and the surface tensional forces and so can therefore also be seen as a secondary nozzle. Furthermore, as a result of this phenomenon, fibre sizes produced using this method of processing can be four orders of magnitude smaller than the needle outlet (Ahmad, Nangrejo *et al.* 2009). Consequently choosing a suitably sized needle bore was taken to be an important consideration as choosing too small a bore size could result in the fibres being too small to be suitable for the investigative aim of this work.

With respect to fibre diameter specifically, the process is governed by the balance between the normal stresses due to surface tension and surface charge repulsion

(Fridrikh, Yu *et al.* 2003) in addition to the vapour pressure, evaporation rate (Shenoy, Bates *et al.* 2005) of the solvent and concentration of the solution. As a result fibre diameter is a product of a significant number of variables

1.4.2 Scaffold Properties

The successful functioning of a scaffold will be dependent on its properties. These properties are vital to the performance and need to be evaluated according to the application required.

1.4.2.1 Surface Properties

Surface properties are an important consideration for the design of a scaffold. The surface chemistry influences the point of interaction between scaffolds the micro environment found *in vivo*. Cellular adhesion represents an important stage for the successful application any tissue engineering implant. Synthetic scaffolds do sometimes present a challenge for cell adhesion and a variety of approaches have been adopted to improve this. Modifications to the scaffold can either be in the form of certain bulk additions to the material or by surface modifications (Hu, Eaton *et al.* 2001). These modifications either facilitate cellular attachment directly or influence protein adsorption onto the scaffold surface which, in turn, influences cellular adhesion. The modification can include altering the surface charge on the scaffold, which influences protein adsorption, or also in incorporation of well understood attachment proteins including fibronectin or the peptide Arg-Gly-Asp (RGD) (Hersel, Dahmen *et al.* 2003). A further approach might be to influence the water uptake into the scaffold, by the use of surface washes, which can also aid cellular infiltration and adhesion.

In addition to the surface chemistry, the physical surface topography of the scaffold is also an important factor. Features such as pores, nodes, steps, ridges or grooves have been shown to have an influence on cell morphology, the processes performed by the cell, and the production of autocrine or paracrine regulatory factors when compared to smooth, featureless surfaces (Flemming, Murphy *et al.* 1999). It has been shown that in the case of PLGA scaffolds surface roughening through the use of a simple treatment with sodium hydroxide was shown to increase chondrocyte adhesion, proliferation and increased ECM production (though some of these effects were accounted for by an increase in the porosity along with the surface roughness). It should be added that scaffolds made with synthetic nanofibres have been shown to provide a complex topography which then supports cell and tissue growth (Woo, Chen *et al.* 2003).

While the surface properties are particularly relevant for synthetic fibres this is not the case with naturally derived scaffold. These materials contain a large number of innate biological materials, in addition to the main constituent collagen, which aid in cell attachment and proliferation (Yamada and Yamada 1983).

1.4.2.2 Scaffold porosity

The physical characteristics of any scaffold play an important role in how it is to function *in vivo*. The structure and the geometry of the scaffold have a number of significant effects, with porosity being one of the key parameters. The porosity of a scaffold facilitates the cellular growth into the scaffold and allows for mass transport of nutrients into, and waste products away from, the interior of the scaffold. This is vital for cell growth as cells have to be within 200 μm of a blood supply otherwise risk being placed under oxygen tension the result of which can be cell death (Colton 1995).

The nature of the porosity is also vital. Pore size is one of the well-studied factors which have been shown to affect how a scaffold performs. While there is no definitive consensus as to the ideal pore size for a scaffold for any given application (the requirements of which are likely to be different) there are some broad observations which have been made. In the case of bone tissue engineering there seems a requirement for the pores to be ~100 µm (in diameter)(Hulbert, Young *et al.* 1970; Karageorgiou and Kaplan 2005). In the case of soft tissue engineering, such as the small intestine, pore sizes which have been shown to be successful are at a size of ~250 µm (Kaihara, Kim *et al.* 1999; Kim, Kaihara *et al.* 1999). Additionally pores in the size range of >50 µm are known to better facilitate nutrient transport and cell infiltration and smaller pores in the range of <20 µm have a larger surface area allowing for greater protein adsorption, ionic solubility, and cell attachment (Woodard, Hilldore *et al.* 2007). Additionally the pore size of 10 µm has been suggested to be optimum for cellular infiltration (Zhang, Ouyang *et al.* 2005). Consequently, for the purposes of soft tissue engineering the range of 10-250 µm seems to be suitable range. It should also be added that the combination of micro- and macro-pores have, in the case of bone tissue engineering at least, been shown to improve drug delivery and strength and stiffness (when compared to exclusively micro- or macroporous).

Pore interconnectivity (or tortuosity) is another important characteristic. Good interconnectivity is vital for mass transport (including nutrients growth factors and cytokines), cellular infiltration and for the formation of neovasculature. All these factors need to be taken into consideration where good porosity characteristics providing a higher surface area (and consequently a high surface area to volume ratio) and good mass transport, thus allowing for high cellular infiltration, attachment and growth (Yang, Leong *et al.* 2001). These factors all need to be balanced by the

mechanical requirements of the scaffold as excessive porosity can compromise the mechanical integrity of the scaffold (Yoon and Fisher 2006).

1.4.2.3 Biodegradability

For the purposes of tissue engineering a scaffold should ideally provide a temporary structure and support for the growth of new tissue and then once this growth has been established it should naturally degrade. This degradation should ideally also occur at an equal rate to tissue formation (or wound healing), however, this is difficult to achieve. In addition the differences which may occur in scaffold degradation on an individual basis, there are also a large number of factors which can affect the scaffolds degradation profile *in vivo* including the levels of cellular activity, cell-induced pH changes, the presence or absence of enzymes or proteins. The physical properties of the scaffold can also have a large effect including the scaffold porosity, fibrous structure, polymer molecular weight, glass transition temperature, crystallinity, and polydispersity (Engineer, Parikh *et al.* 2001).

The actual process of degradation occurs by two mechanisms namely; surface or bulk erosion. Surface degradation is primarily localised at the surface of the material and is characterised by the material retaining its mechanical properties but gradually decreasing in size. Bulk degradation is where the material degrades throughout the volume of the scaffold and is characterised with the material losing mechanical strength but maintaining a relatively intact surface. The retention of surface integrity in bulk degradation does allow for better cell attachment when compared to surface degrading scaffolds (Yoon and Fisher 2006). Polyester scaffolds, like PCL and PLGA, tend to undergo bulk degradation, however one potential negative effect of this is the accumulation of degradation products. In the case of PLGA, which is made of lactic and glycolic acid, it is the acidic nature of the products may have a negative effect on the tissue.

1.4.2.4 Mechanical Properties

All scaffolds which are placed *in vivo* are usually subject to some form of mechanical stress usually equivalent to the stress experienced by the surrounding tissue. Consequently, the mechanical properties of the scaffold should resemble those of the surrounding tissue and should be able to sustain any expected forces which are applied to it. Moreover, these properties should also be sustained for the duration required for new tissue formation (Hayashi 1994). A large number of physical factors may influence the mechanical properties of a scaffold, including fibre characteristics, porosity and surface properties to name a few. In addition to these the mechanical properties of scaffolds will also be governed by the bulk properties of the constituent materials.

1.4.2.5 Polymers

The use of polymer biomaterials is very established and there are a number of important properties which make them highly useful. Polymer biomaterials have a very high level of processability and can be produced into a large number of forms (films, sheets, fibres, particles etc.) and they can also have their properties chemically altered in a large number of ways which can affect their mechanical, chemical, physical and biological properties. These materials can also be biodegradable, which is particularly useful for tissue engineering applications, have reasonable cost and availability, and have a reasonable degree of biocompatibility (a number of them having gained FDA approval for clinical use). Many of the commonly use polymers are polyesters, such as PCL and PLGA, and degrade through non-specific hydrolysis of their ester bonds and consequently degradation results in a loss of polymer molecular weight (Vert, Li *et al.* 1992).

1.4.2.6 Poly(ε-caprolactone) (PCL)

PCL is a semi-crystalline polymer that is that is produced through the ring-opening polymerization of lactone monomer ε-caprolactone. The polymer properties include toughness and flexibility with a meting point of 58-65°C and a glass transition temperature of around -60°C. The degradation rate is described as quite slow, when compared to polymers such as PLLA, and consequently it is considered a polymer suitable for long term drug release (Yoon and Fisher 2006). The degradation rate may be enhanced through the copolymerisation with other monomers such as lactide and glycolide.

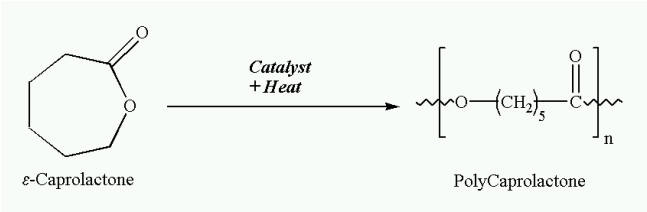

Figure 1.5 Synthesis and structure of Poly(ε-caprolactone)

1.4.2.7 Poly(lactide-co-glycolide) (PLGA)

PLGA is a polymer which is produced through a random ring opening polymerisation of lactide and glycolide. Glycolide is a dimer of glycolic acid and is in the form of a cyclic diester. This can be polymerised to poly glycolic acid (PGA) (Pachence, Bohrer *et al.* 2007).

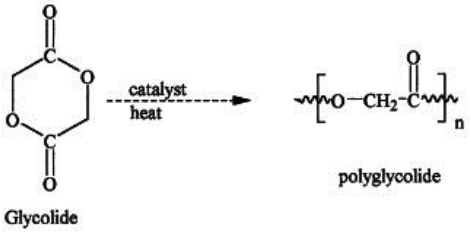

Figure 1.6 Chemical structure of glycolide and polyglycolic acid/poly(glycolide) (PGA).

Lactide is cyclic diester form of lactic acid and can be polymerised to form polylactic acid (PLA). However, the lactic acid molecule has an addition methyl group on the α-carbon compared to the glycolic acid molecule making it a chiral molecule, therefor when polymerising with lactide there can be L-, D- and mixed (D, L-) forms of PLA. This additional methyl group also means that PLA is more hydrophobic than PGA and this results in a slower hydrolysis rate. The L-PLA form is more frequently employed than D-PLA, since the hydrolysis of L-PLA yields L-lactic acid, which is the naturally occurring stereoisomer of lactic acid (Pachence, Bohrer *et al.* 2007).

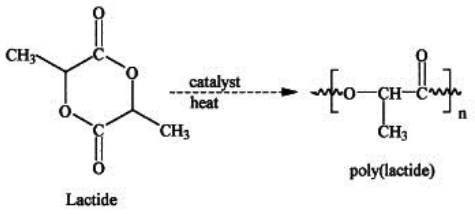

Figure 1.7 Chemical structure of lactide and polylactic acid/poly(lactide) (PLA).

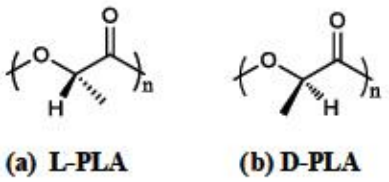

Figure 1.8 Chemical structure of polylactic acid isomers: (a) L- PLA and (b) D-PLA

PLGA is the result of the co-polymerisation of the two monomers mentioned above. The monomers are linked together to form a linear aliphatic polymer. The polymer PGA is crystalline in form, however when it is co-polymerised with PLA there is a reduction in the degree of crystallinity. This reduction results in the polymer becoming more susceptible to hydration and hydrolysis. Consequently the ratio of the two monomers can result in changes in the degradation behaviour of the polymer. It is understood that that the higher the glycolide content (the more hydrophilic of the two), the faster the rate of degradation of the PLGA polymer with

the exception of the 50:50 ratio (see Fig 1.9b.)(Middleton and Tipton 2000). An example of this is that over a 4 week time period, PLGA 85:15 was found to lose 10% of its mass as opposed to 50% for PLGA 75:25 and 70% for PLGA 50:50 (Intra, Glasgow *et al.* 2008). These rates are related to the *in vitro* properties of these materials, however a similar pattern can be observed *in vivo*. Work involving implanted PLGA scaffolds showed that post implantation that the PLGA 50:50 scaffold lost structural integrity by two weeks, with the PLGA 75:25 scaffold lost approximately half of its mass by 3 months and the PLGA 85:15 scaffold was found to lose half of its mass after 4 months (Blackwood, McKean *et al.* 2008).

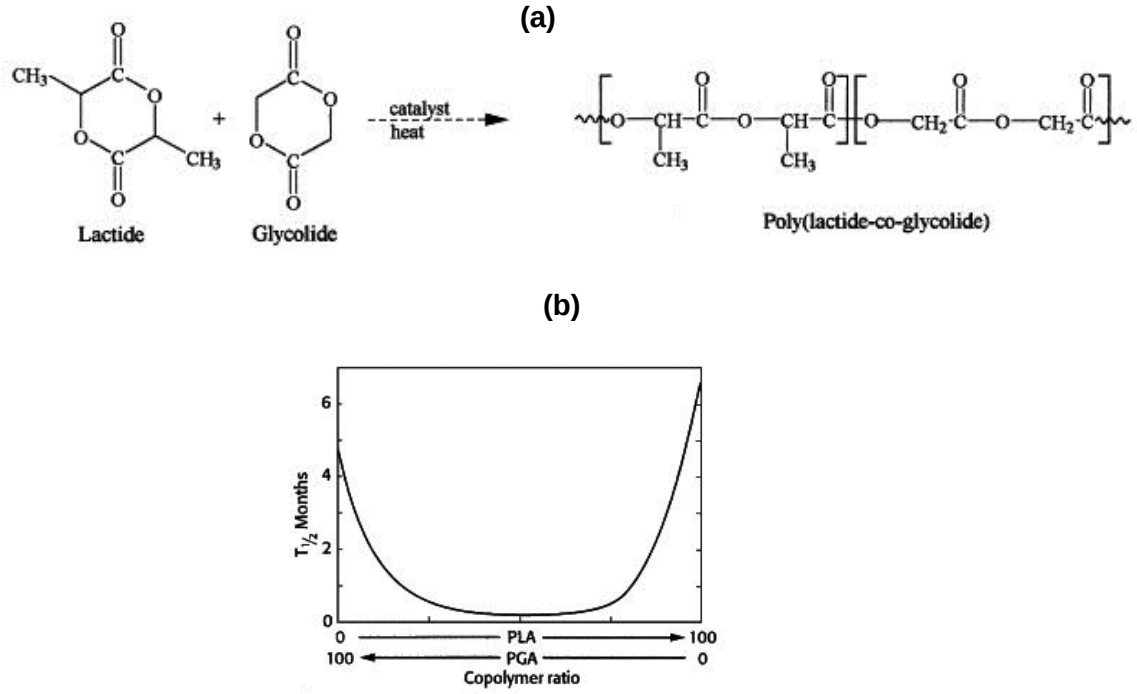

Figure 1.9 (a) Synthesis of PLGA (b) Half-life of PLA and PGA homopolymers and copolymers (Middleton and Tipton 2000).

PLGA as a polymer degrades by direct or enzyme-catalysed hydrolysis in four steps: 1) the amorphous region is penetrated by water and there is a disruption of secondary forces 2) hydrolysis of the covalent bonds of the polymer backbone occur 3) mass loss begins due to increased cleavage of the polymer backbone then 4) erosion occurs with large scale weight loss (Catiker, Gumusderelioglu *et al.* 2000).

In addition to the ratio of monomers the rate of degradation is also affected by the polymer crystallinity (which is dependant, in part, on the monomer ratio), the temperature and the pH (Lu, Peter *et al.* 2000). Once degraded the components take the form of lactic and glycolic acids, which while acidic are biocompatible.

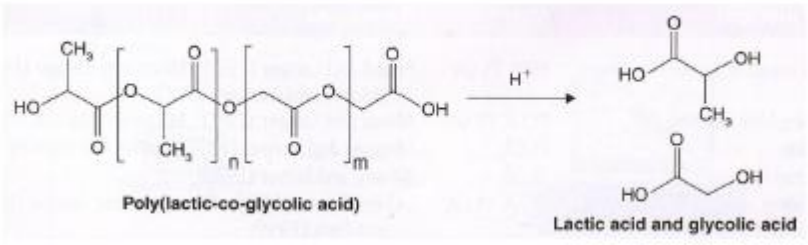

Figure 1.10 Structure of polylactic-co-glycolic acid and its decomposition in lactic and glycolic acid (Hacker and Mikos 2011)

One of the limitations of PLGA as a biomaterial used in tissue engineering is that the material possesses a relatively high degree of hydrophobicity. As a result the material exhibits sub-optimal cellular adhesion and growth at the surface. It also results in there being relatively low hydraulic permeability, which can be useful for controlling mass transport (Shearer, Ellis *et al.* 2006). That being said, this is quite a critical assessment of the material's properties and in a broader context the material has been shown to perform well with suitable levels of cellular adhesion when implanted *in vivo* (Blackwood, McKean *et al.* 2008; Pan and Ding 2012).

1.4.2.8 Fibre Alignment

As mentioned previously, there are a large number of factors which can affect the properties of electrospun polymer fibres. In addition to those mentioned with electrospun fibres there is also the potential to produce fibres which are aligned. Alignment can be achieved by a number of different approaches and have been applied to various different polymers.

A large number of alternative approaches have been taken which have successfully produced aligned fibres using a variety of methods, including against flat rotating discs, onto arrays of aligned needles, between ring-shaped electrodes and the "reeling" of already electrospun fibres collected on liquid (Teo and Ramakrishna 2006). However, the most common approach is through the use of a rotating drum with the rotational speed of the drum having been shown to have a direct influence on this.

One method used was with a rotating plastic drum at a very slow speed of 1 rpm, a hollow drum being embedded with copper wire and while aligned fibres were observed the placement of the wires had additional effects on the localised alignment as the wires were causing a higher degree of attraction and therefore the results were not ideal (Katta, Alessandro *et al.* 2004).

Stitzel *et al.* did not achieve any alignment of fibres when making a tube of PLGA for vascular use at 500 rpm when carried out with a cylindrical mandrel. Here it was noted that at a relative low speed (500 rpm) and a small diameter mandrel (4.75 mm) the fibres were highly randomised (Stitzel, Liu *et al.* 2006).

Alignment has been demonstrated with a rotating mandrel at 1000 rpm, and compared to a randomly aligned sample at 100 rpm (Boland, Wnek *et al.* 2001). Also Sundaray *et al* used a pin and a rotating thin plastic sheet folded into a cylinder rotating at 2000 rpm with some alignment in addition to a criss-cross pattern being observed (Sundaray, Subramanian *et al.* 2004).

It was demonstrated that fibre alignment resulted in the alignment of smooth muscle cells which were cultured on them. It was also shown that while affecting the orientation of the cells, there did not change in phenotypic expression of the cells (Jia, Prabhakaran *et al.* 2014). Using aligned nano-fibrous P(LLA-CL) scaffolds it was also shown that there was improved vascular SMC adhesion, parallel

organisation and a higher degree of contractile phenotype when compared to unaligned samples (Nivison Smith and Weiss 2012).

With the ability to produce alignment in electrospun fibres it has since been shown to alter the mechanical properties of fibre scaffolds produced using this method. Elastic modulus and strain to failure were tested and significant differences observed between the aligned and unaligned scaffolds, with the higher being observed in the aligned fibre constructs (Boland, Wnek *et al.* 2001).

Interestingly, while the rotation speed of the mandrel has been shown to have an effect on the alignment of the fibres produced it has also been shown by Choi *et al.* that this does not impact the diameter of the fibres produced (Choi, Lee *et al.* 2008).

1.4.2.9 Adherence

While the concept of electrospinning fibres onto the surface of an ECM material does appear straightforward, in practice this does not appear to be the case. In work spinning PLGA fibres onto mandrel mounted UBM (Urinary bladder matrix) Horst *et al.* found that it was necessary to alter the conditions of the UBM so as to improve attachment. Testing the fibres onto dry, wet, and continuously rehydrated UBM, with the highest degree of attachment found with the continuously hydrated sample (Horst, Madduri *et al.* 2013). In the case of this material, the UBM was never freeze-dried and was maintained in a hydrated state or dried prior to use. UBM has also been successfully used with electrospun fibres made from silk fibroin. The matrix here was flat and the adhesion characteristics of fibroin is likely to vary compared to PLGA (Li, Song *et al.* 2015).

1.4.3 Drug Delivery

1.4.3.1 Background

Electrospinning offers significant flexibility for use in drug delivery applications. Recent studies have demonstrated that a wide spectrum of drug such as antibiotics, anticancer treatments, growth factors and nucleic acids (both DNA and RNA), can all be incorporated into electrospun fibres. A number of different methods have been employed including coatings on the fibres, direct embedding and encapsulation of drug within the fibres via coaxial or emulsion electrospinning (Prabaharan, Jayakumar *et al.* 2012).

1.4.3.2 Vascular Endothelial Growth Factor

Sufficient blood supply is one of the key factors for obtaining a successful tissue-engineered construct. The rapid ingrowth of newly formed blood vessels is an important process, and angiogenesis is the process by which new branches are created from existing blood vessels (Komura, Kim *et al.* 2011). The process begins with the production of angiogenic growth factors, such as vascular endothelial growth factor (VEGF) or basic fibroblast growth factor (bFGF). These factors may be introduced as part of an implant, originate from the host tissue cells due to tissue injury during an implantation procedure, or as a consequence of an inflammatory response to an implant (Laschke and Menger 2012). Endothelial cells present in the local microvasculature are stimulated to produce matrix metalloproteinases which degrade their basement membrane (Carmeliet 2000). The endothelial cells subsequently migrate into the surrounding interstitial tissue, resulting in the formation of vascular buds and sprouts. The walls of these new vessels are finally stabilized by the production of extracellular matrix compounds and the recruitment of smooth muscle cells or pericytes (Anderson, Ponce *et al.* 2004).

VEGF is an angiogenic growth factor specific for vascular endothelial cells that is able to induce angiogenesis *in vivo* (Leung, Cachianes *et al.* 1989). It is a potent, multifunctional cytokine that while known for facilitating angiogenesis and has been known to stimulate a variety of, possibly independent, endothelial cell processes including inducing transient accumulation of cytoplasmic calcium, shape change, cell division and migration and gene expression changes (Dvorak, Brown *et al.* 1995; Lindhorst, Tavassol *et al.* 2010). Most of the research carried out has been one form but it should also be stated that there are a five different VEGF isoforms that are produced by alternative splicing of the VEGF gene to form active disulfide-linked homodimers which vary in function with most abundant being the 165 amino acid form (Neufeld, Cohen *et al.* 1999; Silvestre, Tamarat *et al.* 2003). VEGF exerts its effect through two endothelial receptors, tyrosine kinase VEGFR-1 (Flt-1) and VEGFR-2 (KDR/Flk-1) though there are a number of accessory receptors (Yancopoulos, Davis *et al.* 2000).

While VEGF has been incorporated into electrospun fibres, the process is not a simple one with a variety of different approaches having been used. Methods used are often quite complicated due to the water-soluble nature of VEGF, a property which prevents direct incorporation into many of the most popular polymers in use. A method around this problem is the incorporation of VEGF into a water soluble polymer which can then be coaxially spun, and example of this was carried out along with PLGA fibres (Jia, Zhao *et al.* 2011). This type of process makes VEGF incorporation into electrospun fibres a time-consuming, technically complex and not readily viable. The complexities of the properties of coaxial fibres are quite difficult to ascertain and therefore if fibres are required to be consistent in size and in properties (so as to control degradation rate and the mechanical properties) then coaxial spinning might not be an ideal option.

A simpler method is the direct application of VEGF onto the scaffold and for it to be adsorbed on the surface. Using this method VEGF has been successfully applied onto polymers prior to *in vivo* implantation (Lode, Wolf-Brandstetter *et al.* 2007; Moioli, Clark *et al.* 2008; Freeman and Cohen 2009; Wernike, Montjovent *et al.* 2010; Singh, Wu *et al.* 2012). VEGF has also been successfully applied to collagen coated PLGA scaffolds with the results confirmed *in vivo* (Lindhorst, Tavassol *et al.* 2010).

1.5 - Aims and Objectives

1.5.1 Primary Objective

As mentioned previously, while there are a number of conditions that could be treated using a tissue engineered construct however the most likely condition which benefit from this approach is oesophageal atresia.

With this in mind, the scaffold was designed to be able to address the issues which arise from this condition. Principally, that the scaffold should be able to function as a short segment replacement for malformed or stricture-affected oesophagi in infants with atresia. It is envisioned that the scaffold could be implanted directly, without the use of cells, and be sterilise packaged and cut to the required length much as SIS is today.

The scaffold is expected to under regenerative cellular ingrowth from epithelial and smooth muscle cells from the adjoining oesophageal tissue to which it is sutured. The use of a growth factor which could aid in the survival of these infiltrated cells through the promotion of angiogenesis is appealing and therefore was also investigated. The scaffold is expected to be able to resist the mechanical forces to which it is likely to be exposed and also to remain mechanically patent particularly during the initial 3-4 weeks period where decellularised materials are known to be rapidly remodelled and loose structural strength. The scaffold is expected to then be degraded overtime and replaced with the patient's own tissues.

1.5.2 Hypothesis

It is hypothesized that by combining unmodified SIS with an electrospun reinforcement layer that this would allow the scaffold to have the benefits of an ECM material while overcoming the poor mechanical qualities of these materials and without necessitating modification to the SIS.

1.5.3 Experimental Objectives

To achieve overall objectives of this work of this work the following objectives will have to be addressed:

- Produce a base SIS scaffold which is structurally and biologically suitable for electrospin coating with polymer fibres. This can be achieved by the scaffold: 1) having an optimal tubular shape and 2) being suitably decellularised to prevent rejection.
- To create a protocol for the production of an electrospun fibre layer that reinforces and adheres to the SIS.
- Investigate the potential for the hybrid scaffold to facilitate drug delivery to improve *in vivo* performance.

It is also important to state that the scaffold in question should have the properties expected of any biological scaffold, such as biocompatibility, non-toxicity and adequate porosity. For the purposes of this this work the scaffold would also be expected to have specific physical/mechanical criteria; specifically be able to extend by 50% in the longitudinal direction and to have a diameter of at least 10 mm. For the scaffold to function well, it is also important that the two layers have a suitable level of adhesion so that they are able to function and be handled as a single hybrid scaffold.

2. Decellularisation and Synthesis of Tubular SIS

2.1 - Introduction

As mentioned in the Section 1.1, the goal of this work is to investigate the creation of a hybrid scaffold for use in oesophageal tissue engineering. The decision was taken that the first stage of this would be the creation of a suitable ECM layer to function as a base layer for such a construct. The question was raised whether a suitable SIS scaffold could be made into a seamless tubular form as this would provide a suitable surface onto which electrospun fibres could be spun. Additionally, it was also hypothesized that the lack of a seam could improve mechanical performance and other potential benefits such as the prevention of leakages.

SIS has been commonly made in sheet form and decellularised using peracetic acid under simple agitation (Badylak, Tullius *et al.* 1995; Hodde, Record *et al.* 2002). However if SIS was to be created in a tubular form an alternative decellularisation protocol was considered necessary to adequately decellularised the tissue. With this in mind a variation of perfusion decellularisation was chosen, a techniques applied to a variety of tissues and for which a large number of protocols and agents exist (Gilbert, Sellaro *et al.* 2006; Crapo and Gilbert 2011). In this chapter two perfusion protocols were selected which have been used to decellularise a variety of tissues. The detergent-based protocols were compared with each other, a perfusion protocol using peracetic acid, peracetic acid under agitation, and with an undecellularised control. The aim here was to obtain an optimal decellularisation protocol for tubular SIS.

The first method researched was a perfusion method successfully applied by Ott *et al.* to decellularise intact rat hearts (Ott, Matthiesen *et al.* 2008). This used two detergents: SDS (sodium dodecyl sulfate), an anionic detergent, and Triton X-100 (t-octylphenoxypolyethoxyethanol), a non-ionic detergent considered to be non-denaturing (Gilbert, Sellaro *et al.* 2006). Both detergents have been commonly

applied in cell lysis in other research areas. SDS has been used for a number of years and on a variety of tissue types (see Section 1.3.4.1) , including less commonly decellularised tissues such as the kidney and temporomandibular joint (Crapo and Gilbert 2011). The use of Triton X-100 is also prominent in tissue engineering and was used for decellularisation by Cortijo *et al.* as early as 1987, when it was applied to a number of different tissues including the ileum, arteries and muscles tissue (Cortijo, Dixon *et al.* 1987). The method used by Ott *et al.* was replicated by Akhyari *et al.* and shown to be the best for whole heart decellularisation in a comparison of four different protocols (Akhyari, Aubin *et al.* 2011).

The second protocol consists of a combination of sodium deoxycholate (SD) and Deoxyribonuclease I (DNase). This protocol is discussed in Section 1.3.4.1. In summary, has shown a degree of effectiveness on a number of tissues when used in a perfusion-based arrangement.

For any ECM to function *in vivo* it must be suitably decellularised as the presence of specific cell membrane epitopes and DNA, xenogeneic or allogeneic, could result in an adverse immune response upon implantation (Gilbert, Freund et al. 2009). In reviewing tissue decellularisation Crapo *et al.* proposed potential framework of three criteria to determine satisfactory decellularisation. These criteria are; <50ng dsDNA (double stranded DNA) per mg of ECM (dry weight), a lack of visible nuclear material in tissue sections stained with 4',6-diamidino-2-phenylindole (DAPI) or Hematoxylin and Eosin (H&E), and <200 bp DNA fragment length (Crapo and Gilbert 2011). No substantial work has been carried out which establishes the threshold level of cellular remnants in ECM materials that elicits a negative remodelling response. However, while these criteria are theoretical they are useful as a guideline for decellularisation. For the purposes of this work only the first two criteria will be considered.

2.2 - Materials and Methods

2.2.1 SIS Preparation

Frozen samples of porcine small intestine were obtained at a local abattoir from animals 6 months in age. Initial work carried out showed no difference mechanically between proximal and distally obtained SIS (Appendix A-1). The jejunum/ileum samples were cut into lengths of approximately 20 cm and the excess mesentery tissue carefully removed (Figure 2.1). The samples were thoroughly rinsed with deionised water repeatedly to remove debris. The small intestine submucosa (SIS) was isolated using slight modifications to the well-established method for preparation (Badylak 1989; Lantz, Badylak *et al.* 1990). The sections of small intestine were inverted and then gently abraded using both moist and dry surgical gauze to remove the inner mucosal layer. The tissue was thoroughly washed with deionised water and then re-inverted and the serosal layer was then taken off through the use of a scalpel to create an incision, followed by manual removal of the layer. Finally the outer surface was carefully abraded using damp gauze to remove any remnants of the smooth muscle layers.

The SIS was then carefully washed twice in deionised water for 5 minutes. This involved immersing the SIS in deionised water with regular stirring. The deionised water was changed regularly and then the SIS rinsed. This was the standard washing method throughout this work. The SIS was then stored in PBS (phosphate buffered saline : 0.01 M phosphate buffer 0.0027 M potassium chloride and 0.137 M sodium chloride, pH 7.4, at 25°C). Representative tissue samples were collected at the end of the process and used as controls.

The diameter of the SIS for animals of this age was found to be roughly 2.5 cm and this was deemed suitable as it was larger than the 1 cm required according to the initial objectives.

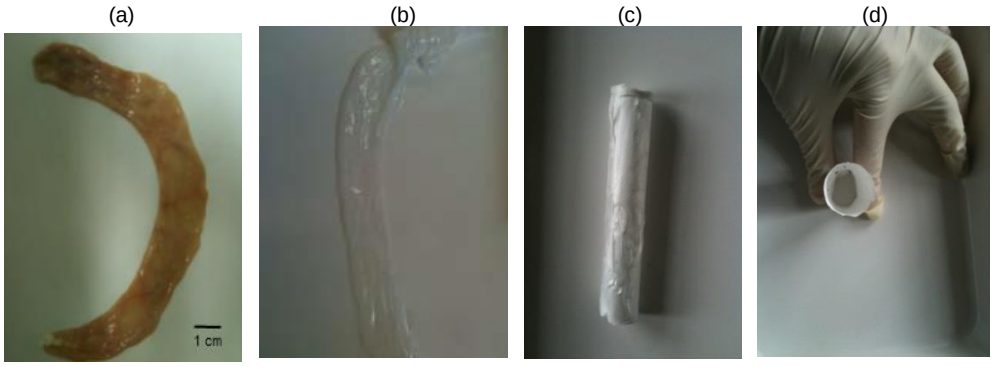

Figure 2.1 Stages of SIS preparation (a) Porcine small intestine section prior to debridement (b) SIS following decellularisation (c) & (d) Final processed form of SIS

2.2.2 Decellularisation Method 1 (Perfusion/Immersion)

Prepared SIS samples were placed in individual sealable plastic containers, secured to adaptors, and connected to a multi-channelled peristaltic pump (Watson-Marlow, Cornwall, UK). The complete arrangement is shown in Figure 2.2a. The input channels were also secured into the same containers. The solutions described below were then placed in the containers creating an isolated chamber and the pump was run to begin perfusion. This was an improvement over an earlier arrangement (Figure A2, Appendix A-3).

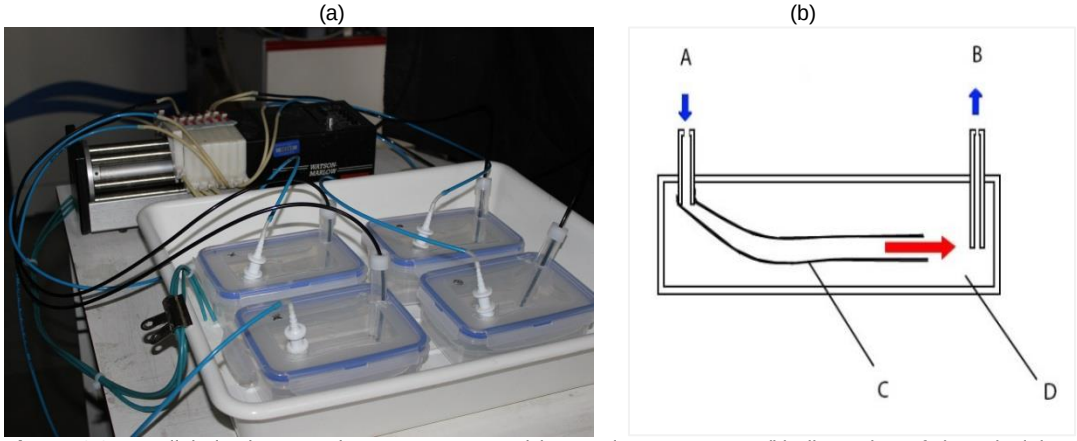

Figure 2.2 Decellularisation container arrangement. (a) Actual arrangement. (b) Illustration of the principle: (**A**) Output from the peristaltic pump which is connected to the SIS (**B**) Return to the peristaltic pump which is not connected to SIS and the SIS and draws the medium from the container (**C**) The SIS to be decellularised (**D**)

Container into which the decellularisation medium would collect and immerse the external surface of the SIS. The red arrow indicates the direction of flow of perfusion decellularisation medium.

This approach allowed the solution to perfuse through the tissue and collect in the vessel, where further immersion occurred then was recycled back to the pump. The benefit of this arrangement is that there is also an element of immersion decellularisation which occurs on the outer surface of the SIS samples as illustrated in Figure 2.2b. Four samples were produced simultaneously using this arrangement.

2.2.2.1 Sodium Dodecyl Sulfate & Triton X-100 (SDS/TX)

The original protocol on which this was based was altered for this particular application in terms of reducing the number the cycles to a single cycle. Each container was filled with 350 ml of 1% solution of SDS (Sigma-Aldrich Company Ltd., Dorset, UK), then the pump was run at 500 ml h^{-1} for 12 hours at room temperature (RT). The SIS was removed and thoroughly rinsed with deionised water, followed by a perfusion wash for 15 minutes with deionised water. The samples were then perfused with 350 ml of 1% Triton X-100 (v/v) for 30 minutes, rinsed, and then perfused with deionised water for a further 15 minutes. The decellularised SIS was then rinsed with deionised water and washed twice in deionised water prior to being given a final rinse. All decellularised SIS was stored at 4°C in PBS. Changes from the protocol as outlined by Akhari *et al.* include removing steps which were more suited to heart decellularisation including the use of a final stage of additional perfusion for 124 h in PBS (phosphate buffered saline) containing penicillin-G, streptomycin and amphotericin B (Akhyari, Aubin *et al.* 2011).

2.2.2.2 Sodium Deoxycholate & DNase (SD/DN)

In this protocol each container was filled with 350 ml of 4% SD (Sigma-Aldrich Company Ltd., Dorset, UK) then the pump run at 500 ml h^{-1} for 12 h at RT. Following this the samples were removed and thoroughly rinsed with deionised water followed by a perfusion wash for 15 minutes, also with deionised water.

The SIS was then perfused with DNase I (Sigma-Aldrich Company Ltd., Dorset, UK) at a quantity of 2000 kU in 300 ml of 1M NaCl solution at RT for 3 h. At the end of 3 h an additional 1000 kU in 50 ml of 1M NaCl was further added and the perfusion was allowed to run for a further 1 h followed by rinsing, a final wash and rinse as described previously. The samples were stored at 4°C in PBS. The original protocol was run in a number of cycles of 4 - 6 h per cycle, here this was increased to 12 h to simulate approximately 2 cycles. The DNase I amount was increased to 3000 kU (from 2000 kU in the original protocol), and the time was extended to 4 h (from 3 h) (Jungebluth, Go *et al.* 2009). The additional quantity of enzyme (1000 kU) was only added in the final hour. Though not doubling, this did extend the DNase portion of a single cycle.

2.2.2.3 Peracetic acid (PAA-12h)

Peracetic acid was used for the final perfusion protocol. This protocol was run as described previously but using 350 ml of 0.1% solution of peracetic acid (v/v) acid (Sigma-Aldrich Company Ltd., Dorset, UK) per length of SIS and run for 12 h at RT.

2.2.3 Decellularisation Method 2 (Immersion/Agitation)

SIS samples used were placed in clean screw-top specimen containers (150ml capacity) and then an orbital–shaker (Stuart Model SSM1) to provide constant mechanical agitation as shown in Figure 2.3. The containers were filled to capacity

with 0.1% solution (v/v) of peracetic acid with care taken to immerse the samples completely and remove any trapped air bubbles. Decellularisation in peracetic acid was carried out for 2 h under mechanical agitation at 100 rpm. The SIS samples were removed and thoroughly washed in deionised water as described previously, and stored at 4°C in PBS. A summary of these methods are shown in Table 2.1.

Figure 2.3 Orbital shaker arragment for agitation decellularisation.

Table 2.1 Experimental conditions for SIS production.

Decellularisation Method	Reagents	Method	Samples Tested	Processed and Tested	Total number of sample sets
uSIS	untreated	-	Untreated	yes	2
PAA-2hA	Peracetic acid	Immersion /Agitation	2h	yes	2
PAA-12h	Peracetic acid	Perfusion	12h	yes	2
SD/DN	Sodium Deoxycholate & DNase	Perfusion	4h, 8h, 12h and Final stage (16h)	yes	5
SDS/TX	Sodium Dodecyl Sulfate & Triton X-100	Perfusion	4h, 8h, 12h and Final stage (12.5h)	yes	5

2.2.4 Post-decellularisation Processing

The SIS sections were stretched over 1.9 cm diameter (3/4 inch) porous polyethylene tubing (60 µm pores) (Porex Corporation, Fairburn, United States)

(Figure 2.4a). These samples were then vacuum-dried in sealable sterile specimen bags and placed under low vacuum conditions (approximately 10 mbar) for 12 hours to compress and dry the samples as shown in Figure 2.4b. The dried SIS samples were subsequently lyophilised by rapid immersing in liquid nitrogen for 1 minute and then placed into a vacuum freeze-drier (Heto Dry Winner) for 12 h. Preliminary testing involved using SIS which was frozen at -80°C, however when this was tested mechanically it was found to fail with strain levels which were below the 50% required in the objectives. This was attributed to the slow-forming ice crystals compromising the material. The final appearance of the processed SIS is shown in Figures 2.1 (c) and (d). The further processing allowed creation of SIS with a rigid cylindrical shape. The lyophilisation additionally aided in extending the storage capacity of the SIS. These were stored in sterile 50 ml Falcon tubes.

(a) (b)

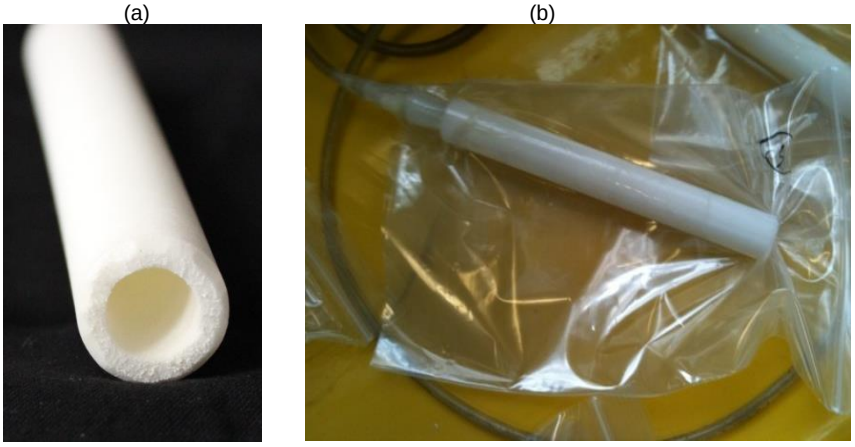

Figure 2.4 SIS processing equipment (a) porous tube (b) vaccuum drying arrangment

2.2.5 Analysis

For the two detergent based protocols (denoted SDS/TX and SD/DN), sections were taken from the SIS at time points 4 h, 8 h, 12 h and upon completion of the protocol, by cutting 2.5 cm segments during decellularisation process. The presence of two stages in these protocols, i.e. a 12h stage followed by shorter stage, brought about the decision to test the tissue at regular intervals to assess the impact of the final stages, though this was extended to some time-points.

Sections were also taken from SIS produced from the groups decellularised by peracetic acid over 12 h (PAA-12h), by peracetic acid for 2 h under agitation (PAA-2hA) at completion, as well as from the untreated control SIS (uSIS). Test sections were also taken from all SIS samples following processing. The sample segments were then sectioned further and stored according to the method of analysis.

2.2.6 Histology

SIS samples to be processed for histology were fixed in 10% formalin. The samples were embedded in paraffin wax, sectioned to 3 µm thickness and stained by haematoxylin and eosin (H&E) and Elastic Van Gieson's (EVG). At least two sections were taken from each sample. Images of the sections were acquired using a light microscope (Olympus BX50) and analysed using Image-Pro Plus (Media Cybernetics, USA) and the images were processed using ImageJ.

2.2.7 Scanning electron microscopy (SEM)

Samples for SEM were prepared alternatively depending on whether they had been processed or not. The non-lyophilised intact tissue samples were fixed in 3% (w/v) glutaraldehyde 0.1M CAB (sodium cacodylate) buffer for 3 h. Following rinsing with PBS the samples were dehydrated by separate 15 minute immersions in graded ethyl alcohol concentrations (50%, 70%, 90% then 100% v/v in deionised water) and then then briefly immersed in hexamethyldisilazane for critical point drying. Sections of dehydrated SIS were cut into sections of 1 mm thickness and mounted on aluminium stubs. Lyophilised samples were cut into 5 × 5mm sections and directly mounted on aluminium stubs using adhesive tabs. The stubs were then placed in a desiccator cabinet for at least 12 hours to ensure any acquired moisture

was sufficiently removed. All sections were then sputter coated with gold/palladium (Polaron E5000, Quorum Technology, UK). The samples were then analysed using scanning electron microscopes (JEOL 5410LV SEM, JEOL UK, UK and Philips XL 30 SFEG, Netherland).

2.2.8 DNA Quantification

To dry the non-lyophilised intact tissue samples these were first frozen and stored at -20°C. These were then placed in a freeze dryer for 6 h to obtain a dry-weight only sample. DNA extraction was carried out using DNeasy Blood & Tissue Kit 50 (Qiagen, Germany). The DNA was quantified using the Quant-iT™ DNA Assay Kit or Qubit® dsDNA HS Assay Kit (Invitrogen, USA), followed by a fluorescence plate reader (Fluoroskan Ascent, Thermo Scientific, USA) or the Qubit® Fluorometer (Invitrogen, USA), respectively.

2.2.9 Mechanical Testing

Test samples were cut into rectangular shapes of dimensions 8 - 14 mm in length and 5 - 8 mm in width, and tested in longitudinal and circumferential directions (relative to the axis of the small intestine). The ends of the samples were enclosed in wire gauze “clamps”, only slightly wider than the samples, to provide grip and stability. The uniaxial tensile testing was carried out using a dynamic mechanical analyser (DMA 7e, Perkin-Elmer Instruments, USA) into which the samples were clamped. The dimensions of the samples were entered into the software (Pyris) and the distance between the two clamps was taken as the length. The tensile test was run with an increasing force value of 500 mN m^{-1}. From the stress-strain graph produced the elastic modulus was then calculated as the gradient of the elastic

region of the curve (E = stress/strain). The processed SIS was rehydrated with deionised water for 30 minutes, prior to testing. Samples which slipped or failed near to the clamps were ignored.

2.2.10 Statistical Analysis

Assessment of the data showed that it did not fit normal distribution models and therefore non-parametric statistical analysis methods were used. The median was found to be a better measure of central tendency than the mean for this type of data and is used in all the mechanical analysis. The group sample data was compared for significant differences using Kruskal-Wallis non-parametric analysis which indicates the presence of significant statistical differences between individual groups. Further analysis was also carried out by post hoc pairwise analysis (Dunnett's Test). Normal distribution statistical testing was carried out using a 2-tailed student's t-test to a 95% confidence interval. All statistical significance tests were done using SPSS version 21 (IBM Corporation).

2.2.11 Cell culture

Primary human oesophageal smooth muscle cells (HESMC) (ScienCell Research Laboratories, Carlsbad, CA, USA) were used for the cellular assays. These cells were cultured in Dulbecco's modified Eagle medium (Gibco, Life Technologies, Paisley, UK) supplemented with 10% foetal bovine serum (Gibco) and 1% penicillin-streptomycin (Gibco) all further references to medium are this composition. The conditions for culture were at 37°C in air with 5% CO_2 and 95% relative humidity. Only cells from passages 3-6 were used for the assays.

2.2.12 Biocompatibility assay

A CellTiter 96 AQueous Non-Radioactive Cell Proliferation Assay (Promega, Southampton, UK) was used to measure the metabolic activity of HESMC's as an indication of biocompatibility, in accordance with ISO 10993 parts 5 and 12 (Appendix A-4) and the manufacturer's protocol. The HESMC's were seeded at a density of 100,000 cells/cm^2 on sections of PAA-12h, PAA-2hA, SDS/TX, SD/DN, uSIS, a commercial scaffold, and with tissue culture plastic (TCP) as a control. The commercial scaffold used in this case was Biodesign® (Cook Medical, UK) and was used to provide a potential alternative to TCP as a control. The sections of SIS were stabilised within the cell culture wells using well inserts (CellCrown, Scaffdex Ltd., Tampere, Finland). The inserts pulled the samples taut and suspend them within the 24-well plates. The cells were then seeded on the abluminal surface with the exception of the commercial scaffold which did not have a specified orientation. The scaffolds were all hydrated with 200 µl of medium approximately 30 minutes prior to seeding cell.

After 24 and 96 h incubation, medium was aspirated from the cells and replaced with six parts of medium and one part MTS solution, which consists of (3-(4,5-dimethylthiazol-2-yl)-5-(3-carboxymethoxyphenyl)-2-(4-sulfophenyl)-2H-tetrazolium) (MTS) and an electron coupling agent phenazine methosulfate. MTS is metabolised forming formazan in the mitochondria of living cells, the result of which is a colour change from yellow to brown that is broadly speaking indicative of cell number. After sufficient colour change was observed (usually after incubation for 1 - 1.5 h), absorbance was measured at 490 nm, with a reference wavelength of 630 nm using an absorbance plate reader (M200, Teccan, Männedorf / Switzerland). The metabolic activity of cells residing on each scaffold was normalised to the TCP control, specific to each time point. Between time-points, MTS-containing medium

was aspirated, the cells rinsed with PBS, and replaced with fresh cell culture medium.

2.3 - Results

2.3.1. Histology

Histological staining with H&E revealed the presence of visible and distinct nuclei in all samples (Figure 2.5), with the relative number of nuclei in the final samples being SDS/TX < PAA-12h < SD/DN < PAA-2hA < uSIS (Figure 2.10a). The numbers of visible nuclei per μm^2 were found to be far higher in the uSIS control and the PAA-2hA groups than those observed in the final stages of SDS/TX, SD/DN and PAA-12h. The SDS/TX group was observed to have the lowest number of histologically visible nuclei per μm^2 of visible tissue by quite a substantial margin. Staining with EVG (Elastic Van Gieson's stain) showed quite an even dispersal of black-stained elastin fibres throughout the intestinal tissue. The decellularisation process did not appear to result in any visible loss of elastin fibres by any of the protocols (Figure 2.6).

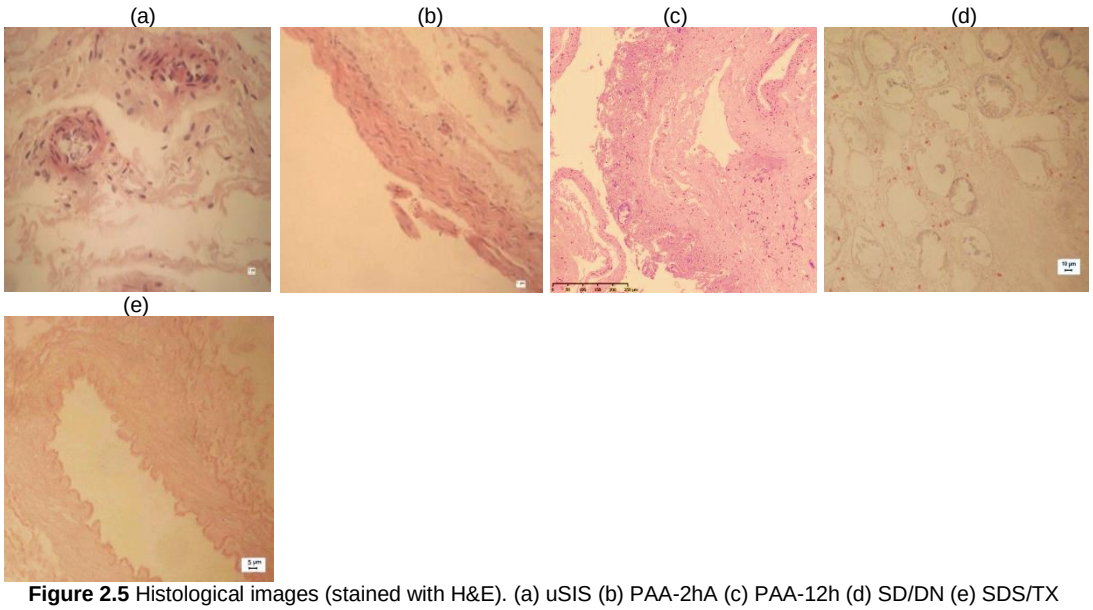

Figure 2.5 Histological images (stained with H&E). (a) uSIS (b) PAA-2hA (c) PAA-12h (d) SD/DN (e) SDS/TX

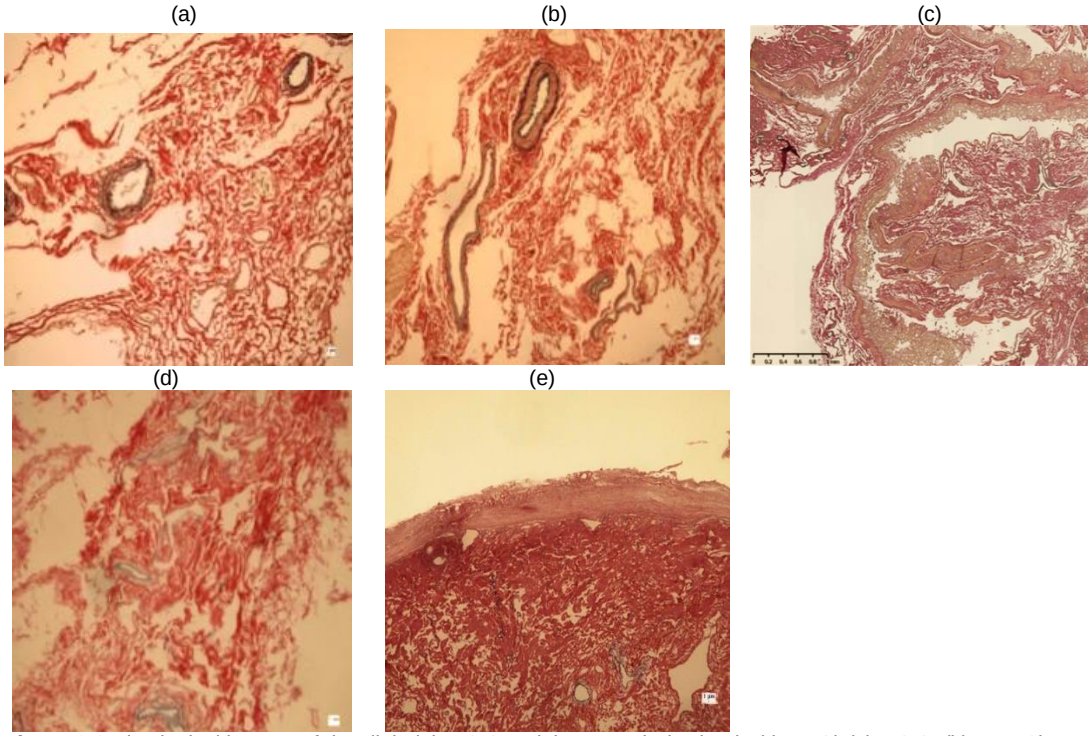

Figure 2.6 Histological images of decellularising SIS and the controls (stained with EVG) (a) uSIS (b) PAA-2hA (c) PAA-12h (d) SD/DN (e) SDS/TX

2.3.2 SEM

The use of SEM imaging did not reveal any visible differences between samples of the 5 groups (Figure 2.7). Additionally there were also no visible differences between samples taken from different time points during the longer multi-stage protocols (SDS/TX & SD/DN). The fibrous structure of the pre-processed SIS samples was clearly visible on some images (Figure 2.7d). The processed form of the SIS produced a characteristic sheet-like regular appearance (Figure 2.7h) in most samples with the exception of the processed PAA-12h, which showed a characteristic appearance with a more irregular and cracked surface with defects (Figure 2.7f and Figure 2.7g).

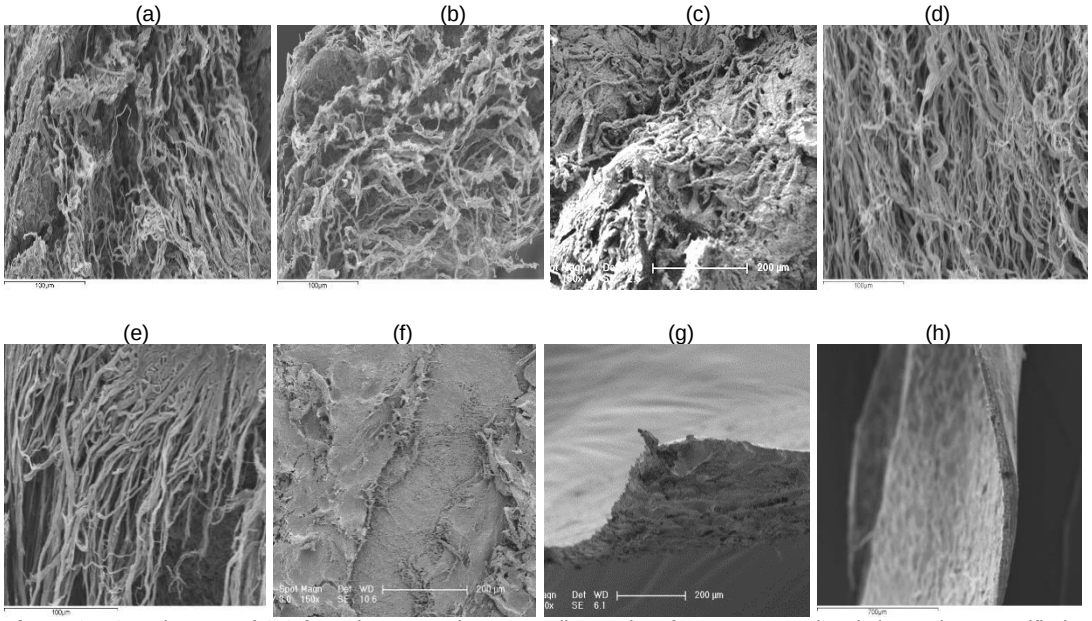

Figure 2.7 SEM images of SIS from the protocol groups. All are taken from cross-sectional view unless specified (a) uSIS (b) PAA-2hA (c)) PAA-12h (d) SD/DNase (e) SDS/TX (f) Luminal view of processed PAA-12h (g) Processed PAA-12 h (h) Processed SD/DNase

2.3.3 Biocompatibility Assay

The results of the biocompatibility assay were expressed in terms of metabolic activity and are represented as a percentage of the TCP control for that time point (Figure 2.8). At day 1 (24 h) the SIS specimens from the groups PAA-2hA and PAA-12h were found to have metabolic activity levels which were similar to the control (TCP), while the SD/DN and the commercial SIS group were found to be elevated to roughly 1.5 and 2 times, respectively, that of the control. The untreated SIS (uSIS) was found to have highly elevated metabolic activity with the average value approximately 4 times that of the control group (TCP) indicating a very rapid increase in the metabolic activity of the cells. The SDS/TX group conversely was found to have significantly lower values than the control and all other samples, indicating lower biocompatibility.

At day 4 (96 h) all specimens showed an increase in metabolic activity from the levels at day 1, including the control group. The SDS/TX specimens still induced very low cellular activity levels and at day 4 the number remained lower than all other groups at day 1, potentially indicating on-going cytotoxicity. Both PAA groups performed similarly to the control indicating a reasonable degree of biocompatibility. At day 4 the SD/DN, commercial SIS and the uSIS all showed numbers at least twice that of the relative control value. While the uSIS finished with the highest activity level there was also a decrease relative to the control, indicating a levelling off after the sudden rapid increase in the first 24 h.

Further work was also carried out as shown in Figure 2.12 which will be discusses in Section 2.4 (Discussion).

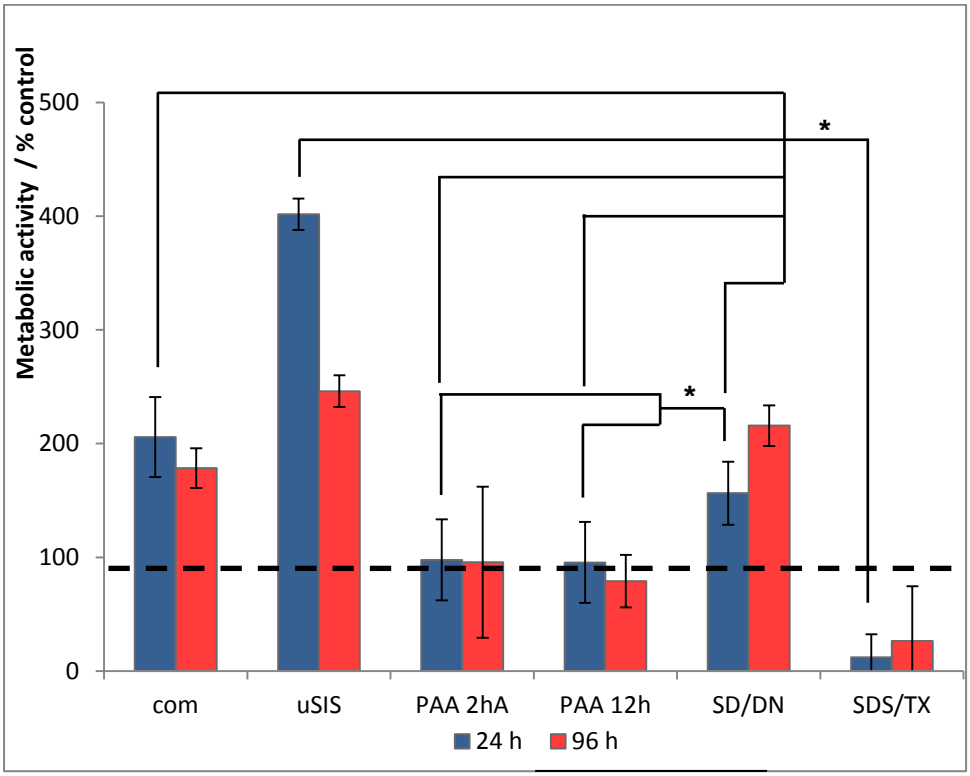

Figure 2.8 Metabolic activity of the cells (HESMC) cultured on the scaffold groups carried out with an MTS assay. The metabolic activity was normalised in relation to the control (tissue culture plastic-TCP with the same surface area) and is expressed here as a percentage of the control, specific to each time point. The dashed line indicates the metabolic activity of the TCP control at each time point. Important values differing significantly from each other are denoted by *; $p < 0.05$.

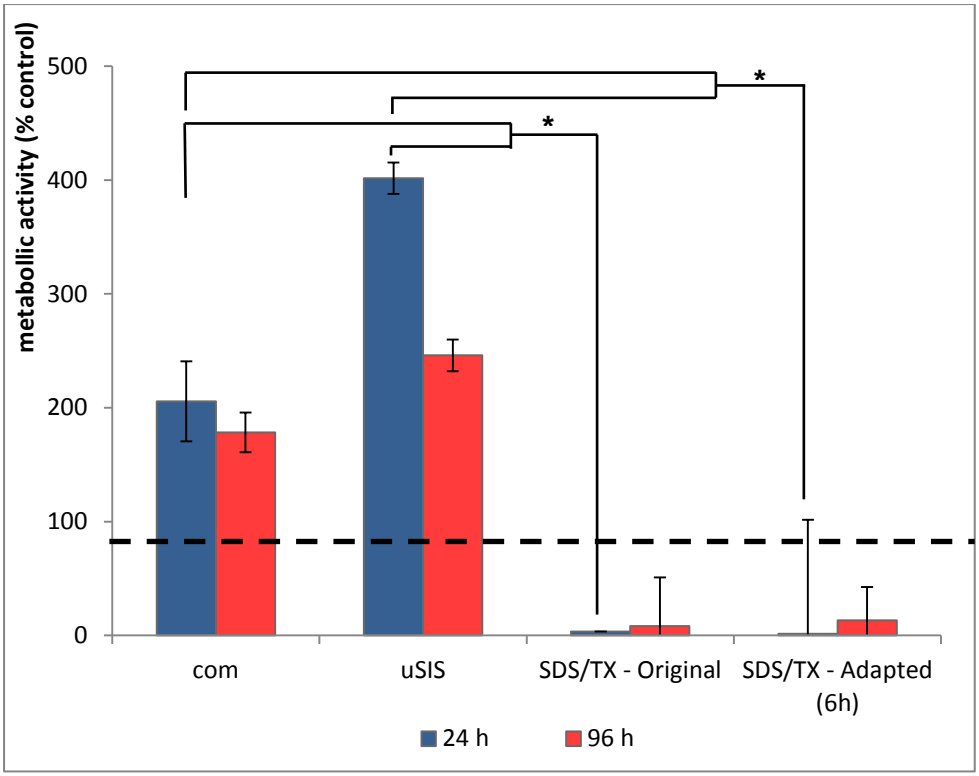

Figure 2.9 Metabolic activity of cells (HESMC) cultured on the SDS/TX scaffolds showing the difference between the original SDS/TX protocol and an adapted protocol with an extended washing regime (increased to 6h and with a continue flow of fresh deionised water). The metabolic activity was normalised in relation to the control (tissue culture plastic-TCP with the same surface area) and is expressed here as a percentage of the control, specific to each time point. The commercial scaffold was added as a reference point for biocompatibility. The dashed line indicates the metabolic activity of the TCP control at each time point. Important values differing significantly from each other are denoted by *; $p < 0.05$.

2.3.4 DNA Quantification

DNA quantification revealed that the SDS/TX group produced the lowest levels of DNA following the completed decellularisation process (Figure 2.10b). SD/DN also proved to be effective at decellularisation producing DNA levels well below that found with the control uSIS. The levels of DNA present in the PAA-2hA samples were not significantly different to that of the control. The level of DNA present in the PAA-12h were also not significantly different from the control but were lower than those observed with the PAA-2hA group.

What was also observed that SD/DN protocol produced no appreciable difference in the DNA quantity detected between time-points 12 h and the final stage (16 h), indicating that the introduction of the enzyme DNase did not appear to affect the quantity of the DNA remaining in the SIS.

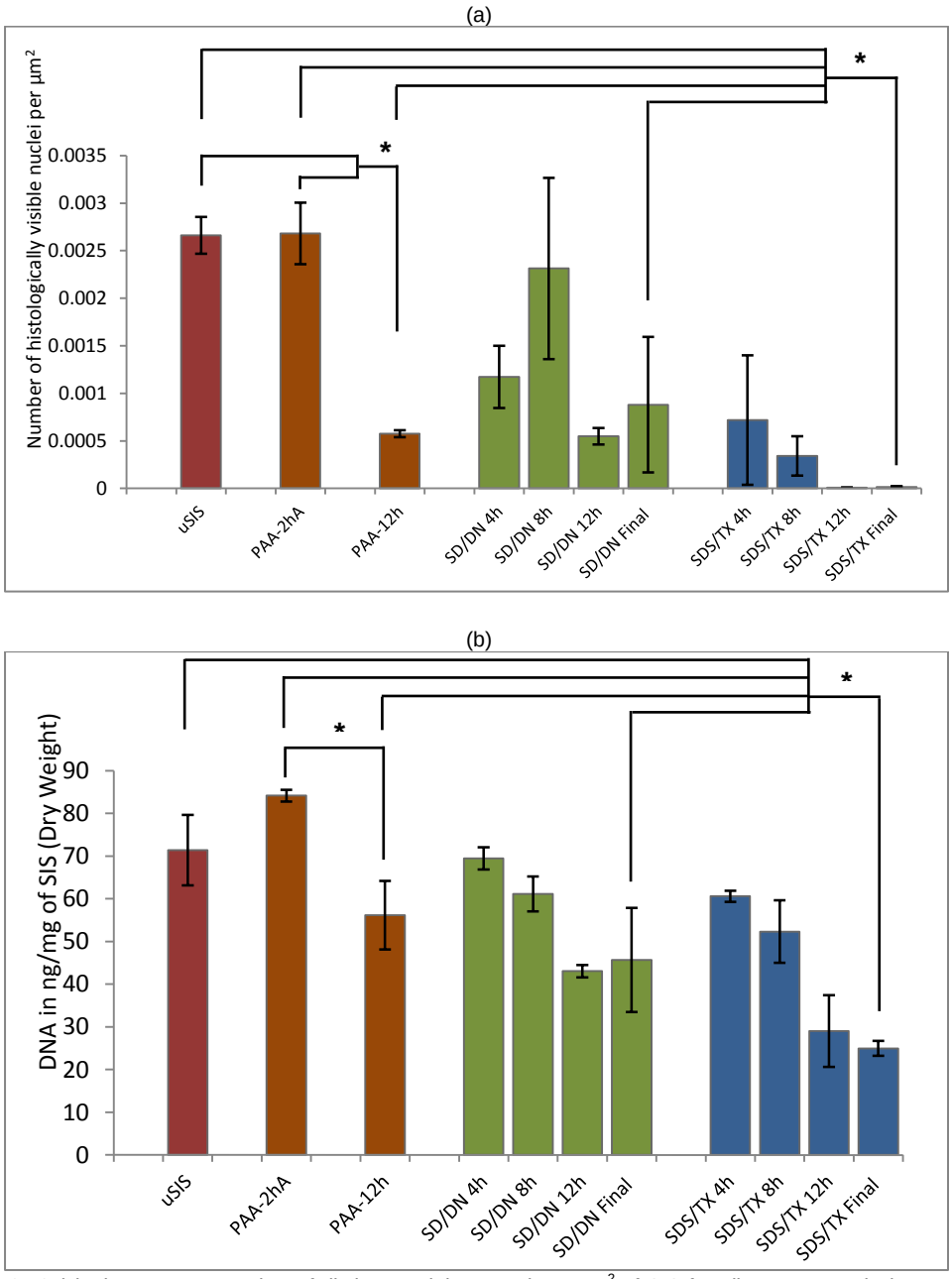

Figure 2.10 (a) The average number of distinct nuclei counted per µm^2 of SIS for all groups. Analysis was carried out on images taken of H&E stained histological sections, with random sites chosen and the nuclei counted using software tools (Image J) (*n* = 10-20). All counts were then averaged together for each stage. Error bars are standard error. (b) DNA quantification values (ng/mg of dry weight) for the all three protocols and the control with each column representing the concentration of DNA at various time-points in the decellularising protocols including the processed SIS (*n* = 4). Error bars are the standard error. Important values differing significantly from each other are denoted by *; $p < 0.05$.

2.3.5 Mechanical Analysis

In longitudinal testing the elastic modulus values were not found to vary significantly between the specimens with the exception of the PAA-12h where values in both directions were found to be high (the longitudinal value being exceptionally high when compared to the other groups) (Figure 2.11a). What was also visually observed is that following decellularisation that the SIS produced from the PAA-12h protocol was physically different to all other SIS samples when handled. The SIS in this group took on a more ridged and less pliable texture not observed in any of the other groups.

Lyophilisation of the all the samples did not affect the elastic modulus values with the exceptions being the PAA-12h group, which fell dramatically and the SDS/TX which when compared longitudinally with the pre-lyophilised form showed a significant increase.

The yield stress was considered an important parameter as it indicates the stress at which the elastic behaviour of the tissue is compromised. The yield stress values showed no significant change between the specimens with the exception of the PAA-12h sample, which again, was found to be significantly larger particularly in the longitudinal direction but also circumferentially when compared to other pre-lyophilised SIS samples (Figure 2.11b). The lyophilisation here was found to cause slight increases in all samples, with the increase in SDS/TX being quite substantial, and the exception being the PAA-12h which fell in longitudinal testing. Circumferentially the only significant increase was found in the PAA-12h specimens which showed, as mentioned previously, substantial increase in the yield strain value. Again here it should be noted PAA-12h SIS produced greatly different behaviour when compared to the other samples.

The failure strain was calculated as being the strain at the point of failure of the test samples during tensile testing. In the longitudinal testing the values for the specimens from SDS/TX, SD/DN and PAA-12h were all found to be similar to the control uSIS or the PAA-2hA (Figure 2.11c) It was also noted that the value for PAA-12h was found to be very low (39.29%) with very low error indicating that while the PAA-12h was very stiff and gave high yield strength values, it had a greatly reduced elasticity when compared to the control uSIS or the other samples tested. In circumferential testing only the PAA-12h protocol failure strain value was found to be significantly lower than that of the control uSIS. Following lyophilisation, the PAA-12h SIS was observed to change in failure strain behaviour with the value increasing following the processing.

The results from the 12 h detergent decellularisation stages (time points 4h, 8h, and 12h) in both the SD/TX and SD/DN (Figure 2.10) do not appear to indicate any quantifiable time-dependant changes in the mechanical properties that occurred during the process.

(a)

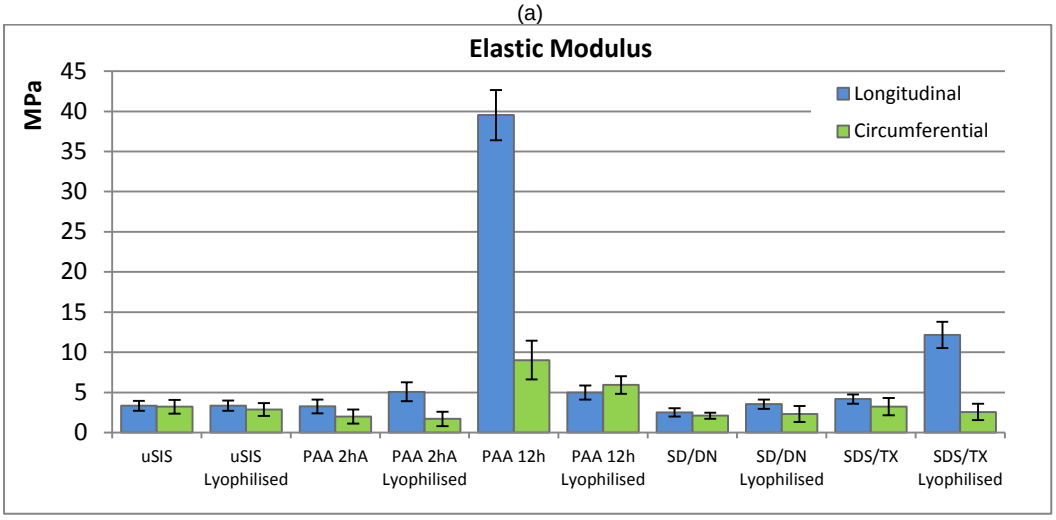

(b)

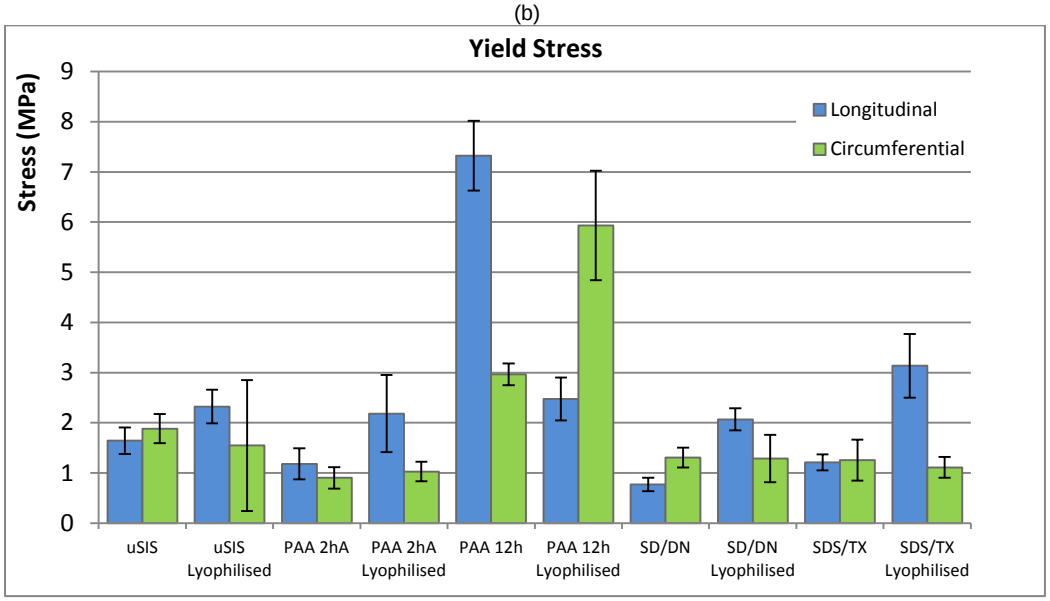

(c)

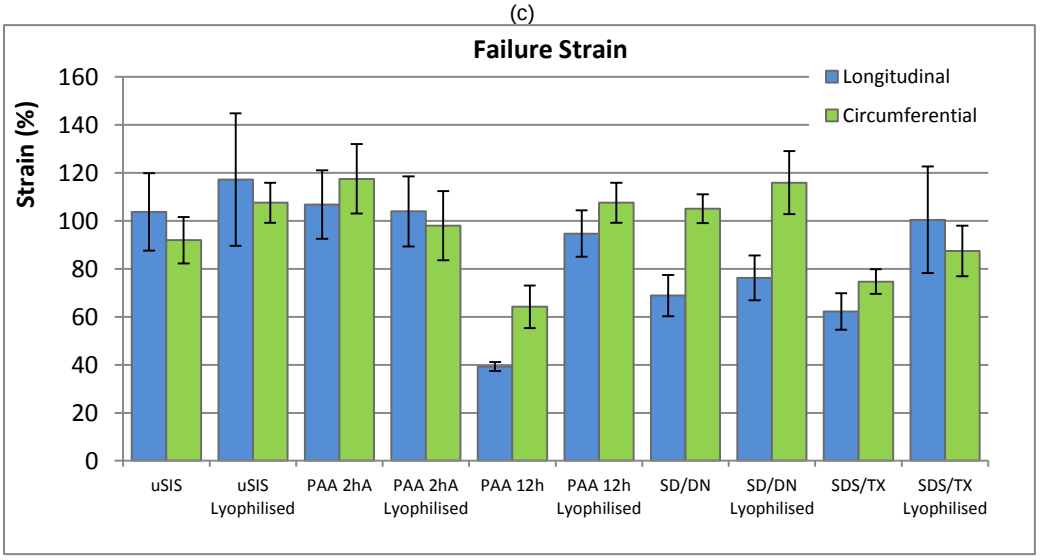

Figure 2.11 Mechanical testing data from the tensile testing of the SIS (a) Elastic modulus values (MPa) for the all final stage SIS along with the lyophilised forms (n = 12) (b) Yield stress values (MPa) for the all final stage SIS along with the lyophilised forms (n = 12) (c) Failure strain values (%)for the all final stage SIS along with the lyophilised form (n = 12). Error bars shown are the standard error. Statistical analysis was done non-parametrically and discussed in the results sections.

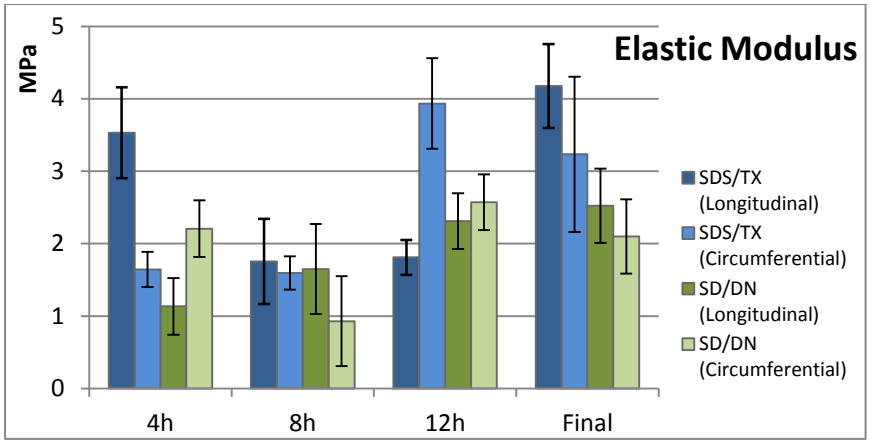

(b)

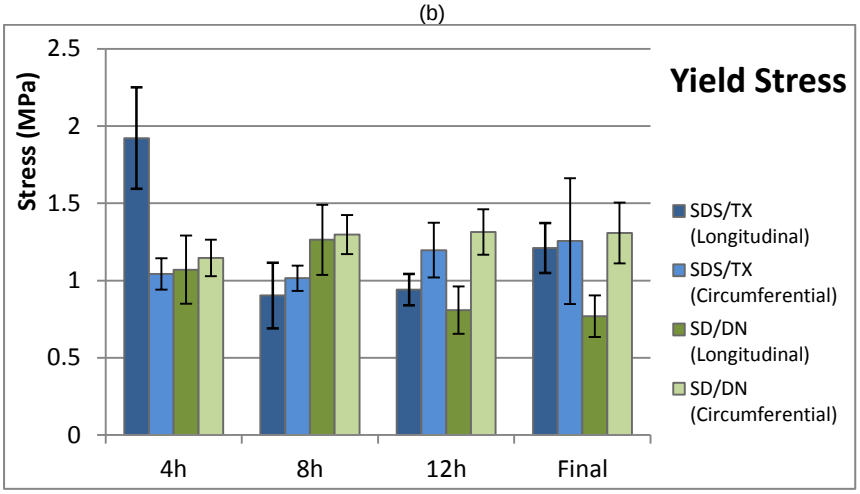

(c)

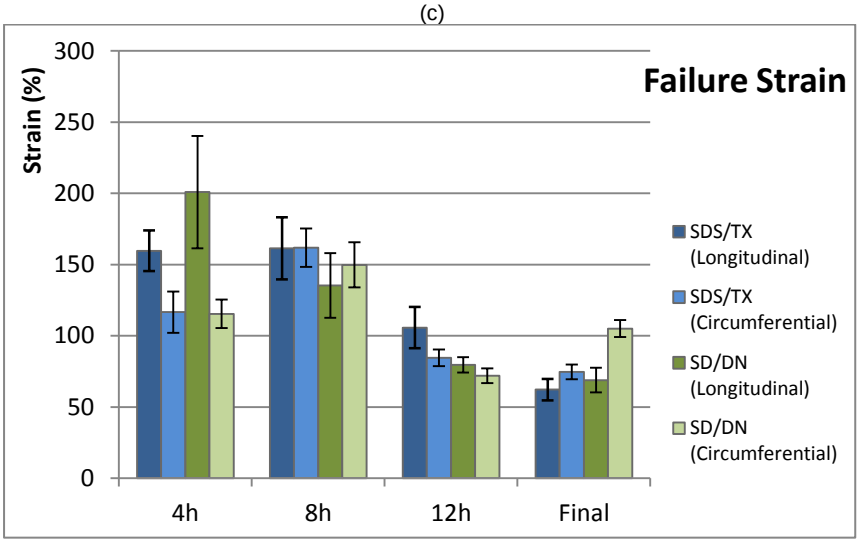

Figure 2.12 Mechanical data from tensile testing SIS from the two detergent-based protocols (SDS/TX and SD/DN) taken from different time points during the decellularisation process. The three analysis criteria being (a) elastic modulus (MPa) (b) yield stress (MPa) and (c) failure strain. The error bars are the standard error. Statistical analysis was done non-parametrically and discussed in the results sections.

2.4 - Discussion

2.4.1 General Discussion

The general aim of this study was to evaluate commonly used decellularisation protocols to create tubular SIS which has both a sufficient level of decellularisation to function as a tissue engineering scaffold and possessing mechanical properties either minimally affected or ideally unaffected by the decellularisation process. The perfusion method has not yet been applied to SIS previously and was hypothesised to be suitable on account of the shape of the tubular SIS produced in this work.

The data from histological and quantitative DNA analysis show that the most effective protocol was the SDS/TX. The SIS produced by this method largely achieved both the criteria highlight by Crapo *et al.* of being below the 50 ng dsDNA per mg of ECM (dry weight) and with no histologically visible nuclei. While it is understood that no work has been carried out that sufficiently evaluates these criteria as indicators of sufficient decellularisation, it does stand to reason that minimising the amount of foreign DNA present in any type of graft tissue would likely increase the chance of successful implantation due to a reduced immune response. It was also found that both detergent-based perfusion methods produced SIS with DNA below the 50 ng dsDNA per mg of ECM (dry weight) threshold. Finally, both methods using peracetic acid did not adequately decellularise SIS though it was observed that there was a significant difference between the two. The question arises as to whether this is due to the effectiveness of the reagents over the time duration of the protocols, or as a result of the physical process of the protocols themselves.

When the effectiveness of the reagents is considered there is evidence to suggest that, by a number of varying criteria, they can all be considered effective at

decellularisation. When applied to sheet SIS peracetic acid is known to be an effective reagent for decellularisation. SDS and Triton X-100 have also been shown to have the capacity to decellularise SIS individually as demonstrated by Oliveira *et al.* where SIS was decellularised to levels below 50 ng dsDNA per mg using concentrations as low as 0.1% over a 24 h period under agitation (Oliveira, Garzon *et al.* 2013). SD while not having been used on SIS has been shown to decellularise the small intestine in a rat model (Totonelli, Maghsoudlou *et al.* 2012). Consequently all three agents are likely to be effective at decellularising SIS, therefore the failure of the SIS to decellularise in this study particularly using PAA is likely not to be entirely due to the effectiveness of the reagent and more likely to be due to the decellularisation methods or the shape and structure of the tissue.

The length of time the protocols are run is another important factor. The level of DNA present in the detergent based protocols (Figure 2.10b) can be seen to steadily decrease over time which undoubtedly shows that time is a vital component of the decellularisation process. Time has also been shown to effect the process of peracetic acid decellularisation and halving the decellularisation time 2h to 1 h has been shown to cause elevated levels of DNA in sheet SIS (Keane, Londono *et al.* 2012). In addition to this the increased effectiveness of the PAA-12h perfusion protocol (in comparison to the PAA-2hA group) does indicate that time likely improved the effectiveness of peracetic acid decellularisation ; however while the amount of DNA was slightly reduced the number of visible nuclei still suggested a less then optimum level of decellularisation (Figure 2.5c).

The final difference with between the protocols was the decellularisation arrangements themselves. As mentioned previously there are no examples of SIS being decellularised using a perfusion arrangement and no work where intact tubular SIS has been consistently studied. Perfusion decellularisation has been previously used on rat small intestine using 4% SD/DNase and this was found to be

an effective means of decellularisation however analysis was limited to histological means (Maghsoudlou, Totonelli *et al.* 2013). Multi-organ decellularisation of rat tissues using SDS perfusion have also been shown to be effective at decellularisation (Park and Woo 2012). In the case of this work, however, it is unclear whether the SIS was actually undergoing true perfusion i.e. though the SIS itself, or creating a flow through the lumen. SIS is a largely impermeable tissue and given the low flow rates used it is highly unlikely that the decellularisation agents perfused through thickness of the tissue. The combination of a constant flow of decellularising agents over the luminal surface of the SIS in addition to the circulating agents on the outer surface have likely produced an environment where suitable decellularisation can occur simultaneously on both surfaces and consequently provide a working method for decellularising tubular SIS.

One of the major observations in the mechanical testing was the extreme variations in the data produced by the PAA-12h protocol. The large increases in the elastic modulus and the yield stress values were also accompanied by a drastic drop in the failure strain to the lowest of all SIS samples at just below 40% (Figure 2.11). This is indicative of SIS tissue which has lost a high degree of elasticity when compared to the control and as a result this SIS can be reasonably excluded from consideration. Furthermore, the human oesophagus also extended by up to 50% under normal conditions and any material which has a failure strain below this level risks failing and compromising the integrity of the construct (Yang, Fung *et al.* 2006; Tan, Chua *et al.* 2012). The SIS produced by peracetic under agitation (PAA-2hA) did appear to match the control, and the SIS from the detergent based protocols, in its mechanical behaviour; however, as described earlier it was poorly decellularised and therefore not suitable as a scaffold. The short exposure of the SIS to the peracetic is what is likely the difference between the two PAA protocols. Currently there does not appear to be any definitive consensus on the effects of individual

decellularisation agents on the mechanical properties of many of the commonly used decellularised tissues (Crapo and Gilbert 2011). It has been shown that some acids when used on ECM can alter the mechanical properties. An example of this is acetic acid which has been shown to alter the stress-strain behaviour of bovine pericardium (Maghsoudlou, Totonelli *et al.* 2013). Peracetic acid has not been reported to alter the mechanical properties of SIS though as in the case here the time of exposures is commonly limited to 2 h as opposed to the 12 h used in this instance (Gilbert, Sellaro *et al.* 2006; Park and Woo 2012).

The two detergent-based protocols also produced decellularised SIS which was not adversely mechanically affected by the decellularisation process according to the three criteria they were evaluated by. Of the two protocols SDS/TX did produce SIS with high values for all three criteria, particularly in terms of the lyophilised form. It should be mentioned that detergents have also been known to disrupt the ECM matrix however this was not observed in this study (Crapo and Gilbert 2011). A possible reason for this is that both these protocol were both adapted in this study to reflect the nature of the SIS, which only consists of a thin layer of ECM and contrasts with intact organs, and were therefore drastically shortened. In the case of other tissues, these profusion protocols are run for a large number of repeated cycles and usually over a number of days. A variation of the SD/DNase protocol has been used to decellularise a human donor trachea, a process taking multiple cycles, though it was found that between cycles 18 and 22 the mechanical properties were so negatively impacted as to render the trachea ineffective (Jungebluth, Go *et al.* 2009). Consequently the limited exposure of the detergents to the tissue in this work could be a possible reason for the preservation of the mechanical properties.

In the mechanical testing some inconsistencies were observed between the longitudinal and circumferential tensile data. This was attributed to the native anisotropy found in SIS, and which contains a high degree of complexity (Orberg,

Baer *et al.* 1983). If both axes are simultaneously secured for example a force applied along one axis would directly result in changes in the stress strain behaviour along the other axis. This behaviour was also found to be asymmetric, with the application of a set forced along the longitudinal, resulting in changes to the circumferential stress–strain behaviour which were more pronounced than if the axes were reversed (Sacks and Gloeckner 1999). This anisotropy has been explained by the angular distribution of the fibres within the ECM of the submucosal layer (Lanir 1979). These fibres have been described as existing in two distinct populations of fibres orientated at approximately ±30° (Orberg, Baer *et al.* 1983; Sacks and Gloeckner 1999). Sacks *et al.* found the ±30° orientated layers as being part of local subdivisions within the tissue which will can vary along its length (Sacks and Gloeckner 1999). This is also reinforced by the description of the fibres on a macro scale being aligned in a spiral which can be considered conducive to peristalsis (He and Callanan 2012).

The vacuum-compression and lyophilisation of the SIS were also found to alter mechanical properties of the material. The exact mechanism for these changes was not entirely clear though differences between the longitudinal and circumferential directions can be explained partially terms of the properties of the native tissue as mentioned previously. What can be observed from the data in Figure 2.11 is that in the longitudinal direction there were particular changes in terms of the failure strain for all samples. A possible mechanism for this is that the vacuum compression of the SIS results in an increase level of interaction between the ECM components particularly the collagen fibres present and thereby altering the mechanical properties. It should be noted that following rehydration the processed samples did not expand to the same thickness as pre-processed SIS samples. In addition to changes in the mechanical properties, it has been shown that processing decellularised SIS can cause a change to the in vivo properties. Vacuum pressed

SIS has been compared to lyophilised SIS and the vacuum pressed SIS was found to be more resistant to enzymatic degradation and with a slower rate at which angiogenesis occurred. These affects were attributed to poor cellular infiltration. The compressed SIS test was found to have a far lower degree of porosity and still retained a compressed appearance after rehydration (Janis, Johnson *et al.* 2011).

The biocompatibility of any scaffold is an important consideration for their potential use. The data here showed clear differences between decellularisation protocols. While both peracetic acid protocols demonstrated a good degree of biocompatibility, cells cultured on the SDS/TX had lower levels of metabolic activity than all other samples. While mechanically, and in terms of the decellularisation, the SIS produced from this method was found to be most ideal, this level of biocompatibility makes it highly unsuitable. Furthermore, follow up work (Figure 2.9) where SDS/TX was created and then washed for 6 h using an improved washing method (Appendix A-2) failed to significantly improve the biocompatibility. This protocol does involve the use of two separate detergents which have each been shown to be cytotoxic i.e. SDS and Triton X-100 and with this increased exposure there is also an increased likelihood of some detergent being retained within the SIS itself. As both the reagents have been used successfully in decellularisation it is probable that a far longer washing protocol would eventually achieve adequate removal though it would require additional work to ascertain the balance between the time taken to remove the reagents and point at which the mechanical properties of the material would begin to deteriorate.

SD is also a cytotoxic detergent and it should be noted that in the SD/DN protocol, had the best biocompatibility of all the decellularised SIS produced. The SIS here was also exposed to a 4 h rinse with a salt solution (containing the DNase) following detergent exposure and this could potentially have aided in removing the detergent sufficiently from the SIS to produce the observed results. While the SIS produced

with the SD/DN protocol had very high biocompatibility (higher than the commercial SIS) the presence of the DNase enzyme, while likely to have minimal effects on cell growth *in vitro*, and may have more negative impact if applied *in vivo* and this remained a concerned.

The uSIS demonstrated a high degree of biocompatibility which may be attributed to the fact the internal structure was likely preserved and the tissue components all entirely retained. An intact ECM, in addition to any remaining growth factors, could potentially stimulate cellular activity. While *in vitro* testing of this scaffold indicated acceptable biocompatibility it will, of course, be unsuitable for *in vivo* applications due to the potential for a severe immune response.

2.4.2 Conclusion

In conclusion, the conventional peracetic acid/agitation method for SIS decellularisation is not suitable for SIS when made in intact tubular form. The primary reason for this is the insufficient level of decellularisation. Peracetic acid when used over 12 h with the perfusion method was also found to be an unsuitable owing to a drastic drop in the elasticity of the tissue following decellularisation, in addition to an inadequate level of decellularisation. The two detergent/perfusion protocols were found not only to provide adequate decellularisation of the SIS, but in several instances were found to possess less adversely affected mechanical properties over the SIS produced from peracetic acid (or the control following processing). There are, however, limitations associated with both methods. It was concluded that SDS/TX was the most suitable protocol for producing scaffolds on account of the highest level of decellularisation and therefore the least risk of immune response and/or graft rejection, the best mechanical properties following the processing stage, and having the added benefit of the protocol lacking enzymes

as used in SD/DNase which may potentially increase the risk of rejection, however it was found to have poor biocompatibility. Also as shown in Figure 2.12, the biocompatibility of the scaffold could not be improved even with increasing the washing time to 6 h with an improved washing protocol. Consequently whilst there may be some merit in researching improved wash cycles, it was deemed that researching longer time periods would not be practical given that there was no improvement observed with a single increase. It was observed that whilst SD/DN may show acceptable *in vitro* biocompatibility and suitable mechanical properties it does have the limitation of using the DNase enzyme which may be unsuitable for clinical application however this shown to not affect the level of decellularisation of the SIS during the protocol. In conclusion SIS produced using SD with the elimination DNase enzyme stage was chosen as the ideal basis for all further work.

3. Electrospinning

3.1 - Introduction

As discussed in Chapter 1, electrospinning is a useful method for the preparation of scaffolds and therefore tissue engineering and related processes. In this chapter it has been attempted to overcome some of the inherent disadvantages of electrospun scaffolds, along with some of the disadvantages of extracellular materials, by combining the two materials together in a single hybrid scaffold.

If these two materials are to be successfully combined one of the key hurdles which needs to be overcome is the issue of attachment between the two materials. With high surface area and an inherent flexibility, electrospun fibres have been observed to have a degree of adhesiveness (Bye, Wang *et al.* 2012) . A similar objective was attempted by Horst *et al.* where urinary bladder matrix (UBM) was combined with electrospun PLGA fibres. In that work the UBM was in the form of a flat sheet and an issue of attachment was identified. Attempts were made to improve this with the outcome being that the UBM was maintained in a wet state during spinning (Horst, Madduri *et al.* 2013). This issue would need to be considered here and any problems overcome if a suitable hybrid scaffold was to be created for potential use in oesophageal tissue engineering.

The aims of this chapter are for the establishment of protocol 1) a viable layer of electrospun polymer and 2) to produce suitable attachment between the tubular SIS decellularised scaffold produced in Chapter 2 and the layer of electrospun polymer.

3.2 - Materials and Methods

3.2.1 SIS preparation

3.2.1.1 SIS Isolation

The SIS was prepared as described in Chapter 2. Briefly, the jejunum/ileum samples were cut into lengths of 20 cm, and cut and prepared as described previously. Following preparation the SIS was then carefully washed twice in deionised water for 5 minutes. The SIS was then stored in PBS (phosphate buffered saline : 0.01 M phosphate buffer 0.0027 M potassium chloride and 0.137 M sodium chloride, pH 7.4, at 25 °C).

3.2.1.2 Decellularisation

The initial SIS used in this work was decellularised by the perfusion method described in Section 2.2.2, and using the protocol SDS/TX (Sodium Dodecyl Sulfate & Triton X-100) described in Section 2.2.2.1. In this protocol each container was filled with 350 ml of 1% solution of SDS (Sigma-Aldrich Company Ltd., Dorset, UK), then the pump was run at 500 ml h^{-1} for 12 h at room temperature. The SIS was removed and thoroughly rinsed with deionised water, followed by a perfusion wash for 15 minutes with deionised water. The samples were then perfused with 350 ml of 1% Triton X-100 (v/v) for 30 minutes, rinsed, and then perfused with deionised water for 15 minutes. The SIS was then washed twice in deionised water as described previously and stored at 4 °C in PBS.

3.2.1.3 Post Decellularisation Processing – Initial Method

The SIS sections were stretched over 1.9 cm diameter (designated by the manufacturer as 3/4 inch) porous polyethylene tubing (60 µm pores) (Porex Corporation, Fairburn, United States). These samples were vacuum-dried in sealed

sterile specimen bags and placed under low vacuum conditions (approximately 10 mbar) for 12 h to compress and dry the samples. The dried SIS samples were subsequently lyophilised by immersing in liquid nitrogen for 1 minute and then placed into a vacuum freeze-drier (Heto Dry Winner) for 12h.

3.2.1.4 - Post Decellularisation Processing – Altered Method

As a results of changes made to the method as a results of the data described in Section 3.3.2.5 changes were made to the SIS producing method and the porous tubes were changed to 2.54 cm diameter (described as 1 inch) porous polyethylene tubing (60 µm pores) (Porex Corporation, Fairburn, United States). The differences between the two sizes are shown in Figures 3.1a & b.

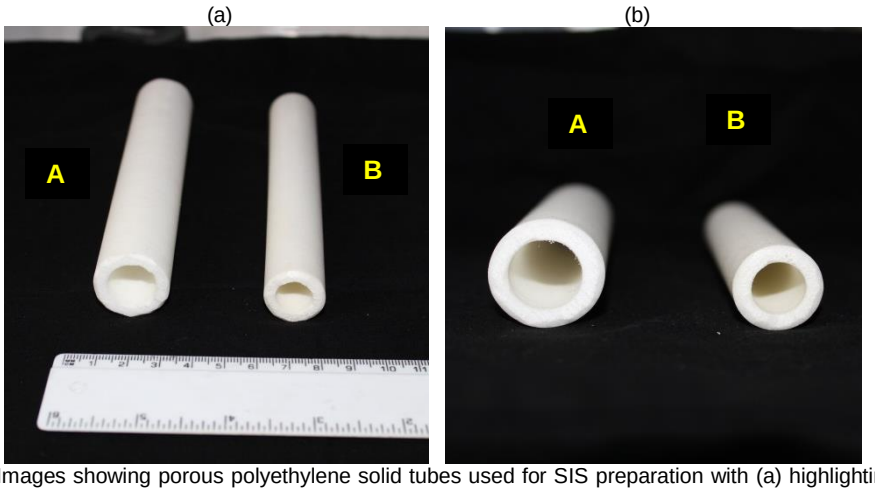

Figure 3.1 Images showing porous polyethylene solid tubes used for SIS preparation with (a) highlighting the size difference and (b) the cross-section. In both images “A” represents the new 2.54 cm diameter tube and “B” the old 1.9 cm diameter tube.

3.2.2 Electrospinning

3.2.2.1 Arrangement 1 (Series 1)

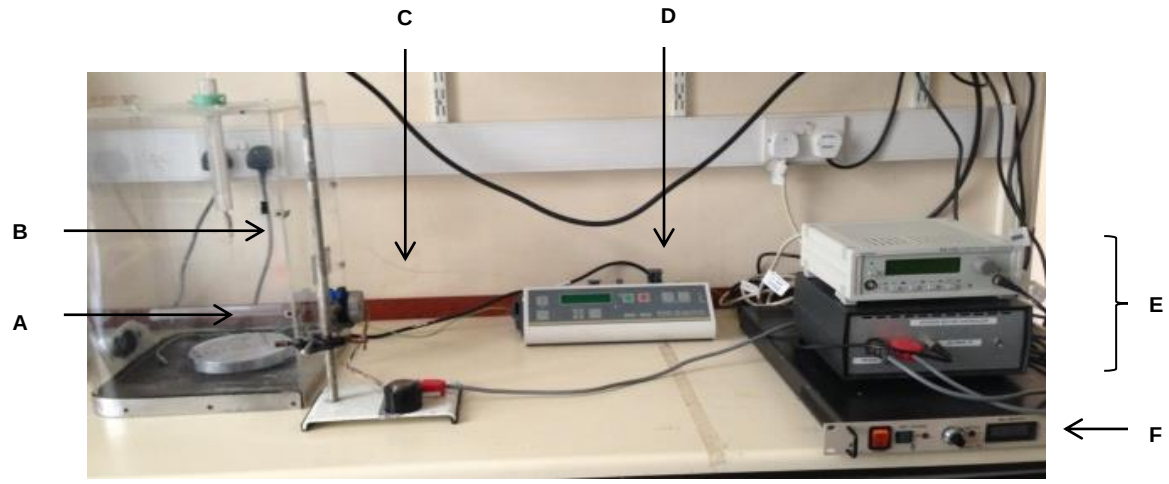

Figure 3.2 Electrospinning arrangement used in Series 1. A) Mandrel B) Needle and power connector C) Step motor D) Syringe Pump E) Motor controller and switch F) Power Source

The basic arrangement was set up as shown in the Figure 3.2. The needle used was an 18 Gauge (0.838 mm) diameter. The tip of the needle was ground level using hand-held power tools and then smoothed using sand paper. The needle was suspended in a fan-ventilated acrylic box of dimensions 45 × 25 × 25 cm, as seen in Figure 3.1. Tubing made of polytetrafluoroethylene (PTFE) tubing was used to connect the needle to a 10 ml syringe, which was then placed in a Graseby 3150 syringe pump (Graseby Dynamcs, Smiths Detection Group Plc, Watford, UK). The needle was connected to a high voltage power supply (Glassman Europe Limited, Bramley, UK) which is able to generate positive DC voltages up to 30 kV. Initial work used a grounded stainless steel collection platform was then placed below the needle with an adjustable height to allow for a variable collection distance. The fibres created were collected on glass slides placed over the collection plate or onto aluminium foil used to cover the collection plate. Later work the collection of the fibres took place on a rotating mandrel which was connected to a step motor. The speed of the mandrel was controlled through the use of a controller and a custom made switch. As there was very little torque required the step motor was allowed to

function as a uniphase motor with the controller providing a wave form signal for drive. The frequency of the wave form was used to equate the rotational speed of the mandrel. The mandrel was covered in aluminium foil and was earthed through the use of a ring-shaped rolling contact.

3.2.2.2 Protocol 1 (Series 1)

The polymer which was selected for Series was poly-Ɛ-caprolactone (PCL) (Sigma, UK). As mentioned in Section 1.4.2.6, the polymer was selected because properties include toughness and flexibility in addition to having a slow degradation rate which was particularly relevant given the properties required of the scaffold in line with the objectives of this work. In addition to this the electrospinning work using this polymer is extensive. The solution was prepared by dissolving the PCL granules in the liquid dichloromethane (DCM) (Sigma, UK). The solution was then mechanically stirred for at least 3 hours. The complete dissolution of the granules into the solvent was carefully confirmed by visual inspection prior to usage. The polymer solution was then stored at 8°C. The polymer solution was returned to room temperature prior to use. The polymer (PCL) was made into a variety of concentrations; 10%, 15%, 20% with the concentrations being weight by volume (w/v).

For the actual spinning process involved cutting tubular SIS into lengths of 3.5 cm in length. These lengths were then secured to the mandrel using a small quantity of adhesive tape, the tape was limited to the final 0.5 cm which would then be cut away and discarded at the end of the process, leaving a 3 cm length free of adhesive and the focus of the spin-coating. The PCL solution was prepared to the concentrations mentioned earlier. Electrospinning was carried out with a polymer solution flow rate of 15 ml h^{-1}, with voltage at 20 kV and a height of 15 cm. The spinning was conducted for 15 minutes for each sample (5 m for each cm of SIS) and the control speed was 540 rpm. The mandrel was advanced at an increment of 1 cm every 5 m. Samples were creating at various mandrel rotational speeds.

Vacuum drying was used to remove any excess solvent using a vacuum freeze-drier (Heto Dry Winner) and they were then stored in sterile 50 ml falcon tubes at room temperature.

For the purposes of attachment analysis the starting condition of the SIS was varied and the SIS was wetted using a spray bottle of deionised waster either initially or repeatedly while stopping the electrospinning to keep the SIS constantly wet, depending on the variable tested. The SIS was also tested by dripping acetone over the surface in a further variable.

The speed of the mandrel was also varied to analyse whether the speed of rotation affected the alignment of the fibres. The speeds used were 540, 1260, 1440, 1620, 1800 rpm. A list of the key variables is in Table B1 (Appendix B-3).

3.2.2.3 Arrangement 2 (Series 2)

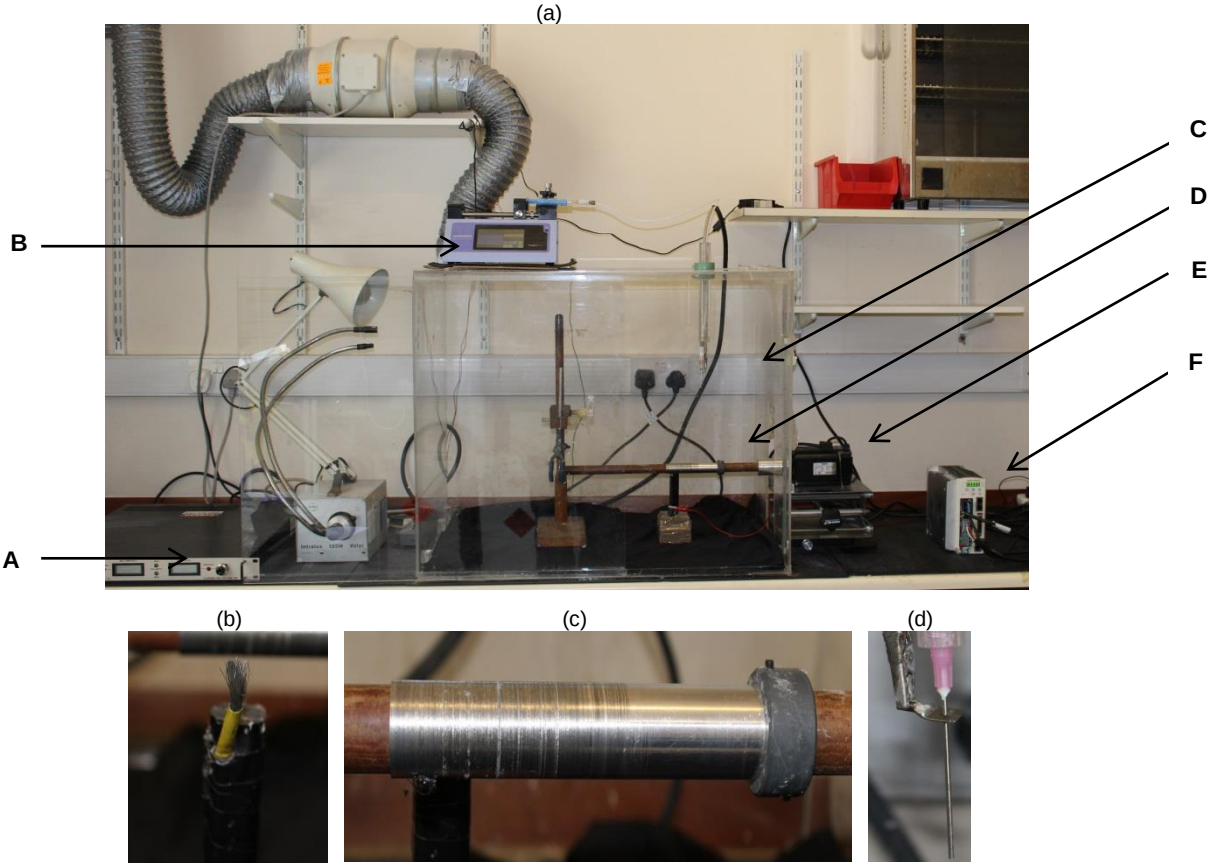

Figure 3.3 (a) Electrospinning arrangement used in Series 2: A) Power Source, B) Syringe Pump, C) Needle and power connector, D) Mandrel, E) Servo motor, F)Motor controller. (b) Brush ground contact (c) Custom collector (d) Needle and power arrangement.

The basic arrangement for electrospinning were kept the same, however a number of changes were made to improve the process by solving particular challenges in addition to other changes which were general improvements (Figure 3.3). In this arrangement the polymer solution was placed in rubberless 10 ml syringes (Appendix B-1) (Terumo medical corporation, Somerset, NJ, USA) which were then placed in a syringe pump (Model Pump 11 Elite, Harvard Apparatus, USA). A combined servo and controller arrangement (System Model Lexium 23, Schneider Electric, Rueil-Malmaison, France) were attached to a mandrel of non-conductive Dacron, (2 cm diameter and 60 cm length) for the fibre collection and was run though a cut out in the box. The fibres were collected onto a stainless steel collector which was custom built to be secured onto the mandrel (Figure 3.3c). The earth for arrangement was connected to the collector via a brush contact (Figure 3.2b). The needle for electrospinning was carried out with an 18 Gauge (0.838mm) needle prepared as described previously. The needle was connected to the power source using the same arrangement described earlier (shown in Figure 3.3d). The electrospinning was moved to a larger acrylic box (dimensions 75 × 60 × 60 cm), increasing the space to provide space for an additional mandrel support including a bearing to provide stability at higher rpm. The ventilation was also improved to allow for better fibre production.

3.2.2.4 Protocol 2 (Series 2)

The polymer adopted for Series 2 was poly(lactic-co-glycolic acid) (PLGA) (Purac® PURASORB, PLG 8523, 85/15 L-lactide/glycolide copolymer) (Corbion, Amsterdam, The Netherlands). PLGA was selected because it better suited the properties required of the objective. This included better biocompatibility and above all a suitable degradation rate (weeks to months) that was more in line with the goals and would not remain present for longer as might be the case with PCL.

Furthermore the properties of the material could also be varied heavily if required by varying the proportions of the copolymers.

The polymer granules were dissolved weight by volume into the solvent Dichloromethane (DCM) using a magnetic stirrer for at least 3 hours. The polymer solution was then stored at 8 ˚C. The polymer solution was returned to room temperature prior to use. The polymer (PLGA) concentrations which were used were 10%, 15% and 20%.

For the actual spinning process involved cutting tubular SIS into lengths of 3.5 cm in length. These lengths were then secured to the mandrel using a small quantity of adhesive tape, the tape was limited to the final 0.5 cm which would then be cut away and discarded at the end of the process, leaving a 3 cm length free of adhesive and the focus of the electrospun fibre coating. The PLGA solution was prepared to the concentrations mentioned earlier. Electrospinning was carried out with a polymer solution flow rate of 1 ml h^{-1}, with voltage at 14 - 16 kV and a height of 15 cm. The spinning was conducted for 45 minutes for each sample (15 m for each cm of SIS). The mandrel was advanced at an increment of 1 cm every 15 m. Samples were creating at mandrel rotational speeds of 10, 500, 1000, 2000 and 3000 rpm. Vacuum drying was used to remove any excess solvent using a vacuum freeze-drier (Heto Dry Winner) and they were then stored in sterile 50 ml falcon tubes at room temperature.

For the purposes of attachment analysis further samples were produced which had an additional 2 minute coating of the polymer solution at a flow rate of 7 ml h^{-1} with the voltage set to 25 - 30 kV and a slow rotation rate of 10 rpm. The high flow rate and high voltage resulted in a highly unstable spinning jet and only partially coated the sample with a set of large and incomplete fibres. A list of the key variations in the electrospinning process is in Table B1 (Appendix B-3).

3.2.3 SEM Analysis

The spun fibres on the SIS were cut into 1 cm sided squares and directly mounted on aluminium stubs using adhesive tabs. The stubs were then placed in a desiccator cabinet for at least 12 h to ensure any acquired moisture was sufficiently removed. All sections were then sputter coated with gold/palladium (Polaron E5000, Quorum Technology, UK). The samples were then analysed using a scanning electron microscope (Philips XL 30 SFEG, Netherland). The images were analysed using software (ImageJ).

3.2.4 Alignment

SEM images of the electrospun fibres were analysed using the Directionality v2.01 plugin for ImageJ which measures alignment angles for fibres present. All samples were cut into regular shapes and aligned prior to SEM imaging. A minimum of 10 images were analysed. In images with lower magnification the images were cut into multiple images to improve the analysis using Image J.

3.2.5 Mechanical Testing

Uniaxial tensile testing was carried out using a dynamic mechanical analyser (DMA 7e, Perkin-Elmer Instruments, USA). Test sections were cut into rectangular shapes of dimensions 8 - 14 mm in length and 5 - 8 mm in width, and in both the longitudinal and circumferential directions (relative to the axis of the small intestine). The ends of the samples were enclosed in wire gauze to provide grip and stability and the samples were then clamped into the machine. The dimensions of the samples were entered into the software (Pyris) and the distance between the two clamps was taken as the length. The tensile test was run with an increasing force

value of 500 mN min^{-1}. From the stress-strain graph produced the elastic modulus was calculated as the gradient of the elastic region of the curve (E = stress/strain). The samples were rehydrated with deionised water for 30 minutes, prior to testing. Samples which slipped or failed near to the clamps were ignored.

3.2.6 Attachment

Samples of the material were prepared identically as those for mechanical testing i.e. cutting rectangular shapes of dimensions 8 - 14 mm in length and 5 - 8 mm in width. These were placing in individual wells of 24 well cell culture plates and then submerged in deionised water for 2 h at room temperature and placed on an orbital shaker set at 60 rpm. Sample which separated were noted and the rest removed using forceps and place on absorbent paper towels and dried with the said towels using reasonable manual force (but with care taken to apply no torsional forces) and allowed to dry for a further 2 h. Any further separations of the layers were then noted.

3.3 - Results

As mentioned previously the complete spinning variations are listed Table B1 (Appendix B-3). This list includes variations which are also used in Chapter 4.

3.3.1 Series 1 (PCL)

3.3.1.1 SEM Imaging (Concentration)

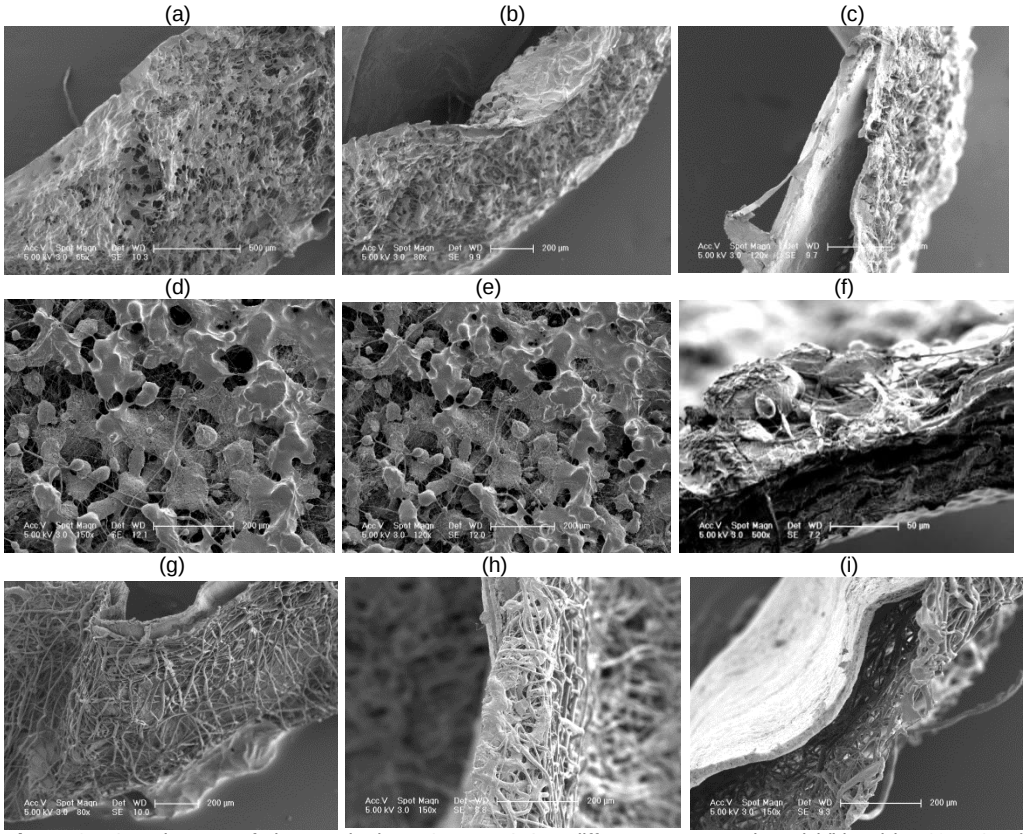

Figure 3.4 SEM images of electrospinning PCL onto SIS at different concentrations (a)(b) & (c): 10% PCL. (d)(e) & (f): 15% PCL. (g)(h) & (i): 20% PCL.

The three concentrations of PCL solution which were test showed different results with only 20% PCL showing consistent and uniform fibres. The samples produced using 10% and 15% PCL showed the characteristics of inadequately dried fibres in the form of large “pools” and droplets of the polymer when collected (as seen in Figure 3.4 a - f). They also showed inconsistent fibre diameters particularly with the distribution consisting of very large fibres (potentially difficult to even classify as fibres) or very thin diameter fibres.

It was also observed that while the fibres produced at 20% were the most desirable, the polymer solution was beginning to reach a viscosity and concentration where it developed a tendency to solidify upon emerging from the needle tip was beginning to arise. With any higher concentration unlikely to be successful and it was decided that 20% would be the standard for further investigation.

3.3.1.2 Fibre Characteristics (Concentration)

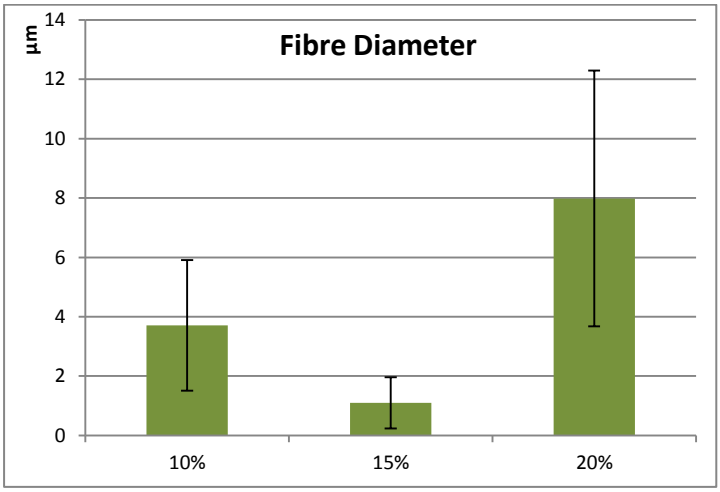

Figure 3.5 The average diameter for PCL electrospun fibres at the PCL solution concentrations of 10% (n = 67), 15% (n = 52) and 20% (n = 93).

The results of the fibre diameter analysis, as shown in Figure 3.5, show that with an increase in the concentration of the PCL solution there was an increase in the average fibre diameter. As mentioned previously the fibres present in 20% were all generally more uniformly fibre shaped with the large “pools” of polymer largely absent. The lower values present for the samples for 10% and 15% were due to the vast majority of fibres being exceptionally thin.

3.3.1.3 Mechanical Properties (Concentration)

The scaffolds were tensile tested and the results shown in terms of the elastic modulus, the yield strength and the failure strain (Figure 3.6). In terms of the modulus and the yield stress the results show that all fibre groups had larger values than the control SIS, with the yield stress result being particularly relevant (i.e.

potentially demonstrating increasingly improved properties over the control material). It was also noted that the certain instances the samples with less regular fibres, such as the 15% PCL fibres, had some slight mechanical advantages particularly in terms of the yield stress.

(a)

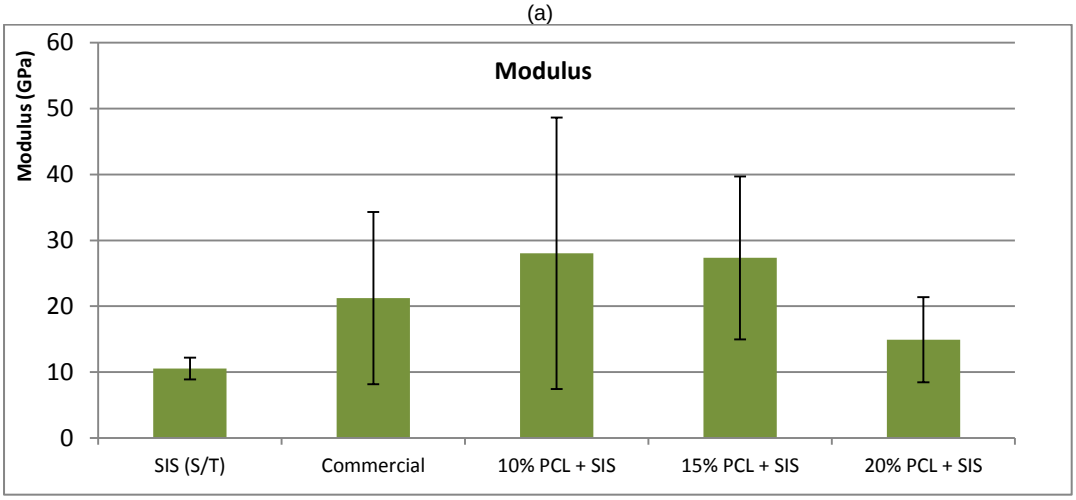

(b)

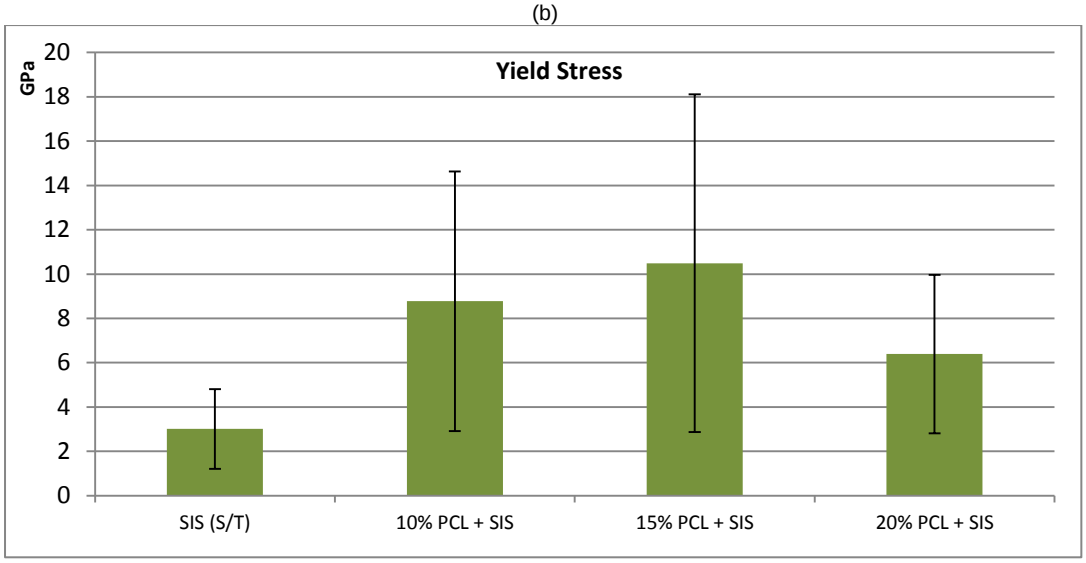

(c)

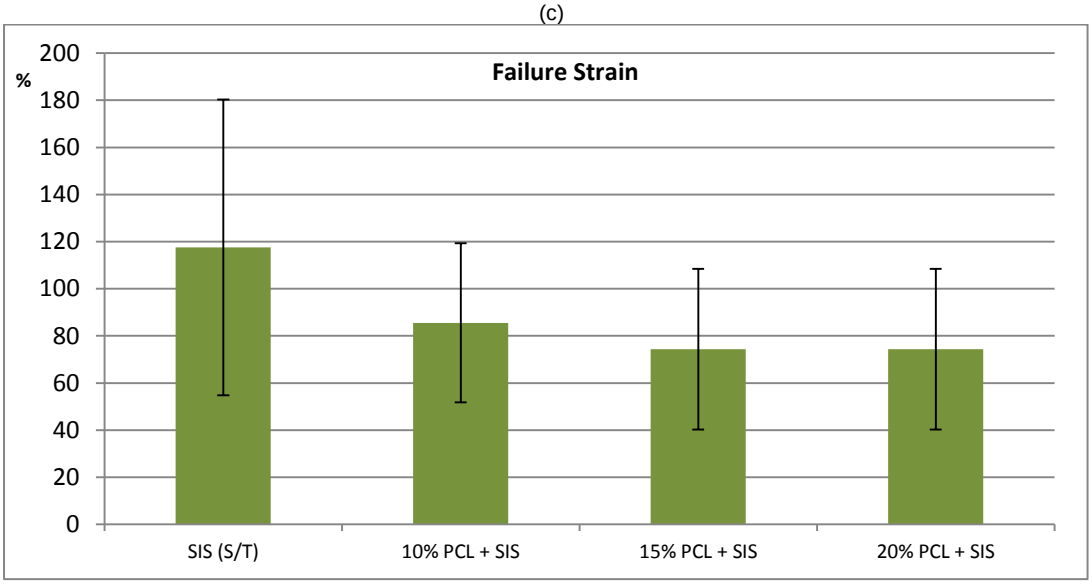

Figure 3.6 Mechanical testing data from the tensile testing of the PCL+SIS scaffolds (a) Elastic modulus values (MPa) (*n* = 6) (b) Yield stress values (MPa) (*n* = 6) (c) Failure strain values (%) (n=6). Error bars shown are the standard deviation. (*n* values for SIS (S/T) = 12).

All the fibre groups showed a decrease in the failure strain when compared to the control. This appears to demonstrate that the addition of the fibres reduced the elasticity of the SIS; however none of the values are reduced to below a failure strain of 75%, which would still be considered a completely suitable level of elasticity. The commercial SIS used in this testing did not fail and therefore did not produced results which could be compared however the results from the modulus tested did show that there was at least a comparable value to the scaffolds produced (Figure 3.6a).

3.3.1.4 Attachment

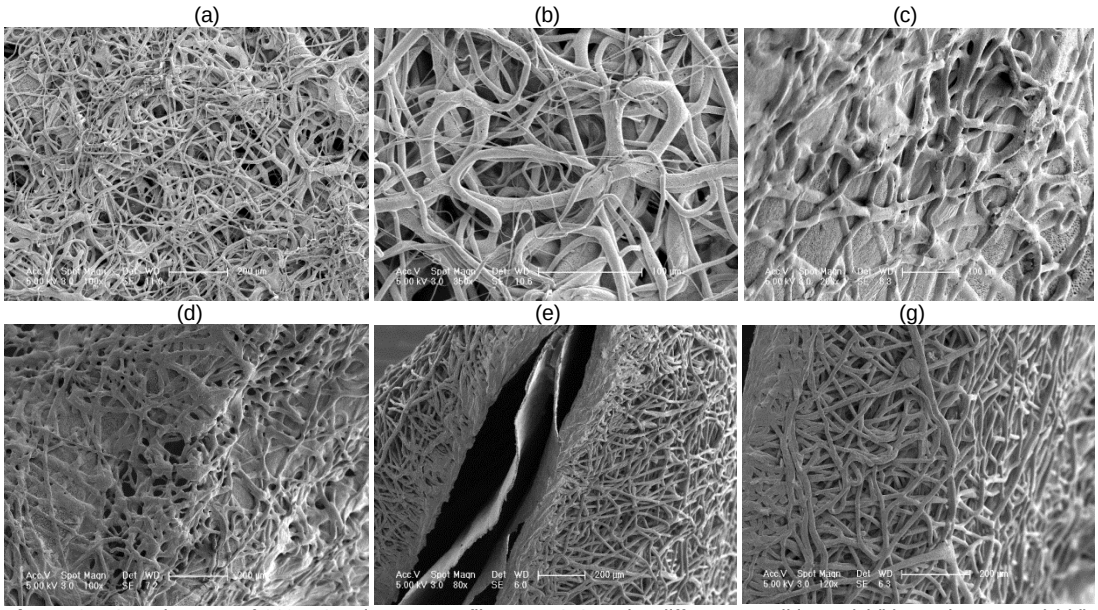

Figure 3.7 SEM images of 20%PCL electrospun fibres on SIS under different conditions: (a)(b) starting wet (c)(d) constantly wet (e)(g) primed SIS with acetone

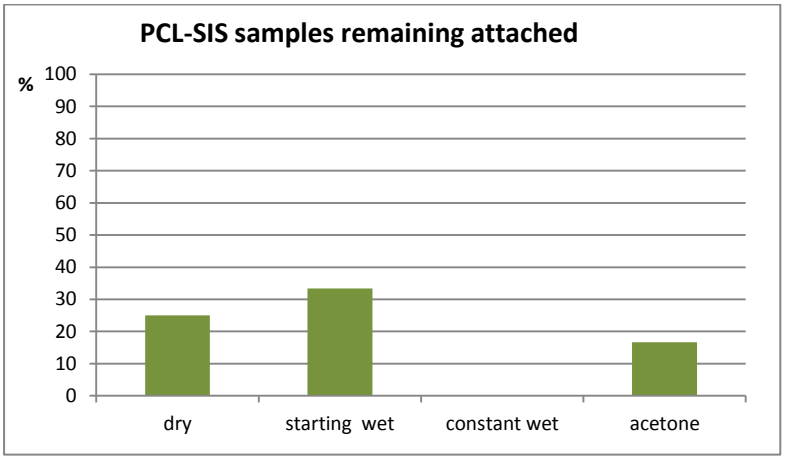

Figure 3.8 Graph representing the percentage of 20% PCL+SIS samples where the layers remained attached following cutting, exposure to deionised water for 30 m and drying (n=12). Values are calculated percentages and so no error bars.

The attachment testing performed after the SEM and mechanical analysis had been carried out and consequently only samples of the 20% PCL were tested (as these were considered the most suitable). The results here showed that the general standard of the fibre-layer attachment using the standard protocol was quite low with the average figure being only 25% (Figure 3.8).

Variations to this method showed that in the samples which were prepared with the SIS starting wet, there was a small increase in the average attachment figure (Figure 3.8). While this appeared to slightly improve the attachment it did not improve it enough for a useful yield. The fibre layers from this method did not appear to be very different from normal dry spun fibres though with SEM imaging it was observed that there were larger variations in fibre diameter as seen in Figures 3.7a & b.

Another variation was to use constant stopping and rehydrating of the SIS however this produced no samples with testable levels of attachment (Figure 3.8). The fibres produced using this method also appear to show signs of inadequate drying as seen in Figures 3.7c&d whether this was only due the wet condition of the SIS or whether the stop-start nature of the method also contributed it is unclear. The additional method of applying acetone to the SIS did not show any improvement over the conventional dry method though it was noted here that the acetone dried very quickly, and the appearance of the fibres resembled that of the default dry method (Figure 3.7e&f).

3.3.1.5 Alignment

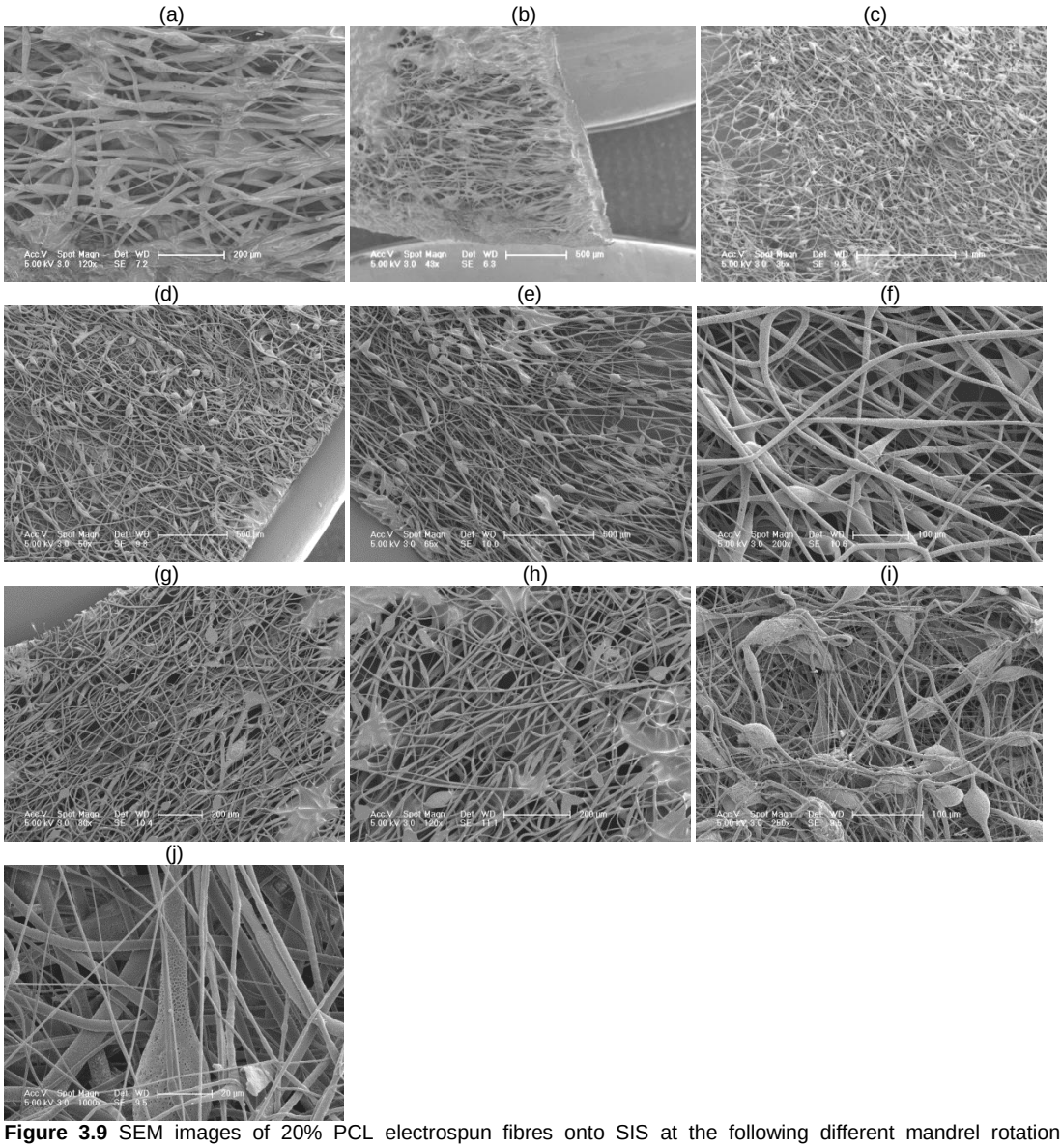

Figure 3.9 SEM images of 20% PCL electrospun fibres onto SIS at the following different mandrel rotation speeds:(a)(b) 540rpm (c)(d) 1260 rpm (e)(f) 1440 rpm (g)(h) 1620 rpm (i)(j) 1800 rpm

Table 3.1 Table listing the variations in speed mandrel speeds for samples of electrospun fibres prepared with 20% PCL onto SIS. All samples were prepared using identical protocols (15 cm, 10-15 kV, 5 m per cm)

Polymer	Concentration	Collection method	Motor Control Frequency	RPM	Alignment Observation
PCL	20%	Mandrel	300Hz	540	unaligned
PCL	20%	Mandrel	700Hz	1260	unaligned
PCL	20%	Mandrel	800Hz	1440	unaligned
PCL	20%	Mandrel	900Hz	1620	unaligned
PCL	20%	Mandrel	1000Hz	1800	Some indication of alignment, however not sufficient

It was investigated whether varying the speed of the mandrel might have the effect of changing fibre alignment (Table 3.1). In the three speeds immediately higher than the base speed of 540 rpm, there were no visible changes to the fibres which were produced (Figure 3.9). However, when the speed was increased to 1800 rpm there were some indications of alignment. It should be added that the alignment was only observed periodically and was not always be reproducible when required.

It was also found that increasing the speed of the mandrel any higher was not possible with this arrangement. Problems identified were the lack if bearing support at the end of the mandrel (space limitation), the use of a rolling ring contact, and a basic step motor, all contributing to high degree of resonant vibration which was a severe limitation. This arrangement was redesigned for Series 2.

3.3.2 Series 2 (PLGA)

As mentioned in the previous section the summary of the principle spinning variations are listed in Table B1 (Appendix B-3). Some preliminary work was carried out using PLGA to ascertain the ideal concentration using a flat collector and is not included in this chapter. The results of this work found that 15% was the ideal concentration, see Figure B2 (Appendix B-4).

3.3.2.1 SEM Imaging

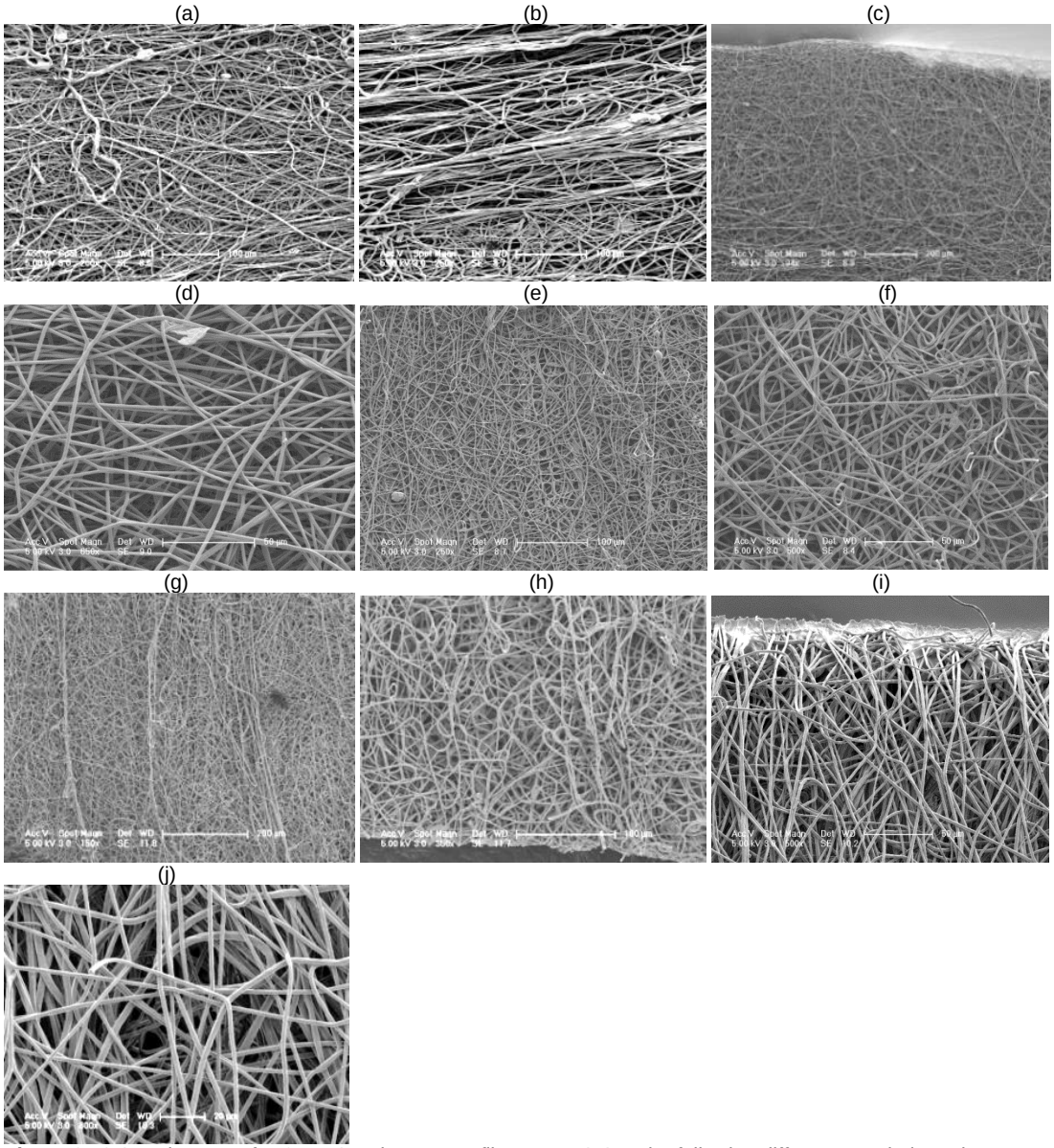

Figure 3.10 SEM images of 15% PLGA electrospun fibres onto SIS at the following different mandrel rotation speeds: (a)(b) 10 rpm (c)(d) 500 rpm (e)(f) 1000 rpm (g)(h) 2000 rpm (i)(j) 3000 rpm

With the changes in the materials, equipment and protocols (see Section 3.4.2) fibres could be made more consistently and at far higher rotational speeds. With faster speeds fibre alignment could be observed and this was taken to be an additional parameter to be investigated. SEM images of the groups tested are shown in Figure 3.10.

3.3.2.2 Fibre Characteristics

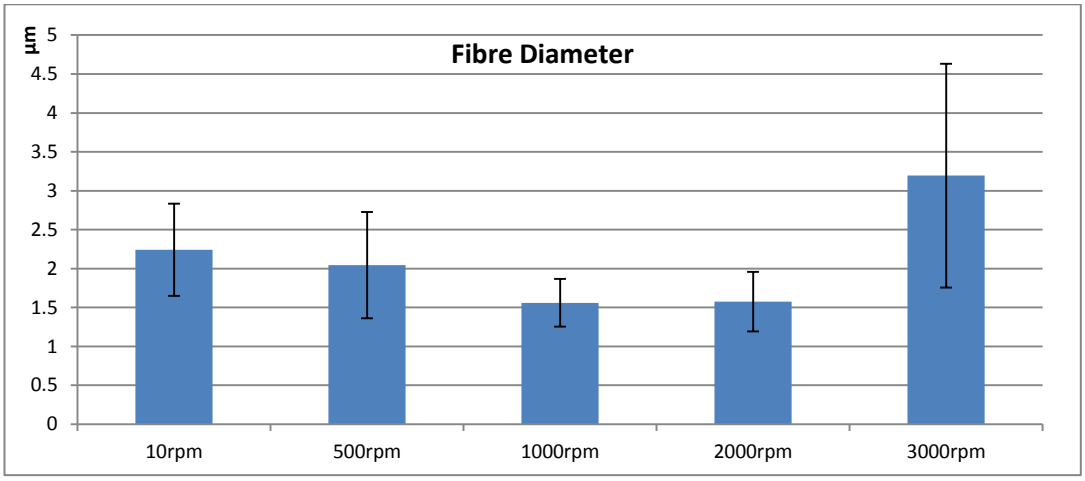

Figure 3.11 Mean fibre diameter of PLGA (15% solution) electrospun fibres produced at the following mandrel speeds (*n* value in brackets): 10 rpm (134), 500 rpm (126), 1000 rpm (115), 2000 rpm (113), 3000 rpm (129).

Image analysis of the fibre diameters from the SEM images showed that while there was some variation, there were no statistically significant differences between the sample groups which were produced (Figure 3.11). Consequently it was concluded that increasing the speed of the mandrel did not affect the fibre diameter.

3.3.2.3 Alignment

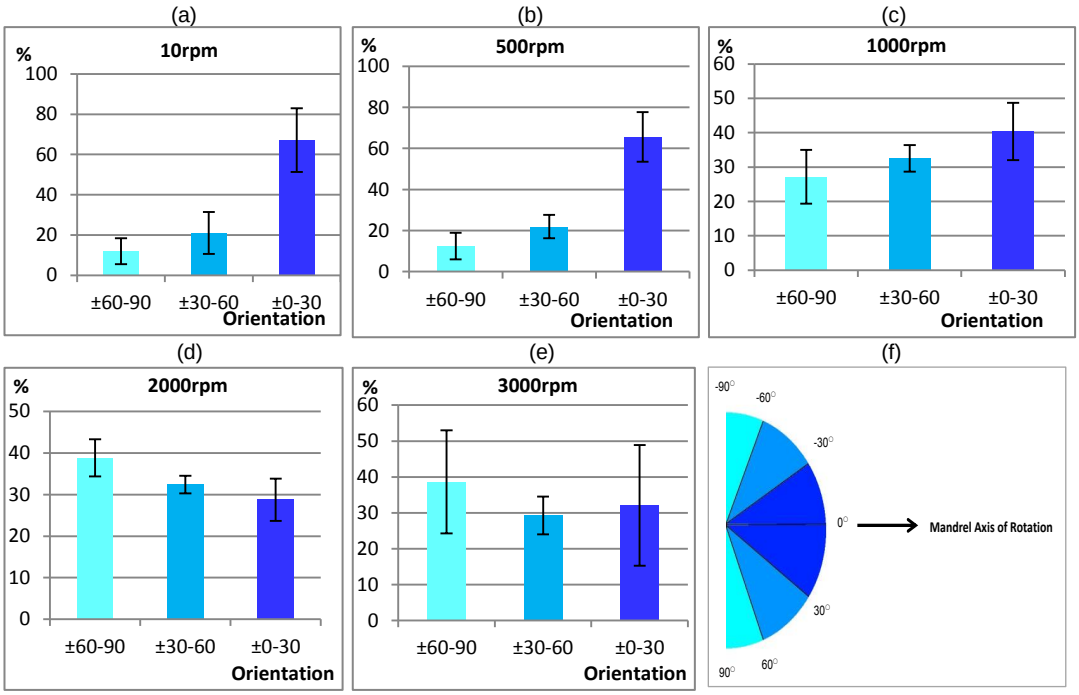

Figure 3.12 PLGA electrospun fibre orientation at the following mandrel rotation speeds (a) 10 rpm (b) 500 rpm (c)1000 rpm (d) 2000 rpm (e) 3000 rpm (f) Legend illustrating the relative fibre orientation relative to the mandrel axis of rotation (shown in degrees removed from the axis of rotation) (n = 10).

The alignment of the PLGA electrospun fibres appears perpendicular to the axis of rotation of the mandrel. This can be quantified by measuring the angle of the fibres relative to the axis (Figure 3.12). At the lowest speed (10 rpm) the highest proportion of fibres fall in the ±0 - 30° orientation group, demonstrating that most of the fibres are actually aligned largely parallel to the axis. Increasing the rotation speed to 500 rpm there is no appreciable difference in alignment. When the speed was increased further to 1000 rpm there was some change but again, the highest percentage grouping is the ±0 - 30° group. Only when speed was increased to 2000 rpm was where the majority of fibres began to show alignment with the highest percentage grouping being the ±60 - 90° group. This alignment is again further evident when the speed was increased to 3000 rpm. The SEM images also show clear charges in alignment as the speed increased (Figure 3.10).

3.3.2.4 Mechanical Properties

The mechanical tensile testing was carried out on samples in both the longitudinal (parallel to the axis of the mandrel) and circumferential (perpendicular to the long axis) shown in Figures 3.13 and 3.14, respectively.

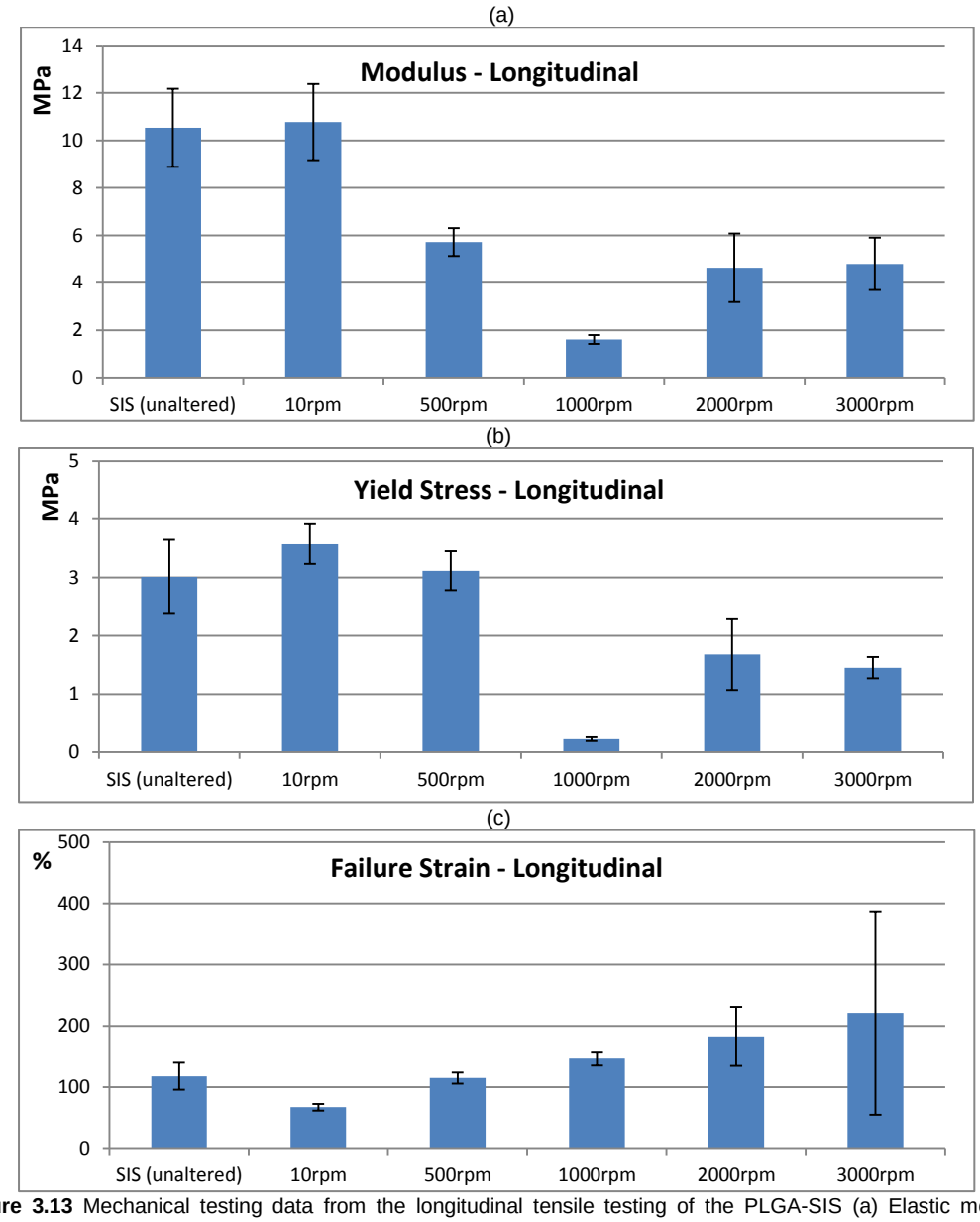

Figure 3.13 Mechanical testing data from the longitudinal tensile testing of the PLGA-SIS (a) Elastic modulus values (MPa) (n = 8) (b) Yield stress values (MPa) (n = 8) (c) Failure strain values (%) (n = 8). Error bars shown are the standard error. (N values for SIS (SDS/TX) = 12). The SIS used was SDS/TX. Statistical analysis was done non-parametrically and discussed in the results sections.

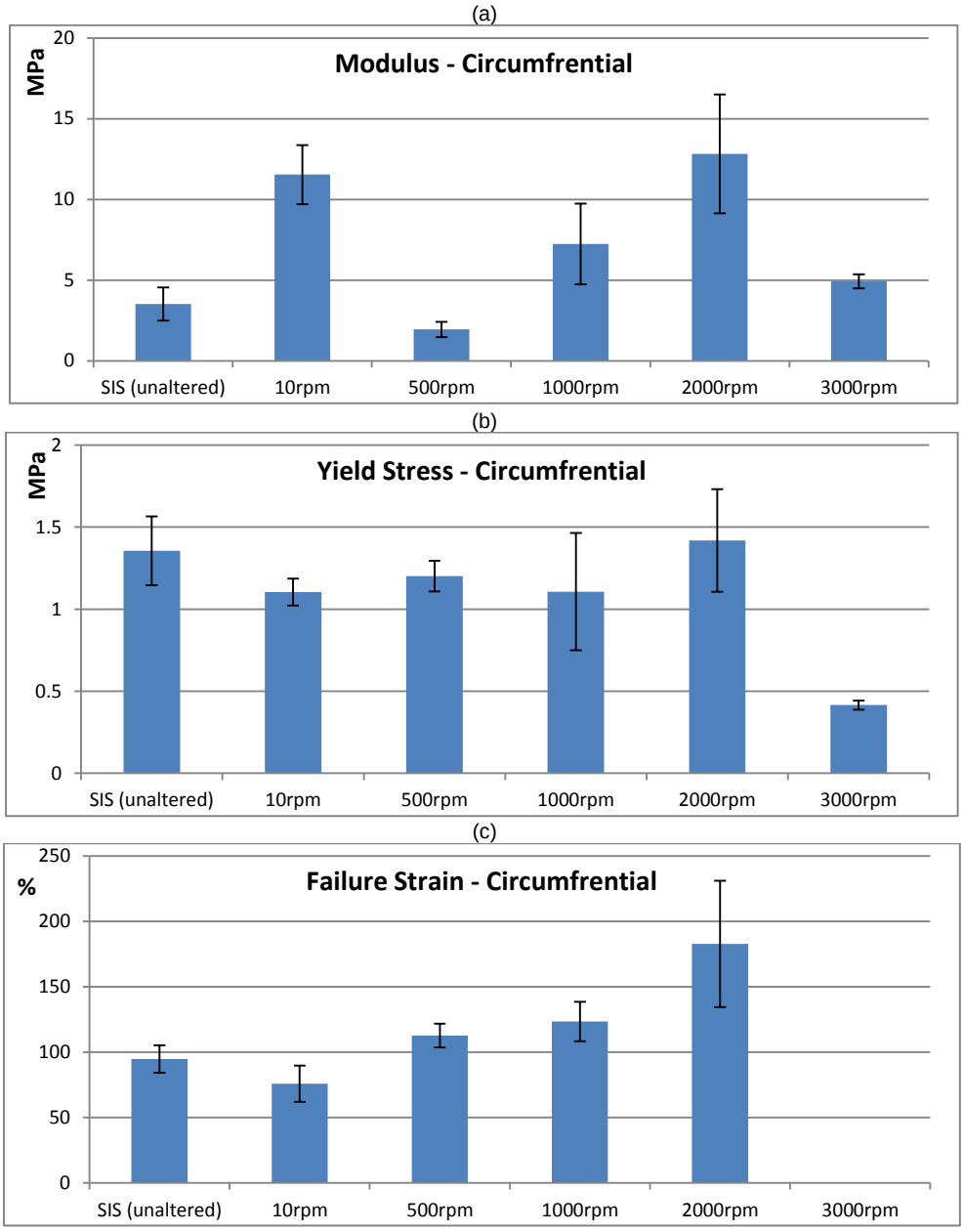

Figure 3.14 Mechanical testing data from the circumferential tensile testing of the PLGA-SIS (a) Elastic modulus values (MPa) (*n* = 6) (b) Yield stress values (MPa) (*n* = 6) (c) Failure strain values (%) (*n* = 6). Error bars shown are the standard error. (*n* values for SIS (SDS/TX) = 12)The SIS used was SDS/TX. Statistical analysis was done non-parametrically and discussed in the results sections.

With longitudinal tensile testing, it was expected that with an increase in perpendicular alignment the effect of the fibres would be decreased. With respect to the modulus and the yield stress this trend does appear to be present. There is a trend of the modulus and the yield stress average values decreasing as the degree of alignment increases. It was also noted that the values for the 1000 rpm group were particularly low though this appears more like a due to a single set of low

values rather than a reflection of any meaningful difference. In the case of the failure strain there did not be any significant difference between the groups, with the exception of the two extreme values, i.e. the 10 rpm and 3000 rpm groups.

In the case of circumferential testing, the modulus data appeared to show a degree of variability with no actual trend in relation to the degree of alignment. The yield stress was again was very consistent with all groups with the exception of the 3000 rpm group which was lower. For the failure strain data, with the increase in alignment there was a definite trend of increasing failure strain as the alignment increased. It should be state that this trend carried on to the 3000 rpm group, however none of the samples tested failed and were limited by the dimensions of the testing rig (which approximated to over 300%). Figure 3.15a illustrates a 3000 rpm sample at full extension with the aligned fibres clearly visible, with figure 3.15b showing a further manual extension using forceps illustrating that the sample did not appear to be at the failure point when the testing stopped and likely could have undergone further strain. It was also observed that the SIS had already failed by this point.

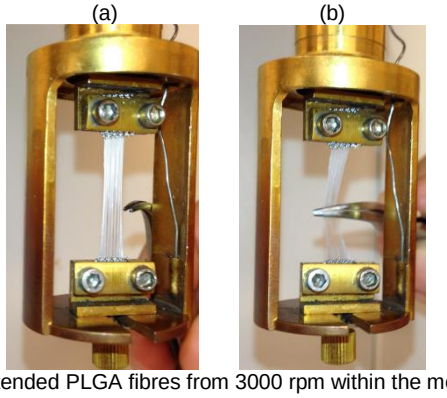

Figure 3.15 (a) Image of highly extended PLGA fibres from 3000 rpm within the mechanical testing arrangement (b) the same fibres manually further extended using forceps.

3.3.2.5 Attachment

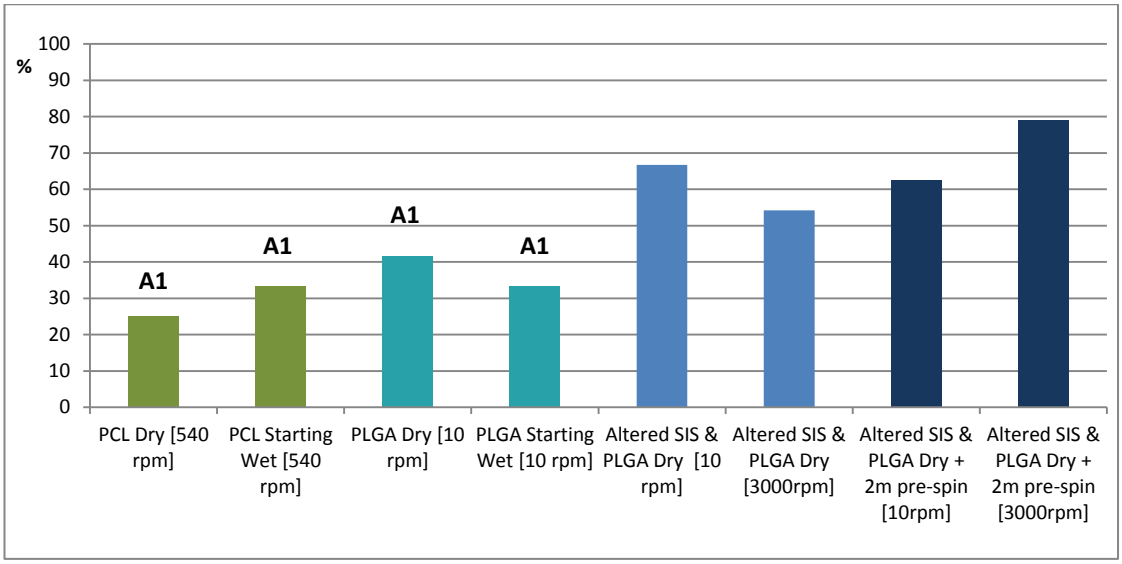

Figure 3.16 Graph comparing the percentage of attached samples from different groups after testing. Groups shown include those from Series 1 (PCL Dry and PCL Starting Wet, *n* = 12), Series 2 (PLGA Dry and PLGA Starting Wet, *n* = 24) and a further 4 test group which will form part of the Chapter 4 (all 15% PLGA, *n* = 24). The A1 denote samples produced with Arrangement 1.

The attachment data is shown in Figure 3.16, and is includes a collection of groups from Series 1, Series 2, and groups which will form part of Chapter 4. Two of the groups (PLGA Dry & PLGA Starting Wet) include PLGA fibres spun using Arrangement 1 and using the old SIS shape (see Section 3.2.2.1). These groups are all shown in Table B1 (Appendix B-3).

The culmination of the trial and error work resulted in a change in technique for SIS creation and consequently a change in shape and surface features. Once the new methods had been used (described in Section 3.2.1.4), then the samples were tested at speeds of 10 rpm (random) and 3000 (aligned).

The results showed that when using Arrangement 1 and the old SIS changing polymers or using wet starting SIS did not appear to change the attachment levels of the polymer fibres to the SIS (Figure 3.16). What did cause a large increase in the levels of attachment was the adoption of the new shape of SIS (the “Altered SIS” groups) and consequently this was the SIS scaffold used in Series 2. Further

work carried out showed that the addition of a further "base" layer of disordered fibres, further increased the levels of attachment particularly in case of 3000 rpm samples (discussed further in Section 3.4.2.1). Generally speaking, the alignment of the fibres does not appear to result in any significant change to the attachment levels. The changes in to the SIS are shown in Figure 3.17 and described also further in Section 3.4.2.1.

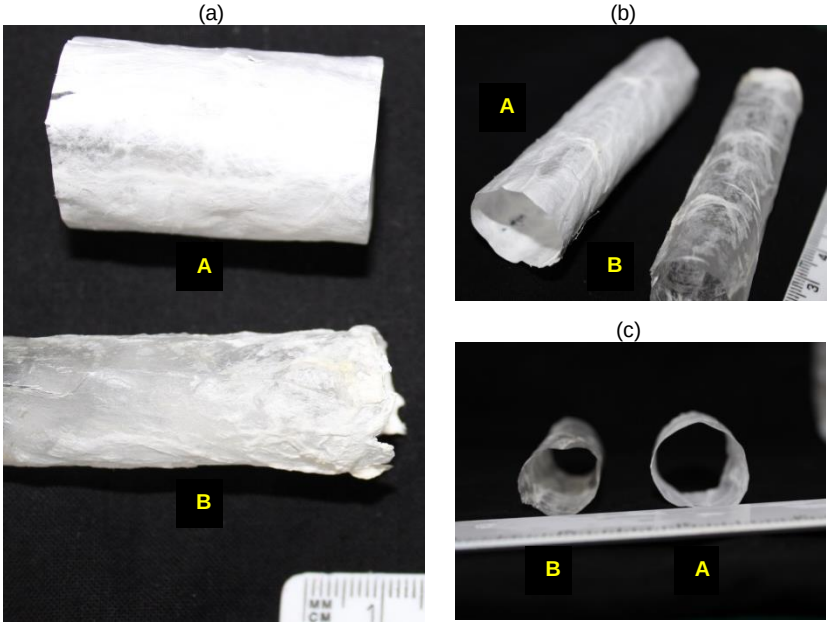

Figure 3.17 Images of the SIS produced using two alternative methods and using two different sizes of tubing. In all images A - new method (2.54 cm diameter) and B - old method (1.9 cm diameter). The change in diameter resulted in improving the surface smoothness of the SIS.

3.3.3 Sample Yield

When electrospinning is used as a production method care needs to be given to the fact that the technique is highly sensitive and quite variable and efforts made to minimise this. In this work (including this chapter and the next) the temperature and humidity were found to be the most difficult factors hindering the process. These factors could be mitigated only to certain degree though the use of cooling and heating methods applied to the lab environment or locally (such as running the tubing through ice packs). Consequently at any given time the yield of suitable scaffold produced was only approximately 70%. The criteria used to dictate a

suitable sample was informed by trial and error and SEM analysis when samples were found to be poor in quality. Generally speaking, when there was a high degree of solvent evaporation this was accompanied by intermittent spinning resulting in regions of the SIS devoid of fibres and these were discarded. Occasionally there was an excess production of polymer droplets (possibly due to inadequate evaporation) and when this occurred to a high degree the samples were also discarded. In addition to that it was found that the electrospinning could be interrupted by periods of electrospraying and this also necessitated sample loss.

The most important factors of all, however, were the production of a stable Taylor cone and a stable stream of polymer being electrospun. Often the appearance of one of the previously mentioned criteria could be predicted if stable spinning conditions were proving to be excessively difficult to establish and maintain. These established criteria were used throughout this work.

3.4 - Discussion

3.4.1 Series 1 (PCL)

Electrospinning with PCL is a common and well used form of scaffold production. In this work however, the PCL scaffold was also required to attach to, and compliment, the SIS and thus form a hybrid scaffold.

The SEM images of the PCL concentrations tested (Figure 3.4) revealed that only the samples from 20% PCL concentration produced consistent and regular fibres. It was observed when handling the scaffolds that attachment was noticeably higher in the samples produced at concentrations of 10% and 15% PCL when compared to 20%. This was not quantified due to the poor quality of the fibres however; this was an observation which was deemed significant.

As seen in Figure 3.8, the general state of attachment of the fibres to the scaffold was generally very poor with only around 25% of the fibre layers actually remaining attached when testing in the 20% PCL group. It should be added here that this figure reflected the scaffold being subjected to a fairly rigorous test and that the actual percentage of passably attached fibre-layers was likely higher. That said, the yield levels were still far too low, and while enough samples were available for further testing, alternative methods were explored to improve the attachment levels and will be discussed later.

In terms of the mechanical properties of the scaffolds there was appreciable improvement over the control SIS (Figure 3.6). This showed that, in theory, the concept of electrospun reinforcement of SIS held some potential for if there could be improved attachment. As mentioned previously, some elements of improved attachment were observed in the 10% and 15% PCL samples. What was speculated here was that with a lack of adequately dried fibres the observed

"pooling" effect, where globules of polymer form and dry over the SIS (Figure 3.4), may have provided some additional attachment. This was in contrast to the samples of 20% PCL which had poorer adhesion but a layer of consistent electrospun fibres. This could possibly represent the reason why the mechanical properties, particularly for modulus and yield stress were higher (Figure 3.6) for these samples than for the more regular, yet less attached, 20% concentration layer.

Attachment improvement was investigated using a number of different starting conditions for the SIS (Figure 3.8). While there was a slight improvement when the SIS was started wet before the spinning process this did not significantly improve the attachment rate to desirable levels.

Interestingly, the method described by Horst *et al.* of constantly rehydrating the samples produced no attached samples at all (Horst, Madduri *et al.* 2013). In that study decellularised urinary bladder matrix (UBM) was coated with electrospun PLGA fibres and it was, as in this work, noted there was an issue was attachment. In their work attachment was achieved through a layer by layer spin process where the matrix was constantly rehydrated. It should be added that in that case the UBM was in flat sheet form. A similar solution was adopted here but as mentioned above the result not achieved. However the shape of the SIS in this work and the rotation of the mandrel may have prevented this method from working. It was also observed that the constant rehydration caused the SIS to sag on the mandrel. Thus, when rotation was recommenced, this created a mobile and less stable surface onto which the electrospun fibres could attach. This contrasts significantly with the circumstances of a flat matrix where hydration might actually increase the stability of the surface of the matrix. Rehydration, by causing expansion, could have removed potential "wrinkling" when on a flat surface, and also the increased surface tension of the wet matrix to the flat electrode underneath could also have had an effect.

The use of acetone to wet the SIS was another attempt to improve attachment; the hypothesis here being that the initial fibres which contacted the acetone might soften and therefore deform enough to grip the surface. However it was observed that with the arrangement being under a slight vacuum, along with the rotation of the mandrel, there was an increased air flow around the mandrel. Consequently a volatile solvent such as acetone could not remain on the surface of the SIS for any appreciable time. Therefore this method was unsuccessful.

The final analysis of the PCL/SIS scaffold produced was carried out by varying the speed of the mandrels rotation (Table 3.1). With increasing the rotational speed of the mandrel there was no great increase in the alignment of the fibres produced with only a slight increase in the observable alignment at the speed of 1800 rpm. As mentioned in the Section 3.3.1.5 it was also noted that when the speeds were increased a number of problems arose. Size limitations in the arrangement box there was no room to add a bearing at the free end of the mandrel. Consequently at higher speeds the mandrel developed some resonant vibration, one of the results being that the ring contact would “bounce” while on the mandrel and break contact repeatedly or it would vibrate off the mandrel entirely. In addition to this there was the physical limitations of the step-motor and switch arrangement which could not achieve higher speeds. It was concluded that if faster rotational speeds were required a new arrangement would need to be devised (Figure 3.3).

With the decision to change the arrangement, the selection of the polymer was also brought into question. One the potential future issues which might arise through the use of PCL was that there would a slow degradation rate when compared to other commonly used polymers (Woodruff and Hutmacher 2010). In the case of the objectives of this work the polymer would only need to persist *in vivo* for a number of months and not for an extended period. In addition to this the semi-crystalline nature of PCL means that in certain solvents such as dimethylformamide it has a

low solubility and this results in rapid evaporation which caused potential clogging difficulties in electrospinning (Woodruff and Hutmacher 2010).

PLGA was selected as an alternative to PCL. It is known to have better biocompatibility, in addition to have improved effects on cell adhesion and proliferation when compared to PCL (Kim and Cho 2009). PLGA also has more potential for controlling the properties of the polymer through changing the ratio of the copolymers.

3.4.2 Series 2 (PLGA)

3.4.2.1 Adhesion

A large amount of work went into improving the attachment of the electrospun fibres to the SIS. The basis of this work was that it was observed that the early had a very wrinkled and uneven surface (Figure 3.17a). The reason for this was due to the disparity in the diameter of the SIS and the smaller diameter of the porous polyethylene tubing onto which it was placed prior to vacuum drying (Figure 3.1). This resulted in “slack” along the SIS lengths becoming compressed and drying in a variety of peaks and troughs. This in turn not only provided a rough surface (Figure 3.17b) onto which to electrospin but the topography also allowed for spans of electrospun fibres having no surface contact with the SIS.

Further work showed by increasing the diameter of the porous tubing enough that the SIS was required to be stretched to be placed over the tubing. While this made the process slightly more difficult the result was highly apparent (Figure 3.17). It was also found that the smoother surface provided by the stretching was further enhanced by the action of the vacuum drying as the bag compressed and improved the smoothness of the SIS, rather than compressing the excess and exacerbating the problem (shown in Figure 2.4b). When the new surface was electrospun onto it showed a great improvement in the levels of attachment over fibres spun using Arrangement 1, as seen in Figure 3.16.

As mentioned in the Section 3.4.1, with PCL fibres it was noted that inadequate drying resulted in incomplete fibres which has the result of causing some increased attachment. It was therefore hypothesized, that the addition of an initial dispersed layer of disordered and “sticky” fibres might increase adhesion. Consequently work was carried out which tested this theory (Table B1, Appendix B-3). As a result of some simple adhesion testing it was shown that the addition of a 2 minute layer of

such fibres resulted in an improvement in the adhesion of the fibre layer as a whole (Figure 3.16). This was deemed a suitable limit as any longer might have resulted in a complete covering, something not desirable as issues such as the porosity of the scaffold would come into question. Consequently the 2 minute only laid down a loose network of fibre around the scaffold. This additional stage to the method was not used in Chapter 3, though would be adopted for all scaffolds produced for use in Chapter 4.

The final result of all this work was to obtain a methodology, which could be finally used to make consistent hybrid scaffolds in terms of decellularisation, fibre characteristics, and attachment.

3.4.2.2 Alignment

The new arrangement increased the capacity for higher speeds of mandrel rotation. Improvements also included the addition of a brush earth contact for the metal collector (Figure 3.3b) which allowed for constant contact irrespective of the rotational speed and is a method commonly used with rotating disc collectors (Xu, Inai *et al.* 2004). Work on Series 1 showed no alignment at lower speeds and this was again observed here with the PLGA fibres produced at 10 or 500 rpm producing no alignment (Figure 3.12). This agrees with examples seen in the literature such as a similar arrangement using PLGA at 500 rpm producing fibres which were unaligned (Stitzel, Liu *et al.* 2006).

While some changes in alignment were detected at 1000 rpm it was at 2000 rpm where the predominant alignment was perpendicular to the axis of rotation. This point of around 2000 rpm was observed to some degree in Series 1 at 1800 rpm and has also been described in other work. Alignment has been demonstrated at the rotational speed of 1500 - 2000 rpm where a rotating cylinder was used to collect polystyrene (PS) and polymethylmethacrylate (PMMA) fibres (Sundaray,

Subramanian *et al.* 2004). Additional work using polyurethane and a polyurethane/collagen blend also allowed showed alignment of electrospun fibres at 2000 rpm (Jia, Prabhakaran *et al.* 2014). PCL fibres have also been made to align with a similar process where the rotational speeds were found to be between 1000 - 2000 rpm (Zhu, Cao *et al.* 2010)

3.4.2.3 Mechanical Properties

The mechanical properties were not straight forward to analyse with respect to the samples produced. When observing the results what needs to be taken into account is that for a large number of samples tensile testing resulted in uniquely bi-phasic behaviour. Figure 3.18 illustrates the difference between (a) SIS (in addition to most non-viscoelastic “softer” materials) and (b) the hybrid scaffolds in question. In the case of these materials it appears that the materials often have one layer take part in an initial stress yield, the material then recovers its elastic behaviour, and this is followed by a second yield. The failure behaviour is straightforward however as the failure of the entire scaffold is singular event. What these means is that the layers can fail separately, and a decision was made than all modulus and yield stress data would be selection from the first elastic region of the stress/strain curve particularly in the context that a yielding of the elastic behaviour of a material is an indication of permanent change of the mechanical behaviour. It should also be born in mind that these materials will have a degree of redundancy which is useful from an implant perspective as failure in one layer will not result in structural compromise of the entire scaffold and potentially give rise to perforations.

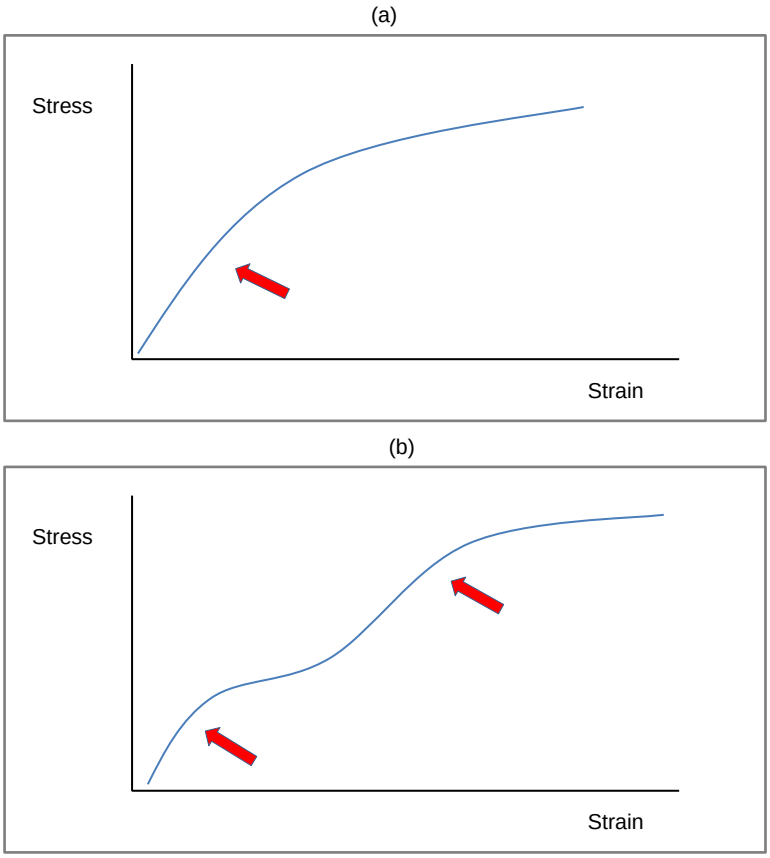

Figure 3.18 Generalised illustration of a typical stress-strain graph for (a) SIS and (b) PLGA-SIS hybrid materials. The red arrows denote the yield point occurring at the end of an elastic region of the stress-strain curve.

There is evidence that the alignment has a direct effect on the mechanical properties of the hybrid scaffold. The was particularly relevant in the case where the high alignment of the PLGA fibres largely prevented samples from the 3000 rpm group from failing well past the 300% strain (this figure is by visual observation of the testing machine). This result is significant as it represents a clear mechanical advantage to having aligned fibres of a particular orientation, here giving rise to a situation where if a sudden force were to extend the scaffold, i.e. such as a bolus, then that extension would not cause the scaffold to be compromised. It was also generally observed with the modulus results, that the randomly aligned scaffolds were found to have higher values, which loosely equates to an increased “stiffness”.

Other studies have shown that the mechanical properties will change as the fibre alignment changes. Polyurethane and polyurethane/collagen blends showed far higher values for ultimate tensile stress and the modulus for aligned samples

compared to non-aligned. The samples tested were parallel to the fibres and when perpendicular tested they behaved as random fibre samples (Jia, Prabhakaran *et al.* 2014). In another case using polyacrylonitrile, the stress-strain behaviour of the scaffolds changed along with fibre alignment as samples were produced with increasing rotational speeds (Heidari, Mosavi Mashhadi *et al.* 2013). PLGA fibres in another study had higher values for aligned fibres in terms of the tensile stress and modulus values when compared to randomly orientated fibres (Shang, Yang *et al.* 2010). Using electrospun synthetic elastin it was found that aligned fibres produced higher values for ultimate tensile stress and strain, however the modulus was found to be lower (Nivison Smith and Weiss 2012). This does not match with other examples in the literature though it is interesting to note that different polymers, in this case elastin, can have different results with respect to mechanical properties even with alignment.

3.4.2.4 Fibre Diameter

The lack of change of fibre diameter is a commonly found observation. Fibre diameters produced with electrospun gelatine over a greater range of speeds, i.e. did 200 - 7000 rpm, have been produced with no change in diameter (Ayres, Bowlin *et al.* 2006). It can therefore be said that providing the fibres are fully dried by the time they reach the collector any change to their physical dimensions is unlikely.

3.4.3 Conclusion

A number of important things were concluded; firstly that successfully electrospinning a polymer layer onto tubular SIS (with two different polymers) was possible but that attachment was a limitation. Through further work it was concluded that a number of things could be done to improve the level of attachment including; changing the shape and surface texture of the ECM to make an even and smooth surface, along with the addition of a small amount of poorly dried “sticky” fibres. It was also concluded that the speed of rotation of the mandrel could be used to create fibre alignment and this, in turn, could be used to change the mechanical behaviour of the scaffold.

4. Hybrid Scaffolds

4.1 - Introduction

In Chapters 2 and 3 two separate materials have been brought together with the aim of producing a true hybrid scaffold for the purposes oesophageal of tissue engineering. Improvements were made in the production of the each of two layers and the hurdle of adhesion between the two layers was also overcome. Further evaluation of hybrid the scaffold would need to be carried out and the final variable, the alignment of the fibres within the electrospun layer, also studied in more detail.

In vascular tissue engineering scaffolds have been used for some time with aligned fibres. These are used to induce alignment in smooth muscle cells with the aim of encouraging contractility (Jia, Prabhakaran *et al.* 2014). This concept is important here as restoring oesophageal contractility through a similar process of culturing of aligned smooth muscle cells seems to be an ideal approach to tissue engineering the oesophagus. This is particularly significant as studies with sectional oesophageal replacement commonly report lack of significant muscle growth along with the more common complications including stricture, dilation and leakage. (Doede, Bondartschuk *et al.* 2009). The work so far has been to address the physical aspects of these failures however the potential to also address the lack of muscular growth is an appealing one. As a result human oesophageal smooth muscle cells were cultured and used to assess the viability of the hybrid scaffolds. While it was unfortunately beyond the scope of this work to biopsy, culture and implant an intact scaffold *in vivo*, work was carried out to take steps towards achieving that goal.

In this chapter the scaffolds were created using all the information gathered from the previous chapters. Some studies have demonstrated highly aligned fibres at speeds higher than the maximum of 3000 rpm used in Chapter 3, examples include highly aligned PCL/gelatin blend fibres produced at 4000 rpm (Gupta, Venugopal *et al.*

2009) and highly aligned collagen fibres at 4500 rpm (Matthews, Wnek *et al.* 2002). Consequently the maximum speed of rotation was increased up to 5000 rpm.

The final change to the overall scaffold design was the addition of VEGF to the scaffold (the benefits of VEGF are outlined in Chapter 1). The decision was made in an effort to maximise the potential long-term performance of the hybrid scaffolds, the lack of angiogenesis being a common reasons for scaffold failure (Laschke and Menger 2012). The addition of a pro-angiogenic agent was seen as a logical step to improve a scaffold design.

The aim of this chapter is to assess the hybrid scaffold as a whole through physical, *in vitro* and *in vivo* means. The different alignment variations would also be assessed to see if an optimal alignment could be chosen. Finally the effectiveness of the incorporation of VEGF would also be assessed.

4.2 - Materials and Methods

4.2.1 SIS Preparations

4.2.1.1 SIS Preparation

The SIS was prepared as described in Chapter 2. Briefly, the jejunum/ileum samples were cut into lengths of 20 cm, and prepared as described previously. Following preparation, the SIS was then carefully washed twice in deionised water for 5 minutes. The SIS was then stored in PBS (phosphate buffered saline: 0.01 M phosphate buffer 0.0027 M potassium chloride and 0.137 M sodium chloride, pH 7.4, at 25 °C).

4.2.1.2 Decellularisation

The SIS was decellularised with a variation of the SD/DNase (perfusion) method of decellularisation described in Section 2.2.2. There were a few changes made to the protocol made as it was described previously to reflect the findings of the Chapter 2. The method was altered in that the DNA was eliminated from the protocol as was shown to have no discernable effect on the levels of decellularisation of the SIS produced.

Each container was filled with 350 ml of 4% SD (Sigma-Aldrich Company Ltd., Dorset, UK) then the pump run 500 ml h^{-1} for 12 h at room temperature. The samples rinsed with deionised water followed by a perfusion wash for 15 minutes, also with deionised water.

4.2.1.3 SIS Washing

Following the initial rinse the SIS was washed using a variation of the altered washing method outlined in Appendix A-2. In this method the containers were filled with deionised water, and the input channels connected to a large separate

reservoir of deionised water. The pump was then run for a further 5 hours. With this arrangement deionised water was allowed to overflow out of the vessels creating a one way flow to allow constant washing with fresh deionised water. The SIS was then rinsed and placed into a further container containing deionised water for a short rinse. All decellularised SIS was stored at 4°C in PBS.

4.2.1.4 - Post Decellularisation Processing

The SIS sections were stretched over a 2.54 cm diameter (described by the manufacturer as 1 inch) porous polyethylene tubing (60 µm pores) (Porex Corporation, Fairburn, United States). These samples were vacuum-dried in sealed sterile specimen bags and placed under low vacuum conditions (approximately 10 mbar) for 12 h to compress and dry the samples. The dried SIS samples were subsequently lyophilised by immersing in liquid nitrogen for 1 minute and then placed into a vacuum freeze-drier (Heto Dry Winner) for 12 h.

4.2.2 Electrospinning

Electrospinning was carried out using the same arrangement described in Section 3.2.2.3 (Arrangement 2). For the actual spinning process the tubular SIS was cut to lengths of 3.5 cm and secured to the mandrel using a small quantity of adhesive tape. The polymer used was PLGA (85/15 L-lactide/glycolide copolymer). The polymer granules were dissolved into dichloromethane (DCM) and dimethylformamide (DMF) at an 8:2 ratio using a magnetic stirrer for at least 3 hours to make a 15 % weight by volume solution. The solution was prepared in small quantities of 10 ml to prevent solvent loss through the re-use of the polymer solution. The polymer solution was then stored at 8 °C.

The electrospinning was carried out in 2 stages. The first stage was a thin coating layer for which the polymer solution was pumped at flow rate of 7 ml h^{-1} for 2 m at a voltage of 20 kV and with the mandrel rotating at 10 rpm. Following this the actual spinning was carried out where the polymer solution was carried out with a flow rate of 1 ml h^{-1} at a voltage of 14 kV for 45 minutes (the complete parameters are listed in Table B1, Appendix B-3). The mandrel was advanced at an increment of 1 cm every 15 minutes. The samples were vacuum dried to remove any excess solvent.

4.2.3 Mechanical Testing

Uniaxial tensile testing was carried out using a dynamic mechanical analyser (DMA 7e, Perkin-Elmer Instruments, USA). Test sections were cut into rectangular shapes of dimensions 8 - 14 mm in length and 5 - 8 mm in width, and in both the longitudinal and circumferential directions (relative to the axis of the mandrel). The ends of the samples were enclosed in wire gauze to provide grip and stability and the samples were then clamped into the DMA. The dimensions of the samples were entered into the software (Pyris) and the distance between the two clamps was taken as the length. The tensile test was run with an increasing force value of 500 mN min^{-1}. From the stress-strain graph produced the elastic modulus was calculated as the gradient of the elastic region of the curve (E = stress/strain). The scaffolds were rehydrated with deionised water for 30 minutes, prior to testing. Samples which separated during the rehydration were discarded. Samples which slipped or failed near to the clamps were ignored. Any samples which showed rapid separation of the layers during the mechanical testing was noted.

4.2.4 SEM Imaging

The spun fibres on the SIS was cut into 1 cm sided squares and directly mounted on aluminium stubs using fast drying epoxy adhesive. The stubs were then placed in a desiccator cabinet for at least 12 h to ensure any acquired moisture was sufficiently removed. All sections were then sputter coated with gold/palladium (Polaron E5000, Quorum Technology, UK) and then imaging was carried out using a scanning electron microscope (Philips XL 30 SFEG, Netherland). Digital images produced were analysed using software (ImageJ).

4.2.5 Porosity

Samples of the scaffold were weighed out to a weight of 1 g. The scaffold samples were rolled into a consistent shape and were placed into the glass testing vessel of a mercury intrusion porosimeter (Micromeritics Autopore, Micromeritics Instrument Corporation, Norcross, USA). The porosity measurements were carried out using an automated testing cycle (n = between 4 and 6 for each sample). Statistical testing was carried out using a 2-tailed student's t-test to a 95% confidence interval using SPSS version 20 (IBM, Armonk, New York, US).

4.2.6 Biocompatibility

4.2.6.1 Cell Culture

Primary human oesophageal smooth muscle cells (HESMC, ScienCell Research Laboratories, Carlsbad, CA, USA) were cultured in Dulbecco's modified Eagle medium (Gibco, Life Technologies, Paisley, UK) supplemented with 10% foetal bovine serum (Gibco) and 1% penicillin-streptomycin (Gibco) at 37°C in air with 5% CO_2 and 95% relative humidity. Cells from passages 2 - 6 were used for experiments.

4.2.6.2 Biocompatibility Assay

A CellTiter 96 AQueous Non-Radioactive Cell Proliferation Assay (Promega, Southampton, UK) was used to assess the enzymatic activity of HESMC's as an indication of biocompatibility, in accordance with ISO 10993 parts 5 and 12 (Appendix A-4) and the manufacturer's protocol. Briefly, HEMSC were seeded at a density of 100,000 cells/cm^2 on the hybrid scaffolds with the PLGA fibres spin at 10 rpm, 1000 rpm, 3000 rpm, 5000 rpm, a commercial scaffold and control TCP 48-wells. The commercial scaffold was Biodesign® (Cook Medical, UK) and was used in this instance only to provide a potential alternative to TCP as a control.

Cell culture inserts (CellCrown, Scaffdex Ltd., Tampere, Finland) were used to pull the samples taut and suspend them within the 24-well plates with the cells seeded on the PLGA nanofibre surface with the exception of the commercial scaffold which did not have a specified orientation. For sterilisation the scaffolds were immersed in a 70% ethanol solution and then allowed to dry completely in a sterile fume hood. The scaffolds were all hydrated with 200 µl of medium approximately 30 m prior to seeding cell.

After 24 and 96 hours incubation, medium was aspirated from the cells and replaced with one part MTS solution in six parts medium, which consists of (3-(4,5-dimethylthiazol-2-yl)-5-(3-carboxymethoxyphenyl)-2-(4-sulfophenyl)-2H-tetrazolium) (MTS dye) and electron coupling agent phenazine methosulfate. MTS is metabolised to form formazan in the mitochondria of living cells, resulting in colour change from yellow to brown that is indicative of cell number. After sufficient colour change was observed (following 1 - 1.5 h incubation), absorbance was measured at 490 nm, with a reference wavelength of 630 nm at each time point using an absorbance plate reader (M200, Teccan, Männedorf / Switzerland). The plates were measured along with a standard plate of known cell concentrations prepared for each time-point (Figure 4.1).

Between time-points, MTS-containing medium was aspirated, the cells rinsed with PBS, and replaced with fresh cell culture medium. The metabolic activity of the cells was normalised to the TCP control at the end of experiment.

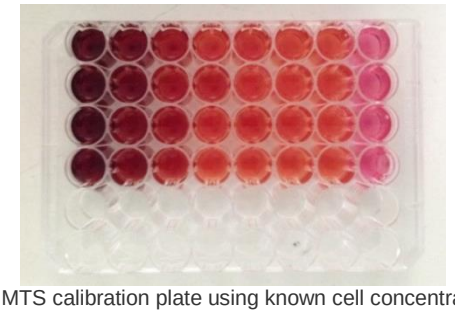

Figure 4.1 MTS calibration plate using known cell concentration values.

4.2.6.3 Live-Dead Assay

The scaffolds (10 rpm, 1000 rpm, 3000 rpm and 5000 rpm) and the commercial SIS were prepared as described previously and in placed in identical arrangements using 24-well plates and CellCrown inserts. The control wells used in this instance were 24-wells with sterile glass coverslip inserts. The glass inserts were simply placed at the bottom of the wells. HEMSC were seeded at a density of 100,000

cells/cm^2. The cells were cultured for 1 day, 7 days and 14 days. At the relevant time points the medium was removed from the wells and a mixture of Calcein AM at a concentration of 4 µM along with Propidium Iodide (PI) at a concentration 20 µM were added in a total volume of 1 ml. The time of incubation was 30 m in the dark and care was taken to ensure that the labelling dyes were not overly exposed to light. The scaffolds were washed with PBS twice and then removed and placed in 50 mm individual wells and then immersed in PBS. The scaffolds were then analysed using a Olympus BX51 confocal microscope. The software used was Lasersharp 2000 and image stacks of the scaffolds were generated. The outputs of the image stacks were merged and then projected into 3D using ImageJ. The 3D projection allowed for direct cell counting within the 3D structure of the scaffolds.

4.2.7 VEGF Incorporation

4.2.7.1 Sample Preparation

SIS/PLGA sample were cut to dimensions 6 mm × 6 mm as used in previous analysis studies. A quantity of 10 µl VEGF (Human Recombinant VEGF, Invitrogen, Camarillo, CA, USA) was added to a solution of 0.1% Bovine Serum Albumin (Sigma) which has been filtered through a 0.22 µm pore sterile filter (Millex®GP, Merck Millipore Ltd. Tullagreen, Co. Cork, Ireland). In sterile conditions the solution was added in very small increments of a maximum of 15 µl to each SIS/PLGA sample up to the required quantity of 500 ng of VEGF per scaffold sample. Following each addition of 15 µl the solution was allowed to dry in the fume hood prior to the addition of the next 15 µl.

4.2.7.2 VEGF Release

The VEGF was added to samples of the PLGA-SIS scaffolds from the 3 sample groups consisting of 10 rpm, 3000 rpm, 5000 rpm, 10 rpm (+VEGF) , 3000 rpm (+VEGF), 5000 rpm (+VEGF) and a commercial SIS. The scaffolds were then individually placed in 15 ml falcon tubes and immersed in 3 ml of solution of PBS with 1% Penicillin-Streptomycin. All tubes were then placed on an orbital shaker (Stuart Model SSM1) and then placed inside an incubator at 37°C and run for 14 days. At days 1, 7 and 14 aliquots of 150 µl were taken and frozen at -80°C.

The VEGF was quantified using a VEGF Human ELISA Kit (Invitrogen, Camarillo, CA, USA). The aliquots were diluted by a factor of 100 to bring the concentration of VEGF into the range of the specific kit (range of kit sensitivity was 0 to 1500 pg mL^{-1} Hu VEGF). The concentration was established through the use of an absorbance plate reader (M200, Teccan, Männedorf / Switzerland). The values were obtained through the use of a standard curve.

4.2.8 CAM Assay

The samples were prepared to a size of 6 × 6 mm cut from the scaffolds. The samples tested in this experiment were the PLGA-SIS scaffolds produced at speeds of 10, 3000, and 5000 rpm. The scaffolds were also separately tested with the addition of VEGF. The addition of VEGF was carried out by first adding the VEGF (recombinant human VEGF; Sf21-derived, 293-VE, R&D Systems, Inc, Minneapolis, USA), to a solution of 0.1% Bovine Serum Albumin (Sigma). In sterile conditions the solution was added in very small increments of a maximum of 15 µl to each SIS/PLGA sample up to the required quantity of 500 ng of VEGF per scaffold sample. Following each addition of 15 µl the solution was allowed to dry in the fume

hood prior to the next quantity. All samples were sterilised by ethylene oxide at 37°C (Person EO50, Person Medical Co., Ltd., Gunpo-si, Gyeounggi-do, South Korea). In addition to the test samples a negative control group was also tested (for all samples $n = 5$).

The method carried out was a modification of the basic methods which have been described previously (Storgard, Mikolon *et al.* 2005). The eggs were first incubated for 12-days in a custom built incubator with care taken to rotate the eggs regularly (Figure 4.2a). Following incubation the eggs were removed and the air pocket was identified by shining a small light source at the egg in a darkened room. Over this air pocket, following a wipe with 70% ethanol, a small hole was bored in the egg shell with care taken not to perforate the inner membrane. Using a sterile needle 2 ml of albumin was removed through the air pocket from the egg and discarded. Any eggs in which the yolk was perforated were discarded.

Following a further wipe with 70% ethanol the holes were sealed up with porous surgical tape and the eggs were returned to incubation for a further 24 hours. Following this period the removal of the albumin would have facilitated the creation of a larger air pocket. The hole was then opened and following a further wipe with 70% ethanol, a larger hole was cut with approximately a 1 cm diameter. It was important at this stage to confirm the viability of the eggs as a reasonable proportion of the eggs were expected to fail due to the procedure being highly technique-sensitive. This was mitigated by the preparation of twice the amount of eggs than experimentally required. Through this hole the scaffold samples were carefully placed onto the CAM using a pair of sterile forceps (Figure 4.2b).

This hole was then covered with a piece of shell with intact inner membrane taken from discarded eggs and then fixed into place using surgical tape. The eggs were

placed in a different incubator (Kingsuro max20, Rcom, Seoul, Korea) with a rocking rotational method and more accurate incubation conditions as shown in Figure 4.2c

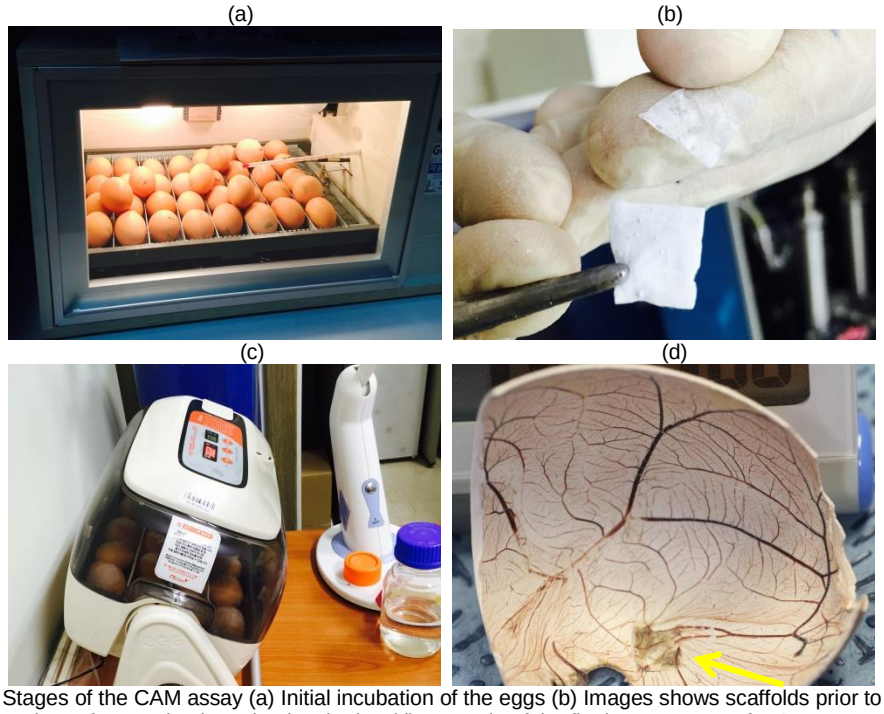

Figure 4.2 Stages of the CAM assay (a) Initial incubation of the eggs (b) Images shows scaffolds prior to insertion (c) Tilting incubator for post implantation incubation (d) Example of the final appearance of a CAM on a portion of egg shell. Yellow arrow indicated the remnants of the scaffold

After incubation the holes were exposed and them 10 - 15 ml of 10% formalin (in PBS) where then injected into the vital part of the eggs. The eggs were then left at room temperature for 24 h. Following this the contents of the eggs was discarded and the shells with the intact CAM's were preserved (as seen in Figure 4.2d). High resolution digital images were then taken of the CAM's. Image analysis was carried out using a custom software package Angioquant (Niemisto, Dunmire *et al.* 2005). The quantification processes the images to identify vessel complexes and produce a vessel "skeleton" from which the calculations are derived. The calculations are carried out using a stepwise imaging processing methodology involving thresholding, segmentation and further modifying processes (Figure 4.3).

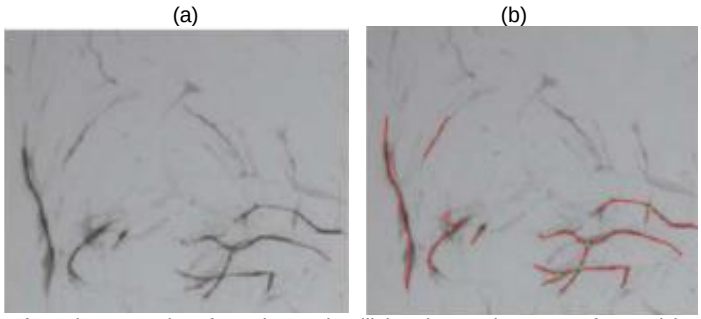

Figure 4.3 Examples of test images taken from the work utilising the Angioquant software (a) Pre-processed image (b) Post-processed image showing highlighted "skeleton" of the vessel complex (Niemisto, Dunmire *et al.* 2005)

4.2.9 *In Vivo* Study

4.2.9.1 Scaffold preparation

The samples were loaded with 35 µl of the VEGF solution to give each sample 500 ng of VEGF. The samples were dried in a sterile fume hood for 24 h.

4.2.9.2 Implantation

This study was approved by and carried out to the standards of Dankook University Institutional Animal Care and Use Committee, South Korea (Appendix C-3). The study was carried out using 22 10-week-old male Sprague–Dawley rats. The rats were kept in a temperature (20 - 24 $^{\circ}$C) and humidity (30 - 70%) controlled environment (30 - 70%), with 12 hour light and dark cycles, and provided with standard pellet foods and water *ad libitum*. Prior to implantation each rat received general anaesthesia via an intramuscular injection of ketamine at 80 mg/kg body weight and xylazine at 10 mg/kg body weight. All surgical procedure was performed under vigorous sterile conditions and within a controlled sterile environment.

For the implantation, the rats were shaved and following a surface wash with iodine solution, a centrally located 2 cm incision was cut along the back of the animal using a scalpel and mayo scissors. From this incision four separate subcutaneous pouches were created by careful instrumentation with the additional use of forceps. Each pouch was located in the region of one of the animal's limbs. In animals which

received samples which were impregnated with the VEGF, only two pouches were created. Within each pouch a single scaffold sample was placed with care taken to place the sample quite deep within the pouch to prevent migration of the sample post implantation. The incision was sutured using monofilament 4-0 absorbable suture material (Prolene). The animals were then returned to the conditions previously mentioned.

During and after surgery, the rats were kept in a temperature controlled environment with rats housed two per cage (identical samples groups but euthanized at different time points). The animals were provided with standard pellet food and water ad libitum.

4.2.9.3 Histological Assessment

The animals were sacrificed at 7 days and 14 days post implantation. The tissue samples were harvested and then fixed in 10% neutral buffered saline for 24 hours. The tissue samples were then immersed in a graded ethanol series for dehydration, and then were embedded in paraffin. Histological sections were cut at a 5 µm thickness from the paraffin blocks using a rotary microtome (Leica RM2245, leicabiosystems, Germany) and were then stained with haematoxylin and eosin (H&E).

4.2.9.4 Digital Image Acquisition and Analysis

The stained slides which were the digitally scanned using a digital slide scanner (Nanozoomer, Hamamatsu, Hamamatsu Photonics K.K., Shizuoka, Japan). Very large high resolution images were then produced of the samples with easily identifiable “encapsulated scaffold” and “surrounding granulation tissue” regions. These images were then sliced into smaller images and categorized according to the regions mentioned. This allowed analysis to be carried out on images which

were of manageable resolution which could be handled by the software used. For region analysis slices were randomised and analysed for each sample group. Cell type counting was carried out using the ImageJ manual cell counting tool.

Nuclei counting was carried out to approximate the number of cells present. The presence of foreign body giant cells made this difficult as these cells could have large numbers of nuclei all of which could not be distinguished from single nuclei by the software methodology. However with the developmental path of FBGC's originating with single macrophages this was deemed a suitable approximation for cell number. Nuclei counting was carried out using Image J. Images were first run through a colour threshold to isolate the stained nuclei. The images were then converted to 8-bit black and white images. The watershed feature allows for clustered particles to be split into individual ones. A particle count was then carried out using the Analyse Particle feature with the parameters defining the size and the circularity expected of a nuclei.

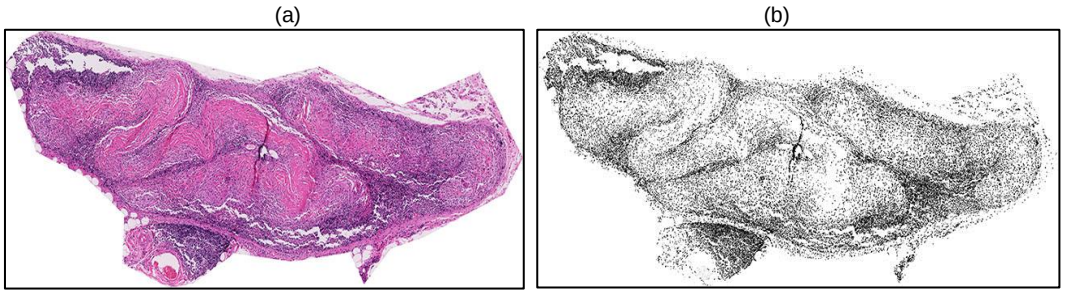

Figure 4.4 Histological image before (a) and after (b) processing to allow for nuclei (particle) counting. The process was carried out using ImageJ software and using mutilple stages described in Section 4.2.9.4.

4.2.10 Analysis

Normal distribution statistical testing was carried out using a 2-tailed student's t-test to a 95% confidence interval. In the case of the mechanical testing basic statistical assessment of the data showed that it did not fit normal distribution models and therefore non-parametric statistical analysis methods were utilised. The median

was found to be a better measure of central tendency than the mean for this type of data and is used in all the mechanical analysis. The group sample data was compared for significant differences using Kruskal-Wallis non-parametric analysis which indicates the presence of significant statistical differences between individual groups. Further analysis was also carried out by post hoc pairwise analysis (Dunnett's Test). All statistical significance tests were done using SPSS versions 20 or 21 (IBM Corporation)

4.3 - Results

4.3.1 SEM Analysis

Analysis was carried out on SEM images a sample of which are shown below in Figure 4.5. All electrospinning variations are listed in Table B1 (Appendix B-3).

(a) 10rpm

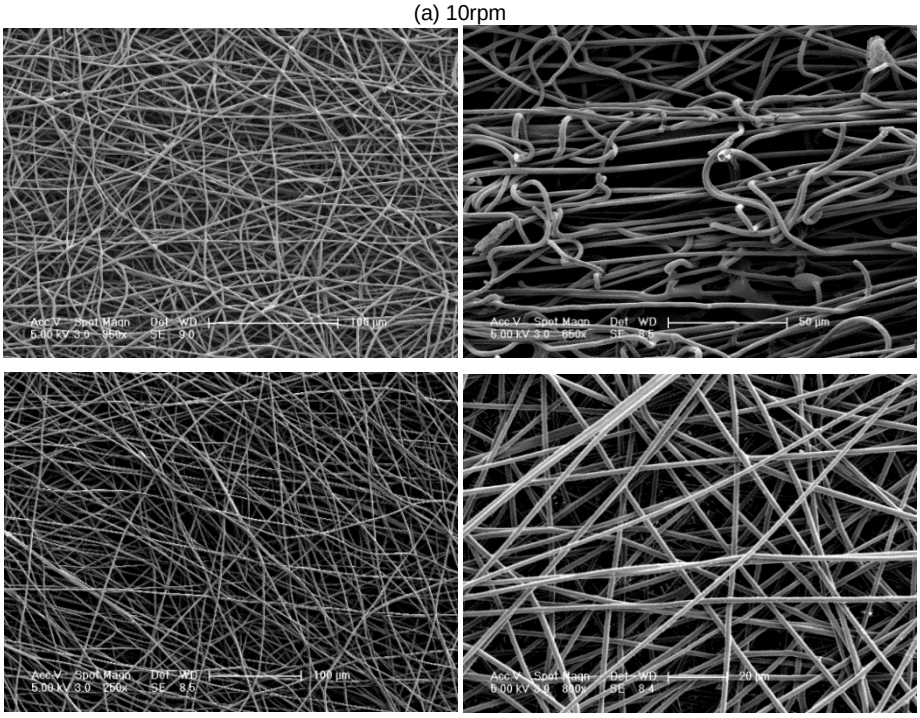

(b) 1000 rpm

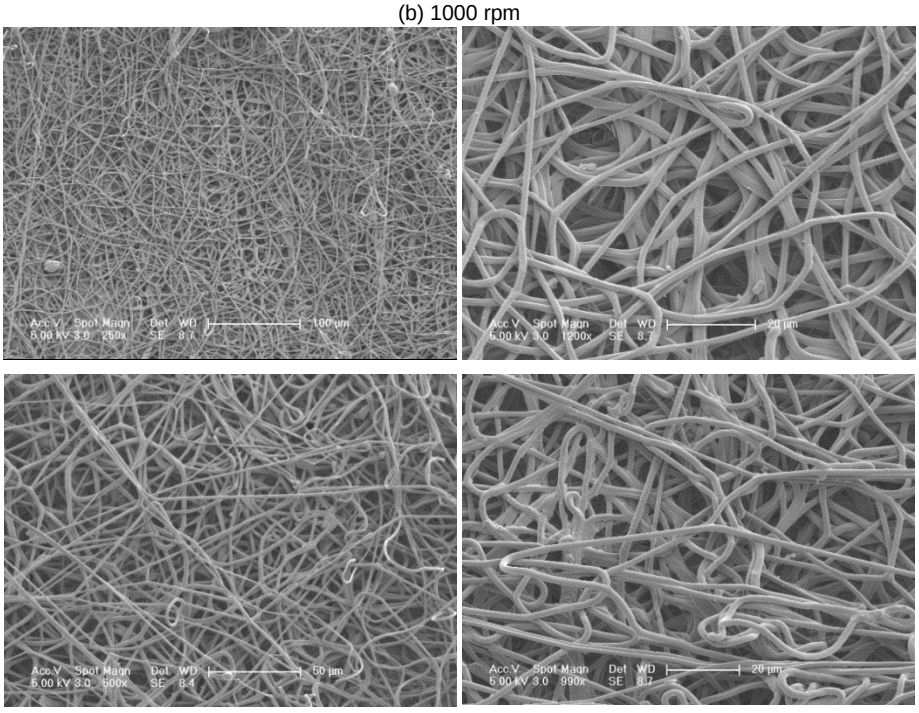

(c) 2000 rpm

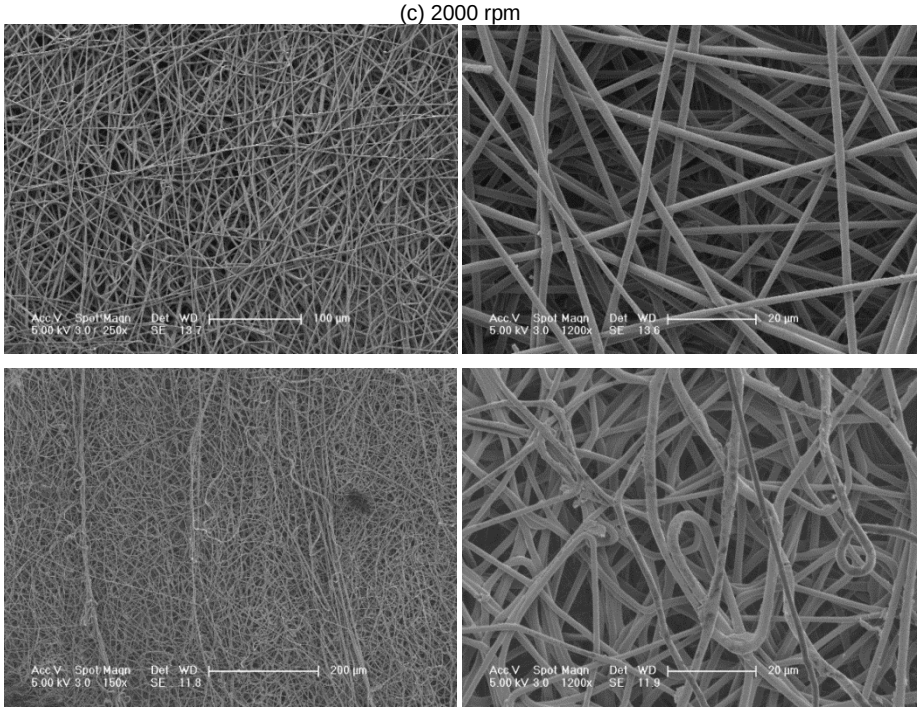

(d) 3000 rpm

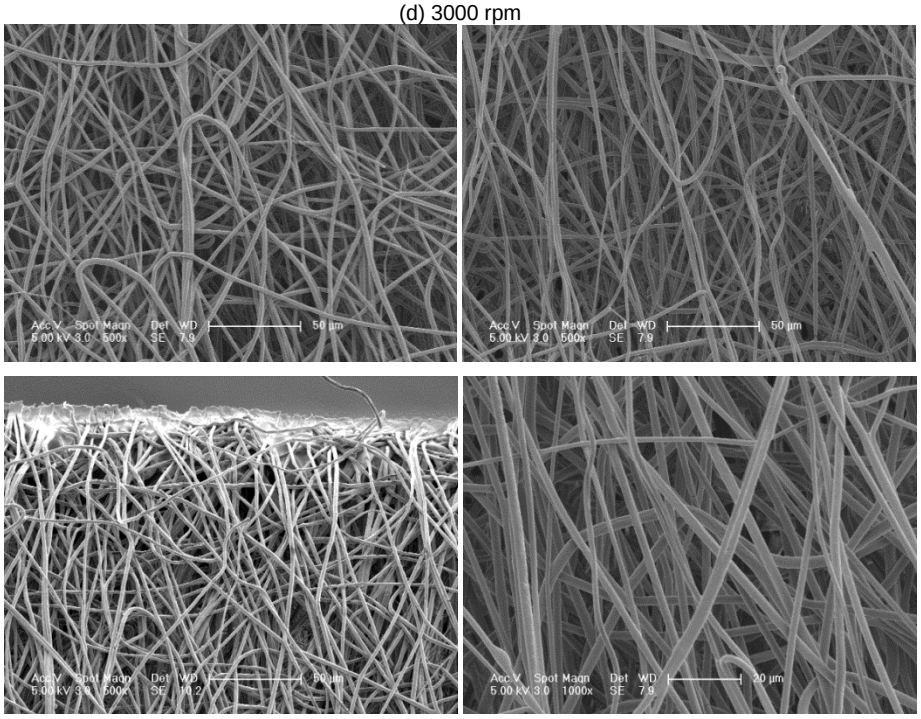

(e) 4000rpm

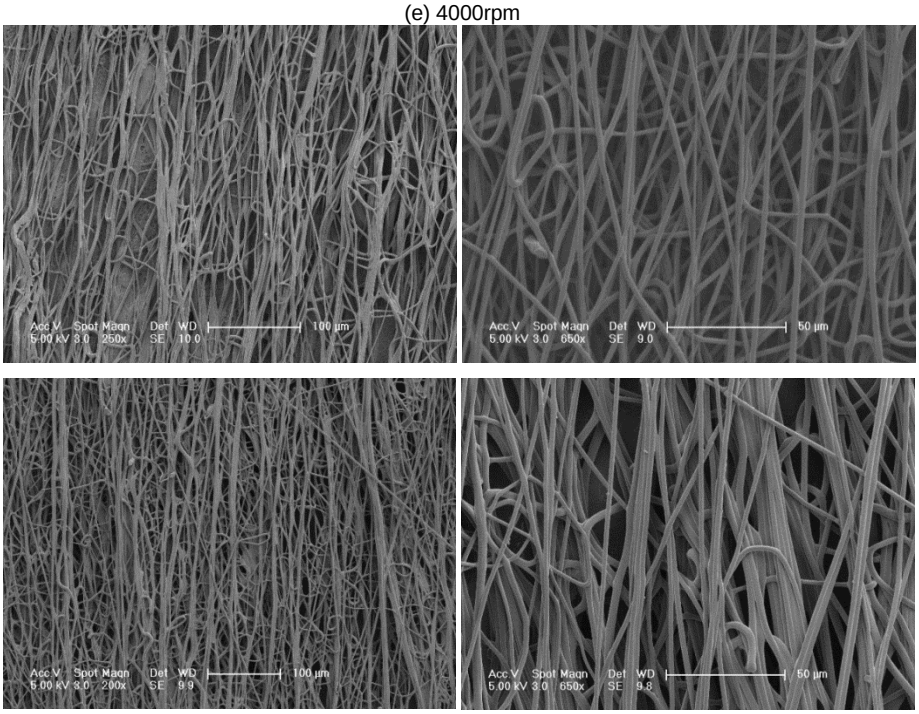

(f) 5000 rpm

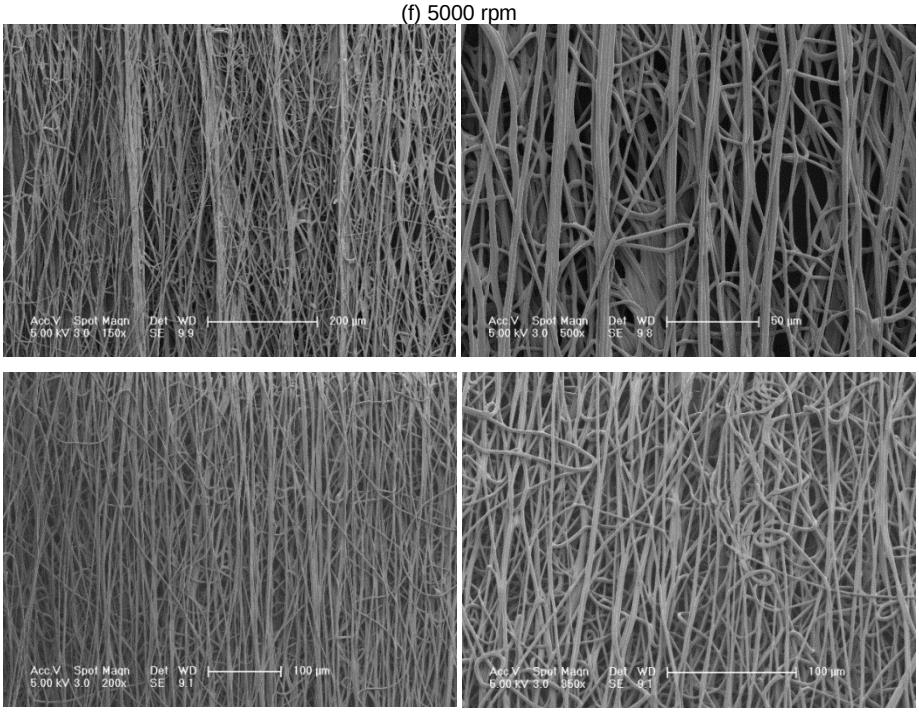

Figure 4.5 SEM images of the PLGA electrospun fibres spun onto SIS at varying mandrel rotational speeds; (a) 10 rpm (b) 1000 rpm (c) 2000 rpm (d) 3000 rpm (e) 4000 rpm (f) 5000 rpm. All images are aligned perpendicular to the mandrel with fibres running left to right being parallel with the mandrel.

4.3.1.1 Fibre Diameter

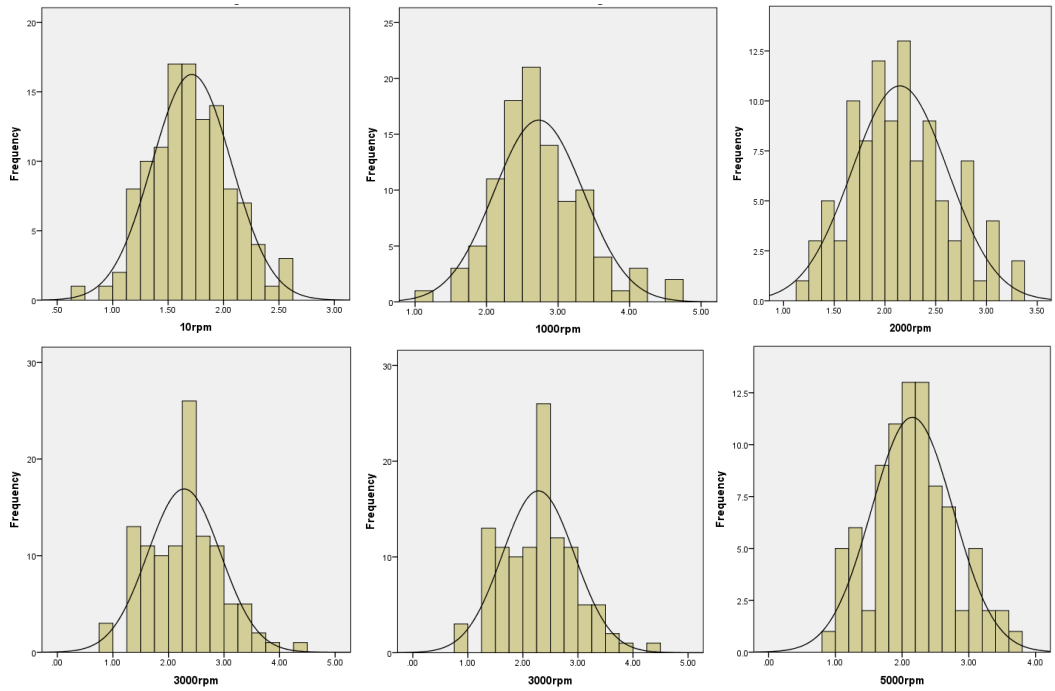

Figure 4.6 Frequency histograms of the fibre diameter data for the samples of PLGA fibres collected on a rotating mandrel at different speeds of rotation. The histograms are overlaid with an ideal normal distribution.

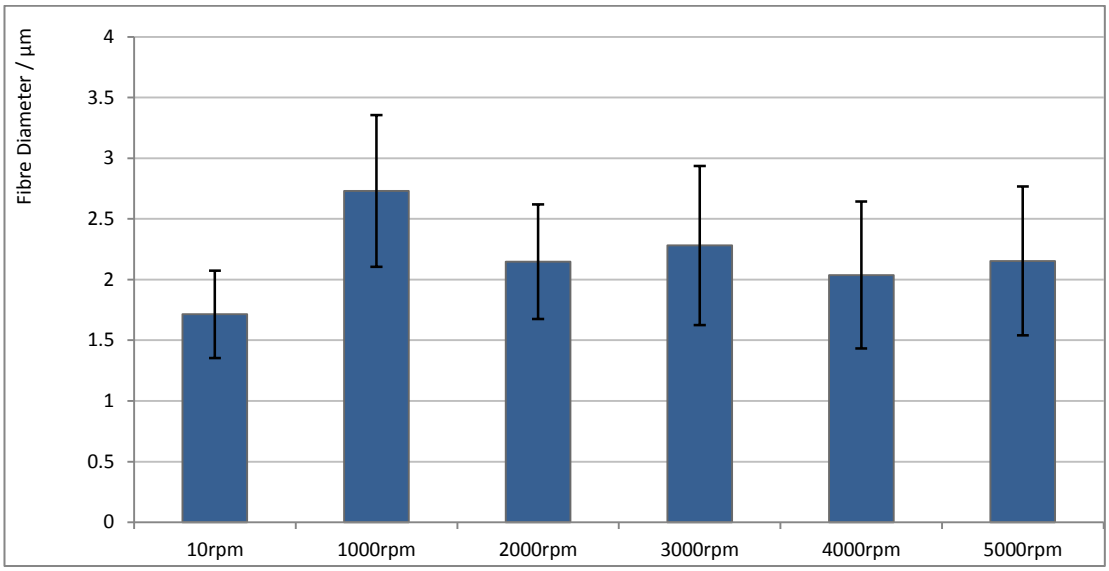

Figure 4.7 The average fibre diameter of electrospun PLGA fibres collected on a rotating mandrel at different speeds of rotation. Analysis was carried out on SEM and the diameters measured using software (Image J) (*n* = 50+). Error bars are standard deviation.

The analysis of the fibre diameter was carried out to ascertain whether the higher rotational speeds in this chapter would result in changes in the diameter of the PLGA fibres.

The first observation of the data was that all groups produced a range fibre diameters which were normally distributed (Figure 4.6). Further analysis of average fibre diameters, shown in Figure 4.7, showed that throughout the entire range of rotational speeds investigated in this work there were no statistically significant differences in the diameter of the fibres produced (the test was carried out with a two tailed T-test). The values of the mean fibre diameters were in the range of 1700 - 2700 nm, with the actual values of fibre diameters being in the 800 - 3000 nm range. The reason for the fibres to be characterised as nanofibres, as opposed to the alternative classification of “microfibres”, is that the range of fibres are all found to be less than 3 micrometres which represents a very small fraction of the µm scale, and a large proportion actually being in the actual nano-scale range.

4.3.1.2 Fibre Alignment

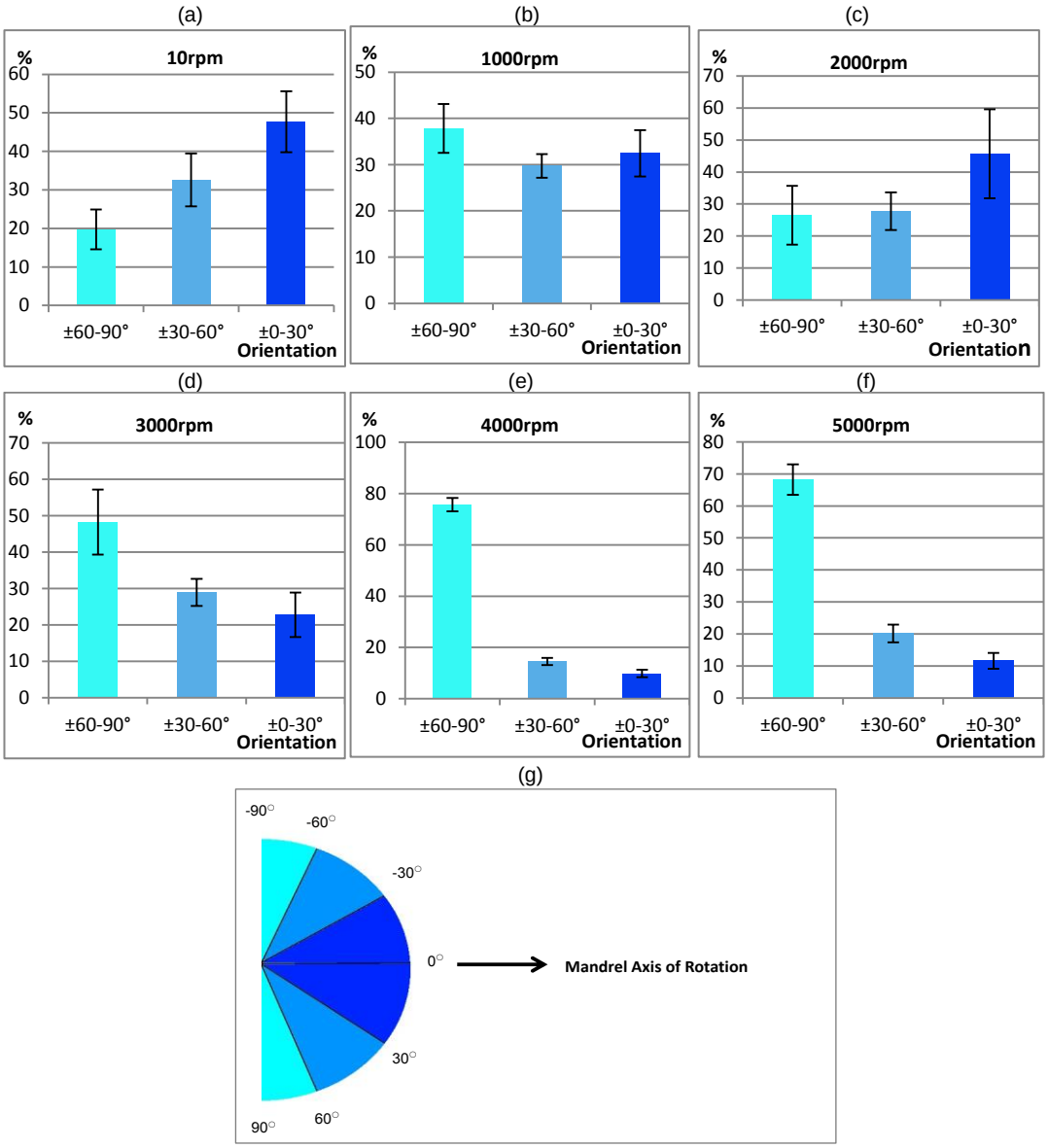

Figure 4.8 PLGA fibre orientation when electrospun onto SIS at different mandrel rotation speeds (a) 10 rpm (b) 1000 rpm (c) 2000 rpm (d) 3000 rpm (e) 4000 rpm (f) 5000 rpm (g) Legend illustrating the fibre orientation relative to the axis of rotation of the mandrel (shown in degrees removed from the axis of rotation) (*n* = 10 - 20). The error bars are standard deviation.

The fibre alignment data shows a very clear trend in the alignment of the fibres (Figure 4.8). As in the previous chapter, it was confirmed that increasing the mandrel's speed of rotation results in an increase in the alignment of the electrospun fibres PLGA fibres perpendicular to axis of rotation. The higher speeds above 3000 rpm showed an increase in alignment however there was little difference the samples produced at 4000 and 5000 rpm.

Some additional work was carried out to ascertain whether the aligned fibres produced aligned cells when cultured on the scaffolds. However due to the three-dimensional nature of the scaffold and the propensity for the calls to grown down into the scaffold, cells growing on the surface of the scaffold were difficult to fix and view from a top-down SEM perspective. While this was attempted this method was found to be inconclusive. That said, there was some partial indication of the orientation of the cells following the direction of the fibres onto which they were cultured in a few images (Figure 4.9).

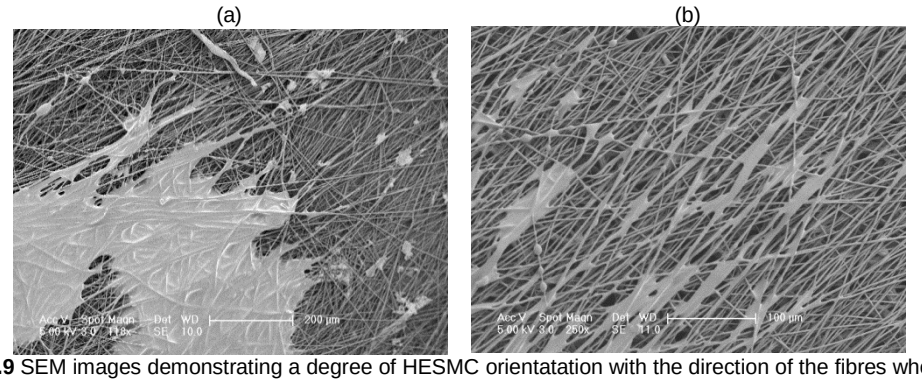

Figure 4.9 SEM images demonstrating a degree of HESMC orientatation with the direction of the fibres when cultured onto the scaffolds produced at (a) 10 rpm and (b) 3000 rpm.

4.3.1.3 Scaffold Thickness

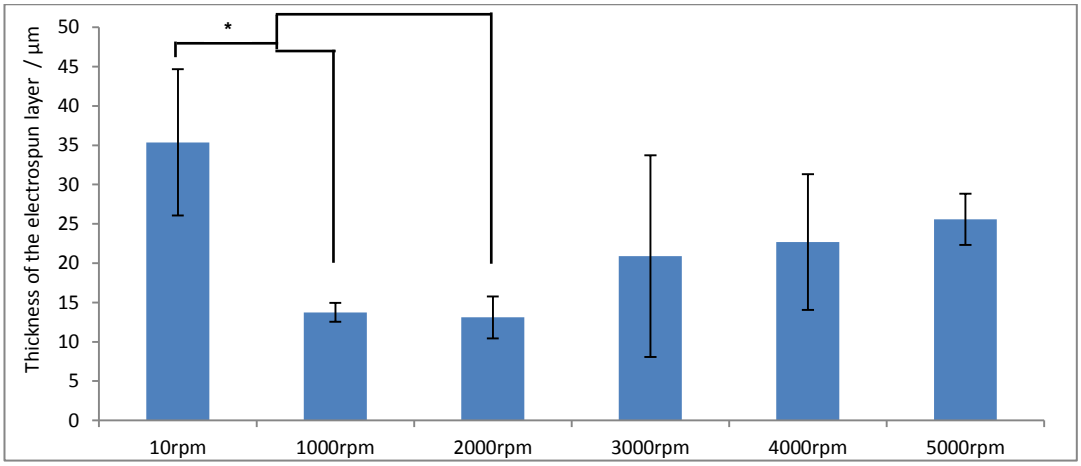

Figure 4.10 The average thickness of the PLGA electrospun layers produced at different mandrel rotational speeds and onto SIS (*n* = 15+). The error bars are standard deviation. Important values differing significantly from each other are denoted by *; $p < 0.05$.

The data here was averaged from SEM image measurements. In some instances, if the thickness of the electrospun layer was not clear but the total scaffold and SIS thickness were clear and thickness were, the value could be calculated. The thickness of the electrospun layer ranged from 11 - 36 µm, as seen in Figure 4.10. The largest values were the for the 10 rpm sample group. This difference was not found to be statistically significant when compared to the aligned fibres from the 3000-5000 rpm range, quite likely due to the levels of variation, however the difference was definitely substantial and noticeable on visual inspection. Care was taken to ensure that the thickness of the electrospun layer was not allowed to get too large and all the samples were produced without the scaffold thickness affecting the electrospinning process. Earlier test work demonstrated that at higher thickness levels the spinning behaviour of the arrangement would change.

4.3.2 Mechanical Testing

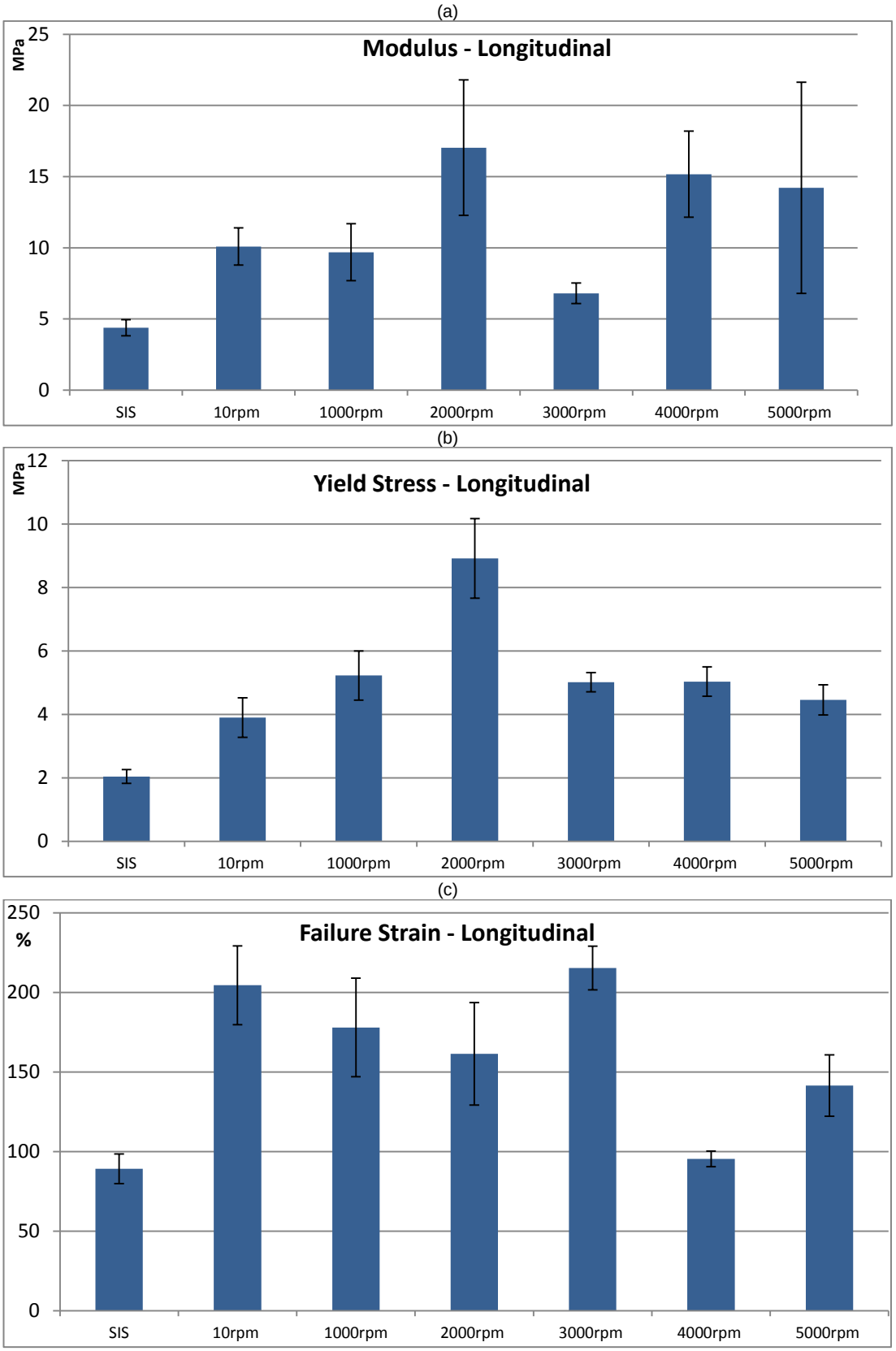

Figure 4.11 Mechanical testing data from the longitudinal tensile testing of the PLGA-SIS showing (a) Elastic modulus values (MPa) (n = 12) (b) Yield stress values (MPa) (n = 12) (c) Failure strain values (%) (n = 12). Error bars shown are the standard error. Statistical analysis was done non-parametrically and discussed in the results sections.

(a)

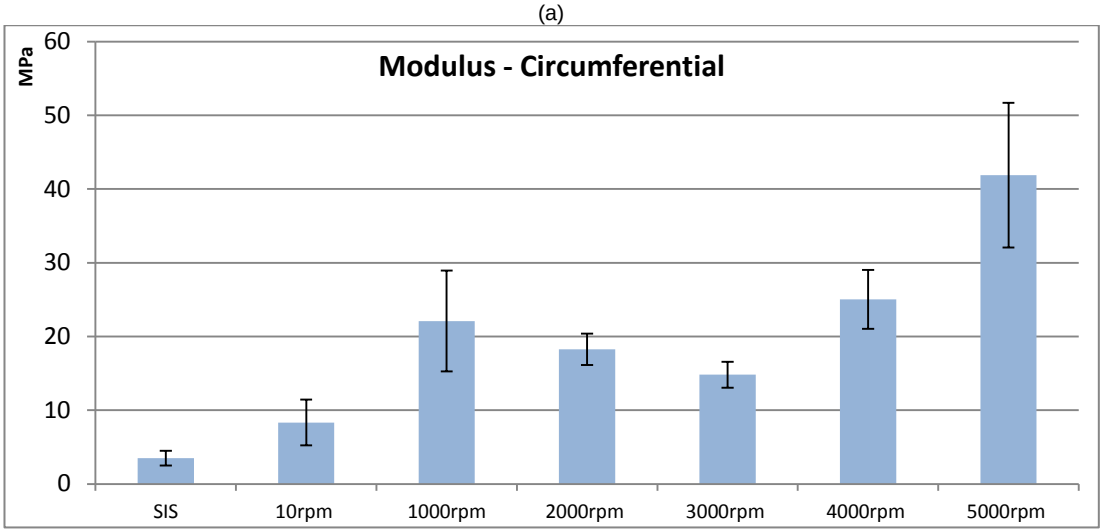

(b)

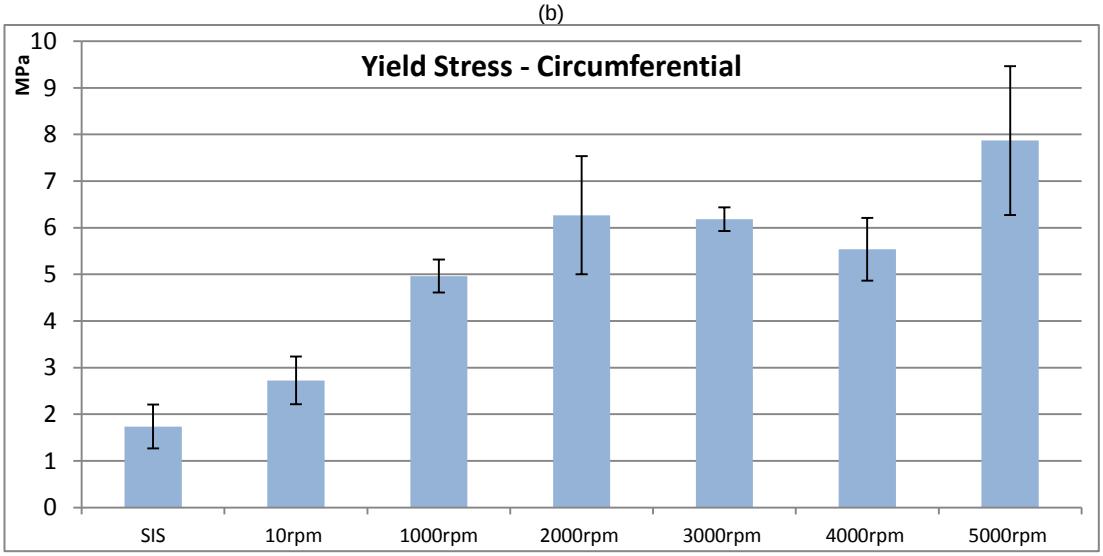

(c)

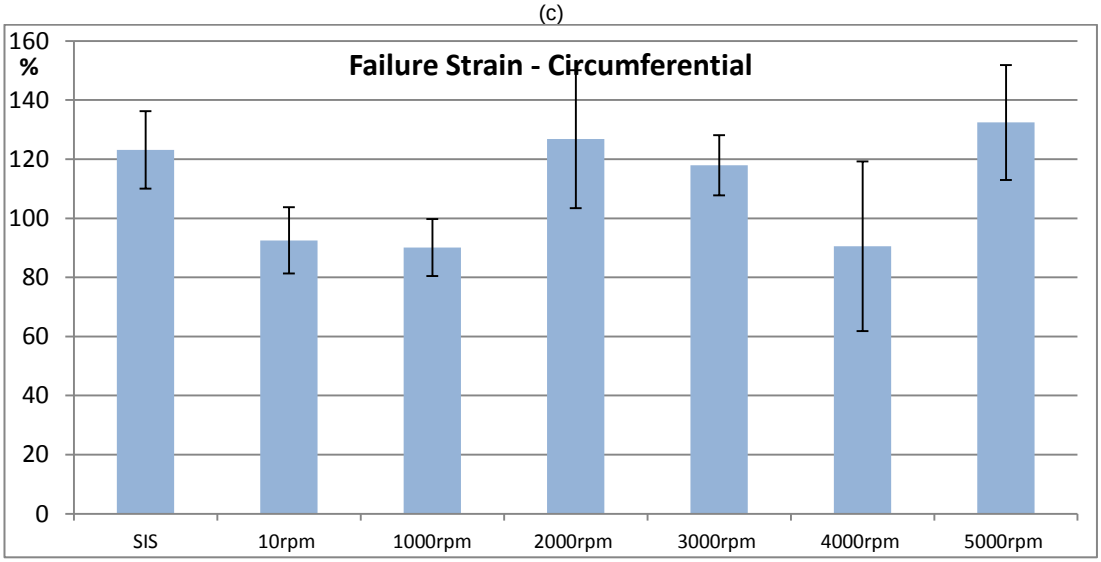

Figure 4.12 Mechanical testing data from the circumferential tensile testing of the PLGA-SIS showing (a) Elastic modulus values (MPa) (n = 8) (b) Yield stress values (MPa) (n = 8) (c) Failure strain values (%) (n = 8). Error bars shown are the standard error. Statistical analysis was done non-parametrically and discussed in the results sections.

A general observation made in the mechanical testing in this chapter was that a lower proportion of the stress-strains curves produced with the scaffolds were of the distinct two stage type which was observed in earlier work in Chapter 3. There were also a number of curves which had features of both categories and produced "stepped" curves which could fall into either category. The criteria for choosing the category into which they fell was unclear and with any distinction being arbitrary it was decided that this could not be quantified. A further general observation was that in nearly all instances of modulus or yield stress the values were higher than those observed in Chapter 3.

As observed in the previous Chapter it was expected that there would again not be large differences between the non-aligned and the highly aligned samples with the longitudinal tensile testing and this was largely again the case (Figure 4.11). While the differences in the modulus did not follow a direct trend all the values were higher than the base SIS so there was an increase with the addition of the PLGA. Yield stress also did not show any distinct trend other than all values being nearly twice as high with the SIS alone. The increase had no trend associated with alignment and was quite constant with the exception of the 2000 rpm sample group which had an elevated value. For the failure strain the values of the test groups were again all higher than the SIS though it was observed that the 4000 rpm sample was only very slightly higher and could be described as having a failure strain value close to that of the control SIS.

In the case of circumferential testing, the modulus values followed a similar lack of trend found in to that found in Chapter 3 (Figure 4.12). Again it was observed that all the values were higher than the SIS alone. It was also observed that for the 5000 rpm sample that the modulus value was found to be extremely high. However, given

the pattern of the other samples it is more reasonable to state that there was no clear trend particularly as the difference in the degree of alignment between the 4000 and 5000 rpm samples is non-existent. In the case of the yield stress there does appear to be evidence of the values generally increasing with the increased alignment of the fibres. For the failure strain values there did not appear to be any trend and with all samples being at levels of at least 85% strain at failure so it could be said that no sample group performed poorly.

4.3.3 Porosity

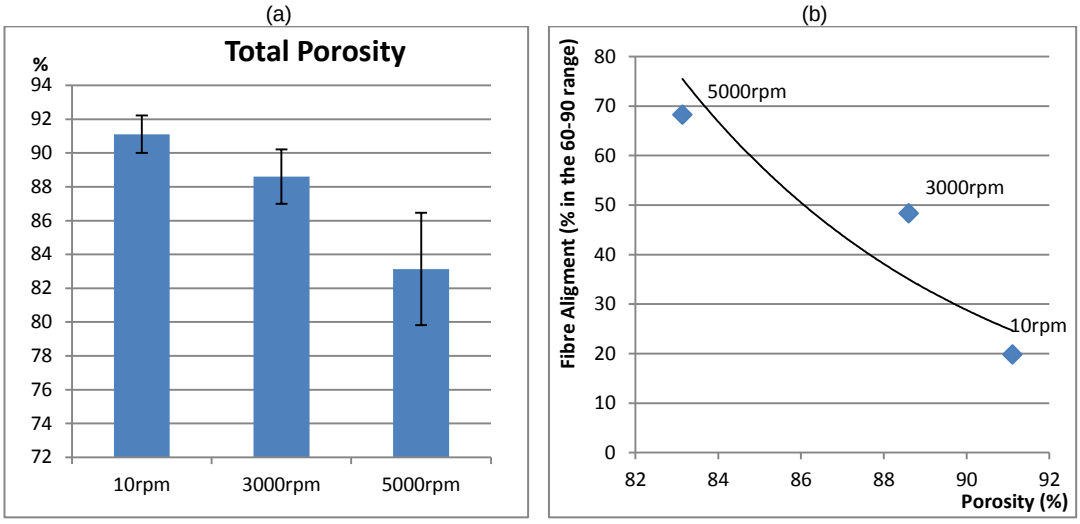

Figure 4.13 (a) Graph representing the porosity of the hybrid scaffolds produced using mercury intrusion porometry (n= 4-6). The errors are bars are standard deviation. (b) Graph illustrating the potential trend between fibre alignment and the porosity of electrospun scaffolds.

The results of the mercury intrusion are shown in Figure 4.13a. The differences between the 10 and 3000 rpm samples, along with the 3000 rpm and 5000 rpm samples, were not found to be significant. However the difference between the 10 rpm and 5000 rpm samples was statistically significant demonstrating that the more random the orientation of the fibres, the higher the degree of porosity. It should also be noted that the porosity levels of all the scaffolds in question were generally quite high and even in the instance of the 5000 rpm sample the porosity was as high as 83.13%.

A further graph was made to assess any relationship between the actual degree of alignment and the porosity and is shown in Figure 4.13b. While there could potentially be indications of a trend for it meaningful a larger sample size would likely be required. That said, the results do show, in part, that the degree of alignment correlated negatively with the porosity.

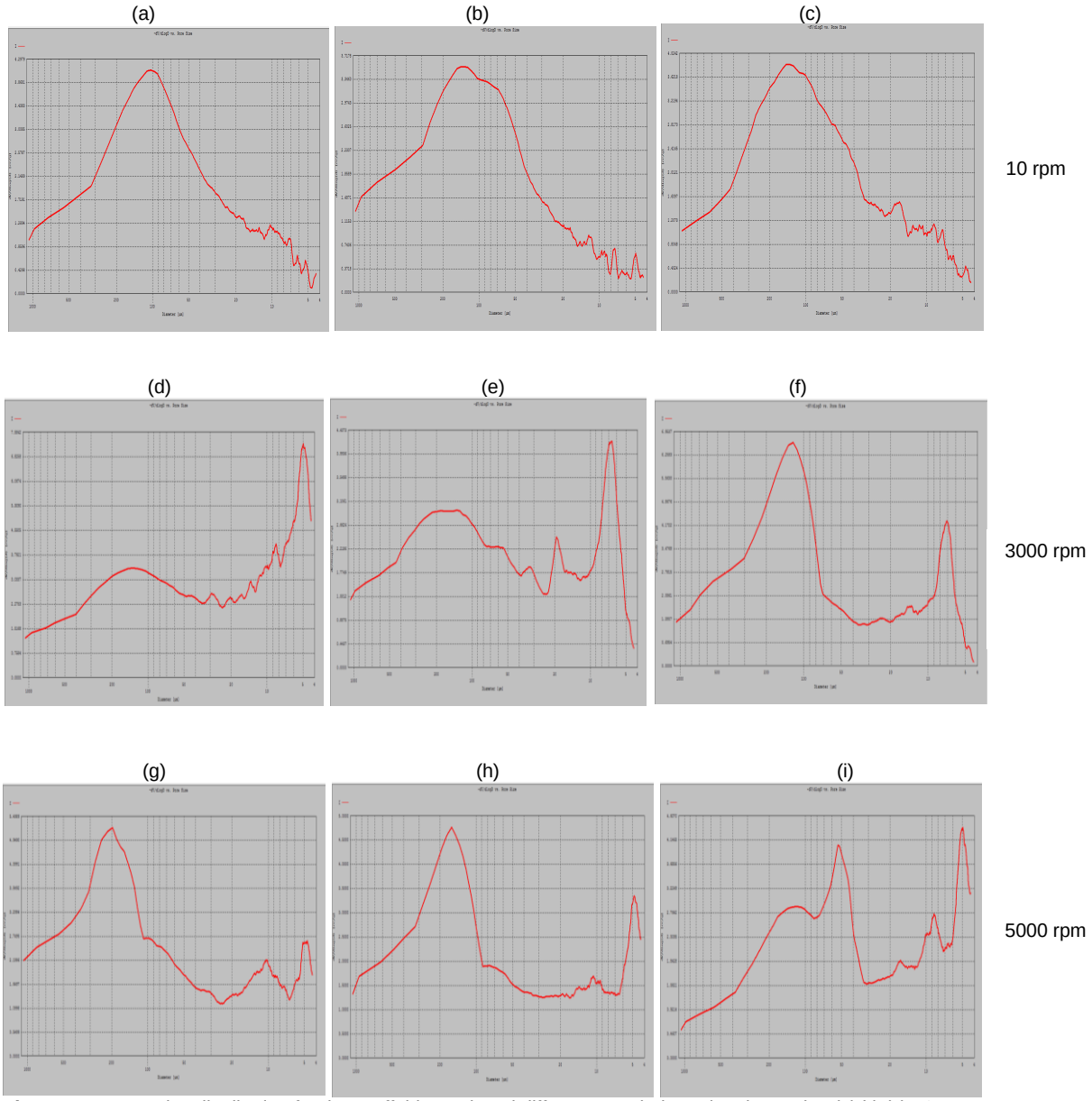

Figure 4.14 Pore size distribution for the scaffolds produced different mandrel rotational speeds: (a) b) (c) 10 rpm (d) (e) (f) 3000 rpm (g) (h) (i) 5000 rpm. The left of the x-axis represents the diameter of the pores in µm. Full size versions of these graphs are in the Figure C2 (Appendix C-2).

In the case of pore size distribution (Figure 4.14), it is quite clear to see that for the randomly organised 10 rpm fibre scaffolds that the values represent a largely

normal distribution of the diameter values centred in the 100-150 µm region. In the case of the 3000 rpm samples the distributions are separated into 2 peaks with a potentially higher peak at the 5 - 7.5 µm region, which shows a large increase in the proportion of very small diameter pores and a reduction in the larger diameter. This trend of 2 peaks continues with the 5000 rpm samples however there does appear to a slight increase in proportion of the larger diameter peak potentially showing a shift to an increase in the proportion of larger pores. It should be emphasized that the distribution of the pores is independent of the total porosity of the scaffold. For clarity, larger versions of the graphs are shown in Figure C2 (Appendix C-2).

4.3.4 Smooth Muscle Actin

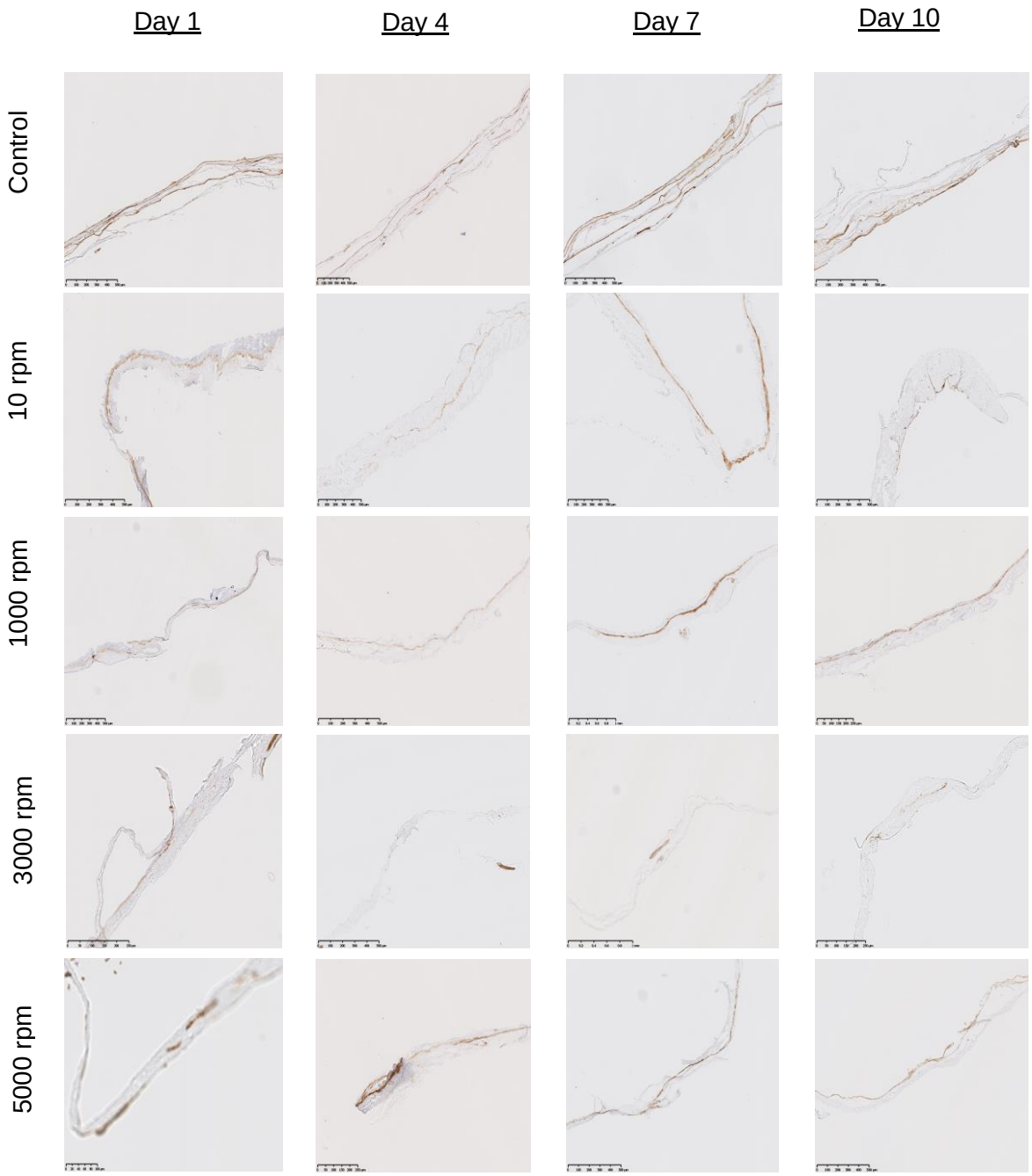

Figure 4.15 Histological images staining for smooth muscle actin (SMA) showing HESMC's cultured on the PLGA-SIS scaffolds at Days 1, 4, 7 and 10, and in 24-well plates. The presence of SMA was detected in all samples and at all time-points.

The scaffold were cultured with HESMC's for the purpose of analysing whether the scaffold impeded the ability of smooth muscle cells from producing smooth muscle actin which is vitally important for the formation of functioning smooth muscle tissue (Rayatpisheh, Heath *et al.* 2013). The results of the SMA staining (Figure 4.15)

demonstrated that SMA was found to be present for all the scaffolds tested and at all the time points.

4.3.5 Biocompatibility

4.3.5.1 Metabolic Activity Assay

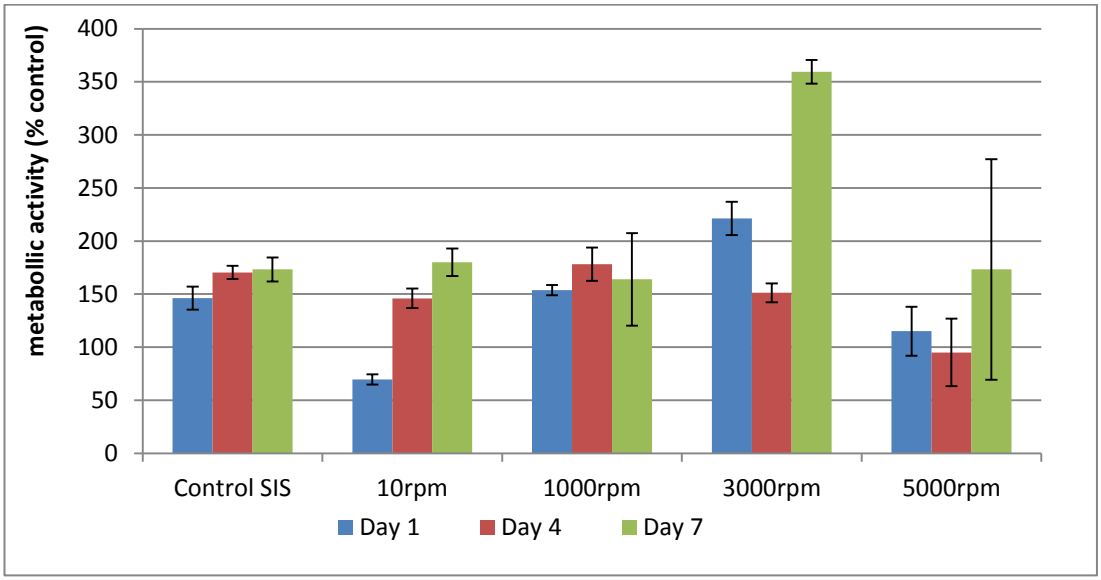

Figure 4.16 Graph representing the normalised levels of metabolic activity as measured by the use of an MTS assay of HESMC's cultured on the scaffold groups at Days 1, 4 and 7. The values are expressed as a percentage of the control (in this case the HESMC's cultured on TCP).

The results of the metabolic activity analysis carried out using MTS were used to evaluate the biocompatibility of the scaffolds (Figure 4.16). What was found was that all the scaffold groups generally performed as well as the control and the commercial (control) SIS. The values of the 3000 rpm scaffold were found to be higher than the other sample groups at days 1 and 7.

4.3.5.2 Live-Dead Analysis

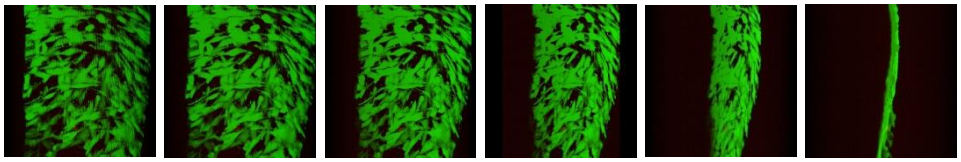

Figure 4.17 Series of confocal images (10 rpm) showing the 3D projections of a stack of confocal images for the purpose of live-dead analysis

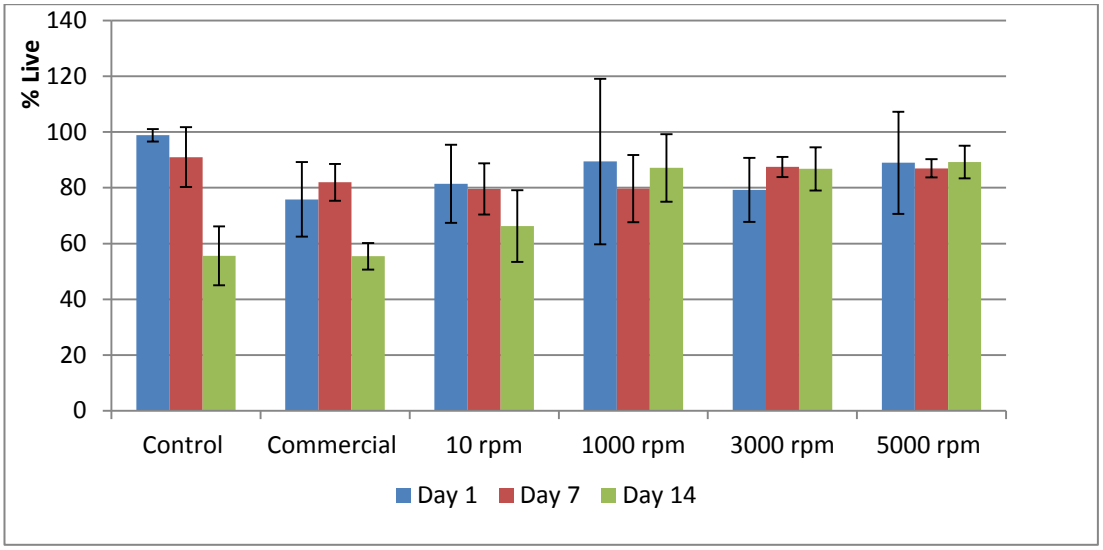

Figure 4.18 Graph representing the percentage of live cells observed by performing a Live-Dead assay on HESMC's cultured on the scaffold groups at Days 1, 7 and 14. The values were obtained cell counts from confocal microscopy images and image stacks (*n* is between 9 and 20 images or image stacks)

As mentioned in Section 4.3.6.3 of the Materials and Method the confocal images of the Live-Dead Assay were created into a 3D projection using Image J a sequence of which is shown in Figure 4.17. What is demonstrated in these images and is that the cultured cells were often found in "seams" which lay inside the 3D structure of the electrospun fibres. There were also a higher concentrations of cells at the base of the scaffold where the SIS was present.

The results of the live-dead assay show a number of important facts (Figure 4.18). Firstly that there was no difference detected between the PLGA-SIS scaffolds which were tested. Secondly, that the PLGA-SIS scaffolds had a similar level of inferred cytotoxicity to the control TCP and the commercial SIS. A final observation was that at day 14 the commercial SIS and the control TCP had higher levels of cell death

though it was noted that the surface area of the TCP wells and the commercial SIS was lower than that of the PLGA-SIS scaffolds.

A further observation was that using the confocal it was easy to identify the alignment of the cells along the orientation of the fibres as seen in Figure 4.19

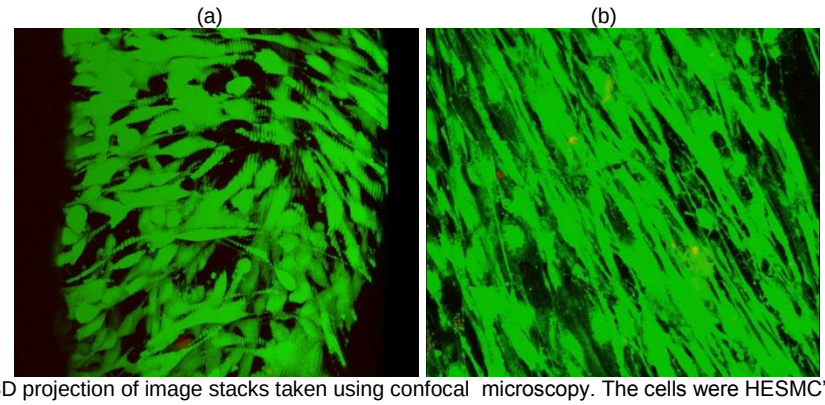

Figure 4.19 3D projection of image stacks taken using confocal microscopy. The cells were HESMC's and cultured in 24-well plates and demonstrate the orientation of the cells within two scaffolds containing different fibre orientations (a) random fibres (10 rpm Day 7) and (b) aligned fibres (5000 rpm Day 14)

4.3.6 VEGF Assay

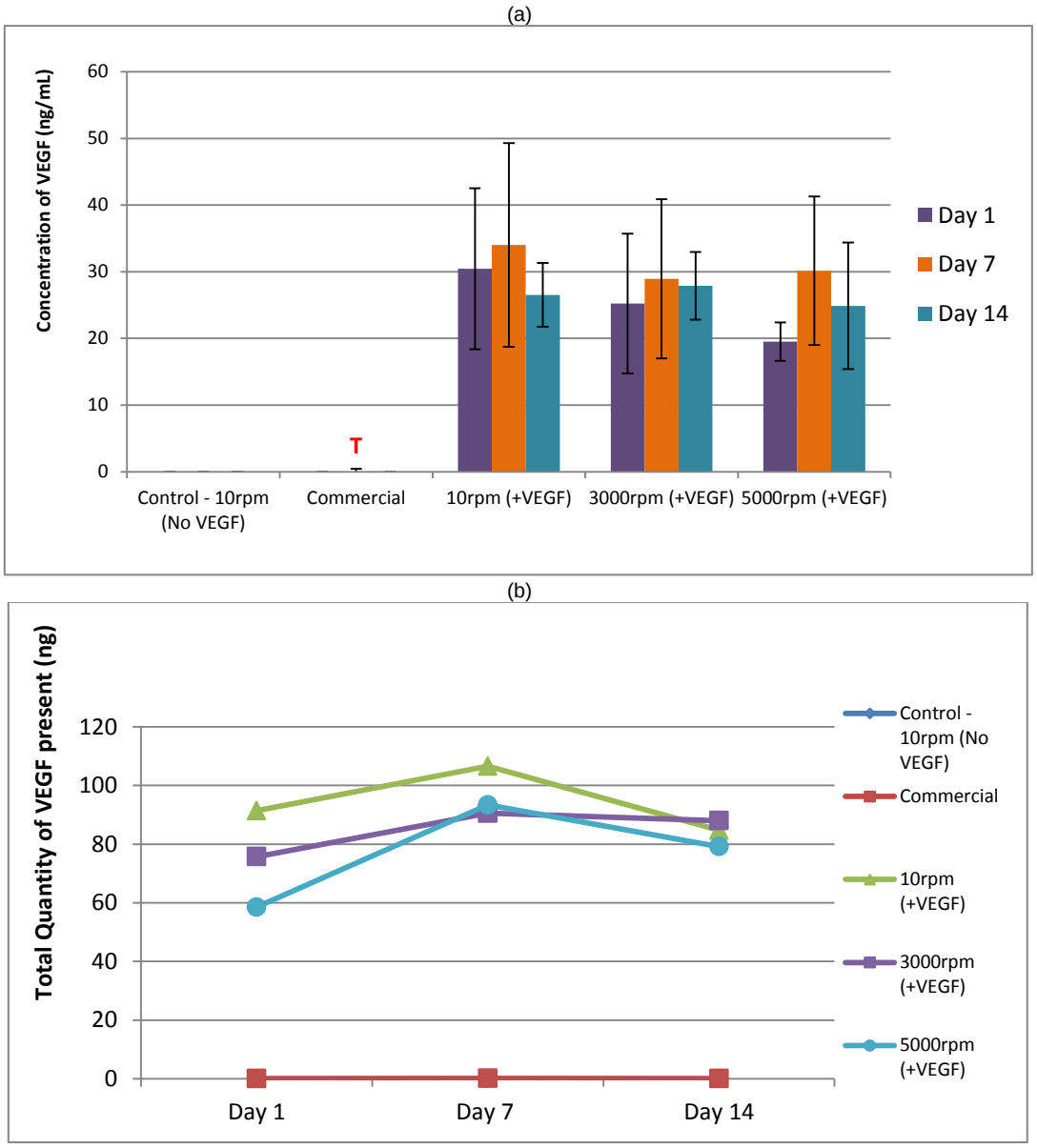

Figure 4.20 (a) Graph representing the concentration of VEGF in solution following scaffold immersed at day intervals of 1, 7 and 14. The "T" denotes a trace amount of VEGF detected in the commercial VEGF on day 7(n = 4 and the error bars are standard deviation). (b) Graph representing the calculated quantity of VEGF present in solution at the same time intervals.

The VEGF assay was carried out to find out i) if the VEGF added to the scaffolds was actually retained and ii) to assess the release profile of the VEGF. The first observation made of the graph shown in Figure 4.20a, is that shows that VEGF was present at detectable levels in all samples to which it added. The VEGF levels did not vary significantly between the samples or over time. It was also noted that a trace amount of VEGF was detected from the commercial control at day 7.

The second graph (Figure 4.20b) shows the same sample data but instead represented as the total calculated quantity of VEGF present in each solution. Here it shows that even the highest average quantity is a little over 100 ng of VEGF. This contrasts with the initial quantity of the VEGF which was 500 ng per sample. This graph also indicated a small fall in the VEGF levels in two of the samples groups between day 7 and day 14.

4.3.7 CAM Assay

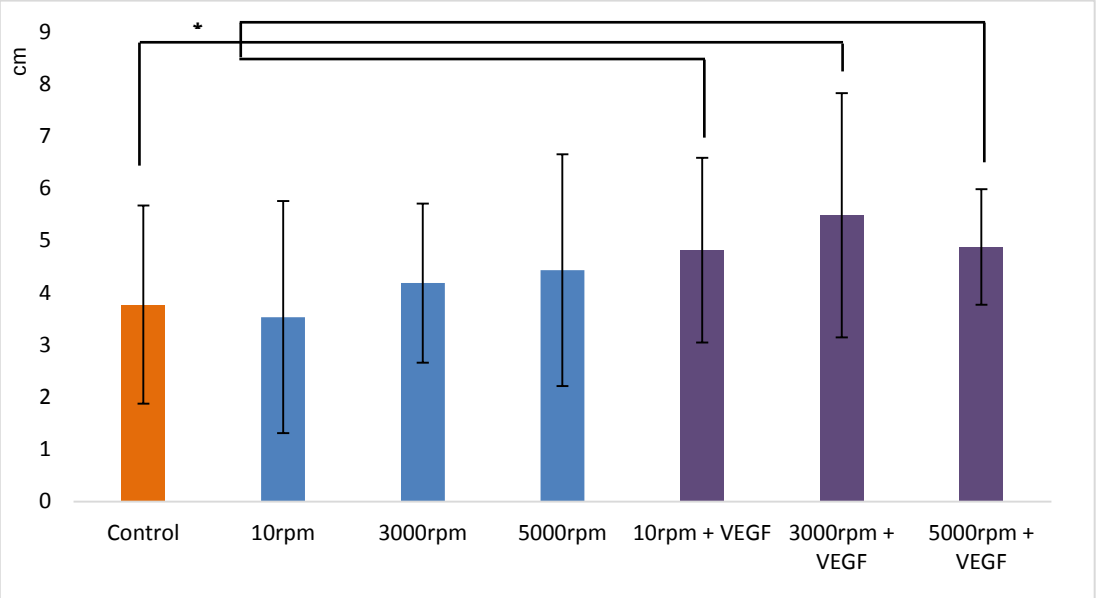

Figure 4.21 The mean length of vessel complex on the CAM as identified by quantification software. The sample groups shown are: Control (*n* = 24), 10 rpm (*n* = 21), 3000 rpm (*n* = 15), 5000 rpm (*n* = 21), 10 rpm + VEGF (*n* = 20), 3000 rpm + VEGF (*n* = 26), and 5000 rpm + VEGF (*n* = 25). The error bars are the standard deviation. Important values differing significantly from each other are denoted by *; $p < 0.05$.

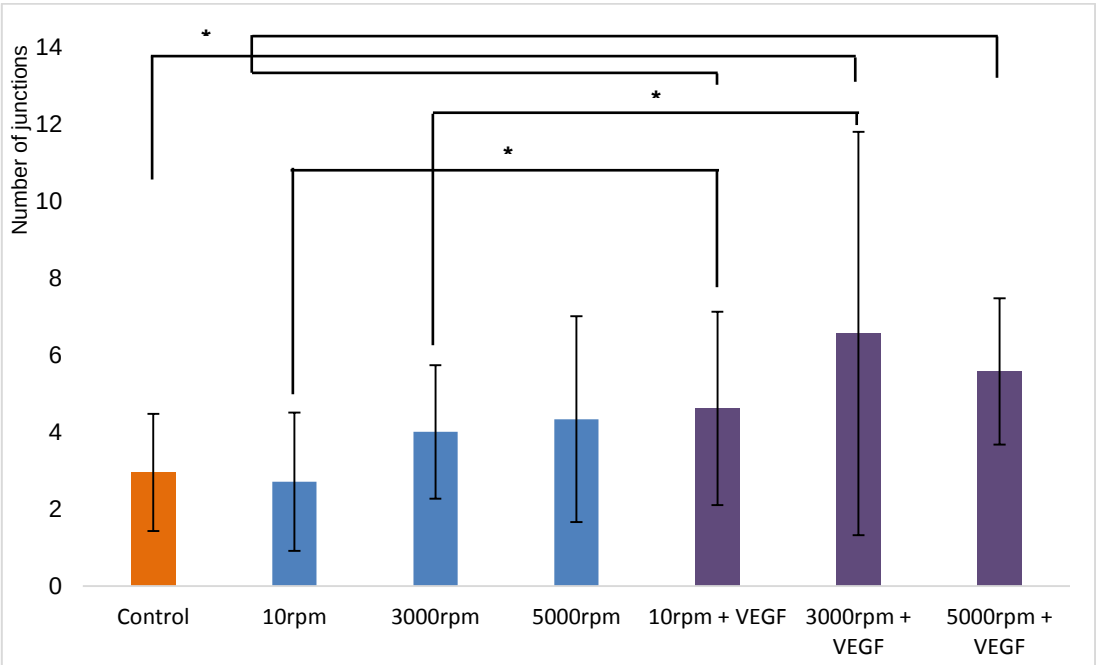

Figure 4.22 The mean number junctions found per vessel complex on the CAM as identified by quantification software. The sample groups shown are: Control (*n* = 24), 10 rpm (*n* = 21), 3000 rpm (*n* = 15), 5000 rpm (*n* = 21), 10 rpm + VEGF (*n* = 20), 3000 rpm + VEGF (*n* = 26), and 5000 rpm + VEGF (*n* = 25). The error bars are the standard deviation. The error bars are the standard deviation. Important values differing significantly from each other are denoted by *; $p < 0.05$.

As mentioned previously the main method of analysis for this experiment were quantified values produced by the Angioquant software. Through this method the data produced was figures for the mean number of junctions and the mean length of blood vessel within each identified vessel complex on the CAM.

Statistical analysis of the data from the average length of the complex (Figure 4.21) found that all samples which lacked VEGF did not differ significantly from the control. It was also found that the samples with VEGF were all statistically larger than the control. When it came to the difference between identical scaffolds with and without VEGF two out of the three were to have larger values with VEGF (the exception being the 5000 rpm groups which was not found to be significantly different). A final analysis was performed where all the non-VEGF samples were combined and were compared with the samples with VEGF and the difference was found to be statistically significant.

The data which was from the mean number of junction is shown in Figure 4.22. Here it was found that in two out of the three samples with VEGF showed no difference with the control (the exception being the 5000 rpm which was found to be larger than the control). All the samples which had VEGF were found to have higher values than both the control samples and their identical non-VEGF samples. It was also found that when the non-VEGF scaffold were combined and compared with the VEGF scaffolds the difference was statistically significant.

4.3.8 *In Vivo* Study

With analysis of the images there was it was observed that there was a district encapsulation of cells around the scaffolds upon implantation. This encapsulation is referred to in this work as the “capsule” and should be differentiated from the fibrous capsule which is a distinct biological formation as the final phase of the inflammatory process. This also differentiates this region form the associated surrounding granulation tissue which was also easily identifiable (Figure 4.23). The cells types and the blood concentration of blood vessels varied in both these regions so they were both analysed independently.

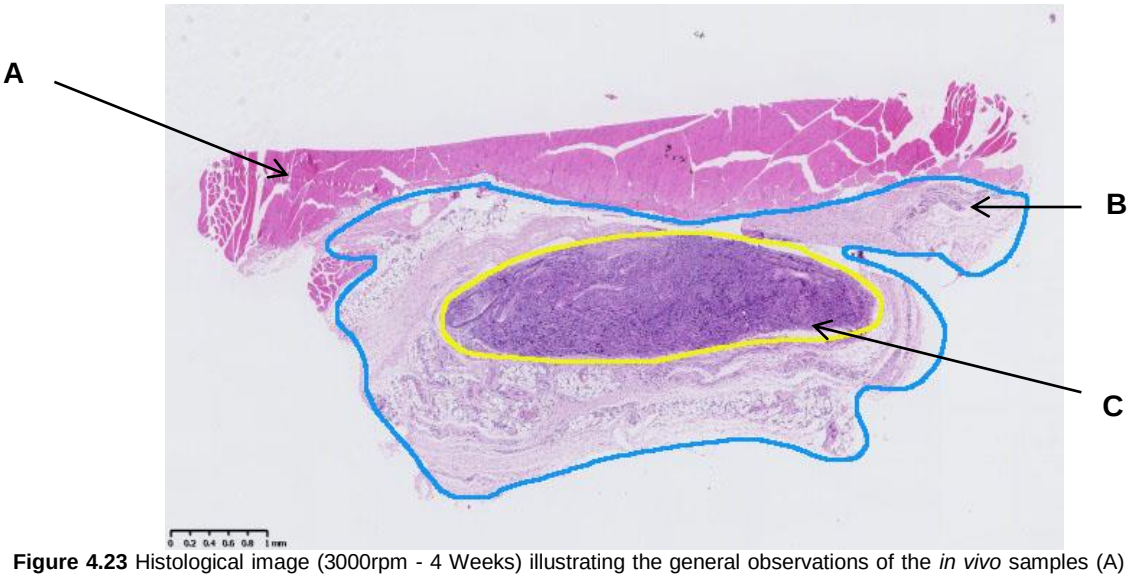

Figure 4.23 Histological image (3000rpm - 4 Weeks) illustrating the general observations of the *in vivo* samples (A) Indicates the underlying muscular tissue (B) The blue line outlines the surrounding granulation tissue (with the encapsulated scaffold within it) (C) The yellow line outlines the “capsule” of cells which forms around the scaffold.

Four cell types were chosen for analysis; eosinophils, lymphocytes, foreign-body giant cells (FBGC) and monocytes (Figure 4.24). It was also observed that the surrounding connective (granulation) tissue was predominately where the blood vessels were located with the capsule region having very low numbers. The importance of this was vital particularly as the effectiveness of VEGF was dependant on the actual number and character of the blood vessels. This difference is illustrated with images in Figure 4.25.

The degree of cellular infiltration also varied between different sample types and this was considered for further analysis. In Figure 4.26, some of the differences in the cellular

responses are shown. For porous, degradable scaffolds to function cells from the host, both immune and otherwise, are required to infiltrate into the scaffold. This is vital for remodelling of the SIS and the eventual resorption of the PLGA fibres. In certain instances it was found that the fibres would form an impentrable barrier with very few cells able to infiltrate (Figures 4.26 c & d). Generally speaking all the pure SIS scaffolds were readily infiltrated, the commercial scaffold were largely poorly infiltrated, though the PLGA-SIS scaffolds varied (Figure 4.26).

The level of infiltration of cells into the scaffolds was quantified using a scale of 0 - 4, with 0 being very poor and 4 being highly infitrated and was averged between 4 different sample images (Figure 4.27). A number of things were observed here; firstly the comercial SIS and the random fibre orientation fibre group (10 rpm) had the lowest infiltration rates. Secondly, there appears to be a trend where that with increasing aligment there was also increasing levels of infiltration with the 5000 rpm being the highest of the PLGA-SIS scaffols. Thirdly, the pure SIS was highest infiltrated with the scaffold sometimes being difficult to clearly define (Figures 4.26a). Finally, it appears that the addition of VEGF did not affect the degree of cellular infiltration (A seletion of the histological images are shown for wach sample group in Figure C1 in Appendix C-1).

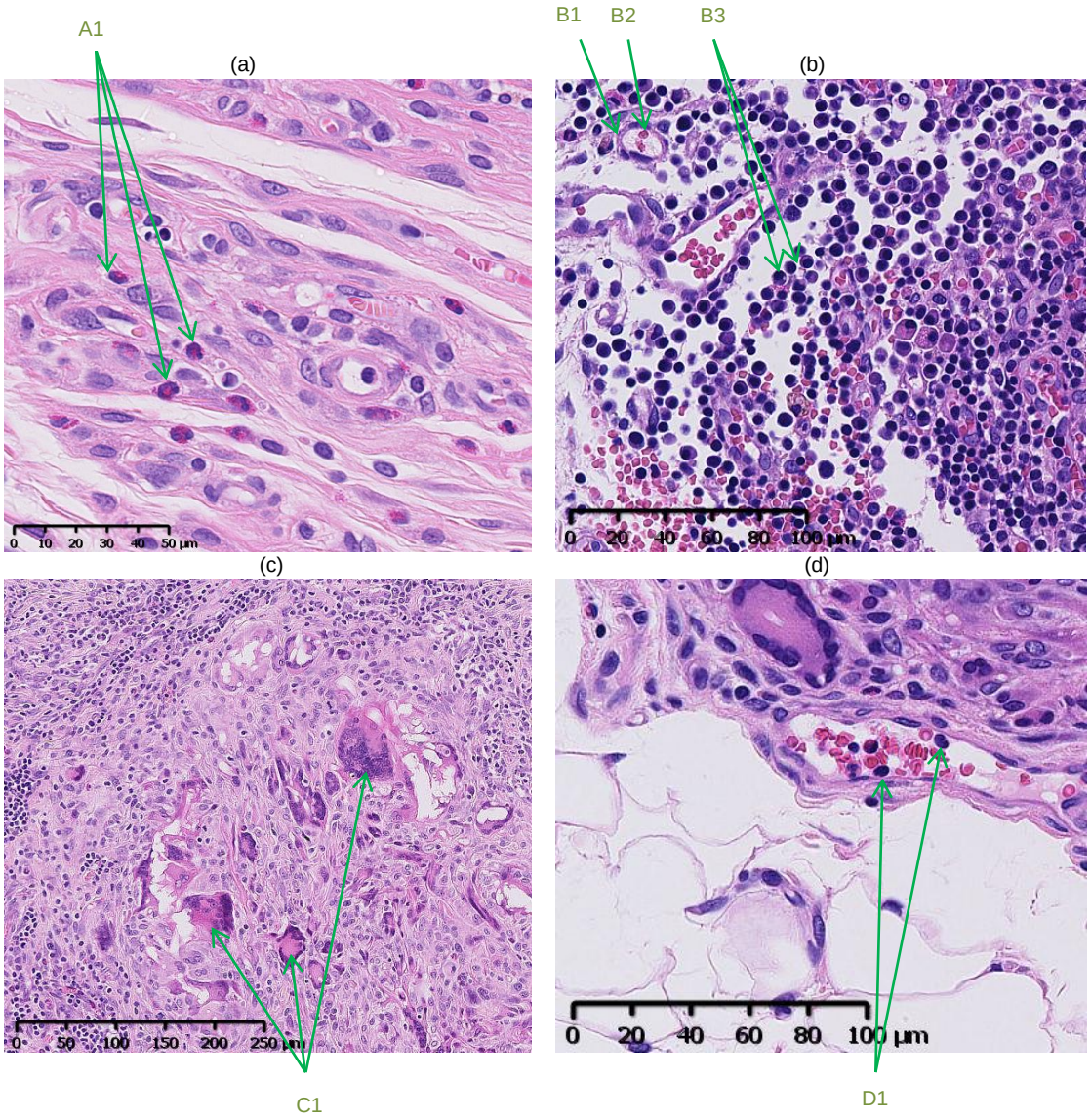

Figure 4.24 Images illustrating the cell types chosen for histological analysis; (a) A1-Eosinophils (b) B3-Lymphocytes, also shown B1- Blood Vessel and B2-Erythrocyte (c) C1-Foreign Body Giant Cells (d) D1-Monocytes. All images are stained with H & E.

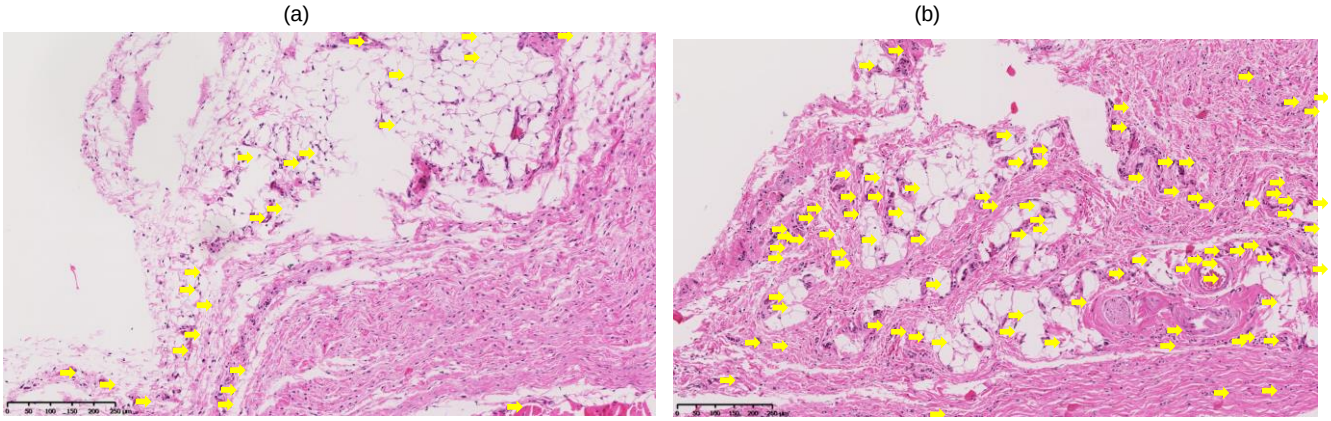

Figure 4.25 Images contrasting the difference in the of density of blood vessels in surrounding granulation tissues for samples with identical fibres and time-points and differing only in the presence of VEGF (a) 5000 rpm at Day 14 without VEGF and (b) 5000 rpm Day 14 with VEGF. Note: The yellow arrows indicate the presence of a blood vessel and may overlay rather than point to the vessel itself.

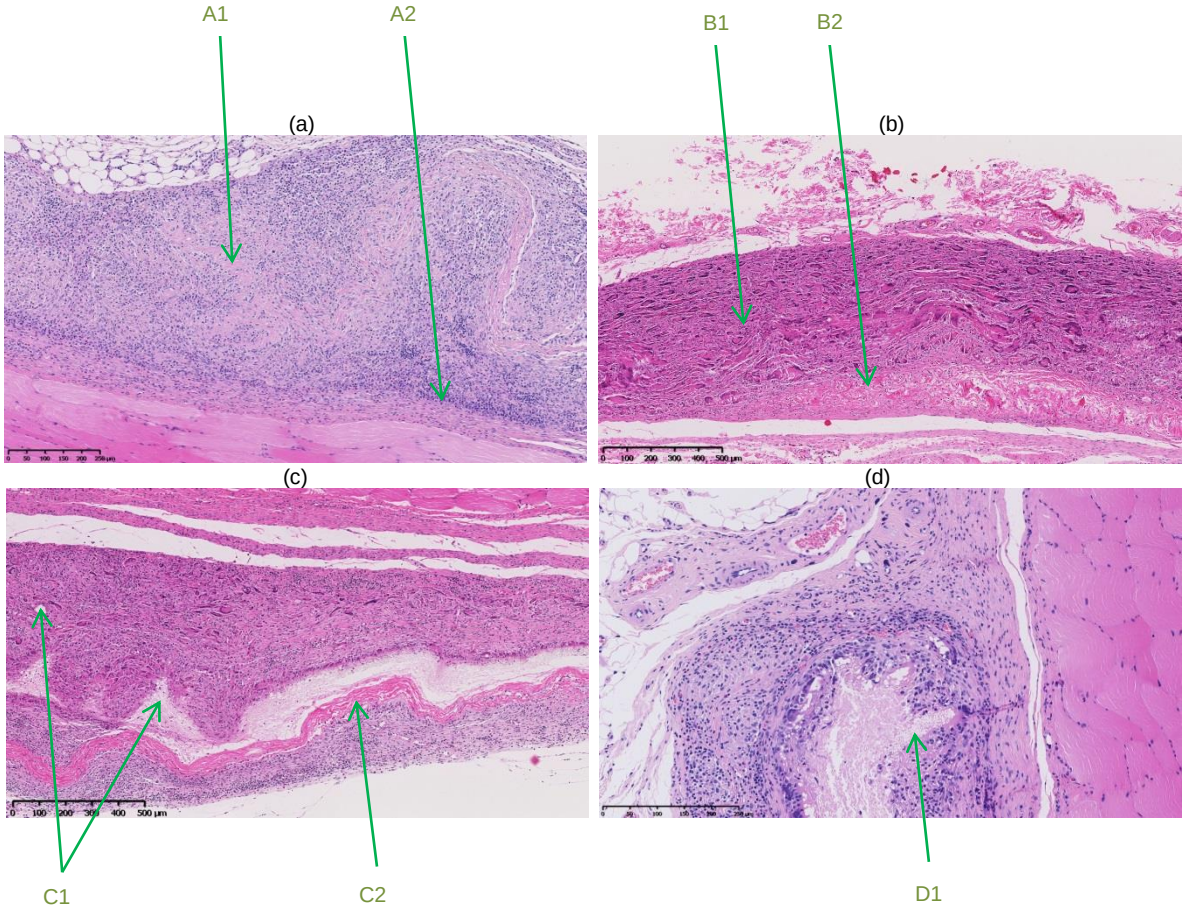

Figure 4.26 Images of features observed in historical analysis; (a) Pure SIS (Day 7), A1-Pink stained collagen-based SIS which is well infiltrated, A2- Boundary between the capsule and the underlying muscle tissue (b) PLGA-SIS 5000 rpm (Day7), B1-Well infiltrated PLGA Fibres ,B2- Well infiltrated SIS (c) PLGA-SIS 5000 rpm (Day7), C1-Poorly infiltrated electrospun fibres, C2- Poorly infiltrated SIS (d) PLGA-SIS 5000 rpm (Day7), D1- Highly visible electrospun fibres (poorly infiltrated)

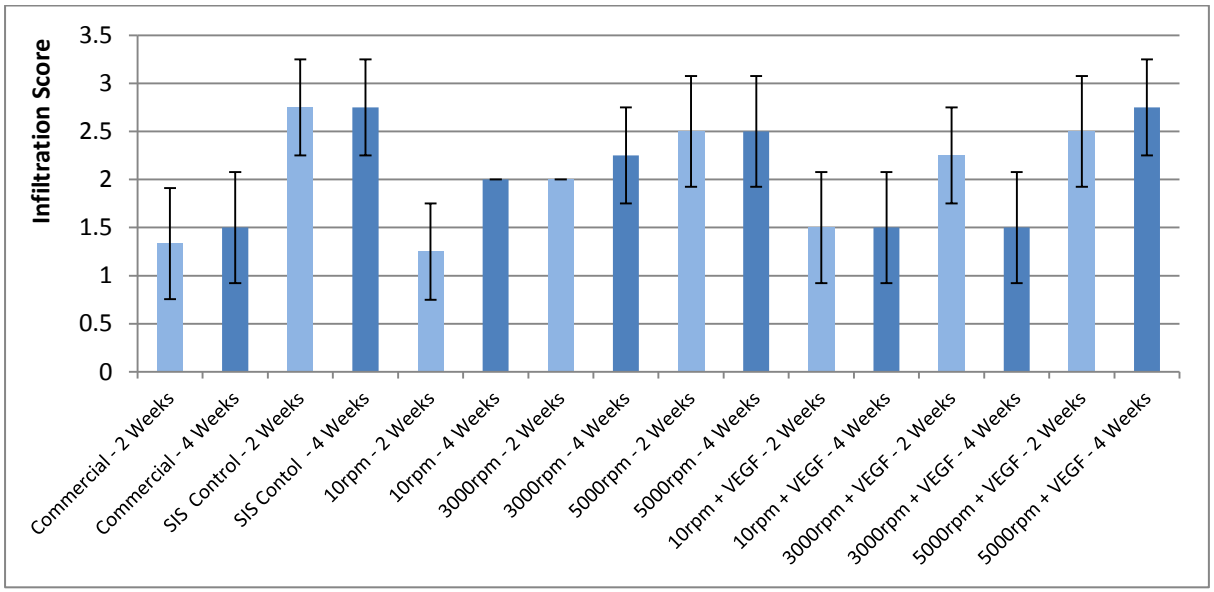

Figure 4.27 Graph of the mean cellular infiltration score for the *in vivo* samples for all the scaffold groups at both 2 and 4 weeks (the point points are differentiated by colour. The images were scored from 0-4 with 0 being poor infiltration and 4 being highly infiltrated (n = 4 and the error bars are the standard deviation).

4.3.8.1 Nuclei Density

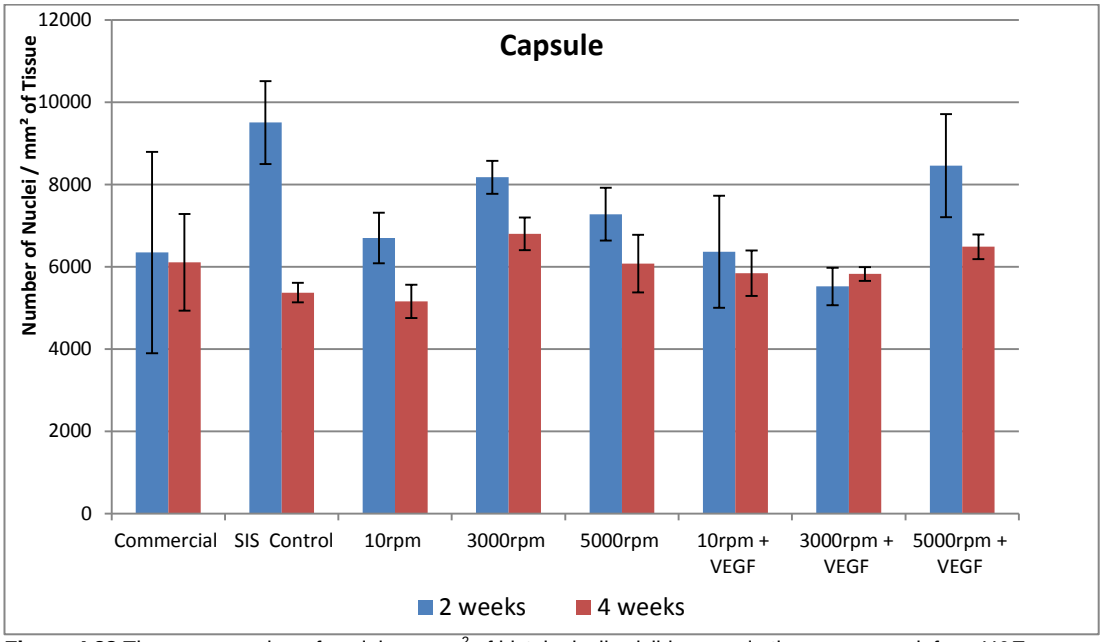

Figure 4.28 The mean number of nuclei per mm^2 of histologically visible capsule tissue averaged from H&E stained images of the scaffold groups at both 2 and 4 weeks (*n* = 4 and the error bars are the standard deviation).

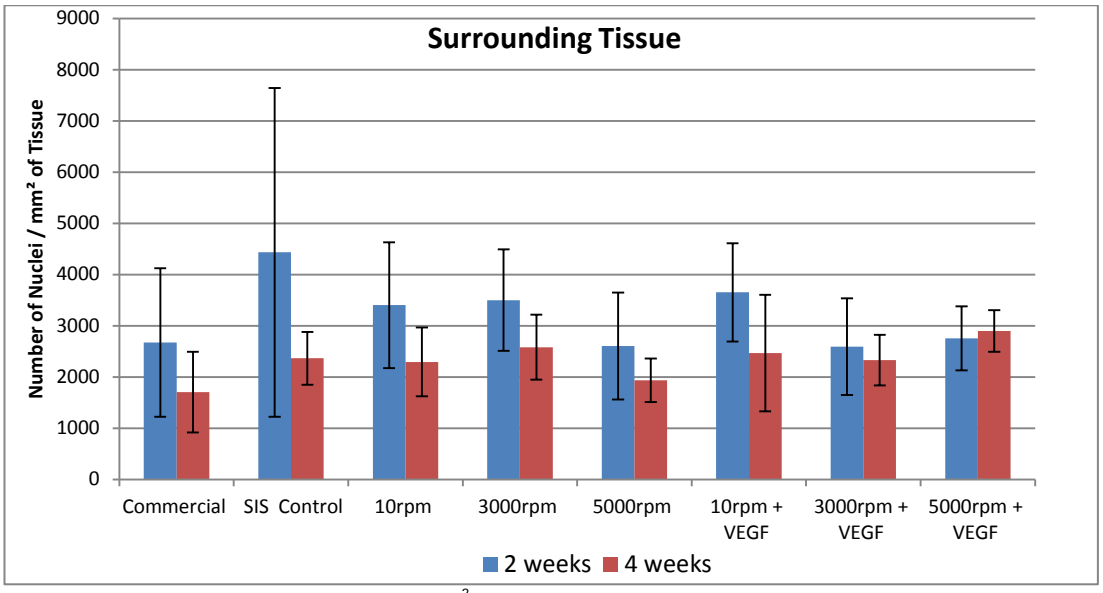

Figure 4.29 The mean number of nuclei per mm^2 of histologically visible capsule-surrounding tissue averaged from H&E stained images of the scaffold groups at both 2 and 4 weeks (*n* = 6 and the error bars are the standard deviation).

The results of the nuclei counting of the capsules indicates that after a two week period the density of nuclei present was largely the same for all sample scaffolds tested (Figures 4.28). The highest value was also observed to be for the control SIS. At four weeks all the samples showed a reduction in the average cell number with the numbers again all being largely similar.

The results of the nuclei counting for the surrounding tissue firstly show that in all instances the nuclei density was lower in the surrounding granulation tissues than within the actual capsules themselves (Figure 4.29). It was also observed that the density was also largely similar across all sample groups after two weeks with the highest numbers again found in the control SIS sample group. After four weeks all the samples were again found to have similar values across all the samples and which were found to be lower than at two weeks.

4.3.8.2 Cell Types

With the nuclei counts being quite similar the observation of the cells types present became more significant. It became clear that there were differences in the ratio of the easily identifiable cells which were present and that this might be useful for analysis. The cells were counted using sectional images of the capsule (Figure 4.30) and the surrounding tissue (Figure 4.31) and both were analysed separately. The first general observation which was made was that there was largely a lack of FBGC's with the control SIS scaffolds and this was easily identifiable through observation at low magnification. Other observations are better described along with immunological explanation and are described in Section 4.4 (Discussion).

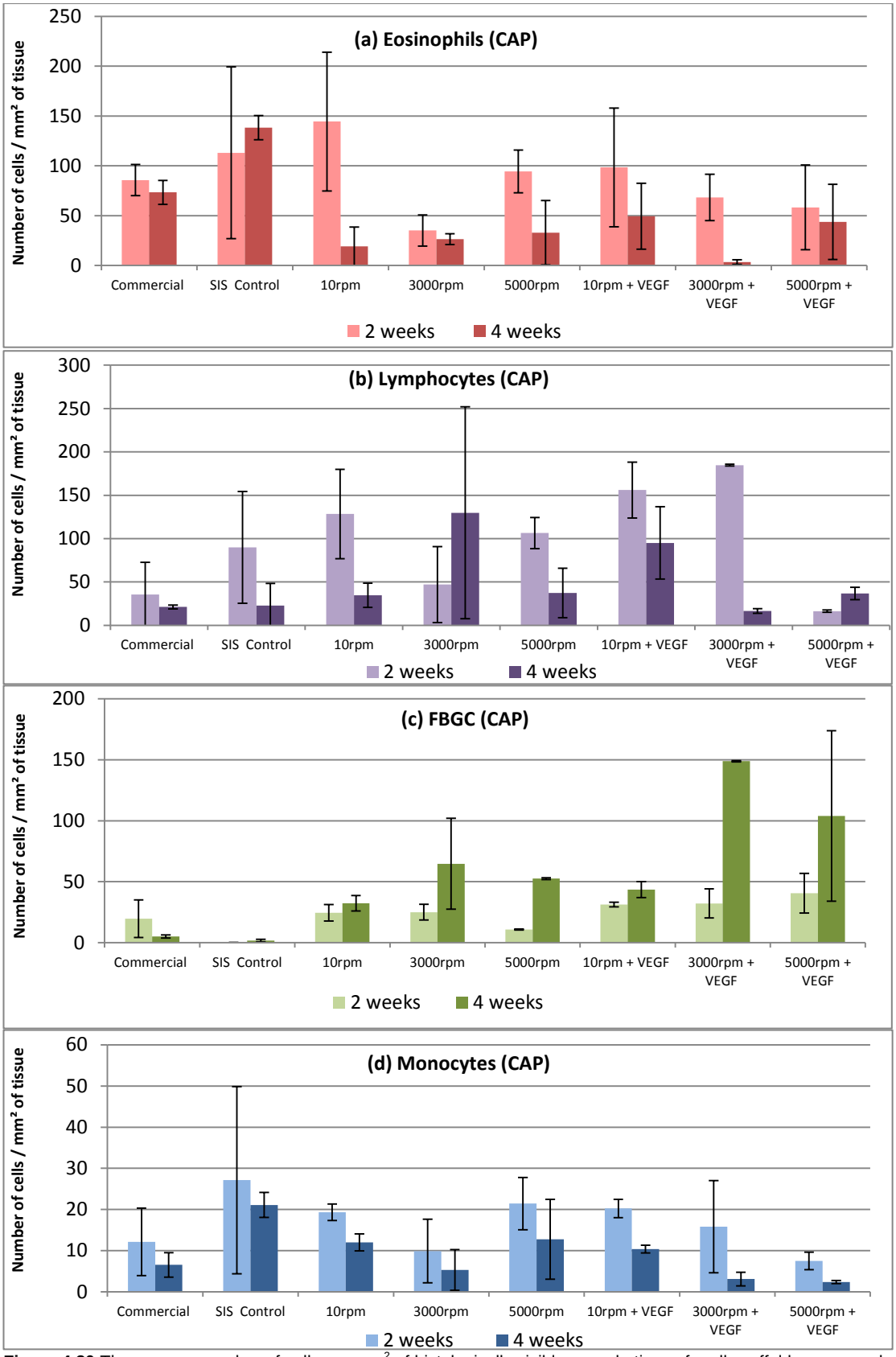

Figure 4.30 The average number of cells per mm^2 of histologically visible capsule tissue for all scaffold groups and at the time points 2 and 4 weeks; the cell types analysed were: (a) Eosinophils (b) Lymphocytes (c) FBGC's (d) Monocytes (n = 3 and the error bars are the standard deviation).

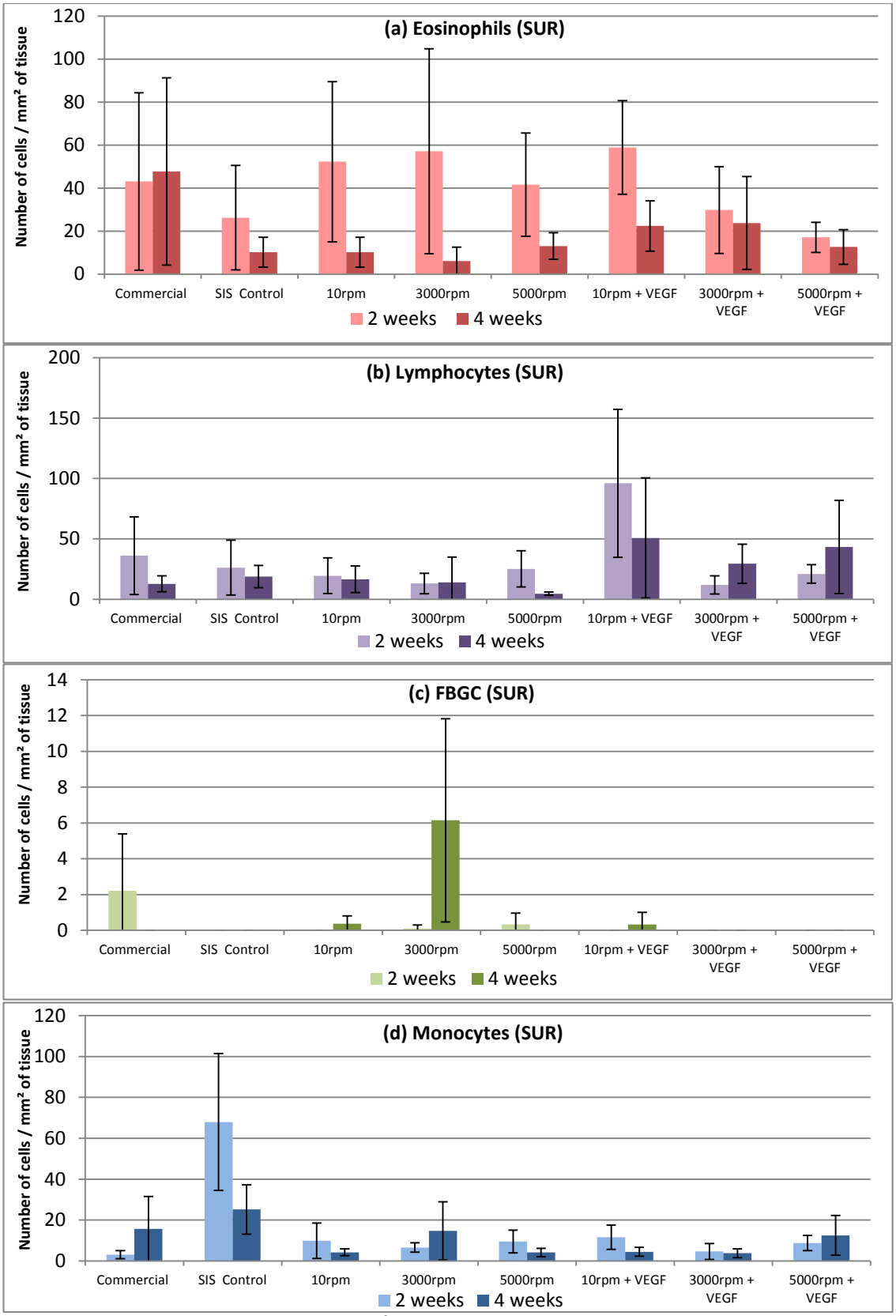

Figure 4.31 The average number of cells per mm^2 of histologically visible capsule sounding tissue for all samples and at time-points 2 and 4 weeks. The cell types analysed were:(a) Eosinophils (b) Lymphocytes (c) FBGC's (d) Monocytes (n = 3 and the error bars are the standard deviation) .

4.3.8.3 Blood Vessel Density

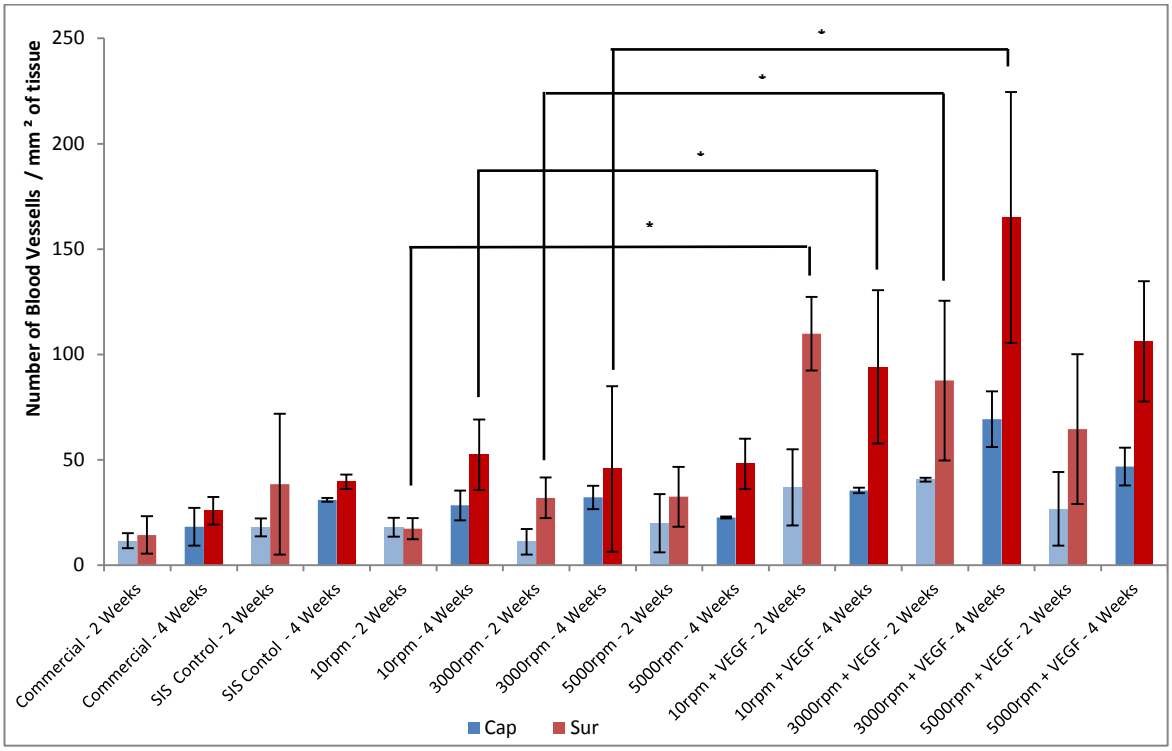

Figure 4.32 The number of histologically visible blood vessels per mm² of tissue based on histological analysis for all sample groups and at 2 and 4 weeks (*n* = 4 for the number of sample images and the error bars are the standard deviation). The bars are alternatively shaded between groups at weeks 2 and 4. Important values differing significantly from each other are denoted by *; $p < 0.05$.

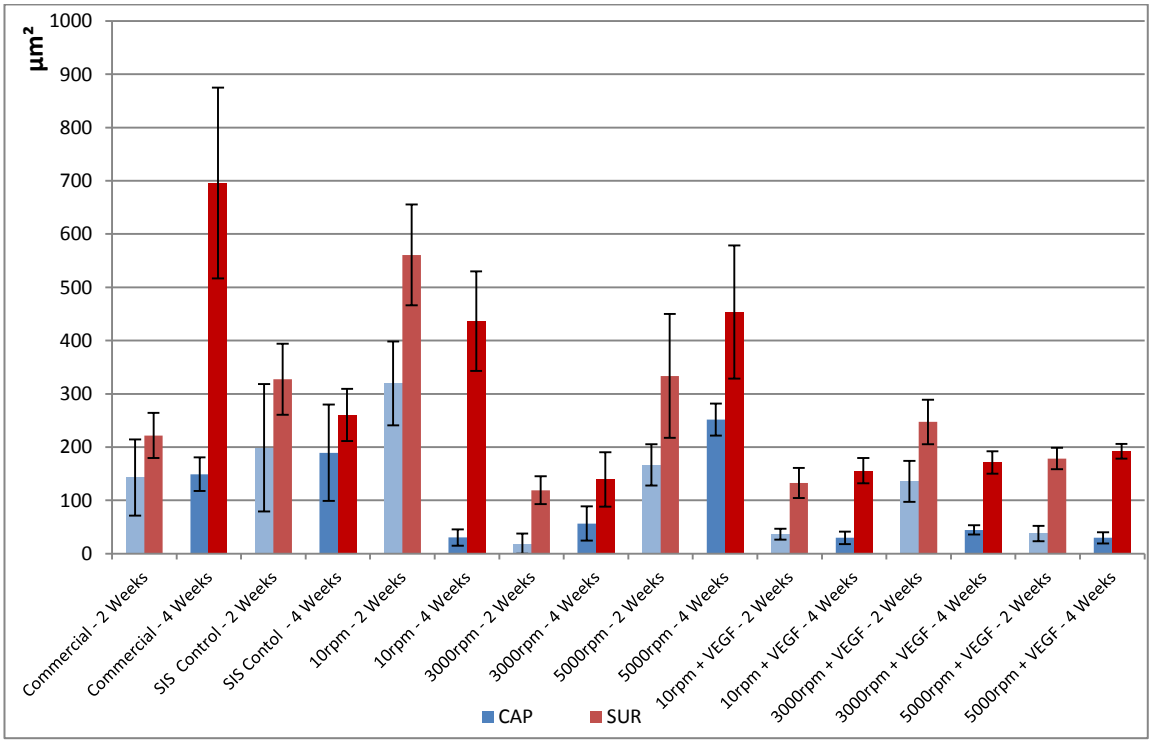

Figure 4.33 The average cross-sectional area of blood vessels of the blood vessels counted in Figure 4.32 (*n* = 4 for the number of sample images and the error bars are the standard deviation). The bars are alternatively shaded between group at weeks 2 and 4.

When the data from the blood vessel density is viewed only in terms of the vessels within the capsules the values were largely the same for all groups, which was not the case for the surrounding tissue (Figure 4.32). As expected, all the sample groups were higher blood vessel density in the surrounding connective tissue than within the capsules themselves.

As mentioned previously, the main area of focus was the surrounding granulation tissue. For the PLGA-SIS scaffolds without VEGF, there was no difference between these samples and the commercial or the control SIS. The main difference observed here were between the PLGA-SIS scaffolds with and without the inclusion of VEGF. Statistical testing of the data showed that when each of the three PLGA-SIS scaffold groups (10, 3000 and 5000 rpm) were compared to the identical group with VEGF then all samples, at both time points, had a significantly higher blood vessel density when compared to the non-VEGF samples (with the single exception being the sample set from 5000 rpm at 2 weeks, though the corresponding sample with VEGF also had a higher values).

A trend with the diameter of the blood vessels was more difficult to ascertain (Figure 4.33). What can be said is that for the samples with VEGF there was a degree of consistency with which diameters remained quite small across all three samples, at both time points, and both in the capsules and the surrounding tissues. This was reinforced by visual observation where the increased density which was observed appeared to be due to an increase in the number of small diameter vessels only.

4.4 - Discussion

4.4.1 General Discussion

The aim of this chapter is to combine the data and findings from the previous three chapters and to create and assess an improved hybrid scaffold for oesophageal tissue engineering from the perspectives of its physical and biological suitability.

With respect to Chapter 2, a limitation of the decellularisation work was that there was the potential to expand the histology work to include staining for basement membrane and this was not carried out. Basement membrane components are important extracellular molecules and serve as attachment sites for cell populations to adjacent tissues. Some basement membrane molecules such as collagen I, collagen IV, laminin, and fibronectin, have been used as surface coatings for biomaterials to facilitate cell attachment and growth and to promote biocompatibility. Processing ECM materials, by decellularization, lyophilization, disinfection, and terminal sterilization can result in disruption to the basement membrane (Brown, Lindberg *et al.* 2006)

Numerous studies show that ECM scaffolds retain basement membrane proteins such as collagen I ,collagen IV and laminin-rich basement membrane after certain types of processing including decellularisation (Badylak, Taylor *et al.* 2011; Barnes, Brison *et al.* 2011). The level of disruption can vary according to the processing the ECM material undergoes including. Given this, the addition of immunostaining for these components would have given vital information on the level of disruption by the decellularisation and processing of the SIS produced here.

In Chapter 2 the fibre diameter was shown to not be affected by rotational speeds up to 3000 rpm and in this chapter this was reconfirmed up to a speed of 5000 rpm. This observation has been confirmed previously and the rotational speed of the

mandrel has been shown not to affect the fibre diameter (Ayres, Bowlin *et al.* 2006). This was important to ascertain as there are examples where a high enough rotational speed can cause a spooling effect where the fibres are thinned by the process (Yang, Murugan *et al.* 2005). The regularity of shape and the consistency of the diameter at different speeds indicate that the fibres were dried and fully-formed when reaching the SIS where the collection took place.

Another physical aspect of the scaffold that had to be monitored was the thickness of the electrospun layer. It has been reported that with an increase in the thickness of the electrospun layer, fibres become disordered as the residual charge accumulation on the deposited fibres interferes with the alignment of incoming fibres (Teo and Ramakrishna 2006; Zhu, Cao *et al.* 2010). At early stages of this work when alignment was not a consideration, it was observed that when the electrospun layer reached a certain thickness then the combined materials eventually had an insulating effect and this caused the fibres to be laterally deflected away from the SIS to the exposed metal mandrel. The results of the thickness shows that for a given time of spinning, i.e. a fixed volume of PLGA per length, of SIS the electrospun layer was found to be thicker for the 10 rpm samples (Figure 4.10). This was not entirely an unexpected result as the more random orientation created a more diffuse structure and would suggest a higher porosity of the scaffold. The porosity of an *in vivo* scaffold presents an important consideration beyond structural properties. For a scaffold to support cell viability in addition to tissue growth and development it must have sufficient porosity to allow for transport of nutrients and the removal of waste products (Sharma and Elisseeff 2004).

Scaffolds which are produced through electrospinning have been described as often being limited in their pore size particularly when consisting of nanofibres (Nguyen, Chen *et al.* 2013). Fibre alignment presents a further challenge as this has been observed to decrease porosity (Ayres, Bowlin *et al.* 2006). The porosity data found

that all the scaffolds produced had a porosity level which was above 80% and that the level of the porosity decreased with the alignment which reinforces the findings in the literature (Figure 4.13a). A potential trend was also observed when the porosity data was plotted against the alignment (further assessment of the effects of alignment will be discussed later) (Figure 4.13b). The highest porosity was observed in the 10 rpm samples which represented completely random fibres and which also explains the observation of why the thickness of the 10 rpm scaffold was the highest. This agrees with the literature and does make logical sense in that the stacking efficiency of aligned fibres is likely to be higher than that that of randomly organised fibres.

Another aspect of the porosity was the pore size distribution. This was shown to change when varying the alignment of the fibres, as observed in Figure 4.14. There were proportionally far fewer small diameter pores within the 10 rpm samples and as the fibres became more aligned there was an increase in the proportion of small diameter pores which also agrees with the idea that better alignment increases packing efficiency, reducing both the pore size and the total porosity. That said in the case of the more aligned scaffolds the total porosity was not at a particularly low level and the presence of smaller pores has been known to have additional benefits and so a decreased overall porosity does not necessarily make the aligned scaffold less biologically effective.

As described in Chapter 1 (Section 1.1.3.1) for scaffolds to work for tissue engineering an outer pore sizes in the range of 50 to 200 μm is able to facilitate cell seeding, and transport of waste and nutrients, and smaller pores in the range of 35 to 70 μm are considered important in the promotion of angiogenesis (Ritchie, Chian *et al.* 2006; Poghosyan, Gaujoux *et al.* 2011; Kuppan, Sethuraman *et al.* 2012; Tan, Chua *et al.* 2012). What was observed here is that there was a fairly broad spread of pore sizes. The two main peak ranges observed, were in the 100 - 150 μm region

for all samples and a second peak for the 3000 and 5000 rpm samples in the 5 - 7.5 µm region. This second peak if taken in isolation could be seen as a problem as it has been shown that that in scaffolds consisting of nanofibres that have small pore sizes (10 µm and below) can act as a barrier to cellular migration (Bye, Bissoli *et al.* 2013). However this effect is mitigated by the first peak showing the presence of larger pore sizes.

The fact that all the scaffolds fall within the aforementioned range established by the literature is a positive one. However, it could be said that the more aligned samples better reflect the actual criteria. The effect of the pore size on the *in vivo* performance will be discussed later.

Another physical aspect of the scaffold was the alignment of the fibres. Culturing cells on an underlying substrate with some form of aligned structure is a well-established method for producing aligned cells with follow the orientation of the substrate through the processes of contact guidance (Shang, Yang *et al.* 2010). Very early work in this area was carried out using smooth muscle cells as early as 1982 (Buck 1982). This phenomenon may not necessarily involve the use of fibres and alternative methods have also been shown to produce these effects. An example of this is the use of a lithographically grooved surface to influence the orientation of cultured human aortic smooth muscle cells on the surface of a hollow cylindrical polydimethylsiloxane (PDMS) substrate (Choi, Piao *et al.* 2014).

This effect has been well-observed in electrospun fibrous scaffolds and has been applied to a variety of cell types. Aligned scaffolds of poly(l-lactide) composite were cultures with mouse osteoblast-like cells (MC3T3-E1 cells) and the cells were observed to orientate themselves along the lengths of the fibres (Tujunen, Fujikura *et al.* 2013). This behaviour has also been observed with the use of mouse fibroblasts which were cultured onto aligned scaffolds of PLGA (Hwang, Park *et al.*

2009). Additionally the orientation of mouse periodontal ligament cells was induced when cultured on aligned PLGA scaffolds (Shang, Yang *et al.* 2010). This effect has even been shown using mouse Schwann cells for applications in neural tissue engineering on aligned PLGA fibres (Subramanian, Krishnan *et al.* 2011)

The use of aligned electrospun fibres with contact guidance dictating the orientation of smooth muscle cells has become a relatively common one in the field of arterial tissue engineering. Here it is a well-established method for getting smooth muscle cells to orientate themselves circumferentially to a cylindrical scaffold with the theoretical aim of establishing contractility. After all, if cells are to contract the vessel radially and then relax to allow for vessel expansion, they must be oriented circumferentially (Bell 2007).

Smooth muscle cells have demonstrated alignment when cultured onto aligned electrospun fibres (polyurethane and collagen) for use in arterial tissue engineering (in this case human aortic smooth muscle cells) (Jia, Prabhakaran *et al.* 2014). Aligned smooth muscle cells were also observed when cultured on synthetic elastin fibres (Nivison Smith and Weiss 2012). In further work, human umbilical artery smooth muscle cells were cultured onto aligned PCL fibres and here it was found that and not only was the orientation and the morphology of the cells influenced by the fibre alignment, but that also the distribution and the organisation of the cytoskeletal proteins within the SMC's were also found to be parallel to the direction of the fibres (Zhu, Cao *et al.* 2010). In addition to orientation, smooth muscle cells cultured in this way have also been shown to express the genes for the contractile proteins (calponin, smooth muscle α-actin (SMA), SM22, and smoothelin) (Rayatpisheh, Heath *et al.* 2013). Furthermore, it has also been observed that following cellular orientation there is also fibrous extracellular matrix formation which also follows the same alignment (Glass-Brudzinski, Perizzolo *et al.* 2002). These phenomena all contribute to potentially addressing the issue prevalent in a wide

variety of regenerative applications where the tissues produced are only in the form of disorganised fibres.

The extension of this concept to oesophageal tissue engineering is a logical one. Arteries and the oesophagus share the same tubular shape and multi-layered structure; with arteries actually performing under slightly more challenging conditions. With constant rise and fall of fluid pressure and with the requirement to contain a complex fluid such as blood a complex challenge is presented (Wong, Liu *et al.* 2013). By contrast, the oesophagus represents a more relatively straightforward challenge, if not a simple one. As mentioned previous in Chapter 1 (Section 1.1.3.2), when tissue engineering constructs have been applied to oesophageal tissue engineering *in vivo* the lack of smooth muscle growth was observed (Doede, Bondartschuk *et al.* 2009). To prevent this it has been suggested here that smooth muscle cells could be cultured onto the construct prior to use. In effect, principles applied to blood vessel tissue engineering also apply to the oesophagus as restoring contractility also represents an ideal target.

In this chapter consistently PLGA aligned fibres were produced and were made to adhere to the underlying SIS to produce the hybrid scaffolds. Smooth muscle cells (HESMC's) were cultured on these scaffolds and through the use of SEM imagining (Figure 4.9) and confocal imaging (Figure 4.19) it was confirmed that in the case of both the 3000 rpm and the 5000 rpm scaffold there was visible evidence of the alignment of the HESMC's.

Another physical consideration for a tissue engineering scaffold are its mechanical properties. As mentioned previously the requirements of an oesophageal scaffold would have to reflect its unique mode of functioning. In blood vessels the differences in mechanical properties (defined in terms of compliance) between graft and tissue can create compliance mismatches resulting in zones of hydrodynamic

instability. This form of consistent instability causes cell signalling cascades resulting in localised cell proliferation and eventual loss of patency (Rapoport, Fish *et al.* 2012). This does not happen with the oesophagus as it acts only intermittently, and does not maintain a constant flow; however it does have to deal with both solids and liquids. The mechanical properties of a graft therefore are not likely to require a very accurate match to the surrounding oesophageal tissue as would be the case with a more sensitive organ such as an arterial blood vessel.

What the results of the mechanical testing show, above, was that with the addition of an electrospun PLGA layer there were improvements to the modulus, yield stress and failure strain over the unaltered SIS in both the longitudinal and the circumferential direction (Figures 4.11 and 4.12). This is a vitally important result and falls in line with the originally stated goals with respect the application and use of SIS in oesophageal tissue engineering and how its short-comings could be overcome (Section 1.3.3.5). More specifically it was found that for the highly aligned scaffolds, in the circumferential direction, the high yield stress values along with the lack of any significant compromise in the failure strain were important result because that is likely to be the fibre direction that would be ideal for smooth muscle bioreactor culture for potential *in vivo* applications. In general the relative mechanical properties of the scaffolds do appear quite favourable when compared to both electrospun materials by themselves and to ECM materials.

Aside from the physical aspects of the scaffolds the biocompatibility was an important consideration for their overall functioning. Biocompatibility was first evaluated using a metabolic activity assay and here it was found that all the scaffold groups performed as well as the control and the commercial SIS. This was an important result particularly when compared to a commercial SIS which is currently in use in the market. With metabolic activity it is necessary to ascertain whether differences in the activity levels are due to scaffold biocompatibility or due to other

effects such as cytotoxicity and/or an increase in cellular activity levels. For this reason a Live-Dead assay was performed and here it was observed that there was no major differences detected between any of the PLGA-SIS scaffolds and both the commercial SIS or the control. At day 14 the MTS assay of the commercial SIS and the control did have slightly lower levels but these can be accounted for by the relatively rapid expansion rate of the cells and that there was a lower surface area present in those samples (lacking electrospun fibres). The scaffolds were also cultured and tested for the presence of smooth muscle actin, a vital component of smooth muscle cell contractility (Figure 4.15). In all instances the presence or alignment of the scaffold neither inhibited nor improved the *in vitro* performance of the scaffold.

When the samples were implanted *in vivo* there results were a little more complex to evaluate. All samples elicited an immune inflammatory reaction around the scaffold and provoked the formation of surrounding granulation connective tissue. Close inspection revealed differences in the immune reactions even though an approximation of the cell numbers showed very little differences between groups. Consequently it could the viewed that the differences were in the nature of the immune reactions rather than the scale.

The first clear observation is that there was cellular infiltration and encapsulation of all samples as expected of a foreign body being placed subcutaneously. The *in vivo* reactions to the scaffolds can be observed from the perspective of the foreign body reaction and mainly concerns the encapsulated scaffolds and not the surrounding granulation tissue though this does have some importance later. Upon implantation there is an immediate reaction which leads to a phase of acute inflammation, which can last up to a week, and which is characterised in its very earliest phases by neutrophils (polymorphonuclear leukocytes). Mast cell degranulation releases histamine (along with the critical Interleukins 3 & 4) and this along with fibrinogen

adsorption on the implanted biomaterial surface, are known to mediate acute inflammatory responses (Zdolsek, Eaton *et al.* 2007).

This is followed by a chronic phase of inflammation which occurs for a longer and more variable period. These overlap and can be better understood as a continuum of overlapping processes. This phase is considered to be defined by the presence of mononuclear cells, i.e. monocytes and lymphocytes, at the site of implantation and is the phase than concerns this work. By this stage of inflammation a number of processes are simultaneously taking place, such as granulation tissue deposition and critical cellular actions, like monocyte adhesion to the surface of the biomaterial, both of which occur after a few days and continue throughout. When chronic inflammation is used to describe the foreign body reaction it is often described as when monocytes, macrophages, and foreign body giant cells are all present at the biomaterial interface. Granulation tissue being present is also a feature with the granulation tissue being considered a precursor to the formation of the fibrous capsule (Anderson, Rodriguez *et al.* 2008).

The formation of FBGC's is an important indicator of the foreign body reaction. Towards the end of the acute phase of inflammation monocytes adhere to the surface of the material; interaction at the material surface causes their differentiation into macrophages. If further conditions are met then these macrophages begin a process of fusion, with the eventual outcome being FGBC's. FBGS's have been shown to exhibit an antigenic phenotype similar to both monocytes and macrophages reflecting their formation from the fusion of monocyte-derived macrophages (Athanasou and Quinn 1990). It has also been shown that lymphocytes also have a role to play in the foreign body reaction. Adherent lymphocytes have been shown to predominately associate with macrophages and FBGC's rather than the surface of the biomaterial itself (Macewan, Colton *et al.* 2005). In *in vitro* co-cultures, lymphocytes have been shown to enhance

macrophage adhesion and fusion while the presence of the macrophages stimulated lymphocyte proliferation (Macewan, Colton *et al.* 2005).

Histological evaluation of the samples here showed that the control SIS did not cause a foreign body reaction. This is quite a significant result in that a largely collagenous xenogeneic decellularised tissue functioned well *in vivo*. The commercial SIS undoubtedly had all the early indications of a foreign body reaction at 2 weeks however by 4 weeks this had resolved itself and the numbers were very low. This again is an important result due to the fact that it appears to indicate a reduction in the foreign body response and this not being observed in the PLGA-SIS samples.

In all test groups the numbers of monocytes fell between weeks 2 and 4. In the case of the control SIS and commercial SIS this could indicate a reduction in the inflammatory process however for the PLGA-SIS samples this could potentially be due to a persistent foreign body reaction as indicated by the increase in the numbers in FBGC's and the reduction in the number of monocytes due to differentiating to macrophages (and, in turn, FBGC's).

In the case of the pure and commercial SIS the numbers of lymphocytes decrease from weeks 2 to 4. This could again be an indication of a decrease in the inflammatory processes. It was also observed that for both the numbers of monocytes and lymphocytes present on the commercial product were far lower than with control SIS. In the case of the control SIS, with high numbers of both these cell types present at 2 weeks it was remarkable that very few FBGC actually formed especially as both being key cells in FBGC formation. The control SIS also appeared to have high numbers of eosinophils, also reflected in its surrounding tissue, in addition to also having the highest monocyte numbers. This could suggest

a mechanism at work, possibly with respect to the rapid remodelling process, which attracts these cells, but however does not, critically, illicit the foreign body reaction.

For all the PLGA-SIS samples the lymphocyte numbers fall from 2 to 4 weeks (the exception being the 3000 rpm sample however high variability with at least one sample showing an almost unique proportion of cells potentially skewing the mean value). This appears to indicate that by 4 weeks the roles of the lymphocytes in any on-going inflammatory processes were quite reduced. What can also be said is that on visual assessment of the images, that in all samples there was a high number of plasma cells (involved in antibody production). These are successor cells to lymphocytes and could also account for the reduction in number.

Eosinophils were present in all samples and at relatively high numbers in some instances. It is not exactly clear what role these would play in the foreign body reaction. Eosinophils are well known to have immunologic effects though they are often described in specific conditions where there presence, usually in high numbers, is either a symptom or potentially a cause, such as pulmonary eosinophilia, eosinophilic esophagitis, hypereosinophilic syndrome, Churg-Strauss syndrome, eosinophilic granulomatous vasculitis (Akuthota and Weller 2015).

With respect to their actions, eosinophils have the capacity to work in association with T-lyphocytes in a variety of immunologic conditions. Eosinophils have also been shown to be able to selectively produce Th1 or Th2 cytokines, depending upon the immune response present (Alam 2009).

When all the sample groups are consider together it becomes quite clear that the cause of the foreign body reaction to the PLGA-SIS scaffolds is the presence of the PLGA electrospun layer. What should be emphasized here is that this was not an aggressive response and compared well with other instances with other PLGA scaffold which have been implanted *in vivo* (Blackwood, McKean *et al.* 2008; Han,

Jia *et al.* 2013). That being said, there was a limited foreign-body reaction and there are a number of possible reasons for this. During the acute phase of inflammation as mentioned earlier monocytes enter the site of implantation and adhere to the surface of the biomaterial. While they initially adhere to most surfaces quite well they often fail to maintain adhesion over time (McNally and Anderson 2002). The result of this is that materials which do not have the surface properties which encourage attachment can lead to increased levels of detachment, which in turn can lead to anoikis. Anoikis being a type of apoptosis caused by disruption of adhesion signals in cells which are programed to remain adhered to a surface or the cells local environment (Frisch and Screaton 2001). When macrophage fusion levels are high, anoikis levels are low, and it is theorised that under certain conditions when the levels of detachment are high, the cells take an alternative pathway and end up undergoing fusion (Brodbeck, Shive *et al.* 2001). This was not observed with the control SIS and as this consists predominantly of collagen, the main constituent of all extracellular matrices, it could be fair to assume that these cells can adhere to the SIS collagen without undergoing this process.

Given the large number of cells present during an inflammatory reaction even if the rate of detachment is high, there are still a large number of cells which are still attached. Here the surface chemistry of the material can also play a part here as it has been shown that biomaterial surface chemistry can influence apoptosis of adherent macrophages both *in vitro* and *in vivo* (Brodbeck, Shive *et al.* 2001; Brodbeck, Colton *et al.* 2003). With this in mind it has to be said that the surface of PLGA fibres cannot be considered great sites for adhesion. This could be the case here as macrophage fusion has been shown to be material dependant with surfaces requiring an array of absorbed proteins in order for adherent cells to undergo the necessary phenotypic change to fuse into foreign body giant cells (Brodbeck, Shive *et al.* 2001). There is also evidence that in *in vitro* testing that the surface properties

of the material (i.e. composition and charge) can actually affect the phenotypic expression of foreign body giant cells and even alter the interleukin-4 induced fusion of macrophages to form them (McNally and Anderson 2015).

Another physical aspect of the immune reaction is that macrophages are only capable of phagocytosing very small particles (<5 μm) and the presence larger particle sizes (>10 μm) or large fibres, can induce the formation of foreign body giant cells (Anderson, Rodriguez *et al.* 2008). It is also crucial to note that in the case of the PLGA-SIS scaffolds the PLGA was in the form of nanofibres and so with a very high surface area all these effects would be exaggerated and contribute greatly to the foreign body reaction.

With these inflammatory processes in effect it is important to emphasize that the "biomaterial" which is primarily the cause, i.e. the PLGA scaffold, is intended to be a temporary feature. This falls in line with the main objectives of this work in that the PLGA is required to maintain its mechanical integrity for 3-4 weeks and then begin to be degraded as the scaffold gives way to regenerated oesophageal tissue. The PLGA is designed to degrade, and the monomer components, lactic and glycolic acid, degraded in Krebs' cycle. The adhesion of macrophages and FGBC's at the surface of the material produce a distinct microenvironment between the cell membranes and the biomaterial. These cells release degradation mediators such as reactive oxygen intermediates (ROIs, oxygen free radicals), degradative enzymes, and acids into the microenvironments. (Anderson, Rodriguez *et al.* 2008).-[How temporary? Again relate to the product specification.]

In these shielded microenvironments buffering or inhibition of these mediators are delayed or reduced (Anderson 2011). The phagolysosomes found in macrophages have been found to have acidity as low as pH 4 (Haas 2007). The surfaces of biomaterials are exposed to high concentrations of these degradative agents and

thus the biochemistry of the biomaterial will affect how rapidly it is degraded. In the case of PLGA there is the additional problem of the degradation products also being acidic which can contribute to lower the pH of the microenvironments further.

As mentioned previously, for a scaffold such as this to succeed the degradation process is an essential part of the function of the implant. Consequently for this process to actually occur it is essential that the scaffold be infiltrated by the immune cell so that these degradative processes can take place. Large sections of the scaffold which are not infiltrated risk becoming isolated and this will be discussed later. It is also an important result that the fibres were intact at 4 weeks as this is the approximate time scale which was quoted for stent-type material to be required to support SIS after implantation (Doede, Bondartschuk *et al.* 2009).

What was also observed in the cellular infiltration data (Figure 4.27) is that there appears that there was a higher degree of cellular infiltration in the scaffolds with aligned fibres, particularly at 5000 rpm. This result is not what was expected as the smaller pore size and more compact structure could be hypothesized to prevent cells and nutrients from becoming distributed throughout the scaffold. However there is agreement in the literature, in one study scaffolds were inserted *in vivo* and compared in terms of alignment, with the aligned fibres demonstrating better cellular infiltration than random orientation (Kurpinski, Stephenson *et al.* 2010). It has also been shown that fibre alignment does not affect integration (Ionescu and Mauck 2013). The alignment of the fibres have also been described as facilitating cell movement within scaffolds (periodontal cells used in this instance) (Shang, Yang *et al.* 2010).

When considering alignment there is also the question of how this affects the porosity. As mentioned previously, fibre alignment change was found to alter the nature of the porosity. While the more aligned scaffolds were less porous they

actually possessed a more split pore diameter distribution between larger and very small pores and this appears to produce better cellular infiltration *in vivo* which is a positive result. It is important to consider that higher porosity and larger pores not necessarily a measure for better interconnectivity between pores which is also significant for nutrient distribution. Consequently it may be that the aligned fibres allow for a porosity distribution with better interconnectivity between pores and this may account for better cellular filtration.

Another reason why it was vital for there to be adequate infiltration into the scaffold was due to the fact that this could potentially affect the nature of remodelling which occurs. This process begins with the adherent macrophages, present during the inflammation, secreting growth and angiogenic factors that have roles in the regulation of fibroblast proliferation and angiogenesis (Martin and Leibovich 2005). In *in vitro* circumstances it has been shown that human macrophages can be react to biopolymers by stimulating fibroblast activity. Also it has been shown that high fibroblast stimulation correlates to the *in vivo* fibrotic response (Miller and Anderson 1989). In effect, biomaterial adherent macrophages can produce stimulating factors that can cause fibrosis and this, in turn, can result in the development of a fibrous capsule that is known to develop around an implanted material. This fibrous capsule can have a harmful effect on the implant and can interfere with its function (Anderson, Rodriguez *et al.* 2008).

The fibrous capsule is formed of a dense collagen matrix and possesses very low numbers of cells (Anderson 2011). Its primary purpose is to isolate the material from the internal environment which is often not desirable. In the case of degradable materials this is undoubtedly a poor outcome. However this is not the only outcome.

The nature of the foreign-body reaction around a biomaterial may be controlled by a number of factors. The surface properties of the biomaterial, the shape of the

implant, and the surface-to-volume of the implant can all impact on the reaction. High-surface-to-volume implants such as electrospun scaffolds (in addition to fabrics, porous materials, particulate, or microspheres) are found to have higher ratios of macrophages and foreign-body giant cells when implanted as opposed to bulk and smooth-surface implants, which tend to have fibrosis as a significant feature of their implantation (Anderson 2011).

The formation of a fibrous capsule was not found in any of the PLGA-SIS scaffolds. What was found was a large number of FBGC's and monocytes (macrophage precursors) as described in the literature as present with high-surface-to-volume implants. While there was actually was a high level of granulation tissue formed around the scaffolds this was actually quite diffuse in structure, was reasonably well cellularised and of high vascularity. In conclusion, while the foreign body reaction can be considered an undesirable result it can actually occur without formation of a fibrous capsule as was the case with the PLGA-SIS scaffolds used here. As a result it could be speculated that the inflammatory process would undergo resolution leading to the restoration of normal tissue structure.

The final feature of the scaffold was its use as a means of drug delivery. A number of things emerged from the addition of VEGF to the hybrid scaffolds. The first stage of VEGF incorporation was carried out *in vitro*. The VEGF assay showed that there was undoubtedly retention of the VEGF within all the three 3 scaffolds tested (Figure 4.20a). The data also showed that the concentration was largely identical for all three and that there was little difference over the three time points. The graph in Figure 4.20b was the result of the calculations of the actual quantities of VEGF present in the solution. The levels were found to be between 60 - 110 ng of VEGF, which was generally considered quite low given the initial quantity added was 500 ng per sample. Care should be taken when considering these figures as absolute as it is likely that some of the VEGF might have denatured, and a certain amount is

likely to remain associated with the scaffold. What can be taken here, given the drastic reduction, is that the direct loading method employed here was quite inefficient.

Upon testing it was also clear that the VEGF was mostly released in the initial burst release by day 1. In a study also using VEGF adsorption, it was found that there was an initial burst release after 1 day, as observed here though it was additionally observed that there was a small and sustained release over the course of days 2-5 (Singh, Wu et al. 2012). This represents a shorter term than analysed here (days 7 and 14) as opposed to daily, however a small increase was observed by day 7 and a slower release could potentially account for this. In another study there was also a burst release at day one followed by a slow decrease to virtually nothing by day 7 (Lode, Wolf-Brandstetter *et al.* 2007). This trend may also be present here however the time-points were chosen to reflect the proposed *in vivo* work and not carried out on a daily basis as mentioned previously.

To demonstrate the scaffold as a suitable delivery method for VEGF a CAM assay was also performed. It is well established that VEGF can affect the CAM (Wilting, Christ *et al.* 1992; Wilting, Christ *et al.* 1993; Verma, Gu *et al.* 2011). The principle conclusion of the CAM assay was that it demonstrated the effectiveness of incorporating VEGF into a scaffold of this nature. The results of the CAM assay show there was a fair degree of variability however and this can probably be due to the method of loading. The average length of the complexes was statistically higher for the VEGF samples versus the control which was not the case for the non-VEGF samples. It was also statistically demonstrated that when the data from all the VEGF samples were compared to the combined non-VEGF samples that there was a statistical difference between the two sets in terms of the mean number of junctions. In conclusion it was demonstrated that in an *in vivo* model the scaffolds and the

VEGF can have a direct effect by increasing angiogenesis, a result also confirmed in the literature.

The actual implantation *in vivo* results included specific analysis to assess any effects of the VEGF in the scaffolds. There were two basic results from the analysis. Firstly that the incorporation of the VEGF resulted in a statistically significant increases in the blood vessel density in the surrounding granulation tissue when samples with and without VEGF were compared (with a single exception but which still had a higher mean value). In effect, the newly formed connective tissue which formed around the encapsulated scaffolds had, as a result of the initial burst release of VEGF from the scaffold, had an increase in the number of blood vessels after a 4 week period. All the VEGF samples were statistically higher than the commercial control. This is a result which has been observed previously, including increased microvessel density with VEGF added to a PLGA sub dermal implant for bone tissue applications (Lindhorst, Tavassol *et al.* 2010).

The second result was first observed through visual analysis and it was that while the numbers of blood vessels were higher in the samples with VEGF the increase appeared to be in the number of smaller diameter vessels with the numbers of larger vessels remaining similar. The decision was then taken to also analyse the vessel diameters as well counting the numbers. While the trend here was not as clear, the samples with VEGF showed a general trend of have lower mean values. This observation is in line with the literature where the action of VEGF is described as causing the formation of new vascular buds (Anderson, Ponce *et al.* 2004).

It is also important to state that VEGF is an angiogenic factor that has only been used with limited success. There is a large body of work that shows that VEGF, when used in isolation can induce vessels which are immature and leaky, giving rise to local oedema and inefficient tissue perfusion (Alfranca 2009). This has been

found to be mitigated though the use of heparin, which natural binds to the molecule (Ferrara 2004). Heparin-binding VEGF isoforms produce a branching network with vessels which do not have the problems listed previously (Vempati, Popel *et al.* 2014). Consequently this represents a limitation of this work, however the VEGF was also an important method by which quantifiable data could be obtained post *in vivo* implantation to demonstrate that the scaffolds had the potential for drug delivery.

4.4.2 Conclusion

The main points of the conclusion of this chapter will be discussed in more detail in the next chapter and tie into the conclusions of the thesis as a whole.

Within the scope of this chapter alone it can be concluded that the PLGA-SIS scaffolds were found to have good mechanical properties and also found to be highly porous in structure. The fibres could also be produced with consistently alignment and the adhesion between the two layers was also maintained throughout the work in this chapter. These factors point to the potential of this scaffold in terms of its physical properties.

In terms of biocompatibility the hybrid scaffolds were again found not to possess any major limitations in a tissue engineering capacity. When tested *in vivo*, a foreign body reaction was elicited though this did not progress to fibrous capsule formation which is a highly desirable result. While the SIS on its own performed very well *in vivo* it was also concluded that if the immune reaction to the PLGA fibres was reduced then this would improve the performance of the scaffold by limiting the potentially harmful effects of the foreign body reaction.

The final area of concern was the alignment of the PLGA fibres. Here it was concluded that the highly aligned samples (5000 rpm) are likely to present the best possible solution due to the *in vivo* performance with the highest cellular infiltration, the circumferential mechanical advantage and finally due to the potential for smooth muscle cell alignment.

It was also concluded that the addition of VEGF resulted in an increase in the numbers of blood vessels in the granulation tissue surrounding the scaffolds and therefore had the potential for use to improve vascularity in and around the scaffold. It was also shown that VEGF incorporation was possible through the use of the adsorption. While it might not present the ideal method for drug delivery due to its low rate of retention it could be used if an initial burst release is required.

5. Conclusions and Future Work

5.1 - Conclusions

One of the first aims outlined in this work was to produce a base SIS scaffold which is structurally and biologically suitable for spin coating with polymer fibres. The ideal method for the decellularisation of intact tubular SIS was concluded to be using sodium deoxycholate under perfusion (with the elimination of DNase from the protocol). The preference for perfusion decellularisation over agitation for tubular organs was also expressed by Sjoqvist *et al.* when the methods were compared for the rat oesophageal decellularisation (Sjoqvist, Jungebluth *et al.* 2014). After analysis, and further adjustments to the procedure, it was conclude that this type of SIS fulfilled the required criteria and could be consistently produced.

A further aim of this work was for the SIS produced to be suitable for electrospinning. Work carried out in Chapter 3 it was concluded that electrospinning a polymer layer onto tubular SIS (with two different polymers) was possible and that attachment, once refinement of the SIS processing was carried, was suitable between the two layers so they could be treated as a single structure.

The aim of the Chapter 4 was to evaluate the effectiveness of the combined hybrid scaffold and to test its potential for drug delivery. It was concluded that the PLGA-SIS scaffolds were found to have good mechanical properties and were highly porous in structure. Here it was also concluded that the scaffolds showed suitable biocompatibility. The SIS on its own (the control group) had no foreign body reaction and therefore the foreign body reaction found on the hybrid scaffolds was largely due to the presence of the PLGA. A further conclusion was that the highly aligned samples (5000 rpm) are likely to present the best possible solution due to the *in vivo* performance. The final conclusion was that the addition of VEGF showed an increase in the number of blood vessels and so could improve the function of the scaffold.

With all that taken together a few further observations can be made. Firstly that the basic approach of a combined ECM and biopolymer appears to be a potential approach to oesophageal tissue engineering. Secondly, while these scaffolds, and indeed other similar approaches, appear to have potential actually using such systems successfully in a patient presents a large array of further problems. Considering all the literature and news of clinical outcomes for similar organ replacement procedures it appears that there will have to be an increase in complexity and knowledge prior the successful clinical application of such systems. Nevertheless, hybrid systems combining the properties of two or more different materials in addition to a variety cell types remains a positive direction for the development of tissue engineered tubular organs.

5.2 - Future Work

As mentioned previously In studies where a section of oesophagus was replaced common complications included stricture, dilation and the lack of significant muscle growth (Doede, Bondartschuk et al. 2009). One method which has always been part of a theoretical end game of this work was the culture of smooth muscle tissue cells onto the scaffold prior to implantation. Circumferential smooth muscle would very rapidly be exposed to mechanical forces which would aid in their development and the formation of a more functional tissue engineered structure.

Minimising the foreign body reaction is also important as it was this that presented as the greatest potential limitation of the scaffolds. Cell adhesion should be an area for improvement there are a large number of ways to improve the biocompatibility of the PLGA fibres such as the incorporation of fibronectin into the PLGA fibres (Hersel, Dahmen et al. 2003). Work here has shown that the incorporation of these types of biomaterials can improve the immune reaction to, and therefore the in vivo performance of, certain polymers. This is significant particularly for an initial culturing scenario as it is in this microenvironment that the introduced cells, in addition to the native cells, are expected to thrive.

One future potential improvement could be the use of additional layers. While the electrospinning might prevent further additions to the electrospun layer, providing the initial SIS-PLGA layer is produced and intact (to prevent leakages), additional layers could be added by cutting and suturing additional layers of the combined SIS-PLGA over the base layer. This could provide additional mechanical strength while also allowing for different layers to be cultured separately and with different cell types.

Alternative polymers are also a potential area for improvement. While the properties of PLGA are very good there is the potential for a polymer with better elastic properties. This not easy to find and the literature does not offer any clear examples which might easily replace the PLGA here. Polymer blends, particularly using biopolymers such as elastin, might offer some potential avenues.

In addition to this the incorporation of VEGF could be improved by it being present in the fibres themselves. At 4 weeks the fibres were present and intact and therefore being resorbed at a slow rate (which was intended); this represents the ideal circumstances for a sustained low-level release of growth factors which might improve the overall in vivo performance of the scaffold. That said, a small dose of adsorption-introduced VEGF as the initial burst release has been shown to have an appreciable effect and therefore could also be included. Nanoparticle encapsulation of VEGF has been successfully carried out and with some variations to the electrospinning process these could be incorporated into the nanofibres. There is also the potential for the VEGF to be added to water soluble polymers and then coaxially electrospun along with the PLGA fibres.

As mention previously VEGF has been found to function better with heparin and therefore incorporating this into future work in this area would be ideal. This can be achieved through the use of heparin binding to the SIS. This would also have the effect of increasing the retention of the VEGF in addition to increasing its active lifespan in vivo (Vempati, Popel et al. 2014). In recent work tubular SIS was created for arterial tissue engineering and then heparin was bound the surface. To this VEGF was added which was then immobilised by the heparin. This cell-free scaffold was then successfully implanted into the arterial vascular system of an ovine model and developed functioning endothelial and medial blood vessel layers. (Koobatian, Row et al. 2016).

One of the most important directions for future work is for the scaffold to be test *in vivo* as a short-segment oesophageal replacement in an animal model. Previous work has shown that dogs represent a better analogue to pigs in terms of their orientation and relative length.

References

Ahmad, Z., Nangrejo, M. E. E. S*., et al.* (2009). Engineering a material for biomedical applications with electric field assisted processing. *Applied physics. A, Materials science & processing* 97(1): 31-37.

Akhyari, P., Aubin, H*., et al.* (2011). The Quest for an Optimized Protocol for Whole-Heart Decellularization: A Comparison of Three Popular and a Novel Decellularization Technique and Their Diverse Effects on Crucial Extracellular Matrix Qualities. *Tissue Engineering Part C-Methods* 17(9): 915-926.

Akuthota, P. and Weller, P. F. (2015). Spectrum of Eosinophilic End-Organ Manifestations. *Immunology and Allergy Clinics of North America* 35(3): 403-411.

Alam, R. (2009). Foreword: What Do Eosinophils Do in the Gastrointestinal Mucosa? *Immunology and Allergy Clinics of North America* 29(1): xvii-xviii.

Alfranca, A. (2009). VEGF therapy: a timely retreat. *Cardiovascular Research* 83(4): 611-612.

Allman, A. J., McPherson, T. B*., et al.* (2001). Xenogeneic extracellular matrix grafts elicit a Th2-restricted immune response. *Transplantation* 71(11): 1631-1640.

Anderson, C. R., Ponce, A. M*., et al.* (2004). Immunohistochemical identification of an extracellular matrix scaffold that microguides capillary sprouting in vivo. *Journal of Histochemistry & Cytochemistry* 52(8): 1063-1072.

Anderson, J. M. (2011). CHAPTER 38 - Biocompatibility and Bioresponse to Biomaterials. Principles of Regenerative Medicine (Second edition). A. A. L. A. T. Nerem. San Diego, Academic Press: 693-716.

Anderson, J. M., Rodriguez, A*., et al.* (2008). Foreign body reaction to biomaterials. *Seminars in Immunology* 20(2): 86-100.

Andrady, A. L. (2008). Science and Technology of Polymer Nanofibers. Hoboken, New Jersey, John Wiley & Sons, Inc.

Arul, G. S. and Parikh, D. (2008). Oesophageal replacement in children. *Annals of the Royal College of Surgeons of England* 90(1): 7-12.

Ashley, R. A., Roth, C. C*., et al.* (2010). Regional variations in small intestinal submucosa evoke differences in inflammation with subsequent impact on tissue regeneration in the rat bladder augmentation model. *Bju International* 105(10): 1462-1468.

Athanasou, N. A. and Quinn, J. (1990). Immunophenotypic differences between osteoclasts and macrophage polykaryons: immunohistological distinction and implications for osteoclast ontogeny and function. *Journal of Clinical Pathology* 43(12): 997-1003.

Ayres, C., Bowlin, G. L*., et al.* (2006). Modulation of anisotropy in electrospun tissue-engineering scaffolds: Analysis of fiber alignment by the fast Fourier transform. *Biomaterials* 27(32): 5524-5534.

Bach, F. H., Ferran, C*., et al.* (1997). Accommodation of vascularized xenografts: expression of "protective genes" by donor endothelial cells in a host Th2 cytokine environment. *Nature Medicine* 3(2): 196-204.

Bader, A., Schilling, T*., et al.* (1998). Tissue engineering of heart valves - human endothelial cell seeding of detergent acellularized porcine valves. *European Journal of Cardio-Thoracic Surgery* 14(3): 279-284.

Badylak, S., Kokini, M*., et al.* (2001). Strength over time of a resorbable bioscaffold for body wall repair in a dog model. *Journal of Surgical Research* 99(2): 282-287.

Badylak, S., Meurling, S*., et al.* (2000). Resorbable bioscaffold for esophageal repair in a dog model. *Journal of pediatric surgery* 35(7): 1097-1103.

Badylak, S., Obermiller, J*., et al.* (2003). Extracellular matrix for myocardial repair. *Heart Surgery Forum* 6(2): E20-E26.

Badylak, S. F. (1989). Small intestinal submucosa as a large diameter vascular graft in the dog. *The Journal of surgical research* 47(1): 74-80.

Badylak, S. F. (2004). Xenogeneic extracellular matrix as a scaffold for tissue reconstruction. *Transplant Immunology* 12(3-4): 367-377.

Badylak, S. F. (2005). Regenerative medicine and developmental biology: The role of the extracellular matrix. *The Anatomical Record Part B: The New Anatomist* 287B(1): 36-41.

Badylak, S. F., Freytes, D. O*., et al.* (2009). Extracellular matrix as a biological scaffold material: Structure and function. *Acta Biomaterialia* 5(1): 1-13.

Badylak, S. F. and Gilbert, T. W. (2008). Immune response to biologic scaffold materials. *Semin Immunol* 20(2): 109-116.

Badylak, S. F., Taylor, D*., et al.* (2011). Whole-Organ Tissue Engineering: Decellularization and Recellularization of Three-Dimensional Matrix Scaffolds. Annual Review of Biomedical Engineering, Vol 13. M. L. Yarmush, J. S. Duncan and M. L. Gray. Palo Alto, Annual Reviews. 13: 27-53.

Badylak, S. F., Tullius, R*., et al.* (1995). The use of xenogeneic small intestinal submucosa as a biomaterial for Achille's tendon repair in a dog model. *Journal of Biomedical Materials Research* 29(8): 977-985.

Barber, F. A. and Aziz-Jacobo, J. (2009). Biomechanical Testing of Commercially Available Soft-Tissue Augmentation Materials. *Arthroscopy-the Journal of Arthroscopic and Related Surgery* 25(11): 1233-1239.

Barnes, C. A., Brison, J*., et al.* (2011). The surface molecular functionality of decellularized extracellular matrices. *Biomaterials* 32(1): 137-143.

Basu, J., Mihalko, K*., et al.* (2012). Extension of bladder-based organ regeneration platform for tissue engineering of esophagus. *Medical Hypotheses* 78(2): 231-234.

Beattie, A. J., Gilbert, T. W*., et al.* (2009). Chemoattraction of Progenitor Cells by Remodeling Extracellular Matrix Scaffolds. *Tissue Engineering Part A* 15(5): 1119-1125.

Beckstead, B. L., Santosa, D. M*., et al.* (2006). Mimicking cell-cell interactions at the biomaterial-cell interface for control of stem cell differentiation. *Journal of Biomedical Materials Research Part A* 79A(1): 94-103.

Bejjani, G. K., Zabramski, J*., et al.* (2007). Safety and efficacy of the porcine small intestinal submucosa dural substitute: results of a prospective multicenter study and literature review. *Journal of Neurosurgery* 106(6): 1028-1033.

Bell, E. (2007). Chapter Seventeen - Models as precursors for prosthetic devices. Principles of Tissue Engineering (Third Edition). R. L. L. Vacanti. Burlington, Academic Press: 241-250.

Bellan, L. M. and Craighead, H. G. (2011). Applications of controlled electrospinning systems. *Polymers for Advanced Technologies* 22(3): 304-309.

Bissell, M. J., Hall, H. G*., et al.* (1982). How Does the Extracellular-Matrix Direct Gene-Expression. *Journal of Theoretical Biology* 99(1): 31-68.

Blackwood, K., McKean, R*., et al.* (2008). Development of biodegradable electrospun scaffolds for dermal replacement. *Biomaterials* 29(21): 3091-3104.

Boland, E. D., Wnek, G. E*., et al.* (2001). Tailoring tissue engineering scaffolds using electrostatic processing techniques: A study of poly(glycolic acid) electrospinning. *Journal of Macromolecular Science-Pure and Applied Chemistry* 38(12): 1231-1243.

Borschel, G. H., Dennis, R. G*., et al.* (2004). Contractile skeletal muscle tissue-engineered on an acellular scaffold. *Plastic and Reconstructive Surgery* 113(2): 595-602.

Brennan, E. P., Reing, J*., et al.* (2006). Antibacterial activity within degradation products of biological scaffolds composed of extracellular matrix. *Tissue engineering* 12(10): 2949-2955.

Brodbeck, W. G., Colton, E.*, et al.* (2003). Effects of adsorbed heat labile serum proteins and fibrinogen on adhesion and apoptosis of monocytes/macrophages on biomaterials. *Journal of Materials Science-Materials in Medicine* 14(8): 671-675.

Brodbeck, W. G., Shive, M. S.*, et al.* (2001). Influence of biomaterial surface chemistry on the apoptosis of adherent cells. *Journal of Biomedical Materials Research* 55(4): 661-668.

Brown, B., Lindberg, K.*, et al.* (2006). The basement membrane component of biologic scaffolds derived from extracellular matrix. *Tissue Engineering* 12(3): 519-526.

Brown, B. N., Barnes, C. A.*, et al.* (2010). Surface characterization of extracellular matrix scaffolds. *Biomaterials* 31(3): 428-437.

Brown, B. N., Valentin, J. E.*, et al.* (2009). Macrophage phenotype and remodeling outcomes in response to biologic scaffolds with and without a cellular component. *Biomaterials.* 30(8): 1482-1491. Epub 2009 Jan 1481.

Buck, R. C. (1982). The Influence of Contact Guidance on the Orientation of Colonies of Subcultured Vascular Smooth Muscle Cells. *In Vitro* 18(9): 783-788.

Bye, F. J., Bissoli, J.*, et al.* (2013). Development of bilayer and trilayer nanofibrous/microfibrous scaffolds for regenerative medicine. *Biomaterials Science* 1(9): 942-951.

Bye, F. J., Wang, L.*, et al.* (2012). Postproduction Processing of Electrospun Fibres for Tissue Engineering. *Journal of Visualized Experiments : JoVE*(66): 4172.

Caione, P., Boldrini, R.*, et al.* (2012). Bladder augmentation using acellular collagen biomatrix: a pilot experience in exstrophic patients. *Pediatric Surgery International* 28(4): 421-428.

Carmeliet, P. (2000). Mechanisms of angiogenesis and arteriogenesis. *Nature Medicine* 6(4): 389-395.

Catiker, E., Gumusderelioglu, M.*, et al.* (2000). Degradation of PLA, PLGA homo- and copolymers in the presence of serum albumin: a spectroscopic investigation. *Polymer International* 49(7): 728-734.

Choi, J. S., Lee, S. J.*, et al.* (2008). The influence of electrospun aligned poly(epsilon-caprolactone)/collagen nanofiber meshes on the formation of self-aligned skeletal muscle myotubes. *Biomaterials* 29(19): 2899-2906.

Choi, J. S., Piao, Y.*, et al.* (2014). Circumferential alignment of vascular smooth muscle cells in a circular microfluidic channel. *Biomaterials* 35(1): 63-70.

Clarke, S. (1981). Direct renaturation of the dodecyl sulfate complexes of proteins with triton X-100. *Biochimica et Biophysica Acta (BBA) - Protein Structure* 670(2): 195-202.

Colton, C. K. (1995). Implantable biohybrid artificial organs. *Cell Transplant* 4(4): 415-436.

Conconi, M. T., De Coppi, P.*, et al.* (2005). Tracheal matrices, obtained by a detergent-enzymatic method, support in vitro the adhesion of chondrocytes and tracheal epithelial cells. *Transplant international* 18(6): 727-734.

Conklin, B. S., Richter, E. R.*, et al.* (2002). Development and evaluation of a novel decellularized vascular xenograft. *Medical Engineering & Physics* 24(3): 173-183.

Cortijo, J., Dixon, J. S.*, et al.* (1987). Influence of some variables in the Triton X-100 method of skinning the plasmalemmal membrane from guinea pig trachealis muscle. *Journal of Pharmacological Methods* 18(3): 253-266.

Crapo, P. and Gilbert (2011). An overview of tissue and whole organ decellularization processes. *Biomaterials* 32(12): 3233-3243.

Daly, K. A., Stewart-Akers, A. M.*, et al.* (2009). Effect of the alpha Gal Epitope on the Response to Small Intestinal Submucosa Extracellular Matrix in a Nonhuman Primate Model. *Tissue Engineering Part A* 15(12): 3877-3888.

Deitzel, J. M., Kleinmeyer, J.*, et al.* (2001). The effect of processing variables on the morphology of electrospun nanofibers and textiles. *Polymer* 42(1): 261-272.

Delgado, L., Pandit, A.*, et al.* (2014). Influence of sterilisation methods on collagen-based devices stability and properties. *Expert Review of Medical Devices* 11(3): 305-314.

Dersch, R., Graeser, M.*, et al.* (2007). Electrospinning of nanofibres: Towards new techniques, functions, and applications. *Australian Journal of Chemistry* 60(10): 719-728.

Derwin, K. A., Baker, A. R.*, et al.* (2006). Commercial extracellular matrix scaffolds for rotator cuff tendon repair - Biomechanical, biochemical, and cellular properties. *Journal of Bone and Joint Surgery-American Volume* 88A(12): 2665-2672.

Doede, T., Bondartschuk, M.*, et al.* (2009). Unsuccessful Alloplastic Esophageal Replacement With Porcine Small Intestinal Submucosa. *Artificial Organs* 33(4): 328-333.

Du, X. F., Kwon, S. K.*, et al.* (2012). Tracheal reconstruction by mesenchymal stem cells with small intestine submucosa in rabbits. *International Journal of Pediatric Otorhinolaryngology* 76(3): 345-351.

Dufrane, D., Mourad, M.*, et al.* (2008). Regeneration of abdominal wall musculofascial defects by a human acellular collagen matrix. *Biomaterials* 29(14): 2237-2248.

Dvorak, H. F., Brown, L. F.*, et al.* (1995). Vascular permeability factor/vascular endothelial growth factor, microvascular hyperpermeability, and angiogenesis. *American Journal of Pathology* 146(5): 1029-1039.

Eberli, D., Filho, L. F.*, et al.* (2009). Composite scaffolds for the engineering of hollow organs and tissues. *Methods* 47(2): 109-115.

Ectors, N., Lismont, D.*, et al.* (2008). Short- and long-term bacterial inhibiting effect of high concentrations of glycerol used in the preservation of skin allografts. *Burns* 34(2): 205-211.

Enayati, M., Chang, M.-W.*, et al.* (2011). Electrohydrodynamic preparation of particles, capsules and bubbles for biomedical engineering applications. *Colloids and Surfaces A: Physicochemical and Engineering Aspects* 382(1-3): 154-164.

Engineer, C., Parikh, J.*, et al.* (2001). Review on Hydrolytic Degradation Behavior of Biodegradable Polymers from Controlled Drug Delivery System *Trends in Biomaterials & Artificial Organs* 25(2): 79-85.

Fallon, A., Goodchild, T.*, et al.* (2012). Remodeling of Extracellular Matrix Patch used for Carotid Artery Repair. *Journal of Surgical Research* 175(1): e25-e34.

Ferrara, N. (2004). Vascular Endothelial Growth Factor: Basic Science and Clinical Progress. *Endocrine Reviews* 25(4): 581-611.

Flemming, R. G., Murphy, C. J.*, et al.* (1999). Effects of synthetic micro- and nano-structured surfaces on cell behavior. *Biomaterials* 20(6): 573-588.

Fong, H., Chun, I.*, et al.* (1999). Beaded nanofibers formed during electrospinning. *Polymer* 40(16): 4585-4592.

Franklin, M. E., Gonzalez, J. J.*, et al.* (2004). Use of porcine small intestinal submucosa as a prosthetic device for laparoscopic repair of hernias in contaminated fields: 2-year follow-up. *Hernia* 8(3): 186-189.

Freeman, I. and Cohen, S. (2009). The influence of the sequential delivery of angiogenic factors from affinity-binding alginate scaffolds on vascularization. *Biomaterials* 30(11): 2122-2131.

Frenot, A. (2003). Polymer nanofibers assembled by electrospinning. *Current opinion in colloid & interface science* 8(1): 64-75.

Freytes, D. O., Badylak, S. F.*, et al.* (2004). Biaxial strength of multilaminated extracellular matrix scaffolds. *Biomaterials* 25(12): 2353-2361.

Freytes, D. O., Rundell, A. E.*, et al.* (2005). Analytically derived material properties of multilaminated extracellular matrix devices using the ball-burst test. *Biomaterials* 26(27): 5518-5531.

Freytes, D. O., Tullius, R. S.*, et al.* (2008). Hydrated versus lyophilized forms of porcine extracellular matrix derived from the urinary bladder. *Journal of Biomedical Materials Research Part A* 87A(4): 862-872.

Fridrikh, S. V., Yu, J. H.*, et al.* (2003). Controlling the fiber diameter during electrospinning. *Physical Review Letters* 90(14).

Frisch, S. M. and Screaton, R. A. (2001). Anoikis mechanisms. *Current Opinion in Cell Biology* 13(5): 555-562.

Gilbert, T. W., Freund, J. M.*, et al.* (2009). Quantification of DNA in Biologic Scaffold Materials. *Journal of Surgical Research* 152(1): 135-139.

Gilbert, T. W., Sellaro, T. L.*, et al.* (2006). Decellularization of tissues and organs. *Biomaterials* 27(19): 3675-3683.

Gilbert, T. W., Wognum, S.*, et al.* (2008). Collagen fiber alignment and biaxial mechanical behavior of porcine urinary bladder derived extracellular matrix. *Biomaterials* 29(36): 4775-4782.

Glass-Brudzinski, J., Perizzolo, D.*, et al.* (2002). Effects of substratum surface topography on the organization of cells and collagen fibers in collagen gel cultures. *Journal of Biomedical Materials Research* 61(4): 608-618.

Glynn, J. J., Polsin, E. G.*, et al.* (2014). Crosslinking Decreases the Hemocompatibility of Decellularized, Porcine Small Intestinal Submucosa. *Acta Biomaterialia*(0).

Goulle, F. (2012). Use of porcine small intestinal submucosa for corneal reconstruction in dogs and cats: 106 cases. *The Journal of small animal practice* 53(1): 34-43.

Grikscheit, T., Ochoa, E. R.*, et al.* (2003). Tissue-engineered esophagus: experimental substitution by onlay patch or interposition. *The Journal of Thoracic and Cardiovascular Surgery* 126(2): 537-544.

Grimes, M., Pembroke, J. T.*, et al.* (2005). The effect of choice of sterilisation method on the biocompatibility and biodegradability of SIS (small intestinal submucosa). *Bio-Medical Materials and Engineering* 15(1-2): 65-71.

Gu, Z. and Zhang (2011). Biocompatibility of genipin-fixed porcine aorta as a possible esophageal prosthesis. *Materials science & engineering. C, Biomimetic materials, sensors and systems* 31(7): 1593-1601.

Gupta, D., Venugopal, J.*, et al.* (2009). Aligned and random nanofibrous substrate for the in vitro culture of Schwann cells for neural tissue engineering. *Acta Biomaterialia* 5(7): 2560-2569.

Haas, A. (2007). The phagosome: Compartment with a license to kill. *Traffic* 8(4): 311-330.

Hacker, M. C. and Mikos, A. G. (2011). Chapter 33 - Synthetic Polymers. Principles of Regenerative Medicine (Second edition). A. A. L. A. T. Nerem. San Diego, Academic Press: 587-622.

Han, F., Jia, X.*, et al.* (2013). Performance of a multilayered small-diameter vascular scaffold dual-loaded with VEGF and PDGF. *Biomaterials* 34(30): 7302-7313.

Hardick, O., Stevens, B.*, et al.* (2011). Nanofibre fabrication in a temperature and humidity controlled environment for improved fibre consistency. *Journal of Materials Science* 46(11): 3890-3898.

Hartel, M. and Wente (2004). Surgical treatment of oesophageal cancer. *Digestive diseases* 22(2): 213-220.

Hartman, R. P. A., Borra, J. P.*, et al.* (1999). The evolution of electrohydrodynamic sprays produced in the cone-jet mode, a physical model. *Journal of Electrostatics* 47(3): 143-170.

Hayashi, T. (1994). Biodegradable polymers for biomedical uses. *Progress in Polymer Science* 19(4): 663-702.

Hayati, I., Bailey, A.*, et al.* (1987b). Investigations into the mechanism of electrohydrodynamic spraying of liquids : II. Mechanism of stable jet formation and electrical forces acting on a liquid cone. *Journal of Colloid and Interface Science* 117(1): 222-230.

Hayati, I., Bailey, A. I.*, et al.* (1987a). Investigations into the mechanisms of electrohydrodynamic spraying of liquids : I. Effect of electric field and the environment on pendant drops and factors affecting the formation of stable jets and atomization. *Journal of Colloid and Interface Science* 117(1): 205-221.

He, M. and Callanan, A. (2012). Comparison of methods for whole organ decellularisation in tissue engineering of bio-artificial organs. *Tissue Eng Part B Rev* 19: 19.

Heidari, I., Mosavi Mashhadi, M.*, et al.* (2013). A novel approach for preparation of aligned electrospun polyacrylonitrile nanofibers. *Chemical Physics Letters* 590(0): 231-234.

Henry, J. A., Burugapalli, K.*, et al.* (2009). Structural variants of biodegradable polyesterurethane in vivo evoke a cellular and angiogenic response that is dictated by architecture. *Acta Biomaterialia* 5(1): 29-42.

Hersel, U., Dahmen, C.*, et al.* (2003). RGD modified polymers: biomaterials for stimulated cell adhesion and beyond. *Biomaterials* 24(24): 4385-4415.

Hodde, J. (2006). Extracellular matrix as a bioactive material for soft tissue reconstruction. *ANZ J Surg* 76(12): 1096-1100.

Hodde, J., Janis, A.*, et al.* (2007). Effects of sterilization on an extracellular matrix scaffold: Part I. Composition and matrix architecture. *Journal of Materials Science-Materials in Medicine* 18(4): 537-543.

Hodde, J., Janis, A.*, et al.* (2007b). Effects of sterilization on an extracellular matrix scaffold: Part II. Bioactivity and matrix interaction. *Journal of Materials Science-Materials in Medicine* 18(4): 545-550.

Hodde, J., Record, R.*, et al.* (2002). Fibronectin peptides mediate HMEC adhesion to porcine-derived extracellular matrix. *Biomaterials* 23(8): 1841-1848.

Hodde, J. P., Badylak, S. F.*, et al.* (1996). Glycosaminoglycan content of small intestinal submucosa: a bioscaffold for tissue replacement. *Tissue engineering* 2(3): 209-217.

Hodde, J. P., Record, R. D.*, et al.* (2001). Vascular endothelial growth factor in porcine-derived extracellular matrix. *Endothelium.* 8(1): 11-24.

Hodde, J. P., Record, R. D.*, et al.* (2002). Retention of endothelial cell adherence to porcine-derived extracellular matrix after disinfection and sterilization. *Tissue engineering* 8(2): 225-234.

Holland, A. J. A. and Fitzgerald, D. A. (2010). Oesophageal atresia and tracheo-oesophageal fistula: current management strategies and complications. *Paediatric Respiratory Reviews* 11(2): 100-107.

Horst, M., Madduri, S.*, et al.* (2013). A bilayered hybrid microfibrous PLGA–Acellular matrix scaffold for hollow organ tissue engineering. *Biomaterials* 34(5): 1537-1545.

Hoshiba, T., Lu, H.*, et al.* (2010). Decellularized matrices for tissue engineering. *Expert opinion on biological therapy* 10(12): 1717-1728.

Hu, W. J., Eaton, J. W.*, et al.* (2001). Molecular basis of biomaterial-mediated foreign body reactions. *Blood* 98(4): 1231-1238.

Huang, Q. H., Dawson, R. A.*, et al.* (2004). Use of peracetic acid to sterilize human donor skin for production of acellular dermal matrices for clinical use. *Wound repair and regeneration* 12(3): 276-287.

Huber, A. and Badylak, S. F. (2011). Chapter 34 - Biological Scaffolds for Regenerative Medicine. Principles of Regenerative Medicine (Second edition). A. Anthony, L.

Robert, A. T. James, R. L. J. A. T. Robert M. NeremA2 - Anthony Atala and M. N. Robert. San Diego, Academic Press: 623-635.

Hulbert, S. F., Young, F. A.*, et al.* (1970). Potential of ceramic materials as permanently implantable skeletal prostheses. *Journal of Biomedical Materials Research* 4(3): 433-456.

Hwang, C. M., Park, J. Y.*, et al.* (2009). Controlled cellular orientation on PLGA microfibers with defined diameters. *Biomedical Microdevices* 11(4): 739-746.

Intra, J., Glasgow, J. M.*, et al.* (2008). Pulsatile release of biomolecules from polydimethylsiloxane (PDMS) chips with hydrolytically degradable seals. *Journal of Controlled Release* 127(3): 280-287.

Ionescu, L. C. and Mauck, R. L. (2013). Porosity and Cell Preseeding Influence Electrospun Scaffold Maturation and Meniscus Integration In Vitro. *Tissue engineering. Part A* 19(3-4): 538-547.

Janis, A. D., Johnson, C. C.*, et al.* (2011). Structural Characteristics of Small Intestinal Submucosa Constructs Dictate In Vivo Incorporation and Angiogenic Response. *Journal of Biomaterials Applications*.

Jansen, E. J. P., Sladek, R. E. J.*, et al.* (2005). Hydrophobicity as a design criterion for polymer scaffolds in bone tissue engineering. *Biomaterials* 26(21): 4423-4431.

Jia, L., Prabhakaran, M. P.*, et al.* (2014). Guiding the orientation of smooth muscle cells on random and aligned polyurethane/collagen nanofibers. *Journal of Biomaterials Applications*.

Jia, X., Zhao, C.*, et al.* (2011). Sustained Release of VEGF by Coaxial Electrospun Dextran/PLGA Fibrous Membranes in Vascular Tissue Engineering. *Journal of biomaterials science. Polymer edition* 22(13): 1811-1827.

Jungebluth, P., Go, T.*, et al.* (2009). Structural and morphologic evaluation of a novel detergent-enzymatic tissue-engineered tracheal tubular matrix. *Journal of Thoracic and Cardiovascular Surgery* 138(3): 586-593.

Kaihara, S., Kim, S.*, et al.* (1999). End-to-end anastomosis between tissue-engineered intestine and native small bowel. *Tissue engineering* 5(4): 339-346.

Karageorgiou, V. and Kaplan, D. (2005). Porosity of 3D biomaterial scaffolds and osteogenesis. *Biomaterials* 26(27): 5474-5491.

Katta, P., Alessandro, M.*, et al.* (2004). Continuous Electrospinning of Aligned Polymer Nanofibers onto a Wire Drum Collector. *Nano Letters* 4(11): 2215-2218.

Keane, T. J., Londono, R.*, et al.* (2012). Consequences of ineffective decellularization of biologic scaffolds on the host response. *Biomaterials* 33(6): 1771-1781.

Kelly, D. J., Rosen, A. B.*, et al.* (2009). Increased Myocyte Content and Mechanical Function Within a Tissue-Engineered Myocardial Patch Following Implantation. *Tissue Engineering Part A* 15(8): 2189-2201.

Khoo, T. L., Halim, A. S.*, et al.* (2010). The application of glycerol-preserved skin allograft in the treatment of burn injuries: An analysis based on indications. *Burns* 36(6): 897-904.

Kim, B. S., Park, I. K.*, et al.* (2011). Design of artificial extracellular matrices for tissue engineering. *Progress in Polymer Science* 36(2): 238-268.

Kim, J. Y. and Cho, D. W. (2009). Blended PCL/PLGA scaffold fabrication using multi-head deposition system. *Microelectronic Engineering* 86(4-6): 1447-1450.

Kim, S. S., Kaihara, S.*, et al.* (1999). Effects of anastomosis of tissue-engineered neointestine to native small bowel. *Journal of Surgical Research* 87(1): 6-13.

Kochupura, P. V., Azeloglu, E. U.*, et al.* (2005). Tissue-engineered myocardial patch derived from extracellular matrix provides regional mechanical function. *Circulation* 112(9): I144-I149.

Komura, M., Kim, J.*, et al.* (2011). Chapter 59 - The Digit: Engineering of Phalanges and Small Joints. Principles of Regenerative Medicine (Second edition). A. A. L. A. T. Nerem. San Diego, Academic Press: 1091-1103.

Koobatian, M. T., Row, S.*, et al.* (2016). Successful endothelialization and remodeling of a cell-free small-diameter arterial graft in a large animal model. *Biomaterials* 76: 344-358.

Kropp, B. P., Cheng, E. Y.*, et al.* (2004). Reliable and Reproducible Bladder Regeneration Using Unseeded Distal Small Intestinal Submucosa. *The Journal of Urology* 172(4, Supplement): 1710-1713.

Kropp, B. P., Eppley, B. L.*, et al.* (1995). Experimental assessment of small intestinal submucosa as a bladder wall substitute. *Urology* 46(3): 396-400.

Kuppan, P., Sethuraman, S.*, et al.* (2012). Tissue engineering interventions for esophageal disorders — Promises and challenges. *Biotechnology Advances* 30(6): 1481-1492.

Kurpinski, K. T., Stephenson, J. T.*, et al.* (2010). The effect of fiber alignment and heparin coating on cell infiltration into nanofibrous PLLA scaffolds. *Biomaterials* 31(13): 3536-3542.

Lanir, Y. (1979). A structural theory for the homogeneous biaxial stress-strain relationships in flat collagenous tissues. *Journal of Biomechanics* 12(6): 423-436.

Lantz, G. C., Badylak, S. F.*, et al.* (1990). Small intestinal submucosa as a small-diameter arterial graft in the dog. *Journal of investigative surgery : the official journal of the Academy of Surgical Research* 3(3): 217-227.

Laschke, M. W. and Menger, M. D. (2012). Vascularization in Tissue Engineering: Angiogenesis versus Inosculation. *European Surgical Research* 48(2): 85-92.

Lawler, M. R., Foster, J. H.*, et al.* (1971). Evaluation of canine intestinal submucosa as a vascular substitute. *The American Journal of Surgery* 122(4): 517-519.

Leung, D., Cachianes, G.*, et al.* (1989). Vascular endothelial growth factor is a secreted angiogenic mitogen. *Science* 246(4935): 1306-1309.

Li, Z. B., Song, L. J.*, et al.* (2015). Tough and VEGF-releasing scaffolds composed of artificial silk fibroin mats and a natural acellular matrix. *Rsc Advances* 5(22): 16748-16758.

Lindhorst, D., Tavassol, F.*, et al.* (2010). Effects of VEGF loading on scaffold-confined vascularization. *Journal of Biomedical Materials Research Part A* 95A(3): 783-792.

Lode, A., Wolf-Brandstetter, C.*, et al.* (2007). Calcium phosphate bone cements, functionalized with VEGF: release kinetics and biological activity. *Journal of Biomedical Materials Research Part A* 81A(2): 474-483.

Lopes, M. F., Cabrita, A.*, et al.* (2006). Esophageal replacement in rat using porcine intestinal submucosa as a patch or a tube-shaped graft. *Diseases of the Esophagus* 19(4): 254-259.

Lu, L., Peter, S. J.*, et al.* (2000). In vitro and in vivo degradation of porous poly(DL-lactic-co-glycolic acid) foams. *Biomaterials* 21(18): 1837-1845.

Luo, C., Nangrejo, M.*, et al.* (2010). A novel method of selecting solvents for polymer electrospinning. *Polymer* 51(7): 1654-1662.

Macchiarini, P., Jungebluth, P.*, et al.* (2008). Clinical transplantation of a tissue-engineered airway. *The Lancet* 372(9655): 2023-2030.

Macewan, M., Colton, E.*, et al.* (2005). Lymphocytes and the foreign body response: Lymphocyte enhancement of macrophage adhesion and fusion. *Journal of biomedical materials research. Part A* 74(2): 222-229.

Mackie, D. P. (1997). The Euro Skin Bank: development and application of glycerol-preserved allografts. *J Burn Care Rehabil* 18(1 Pt 2): S7-9.

Maghsoudlou, P., Totonelli, G.*, et al.* (2013). A Decellularization Methodology for the Production of a Natural Acellular Intestinal Matrix. *Journal of Visualized Experiments*(80): e50658.

Marcal, H., Ahmed, T*., et al.* (2012). A comprehensive protein expression profile of extracellular matrix biomaterial derived from porcine urinary bladder. *Regenerative medicine* 7(2): 159-166.

Martin, P. and Leibovich, S. J. (2005). Inflammatory cells during wound repair: the good, the bad and the ugly. *Trends in Cell Biology* 15(11): 599-607.

Matsumoto, T., Holmes, R. H*., et al.* (1966). Replacement of Large Veins with Free Inverted Segments of Small Bowel - Autografts of Submucosal Membrane in Dogs and Clinical Use. *Annals of Surgery* 164(5): 845-&.

Matsumoto, T., Holmes, R. H*., et al.* (1966). The fate of the inverted segment of small bowel used for the replacement of major veins. *Surgery* 60(3): 739-743.

Matthews, J. A., Wnek, G. E*., et al.* (2002). Electrospinning of collagen nanofibers. *Biomacromolecules* 3(2): 232-238.

McDevitt, C. A., Wildey, G. M*., et al.* (2003). Transforming growth factor-beta 1 in a sterilized tissue derived from the pig small intestine submucosa. *Journal of Biomedical Materials Research Part A* 67A(2): 637-640.

McNally, A. K. and Anderson, J. M. (2002). beta 1 and beta 2 integrins mediate adhesion during macrophage fusion and multinucleated foreign body giant cell formation. *American Journal of Pathology* 160(2): 621-630.

McNally, A. K. and Anderson, J. M. (2015). Phenotypic expression in human monocyte-derived interleukin-4-induced foreign body giant cells and macrophagesin vitro: Dependence on material surface properties. *Journal of biomedical materials research. Part A* 103(4): 1380-1390.

Meezan, E., Hjelle, J. T*., et al.* (1975). A simple, versatile, nondisruptive method for the isolation of morphologically and chemically pure basement membranes from several tissues. *Life Sciences* 17(11): 1721-1732.

Merguerian, P. A., Reddy, P. P*., et al.* (2000). Acellular bladder matrix allografts in the regeneration of functional bladders: evaluation of large-segment (> 24 cm(2)) substitution in a porcine model. *Bju International* 85(7): 894-898.

Middleton, J. C. and Tipton, A. J. (2000). Synthetic biodegradable polymers as orthopedic devices. *Biomaterials* 21(23): 2335-2346.

Miller, K. M. and Anderson, J. M. (1989). In vitro stimulation of fibroblast activity by factors generated from human monocytes activated by biomedical polymers. *Journal of Biomedical Materials Research* 23(8): 911-930.

Misseri, R., Cain, M. P*., et al.* (2005). Small intestinal submucosa bladder neck slings for incontinence associated with neuropathic bladder. *The Journal of Urology* 174(4, Part 2): 1680-1682.

Moioli, E. K., Clark, P. A*., et al.* (2008). Synergistic Actions of Hematopoietic and Mesenchymal Stem/Progenitor Cells in Vascularizing Bioengineered Tissues. *PLoS ONE* 3(12).

Mosser, D. M. (2003). The many faces of macrophage activation. *Journal of leukocyte biology* 73(2): 209-212.

Natarajan, A. and Mahavadi (2011). Preparation of Solid and Hollow Asphaltene Fibers by Single Step Electrospinning. *Journal of Engineered Fibers and Fabrics* 6(2): 1-6.

Neufeld, G., Cohen, T*., et al.* (1999). Vascular endothelial growth factor (VEGF) and its receptors. *Faseb Journal* 13(1): 9-22.

Nguyen, L. T. H., Chen, S*., et al.* (2013). Biological, Chemical, and Electronic Applications of Nanofibers. *Macromolecular materials and engineering* 298(8): 822-867.

Niemisto, A., Dunmire, V*., et al.* (2005). Robust quantification of in vitro angiogenesis through image analysis. *Ieee Transactions on Medical Imaging* 24(4): 549-553.

Nivison Smith, L. and Weiss, A. (2012). Alignment of human vascular smooth muscle cells on parallel electrospun synthetic elastin fibers. *Journal of biomedical materials research. Part A* 100(1): 155-161.

Olde Damink, L. H. H., Dijkstra, P. J.*, et al.* (1995). Influence of ethylene oxide gas treatment on the in vitro degradation behavior of dermal sheep collagen. *Journal of Biomedical Materials Research* 29(2): 149-155.

Oliveira, A. C., Garzon, I.*, et al.* (2013). Evaluation of small intestine grafts decellularization methods for corneal tissue engineering. *PLoS ONE* 8(6): e66538.

Omae, H., Zhao, C. F.*, et al.* (2009). Multilayer Tendon Slices Seeded with Bone Marrow Stromal Cells: A Novel Composite for Tendon Engineering. *Journal of Orthopaedic Research* 27(7): 937-942.

Orberg, J., Baer, E.*, et al.* (1983). Organization of collagen fibers in the intestine. *Connective tissue research* 11(4): 285-297.

Ott, H. C., Matthiesen, T. S.*, et al.* (2008). Perfusion-decellularized matrix: using nature's platform to engineer a bioartificial heart. *Nature Medicine* 14(2): 213-221.

Pachence, J. M., Bohrer, M. P.*, et al.* (2007). Chapter Twenty-Three - Biodegradable polymers. Principles of Tissue Engineering (Third Edition). R. L. L. Vacanti. Burlington, Academic Press: 323-339.

Paine, M. D., Alexander, M. S.*, et al.* (2007). Nozzle and liquid effects on the spray modes in nanoelectrospray. *Journal of Colloid and Interface Science* 305(1): 111-123.

Pan, Z. and Ding, J. D. (2012). Poly(lactide-co-glycolide) porous scaffolds for tissue engineering and regenerative medicine. *Interface Focus* 2(3): 366-377.

Park, K. M. and Woo, H. M. (2012). Systemic decellularization for multi-organ scaffolds in rats. *Transplantation proceedings* 44(4): 1151-1154.

Pirayesh, A., Hoeksema, H.*, et al.* (2015). Glyaderm® dermal substitute: Clinical application and long-term results in 55 patients. *Burns* 41(1): 132-144.

Poghosyan, T., Gaujoux, S.*, et al.* (2011). Bioartificial Oesophagus in the Era of Tissue Engineering. *Journal of Pediatric Gastroenterology and Nutrition* 52: S16-S17.

Prabaharan, M., Jayakumar, R.*, et al.* (2012). Electrospun Nanofibrous Scaffolds-Current Status and Prospects in Drug Delivery. Biomedical Applications of Polymeric Nanofibers. R. Jayakumar and S. Nair, Springer Berlin Heidelberg. 246: 241-262.

Qin, H. and Dunn, J. C. Y. (2011). Small Intestinal Submucosa Seeded with Intestinal Smooth Muscle Cells in a Rodent Jejunal Interposition Model. *The Journal of surgical research* 171(1): E21-E26-E21-E26.

Quirk, R. A., Kellam, B.*, et al.* (2003). Cell-type-specific adhesion onto polymer surfaces from mixed cell populations. *Biotechnol Bioeng.* 81(5): 625-628.

Raeder, R. H., Badylak, S. F.*, et al.* (2002). Natural anti-galactose α1,3 galactose antibodies delay, but do not prevent the acceptance of extracellular matrix xenografts. *Transplant Immunology* 10(1): 15-24.

Raghavan, D., Kropp, B. P.*, et al.* (2005). Physical characteristics of small intestinal submucosa scaffolds are location-dependent. *Journal of Biomedical Materials Research Part A* 73A(1): 90-96.

Rapoport, H., Fish, J.*, et al.* (2012). Construction of a Tubular Scaffold that Mimics J-Shaped Stress/Strain Mechanics Using an Innovative Electrospinning Technique. *Tissue Engineering Part C: Methods* 18(8): 567-574.

Rayatpisheh, S., Heath, D. E.*, et al.* (2013). Combining cell sheet technology and electrospun scaffolding for engineered tubular, aligned, and contractile blood vessels. *Biomaterials*(0).

Rayleigh, J. W. S. (1882). On the Equilibrium of a Liquid Conducting Masses charged with Electricity. *Philosophical Magazine* 14: 184-186.

Rehfeldt, F., Engler, A. J.*, et al.* (2007). Cell responses to the mechanochemical microenvironment - Implications for regenerative medicine and drug delivery. *Advanced Drug Delivery Reviews* 59(13): 1329-1339.

Reing, J. E., Brown, B. N.*, et al.* (2010). The effects of processing methods upon mechanical and biologic properties of porcine dermal extracellular matrix scaffolds. *Biomaterials* 31(33): 8626-8633.

Reneker, D. and Yarin, A. L. (2008). Electrospinning jets and polymer nanofibers. *Polymer* 49(10): 2387-2425.

Reneker, D. H. and Chun, I. (1996). Nanometre diameter fibres of polymer, produced by electrospinning. *Nanotechnology* 7(3): 216-223.

Reneker, D. H., Yarin, A. L.*, et al.* (2000). Bending instability of electrically charged liquid jets of polymer solutions in electrospinning. *Journal of applied physics* 87(9): 4531-4547.

Reneker, D. H., Yarin, A. L.*, et al.* (2007). Electrospinning of nanofibers from polymer solutions and melts. Advances in Applied Mechanics, Vol 41. San Diego, Elsevier Academic Press Inc. 41: 43-195.

Ricchetti, E. T., Aurora, A.*, et al.* (2012). Scaffold devices for rotator cuff repair. *Journal of Shoulder and Elbow Surgery* 21(2): 251-265.

Ritchie, A., Chian, K.*, et al.* (2006). Esophagus: A Tissue Engineering Challenge. Tissue engineering and Artificial Organs. J. D. Bronzino, CRC Press: 54-51-54-19.

Roberts, R., Gallagher, J.*, et al.* (1988). Heparan sulphate bound growth factors: a mechanism for stromal cell mediated haemopoiesis. *Nature* 332(6162): 376-378.

Roth, C. C., Mondalek, F. G.*, et al.* (2011). Bladder regeneration in a canine model using hyaluronic acid-poly(lactic-co-glycolic-acid) nanoparticle modified porcine small intestinal submucosa. *Bju International* 108(1): 148-155.

Sacks, M. S. and Gloeckner, D. C. (1999). Quantification of the fiber architecture and biaxial mechanical behavior of porcine intestinal submucosa. *Journal of Biomedical Materials Research* 46(1): 1-10.

Sandusky, G. E., Badylak, S. F.*, et al.* (1992). Histologic findings after in vivo placement of small intestine submucosal vascular grafts and saphenous vein grafts in the carotid artery in dogs. *American Journal of Pathology* 140(2): 317-324.

Saxena, A. K., Ainoedhofer, H.*, et al.* (2009). Esophagus tissue engineering: in vitro generation of esophageal epithelial cell sheets and viability on scaffold. *Journal of Pediatric Surgery* 44(5): 896-901.

Saxena, A. K., Baumgart, H.*, et al.* (2010). Esophagus tissue engineering: in situ generation of rudimentary tubular vascularized esophageal conduit using the ovine model. *Journal of pediatric surgery* 45(5): 859-864.

Sellaro, T. L., Ravindra, A. K.*, et al.* (2007). Maintenance of hepatic sinusoidal endothelial cell phenotype in vitro using organ-specific extracellular matrix scaffolds. *Tissue engineering* 13(9): 2301-2310.

Shang, S., Yang, F.*, et al.* (2010). The Effect of Electrospun Fibre Alignment on the Behaviour of Rat Periodontal Ligament Cells. *European cells & materials* 19: 180-192.

Sharma, B. and Elisseeff, J. H. (2004). Engineering Structurally Organized Cartilage and Bone Tissues. *Annals of biomedical engineering* 32(1): 148-159.

Shearer, H., Ellis, M. J.*, et al.* (2006). Effects of common sterilization methods on the structure and properties of poly(D,L lactic-co-glycolic acid) scaffolds. *Tissue engineering* 12(10): 2717-2727.

Shenoy, S. L., Bates, W. D.*, et al.* (2005). Role of chain entanglements on fiber formation during electrospinning of polymer solutions: good solvent, non-specific polymer-polymer interaction limit. *Polymer* 46(10): 3372-3384.

Shin, Y. M., Hohman, M. M.*, et al.* (2001a). Electrospinning: A whipping fluid jet generates submicron polymer fibers. *Applied Physics Letters* 78(8): 1149-1151.
Shin, Y. M., Hohman, M. M.*, et al.* (2001b). Experimental characterization of electrospinning: the electrically forced jet and instabilities. *Polymer* 42(25): 9955-9967.
Silvestre, J. S., Tamarat, R.*, et al.* (2003). Vascular endothelial growth factor-B promotes in vivo angiogenesis. *Circulation Research* 93(2): 114-123.
Singh, S., Wu, B. M.*, et al.* (2012). Delivery of VEGF using collagen-coated polycaprolactone scaffolds stimulates angiogenesis. *Journal of Biomedical Materials Research Part A* 100A(3): 720-727.
Sjoqvist, S., Jungebluth, P.*, et al.* (2014). Experimental orthotopic transplantation of a tissue-engineered oesophagus in rats. *Nature Communications* 5.
Sokolis, D. P. (2010). Strain-energy function and three-dimensional stress distribution in esophageal biomechanics. *Journal of Biomechanics* 43(14): 2753-2764.
Song, J. J. and Ott, H. C. (2011). Organ engineering based on decellularized matrix scaffolds. *Trends in Molecular Medicine* 17(8): 424-432.
Spechler, S. J. (2000). Barrett's oesophagus: diagnosis and management. *Best Practice & Research Clinical Gastroenterology* 14(5): 857-879.
Spitz, L. (2007). Oesophageal atresia. *Orphanet Journal of Rare Diseases* 2.
Spitz, L., Kiely, E. M.*, et al.* (1996). Long-gap oesophageal atresia. *Pediatric Surgery International* 11(7): 462-465.
Stavropoulou, E. A., Dafalias, Y. F.*, et al.* (2012). Biomechanical behavior and histological organization of the three-layered passive esophagus as a function of topography. *Proceedings of the Institution of Mechanical Engineers, Part H: Journal of Engineering in Medicine* 226(6): 477-490.
Stitzel, J., Liu, J.*, et al.* (2006). Controlled fabrication of a biological vascular substitute. *Biomaterials* 27(7): 1088-1094.
Stokes, T. H. (2011). Successful use of matristem in difficult plastic & reconstructive surgery cases. *Wound repair and regeneration* 19(2): A54-A54.
Storgard, C., Mikolon, D.*, et al.* (2005). Angiogenesis Assays in the Chick CAM. Cell Migration. J.-L. Guan, Humana Press. 294: 123-136.
Subramanian, A., Krishnan, U. M.*, et al.* (2011). Fabrication of uniaxially aligned 3D electrospun scaffolds for neural regeneration. *Biomedical Materials* 6(2).
Sundaray, B., Subramanian, V.*, et al.* (2004). Electrospinning of continuous aligned polymer fibers. *Applied Physics Letters* 84(7): 1222-1224.
Tan, J. Y., Chua, C. K.*, et al.* (2012). Esophageal tissue engineering: An in-depth review on scaffold design. *Biotechnology and bioengineering* 109(1): 1-15.
Taylor, G. I. (1964). Disintegration of Water Drops in an Electric Field. *Proceedings of the Royal Society A*(280): 383-397.
Teo, W. E. and Ramakrishna, S. (2006). A review on electrospinning design and nanofibre assemblies. *Nanotechnology* 17(14): R89-R106.
Thompson, C. J., Chase, G. G.*, et al.* (2007). Effects of parameters on nanofiber diameter determined from electrospinning model. *Polymer* 48(23): 6913-6922.
Totonelli, G., Maghsoudlou, P.*, et al.* (2012). A rat decellularized small bowel scaffold that preserves villus-crypt architecture for intestinal regeneration. *Biomaterials* 33(12): 3401-3410.
Trabuco, E. C., Klingele, C. J.*, et al.* (2007). Xenograft use in reconstructive pelvic surgery: a review of the literature. *International Urogynecology Journal* 18(5): 555-563.
Tujunen, N.-M., Fujikura, K.*, et al.* (2013). Aligned electrospun siloxane-doped vaterite/poly(L-lactide) composite fibremats: evaluation of their tensile strength

and cell compatibility. *Journal of biomaterials science. Polymer edition* 24(18): 2096-2109.

Vaira, D., Gatta, L*., et al.* (2011). Gastroesophageal reflux disease and Barrett's esophagus. *Internal and emergency medicine* 6(4): 299-306.

Valentin, J., Badylak, J*., et al.* (2006). Extracellular matrix bioscaffolds for orthopaedic applications - A comparative histologic study. *Journal of Bone and Joint Surgery; American volume* 88(12): 2673-2686.

Vempati, P., Popel, A. S*., et al.* (2014). Extracellular regulation of VEGF: isoforms, proteolysis, and vascular patterning. *Cytokine & growth factor reviews* 25(1): 1-19.

Verma, K., Gu, J*., et al.* (2011). Tumor Endothelial Marker 8 Amplifies Canonical Wnt Signaling in Blood Vessels. *PLoS ONE* 6(8): e22334.

Vert, M., Li, S. M*., et al.* (1992). Bioresorbability and biocompatibility of aliphatic polyesters. *Journal of Materials Science: Materials in Medicine* 3(6): 432-446.

VoytikHarbin, S. L., Brightman, A. O*., et al.* (1997). Identification of extractable growth factors from small intestinal submucosa. *Journal of Cellular Biochemistry* 67(4): 478-491.

Wainwright, D. J. (1995). Use of an acellular allograft dermal matrix (AlloDerm) in the management of full-thickness burns. *Burns* 21(4): 243-248.

Wang, Z., He, Y*., et al.* (2012). Rapid vascularization of tissue-engineered vascular grafts in vivo by endothelial cells in co-culture with smooth muscle cells. *Journal of Materials Science-Materials in Medicine* 23(4): 1109-1117.

Welling, L. W. and Grantham, J. J. (1972). Physical Properties of Isolated Perfused Renal Tubules and Tubular Basement-membranes. *The Journal of clinical investigation* 51(5): 1063-&.

Wernike, E., Montjovent, M. O*., et al.* (2010). Vegf incorporated into calcium phosphate ceramics promotes vascularisation and bone formation in vivo. *European cells & materials* 19: 30-40.

Wilhelm, O. (2004). Electrohydrodynamic Spraying – Transport, Mass and Heat Transfer of Charged Droplets and their Application to the Deposition of Thin Functional Films. . PhD.

Wilting, J., Christ, B*., et al.* (1993). In vivo effects of vascular endothelial growth factor on the chicken chorioallantoic membrane. *Cell and Tissue Research* 274(1): 163-172.

Wilting, J., Christ, B*., et al.* (1992). The effects of growth factors on the day 13 chorioallantoic membrane (CAM): a study of VEGF165 and PDGF-BB. *Anatomy and embryology* 186(3): 251-257.

Wolf, M. T., Daly, K. A*., et al.* (2012). Biologic scaffold composed of skeletal muscle extracellular matrix. *Biomaterials* 33(10): 2916-2925.

Wong, C. S., Liu, X*., et al.* (2013). Elastin and collagen enhances electrospun aligned polyurethane as scaffolds for vascular graft. *Journal of Materials Science-Materials in Medicine* 24(8): 1865-1874.

Woo, K. M., Chen, V. J*., et al.* (2003). Nano-fibrous scaffolding architecture selectively enhances protein adsorption contributing to cell attachment. *Journal of Biomedical Materials Research Part A* 67A(2): 531-537.

Woodard, J. R., Hilldore, A. J*., et al.* (2007). The mechanical properties and osteoconductivity of hydroxyapatite bone scaffolds with multi-scale porosity. *Biomaterials* 28(1): 45-54.

Woodruff, M. A. and Hutmacher, D. W. (2010). The return of a forgotten polymer—Polycaprolactone in the 21st century. *Progress in Polymer Science* 35(10): 1217-1256.

Woods, T. and Gratzer, P. F. (2005). Effectiveness of three extraction techniques in the development of a decellularized bone–anterior cruciate ligament–bone graft. *Biomaterials* 26(35): 7339-7349.

Xu, C. Y., Inai, R.*, et al.* (2004). Aligned biodegradable nanofibrous structure: a potential scaffold for blood vessel engineering. *Biomaterials* 25(5): 877-886.

Yamada, K. M. and Yamada (1983). Cell-surface interactions with extracellular materials. *Annual review of biochemistry* 52(1): 761-799.

Yancopoulos, G. D., Davis, S.*, et al.* (2000). Vascular-specific growth factors and blood vessel formation. *Nature* 407(6801): 242-248.

Yang, F., Murugan, R.*, et al.* (2005). Electrospinning of nano/micro scale poly(L-lactic acid) aligned fibers and their potential in neural tissue engineering. *Biomaterials* 26(15): 2603-2610.

Yang, S. F., Leong, K. F.*, et al.* (2001). The design of scaffolds for use in tissue engineering. Part 1. Traditional factors. *Tissue engineering* 7(6): 679-689.

Yang, W., Fung, T. C.*, et al.* (2006). Directional, regional, and layer variations of mechanical properties of esophageal tissue and its interpretation using a structure-based constitutive model. *Journal of Biomechanical Engineering-Transactions of the Asme* 128(3): 409-418.

Yang, W., Fung, T. C.*, et al.* (2007). Three-dimensional finite element model of the two-layered oesophagus, including the effects of residual strains and buckling of mucosa. *Proceedings of the Institution of Mechanical Engineers Part H-Journal of Engineering in Medicine* 221(H4): 417-426.

Yarin, A. L., Koombhongse, S.*, et al.* (2001). Taylor cone and jetting from liquid droplets in electrospinning of nanofibers. *Journal of applied physics* 90(9): 4836-4846.

Yoon, M. Y. and Fisher, J. P. (2006). Polymeric Scaffolds for Tissue Engineering Applications. Tissue Engineering and Artificial Organs. J. D. Bronzino. Boca Raton, Fla, CRC Press, Taylor & Francis Group.

Yu, D.-G., Branford-White, C. J.*, et al.* (2010). Electrospinning of Concentrated Polymer Solutions. *Macromolecules* 43(24): 10743-10746.

Zdolsek, J., Eaton, J. W.*, et al.* (2007). Histamine release and fibrinogen adsorption mediate acute inflammatory responses to biomaterial implants in humans. *Journal of translational medicine* 5(1): 31.

Zeleny, J. (1917). Instability of Electrified Liquid Surfaces. *The Physical Review* 10(1).

Zhang, Y. Z., Ouyang, H. W.*, et al.* (2005). Electrospinning of gelatin fibers and gelatin/PCL composite fibrous scaffolds. *Journal of Biomedical Materials Research Part B-Applied Biomaterials* 72B(1): 156-165.

Zhu, Y., Leong, M. F.*, et al.* (2007). Esophageal epithelium regeneration on fibronectin grafted poly(L-lactide-co-caprolactone) (PLLC) nanofiber scaffold. *Biomaterials* 28(5): 861-868.

Zhu, Y. B., Cao, Y.*, et al.* (2010). Macro-Alignment of Electrospun Fibers For Vascular Tissue Engineering. *Journal of Biomedical Materials Research Part B-Applied Biomaterials* 92B(2): 508-516.

Appendix A

A-1 Proximal vs. Distal Small Intestine Submucosa

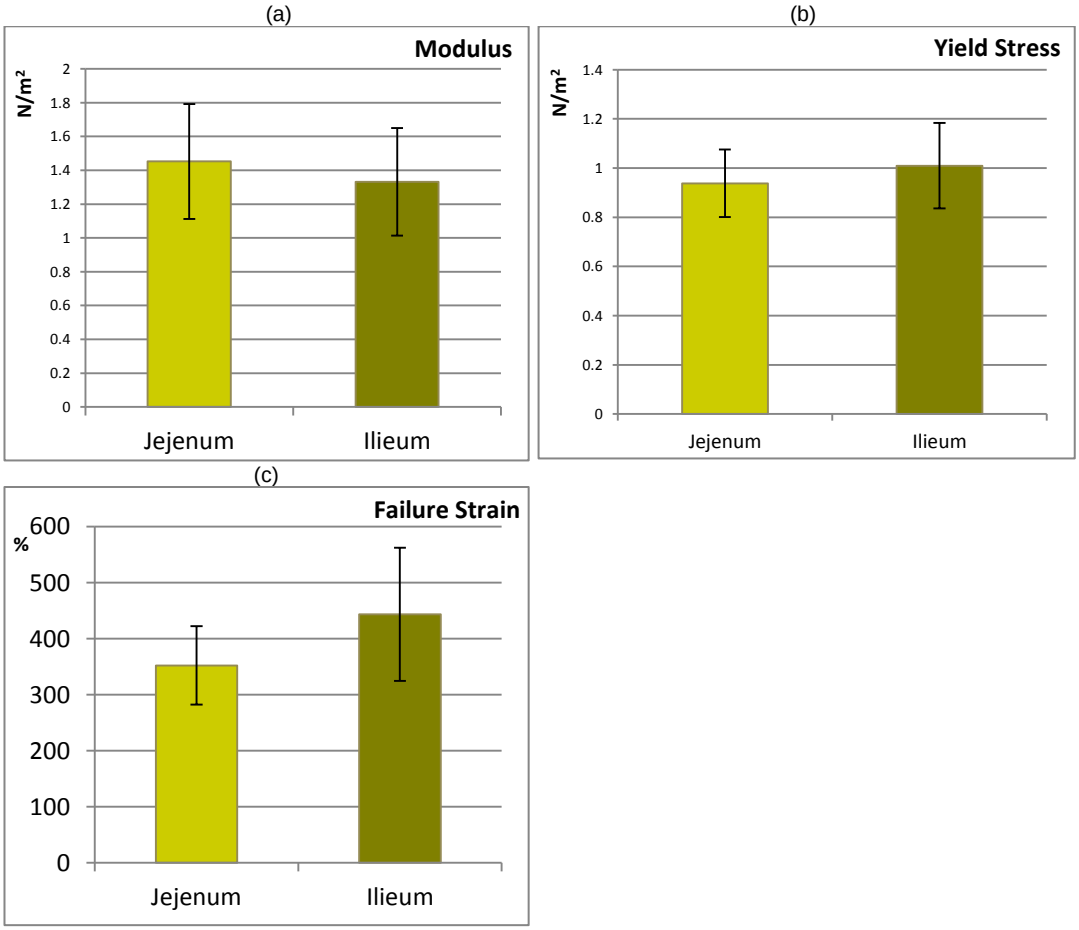

Figure A1 Comparison data from mechanical testing of the proximal (jejunum) and distal (ileum) showing (a) Elastic modulus values (MPa) (*n* = 8) (b) Yield stress values (MPa) (*n* = 8) (c) Failure strain values (%) (*n* = 8). Error bars shown are the standard error.

Mechanical testing (Figure A1) was carried out using fresh porcine small intestine submucosa with a view to ascertain whether using small intestine submucosa from different regions might make a difference to the mechanical performance of SIS. In these tests there appeared to be no differences in the values from the two types of SIS. Consequently the decision was taken to use tissue primarily from the jejunum which is the longest section of the small intestine and from which it is easier to harvest the SIS.

A-2 Improved washing regime

The samples were placed in the containers and then the containers were completely filled with deionised water. Care was taken to ensure that no air bubbles were present. The input channels of all the containers were then placed in a large 5 litre flask filled with deionised water and the pump then allowed to run. The deionised water was then allowed to overflow from each container creating a one-way flow. The 5 litre flask was then topped up with fresh deionised water as required, and the entire arrangement was run for 6 h.

A-3 Earlier Perfusion Rig

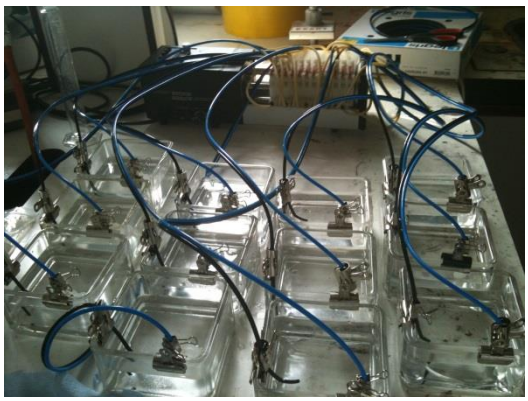

Figure A2 Early perfusion rig. The design was updated to allow for a fully sealed environment,

Early perfusion was carried out using an open-top vessel arrangement (Figure A2). Upon decellularisation these would be covered with plastic wrapping material, however the seal was never complete.

A-4 ISO Standards

- ISO 10993-5:2009(en) Biological evaluation of medical devices — Part 5: Tests for in vitro cytotoxicity. https://www.iso.org/obp/ui/#iso:std:iso:10993:-5:ed-3:v1:en
- ISO 10993-12:2007(en) Biological evaluation of medical devices — Part 12: Sample preparation and reference materials https://www.iso.org/obp/ui/#iso:std:iso:10993:-12:ed-3:v1:en

Appendix B

B-1 Changing Syringe Type

The syringes in initial use were conventional syringes with rubber bungs. With the use of dichloromethane as a solvent the result was that the rubber was being dissolved by the solvent causing decolouration of the polymer. As future research would involve *in vivo* and *in vitro* work preventing any contaminant from entering the polymer became relevant. A rubberless syringe was adopted for future use. In addition to this polymer was also made in small 10 cm^3 batch so that to would not be reused so that potentially contaminants would not accumulate. This method also improved the process as a whole, as repeated use of a polymer solution caused solvent loss. Solvent loss caused the concentration to change, affecting the viscosity, needle tip drying and subsequent clogging, in addition to other factors.

B-2 Salt Leaching

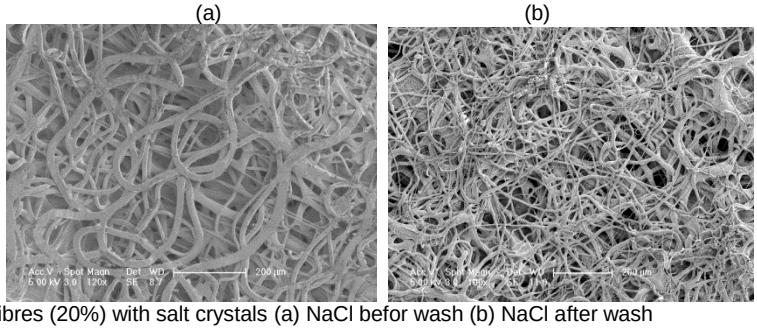

Figure B1 PCL fibres (20%) with salt crystals (a) NaCl befor wash (b) NaCl after wash

No difference and no improvement obeserved. It was likely that the large salt crystals separated from the polymer upon emergence or remained in the syring. While this might be improved through the use of smaller crystals, on appearance the scaffolds appeared to have a resonable amount of porsity.

B-3 Electrospinning Parameters and Variations

Table B1 Key variations of electrospun fibres produced for Chapters 3 & 4. This list is not exhaustive and predominately only includes samples producing using a mandrel. Each variation, in addition to others, were produced using flat collectors such as foil or glass slides placed over a flat plate electrode.

Collection Surface	SIS type	Dia-meter (cm)	Arrange-ment	Polymer	Concentration (% - w/v)	Solvent	Flow Rate (ml h-1)	Needle Size	Height (cm)	Voltage (kV)	Time (m/cm)	Mandrel Speed (rpm)	Additional 1	Additional 2	Comment	Reference
Foil	n/a	n/a	1	PCL	10	DCM	60	21 Gauge (0.514mm)	4	20 – 30	2	9			No clear fibres, pooling of the polymer	
Foil	n/a	n/a	1	PCL	20	DCM	60	21 Gauge (0.514mm)	4	20 – 30	2	9			No clear fibres, pooling of the polymer	
Foil	n/a	n/a	1	PCL	30	DCM	60	21 Gauge (0.514mm)	4	20 – 30	2	9			No clear fibres, pooling of the polymer	
Foil	n/a	n/a	1	PCL	10	DCM	60	21 Gauge (0.514mm)	7	20 – 30	2	9			Very few fibres, still heavy pooling	
Foil	n/a	n/a	1	PCL	20	DCM	60	21 Gauge (0.514mm)	7	20 – 30	2	9			Very few fibres, still heavy pooling	
Foil	n/a	n/a	1	PCL	30	DCM	60	21 Gauge (0.514mm)	7	20 – 30	2	9			Very few fibres, still heavy pooling	
Foil	n/a	n/a	1	PCL	10	DCM	15	18 Gauge (0.838mm)	15	20	2	540			Some fibres present	
Foil	n/a	n/a	1	PCL	20	DCM	15	18 Gauge (0.838mm)	15	20	2	540			Some fibres present	

Foil	n/a	n/a	1	PCL	30	DCM	15	18 Gauge (0.838mm)	15	20	2	540			Very poor fibres	
Foil	n/a	n/a	1	PCL	15	DCM	15	18 Gauge (0.838mm)	15	20	2	540			Improvement over 30% PCL, yet no better than 20%	
SIS	SDS /TX	1.9	1	PCL	10	DCM	15	18 Gauge (0.838mm)	15	20	5	540			Fibres present, irregular and inadequately dried	Chapter 3.3.1
SIS	SDS /TX	1.9	1	PCL	15	DCM	15	18 Gauge (0.838mm)	15	20	5	540			Fibres present, irregular and inadequately dried	Chapter 3.3.1
SIS	SDS /TX	1.9	1	PCL	20	DCM	15	18 Gauge (0.838mm)	15	20	5	540			Improved Fibres	Chapter 3.3.1
SIS	SDS /TX	1.9	1	PCL	20	DCM	15	18 Gauge (0.838mm)	15	20	5	1260			No improved alignment over 540 rpm	Chapter 3.3.1
SIS	SDS /TX	1.9	1	PCL	20	DCM	15	18 Gauge (0.838mm)	15	20	5	1440			No improved alignment over 540 rpm	Chapter 3.3.1
SIS	SDS /TX	1.9	1	PCL	20	DCM	15	18 Gauge (0.838mm)	15	20	5	1620			No improved alignment over 540 rpm	Chapter 3.3.1
SIS	SDS /TX	1.9	1	PCL	20	DCM	15	18 Gauge (0.838mm)	15	20	5	1800			Some improved alignment over 540 rpm	Chapter 3.3.1
SIS	SDS /TX	1.9	1	PCL	20	DCM	15	18 Gauge (0.838mm)	15	20	5	540	attachment			Chapter 3.3.1
SIS	SDS /TX	1.9	1	PCL	20	DCM	15	18 Gauge (0.838mm)	15	20	5	540	starting wet			Chapter 3.3.1
SIS	SDS /TX	1.9	1	PCL	20	DCM	15	18 Gauge (0.838mm)	15	20	5	540	constant wet			Chapter 3.3.1
SIS	SDS /TX	1.9	1	PCL	20	DCM	15	18 Gauge (0.838mm)	15	20	5	540	acetone			Chapter 3.3.1

SIS	SDS /TX	1.9	1	PCL	20	DCM	15	18 Gauge (0.838mm)	15	20	5	540	NaCl	No Wash	No salt crystals detected	Appendix B-2
SIS	SDS /TX	1.9	1	PCL	20	DCM	15	18 Gauge (0.838mm)	15	20	5	540	NaCl	Washed	No salt crystals detected	Appendix B-2
Foil	n/a	n/a	1	PLGA (D- & L-)	10	DCM	15	18 Gauge (0.838mm)	15	20	2	540			Suitable for fibres (but not followed due to changes in the polymer)	
Foil	n/a	n/a	1	PLGA (D- & L-)	15	DCM	15	18 Gauge (0.838mm)	15	20	2	540			Suitable for fibres (but not followed due to changes in the polymer)	
Foil	n/a	n/a	1	PLGA (D- & L-)	20	DCM	15	18 Gauge (0.838mm)	15	20	2	540			Suitable for fibres (but not followed due to changes in the polymer)	
Foil	n/a	n/a	1	PLGA (D- & L-)	25	DCM	15	18 Gauge (0.838mm)	15	20	2	540			Suitable for fibres (but not followed due to changes in the polymer)	
Foil	n/a	n/a	1	PLGA (High Viscosity)	10	DCM	1	18 Gauge (0.838mm)	15	10 – 15	2	540			The viscosity was creating some clogging problems with the needle. Lower concentrations evaporated too quickly.	
Foil	n/a	n/a	1	PLGA (High Viscosity)	15	DCM	1	18 Gauge (0.838mm)	15	10 – 15	2	540			The viscosity was creating some clogging problems with the needle. Lower concentrations evaporated too quickly.	
Foil	n/a	n/a	1	PLGA	10	DCM	1	18 Gauge (0.838mm)	15	10 – 15	2	540			Globules of polymer along with very fine fibres	Appendix B-4
Foil	n/a	n/a	1	PLGA	15	DCM	1	18 Gauge (0.838mm)	15	10 – 15	2	540			Positive result for the polymer	Appendix B-4
Foil	n/a	n/a	1	PLGA	20	DCM	1	18 Gauge (0.838mm)	15	10 – 15	2	540			Clogging present/Good Fibres	Appendix B-4
SIS	SDS /TX	1.9	1	PLGA	10	DCM	1	18 Gauge (0.838mm)	15	10 – 15	5	540				
SIS	SDS /TX	1.9	1	PLGA	15	DCM	1	18 Gauge (0.838mm)	15	10 – 15	5	540			Remained the best option	

SIS	SDS /TX	1.9	1	PLGA	20	DCM	1	18 Gauge (0.838mm)	15	10 – 15	5	540				
SIS	SDS /TX	1.9	1	PLGA	15	DCM	1	18 Gauge (0.838mm)	15	10 – 15	5	540	attachment			Chapter 3.3.2
SIS	SDS /TX	1.9	1	PLGA	15	DCM	1	18 Gauge (0.838mm)	15	10 – 15	5	540	starting wet			Chapter 3.3.2
SIS	SDS /TX	1.9	1	PLGA	15	DCM	1	18 Gauge (0.838mm)	15	10 – 15	5	1440				Chapter 3.3.2
SIS	SDS /TX	2.54	2	PLGA	15	DCM	1	18 Gauge (0.838mm)	15	10 – 15	5	10				Chapter 3.3.2
SIS	SDS /TX	2.54	2	PLGA	15	DCM	1	18 Gauge (0.838mm)	15	10 – 15	5	1000				Chapter 3.3.2
SIS	SDS /TX	2.54	2	PLGA	15	DCM	1	18 Gauge (0.838mm)	15	10 – 15	5	2000				Chapter 3.3.2
SIS	SDS /TX	2.54	2	PLGA	15	DCM	1	18 Gauge (0.838mm)	15	10 – 15	5	3000				Chapter 3.3.2
SIS	SDS /TX	2.54	2	PLGA	15	DCM	1	18 Gauge (0.838mm)	15	10 – 15	5	10	starting wet			Chapter 3.3.2
SIS	SDS /TX	2.54	2	PLGA	15	DCM	1	18 Gauge (0.838mm)	15	10 – 15	5	3000	starting wet			Chapter 3.3.2
SIS	SDS /TX	2.54	2	PLGA	15	DCM	1	18 Gauge (0.838mm)	15	10 – 15	5	10		Initial Spin for 1m at 7ml h-1	Additional layer created an incomplete covering	
SIS	SDS /TX	2.54	2	PLGA	15	DCM	1	18 Gauge (0.838mm)	15	10 – 15	5	10		Initial Spin for 2m at 7ml h-1		Chapter 3.3.2
SIS	SDS /TX	2.54	2	PLGA	15	DCM	1	18 Gauge (0.838mm)	15	10 – 15	5	3000		Initial Spin for 2m at 7ml h-1		Chapter 3.3.2

Foil	n/a	n/a	2	PLGA	15	DCM:DMF (9:1)	1	18 Gauge (0.838mm)	15	10 – 15	2	10			Little reduction of clogging	
Foil	n/a	n/a	2	PLGA	15	DCM:DMF (8:2)	1	18 Gauge (0.838mm)	15	10 – 15	2	10			Significant reduction to clogging	
Foil	n/a	n/a	2	PLGA	15	DCM:DMF (7:3)	1	18 Gauge (0.838mm)	15	10 – 15	2	10			Similar to 8:2	
SIS	SD	2.54	2	PLGA	15	DCM:DMF (8:2)	1	18 Gauge (0.838mm)	15	10 – 15	15	10		Initial Spin for 2m at 7ml h-1		Chapter 4
SIS	SD	2.54	2	PLGA	15	DCM:DMF (8:2)	1	18 Gauge (0.838mm)	15	10 – 15	15	1000		Initial Spin for 2m at 7ml h-1		Chapter 4
SIS	SD	2.54	2	PLGA	15	DCM:DMF (8:2)	1	18 Gauge (0.838mm)	15	10 – 15	15	2000		Initial Spin for 2m at 7ml h-1		Chapter 4
SIS	SD	2.54	2	PLGA	15	DCM:DMF (8:2)	1	18 Gauge (0.838mm)	15	10 – 15	15	3000		Initial Spin for 2m at 7ml h-1		Chapter 4
SIS	SD	2.54	2	PLGA	15	DCM:DMF (8:2)	1	18 Gauge (0.838mm)	15	10 – 15	15	4000		Initial Spin for 2m at 7ml h-1		Chapter 4
SIS	SD	2.54	2	PLGA	15	DCM:DMF (8:2)	1	18 Gauge (0.838mm)	15	10 – 15	15	5000		Initial Spin for 2m at 7ml h-1		Chapter 4
SIS	SD	2.54	2	PLGA	15	DCM:DMF (8:2)	1	18 Gauge (0.838mm)	15	10 – 15	7.5 / 7.5	10 / 3000	[mixed]	Initial Spin for 2m at 7ml h-1	No advantage observed with mechanical testing	
SIS	SD	2.54	2	PLGA	15	DCM:DMF (8:2)	1	18 Gauge (0.838mm)	15	14 – 15	15	10	improved SIS wash	Initial Spin for 2m at 7ml h-1		Chapter 4
SIS	SD	2.54	2	PLGA	15	DCM:DMF (8:2)	1	18 Gauge (0.838mm)	15	14 – 15	15	3000	improved SIS wash	Initial Spin for 2m at 7ml h-1		Chapter4
SIS	SD	2.54	2	PLGA	15	DCM:DMF (8:2)	1	18 Gauge (0.838mm)	15	14 – 15	15	5000	improved SIS wash	Initial Spin for 2m at 7ml h-1		Chapter4

B-4 PLGA Electrospinning

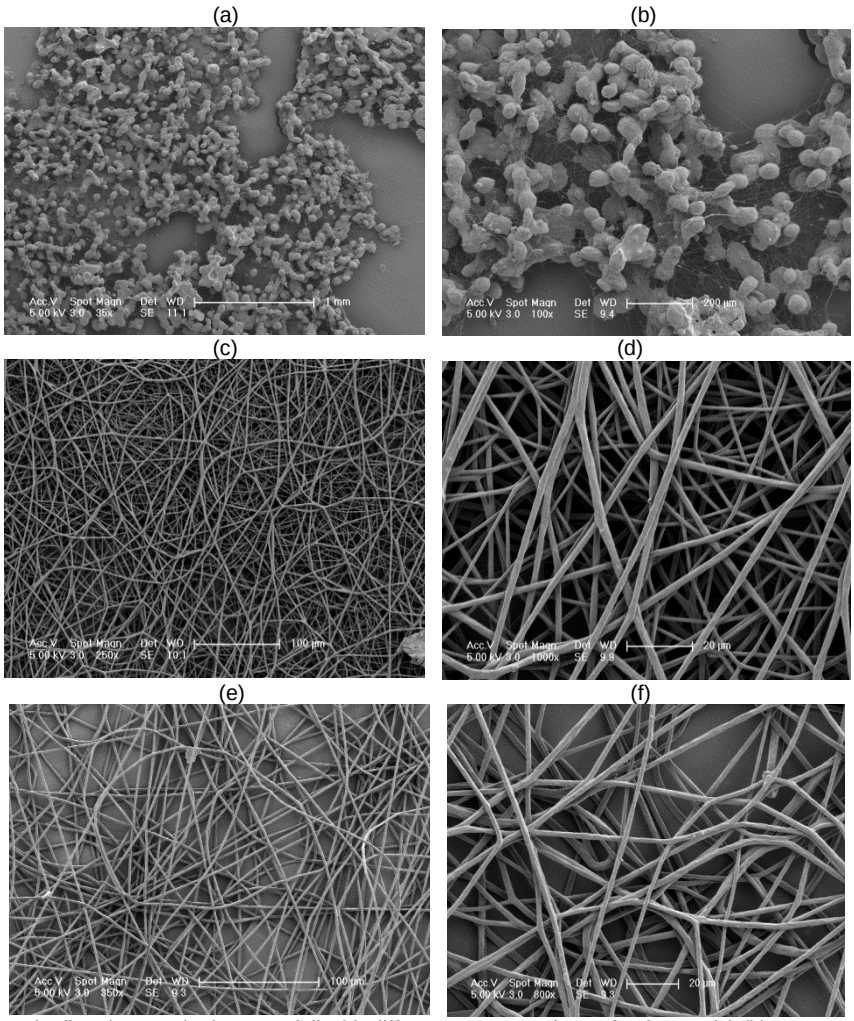

Figure B2 Results flat electrospinning onto foil with different concentrations of polymer; (a) (b) 10% PLGA (c) (d) 15% PLGA (e) (f) 20% PLGA

Preliminary work with varying PLGA concentration using electrospinning to flat surface (aluminium foil). Here it was found that with the 10% PLGA soultion the electrospinning largely failed. For both the 15% and 20% PLGA there was clear electrospun fibres produced, however, with the 20% PLGA solution clogging became an issue. Consequently 15% PLGA became the solution adopted for future work.

Appendix C

C-1 Histological Images

(a) Commercial - 2 Weeks

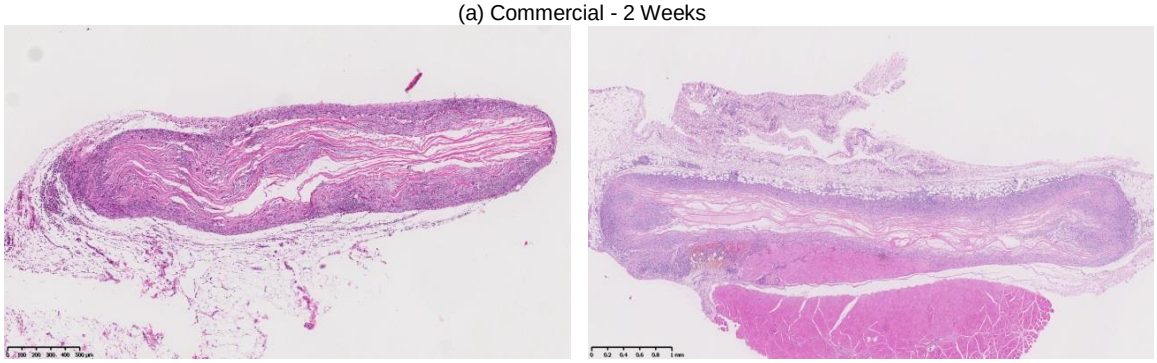

(b) Commercial - 4 Weeks

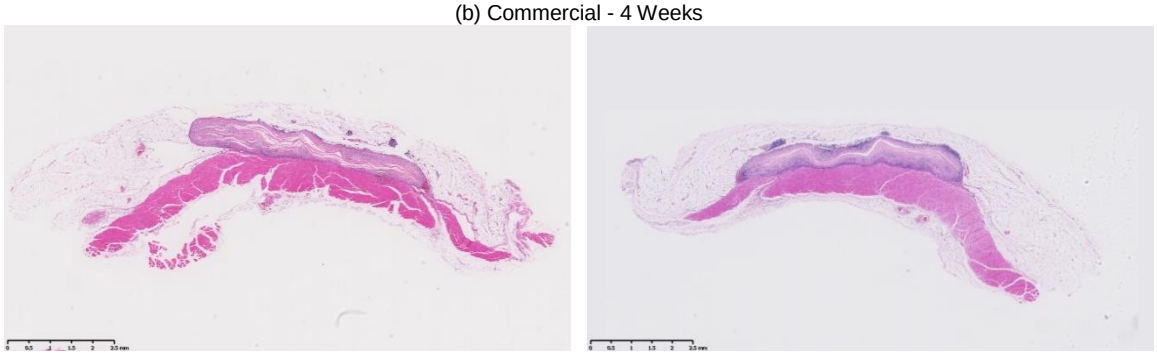

(c) SIS Control - 2 Weeks

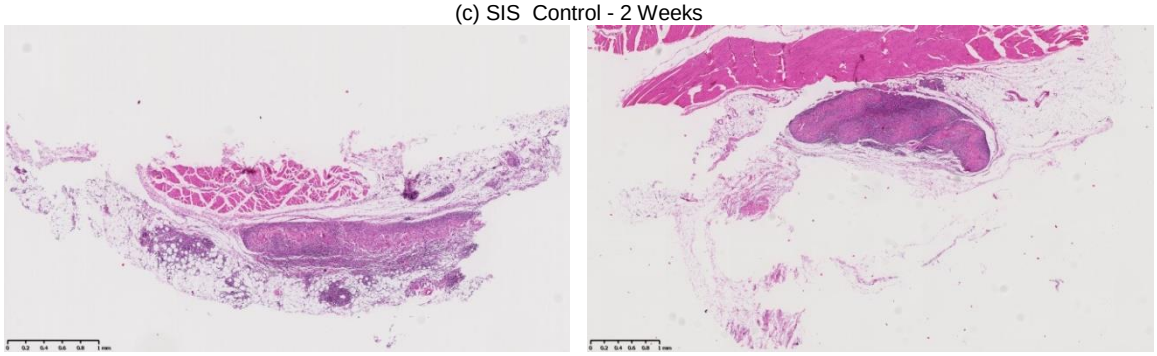

(d) SIS Control - 4 Weeks

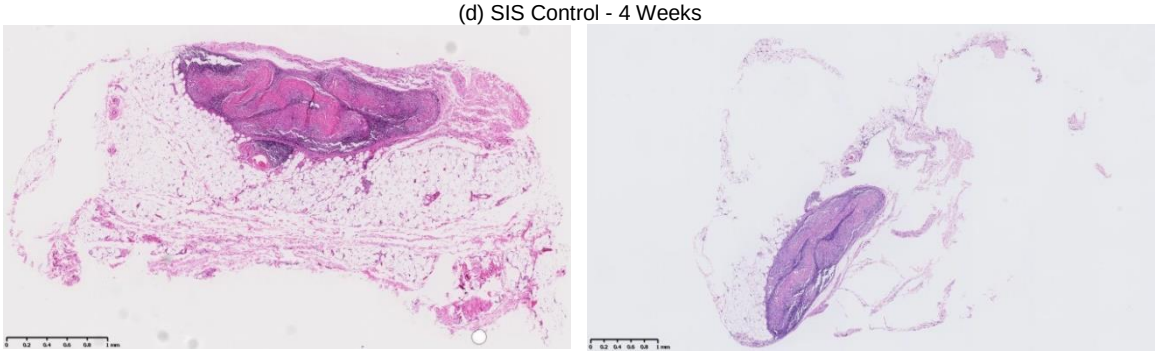

(e) 10rpm - 2 Weeks

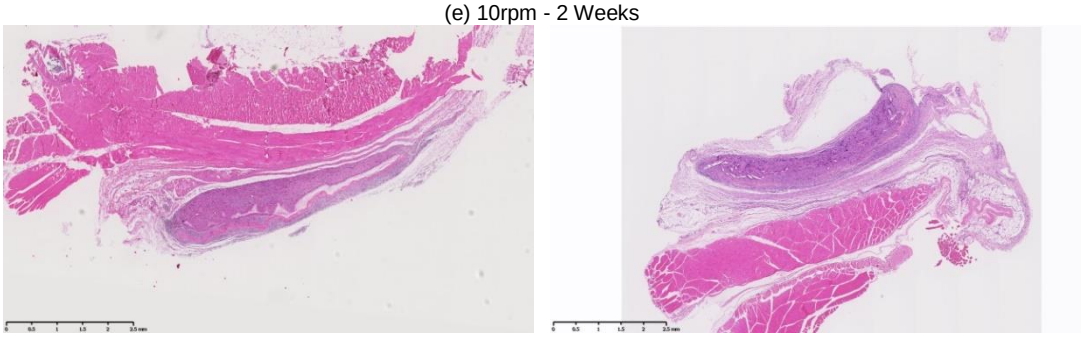

(f) 10rpm - 4 Weeks

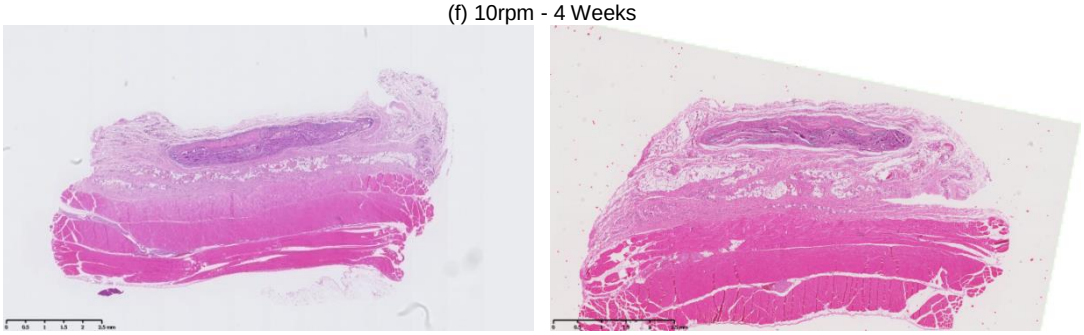

(g) 3000rpm - 2 Weeks

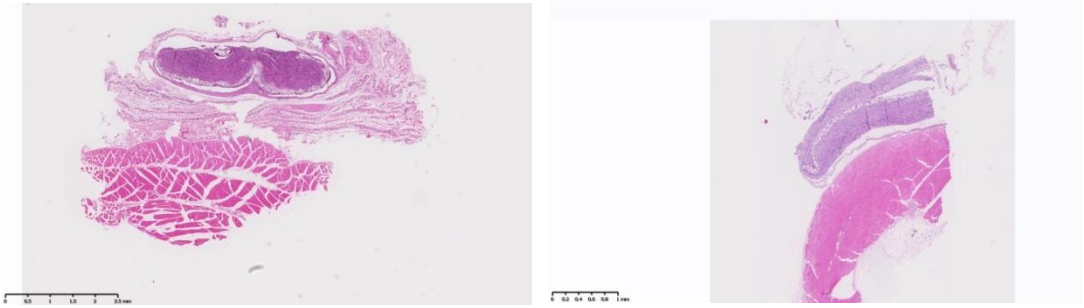

(h) 3000rpm - 4 Weeks

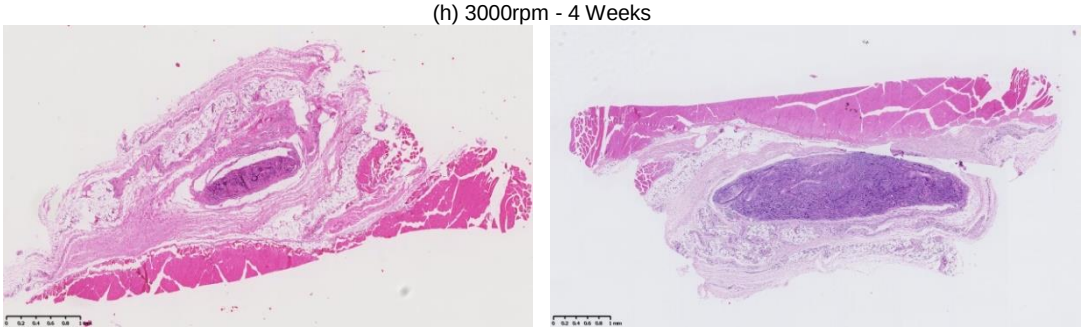

(i) 5000rpm - 2 Weeks

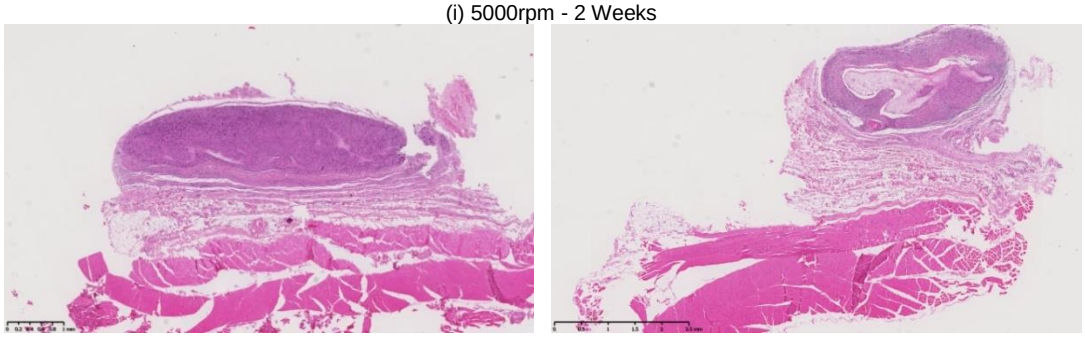

(j) 5000rpm - 4 Weeks

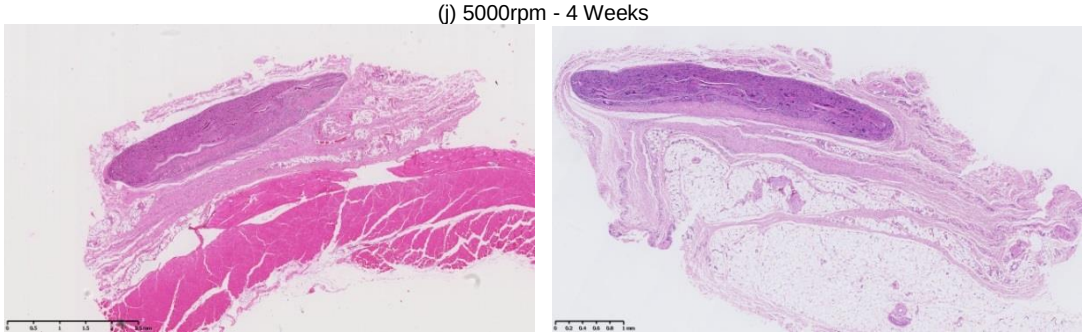

(k) 10rpm + VEGF - 2 Weeks

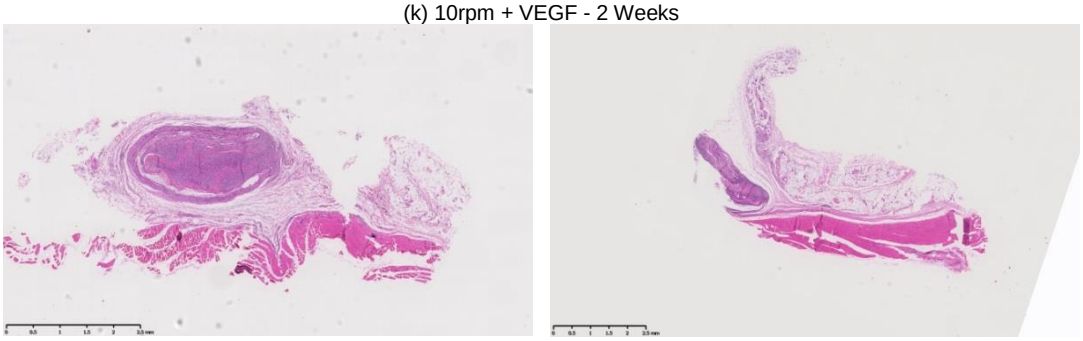

(l) 10rpm + VEGF - 4 Weeks

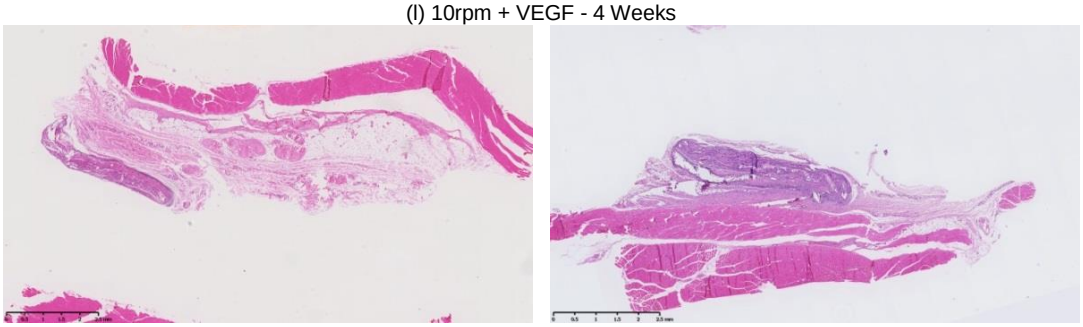

(m) 3000rpm + VEGF - 2 Weeks

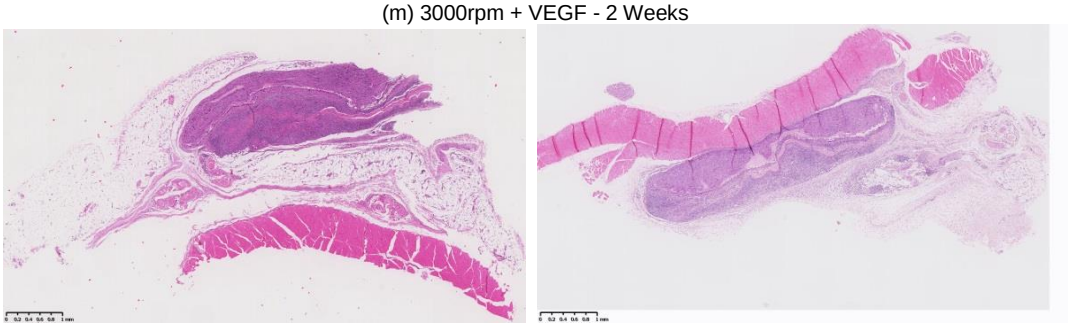

(n) 3000rpm + VEGF - 4 Weeks

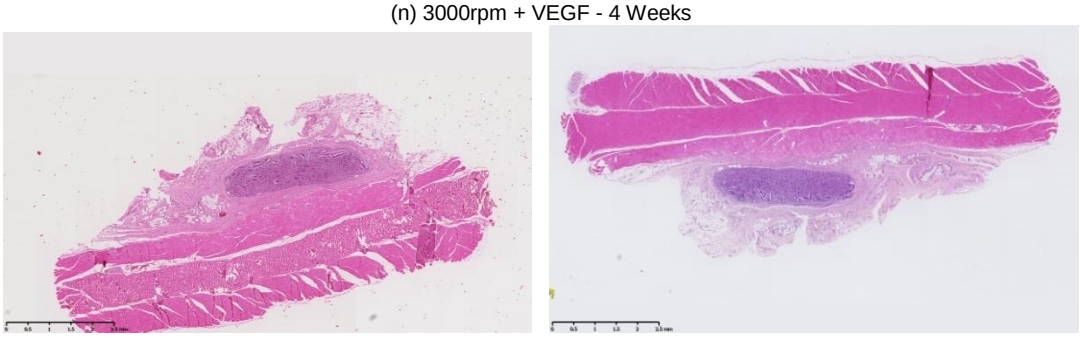

(o) 5000rpm + VEGF - 2 Weeks

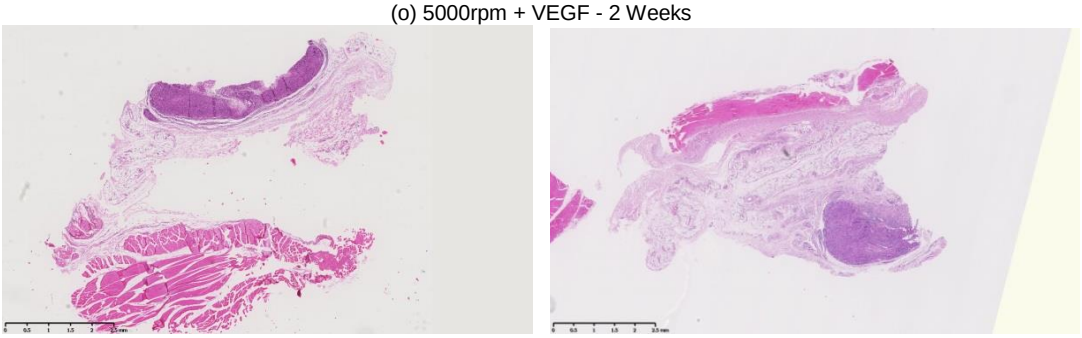

(p) 5000rpm+ VEGF - 4 Weeks

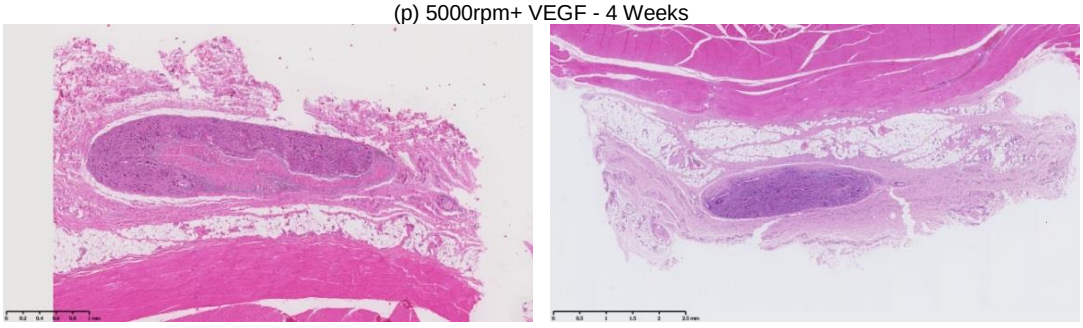

Figure C1 Low resolution histological images (H&E) from the samples groups. The samples type are (a) Commercial - 2 Weeks (b) Commercial - 4 Weeks (c) SIS Control - 2 Weeks (d) SIS Control - 4 Weeks (e) 10rpm - 2 Weeks (f) 10rpm - 4 Weeks (g) 3000rpm - 2 Weeks (h) 3000rpm - 4 Weeks (i) 5000rpm - 2 Weeks (j) 5000rpm - 4 Weeks (k) 10rpm + VEGF - 2 Weeks (l) 10rpm + VEGF - 4 Weeks (m) 3000rpm + VEGF - 2 Weeks (n) 3000rpm + VEGF - 4 Weeks (o) 5000rpm + VEGF - 2 Weeks (p) 5000rpm + VEGF - 4 Weeks

C-2 Mercury Intrusion Porometry

(a) 10 rpm

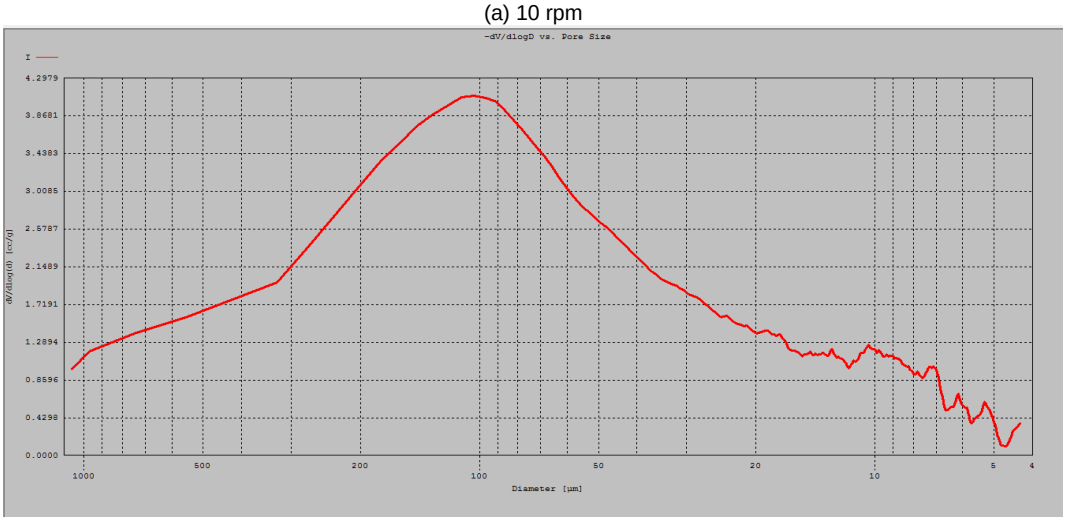

(b) 10 rpm

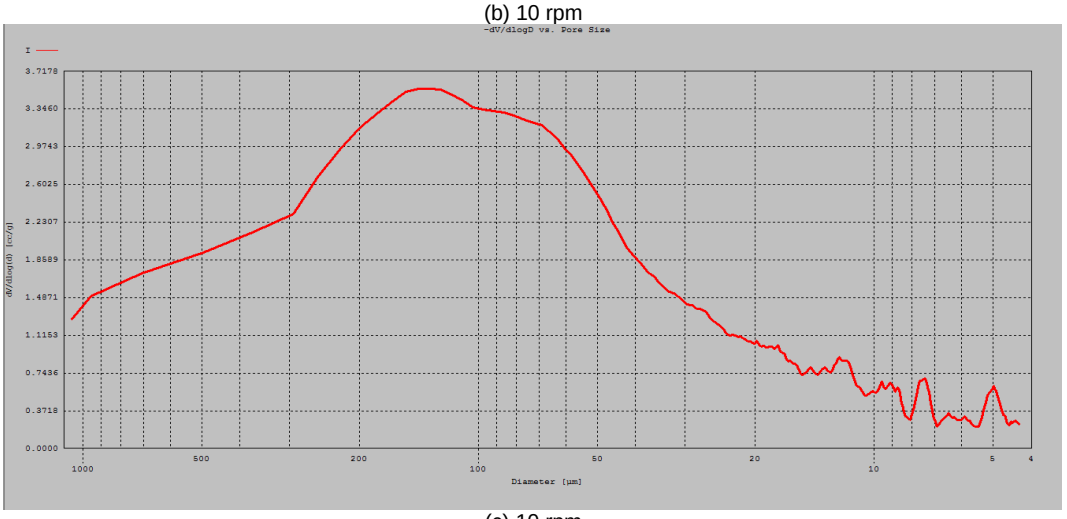

(c) 10 rpm

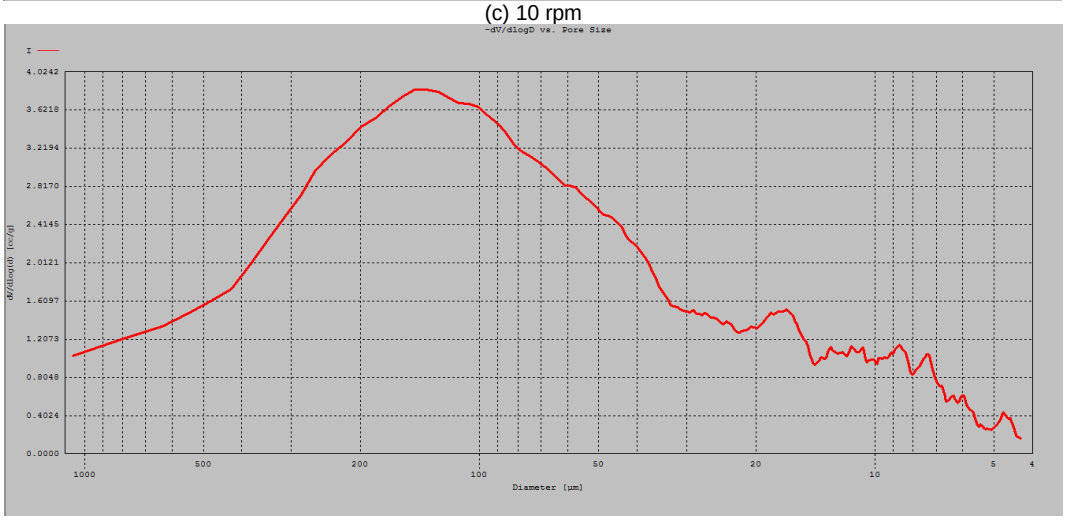

(e) 3000 rpm

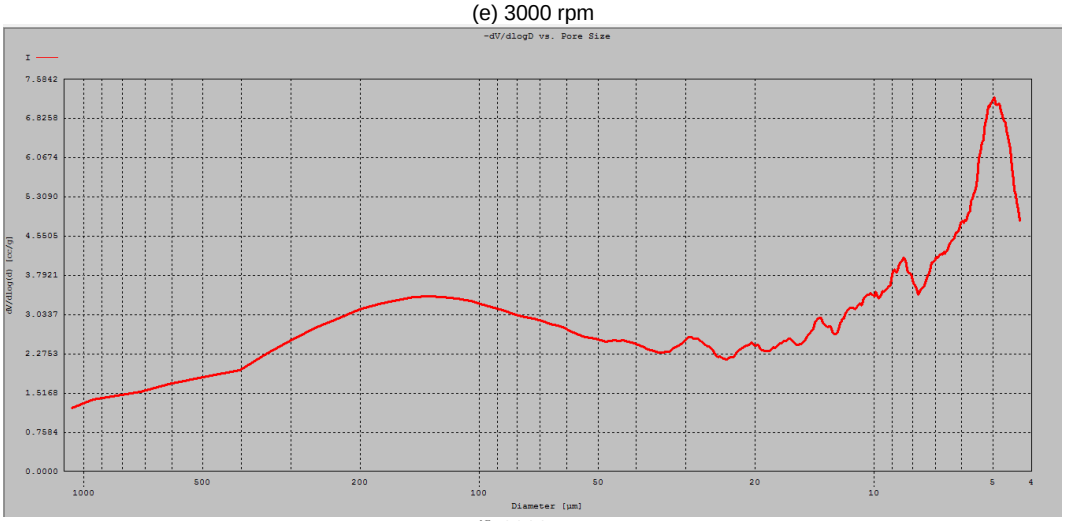

(f) 3000 rpm

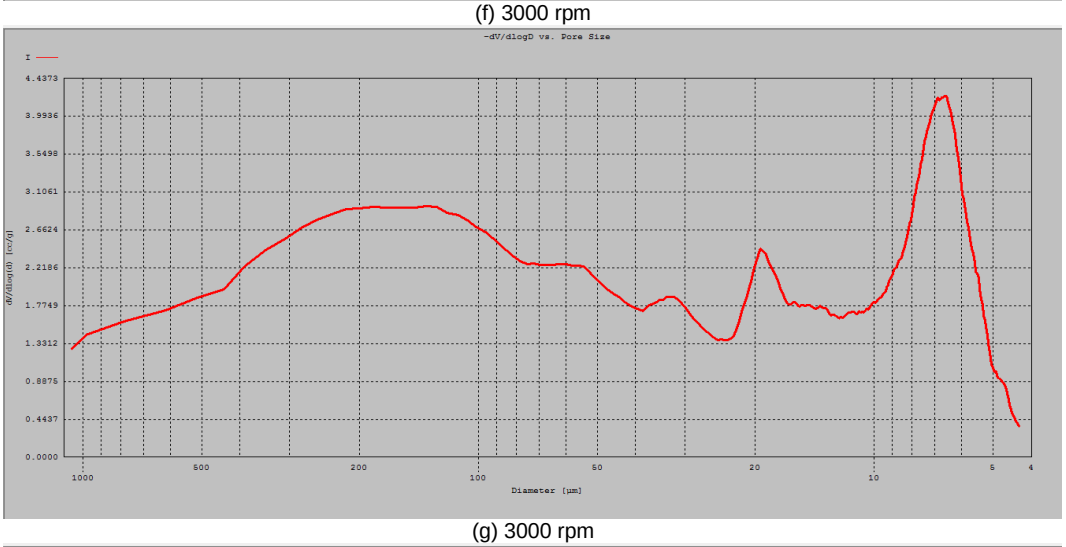

(g) 3000 rpm

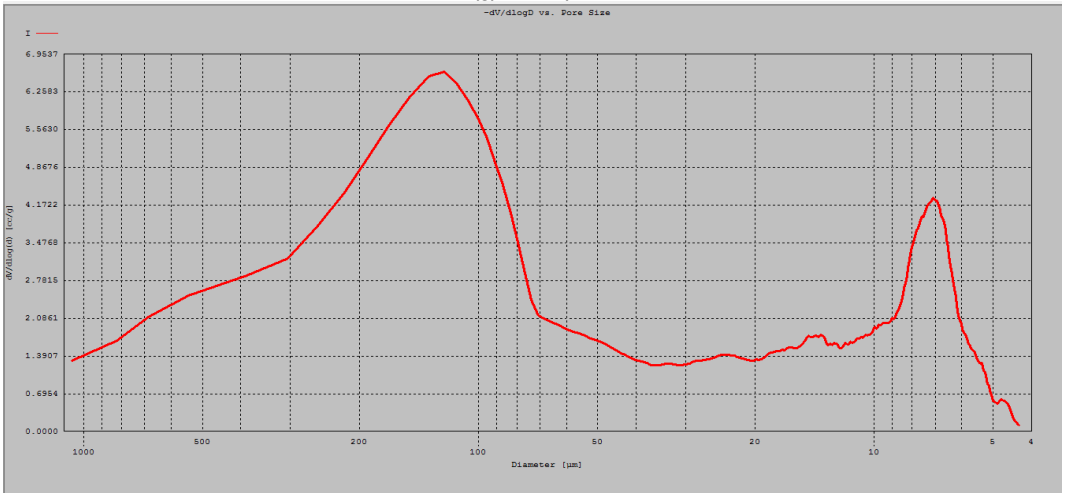

(h) 5000 rpm

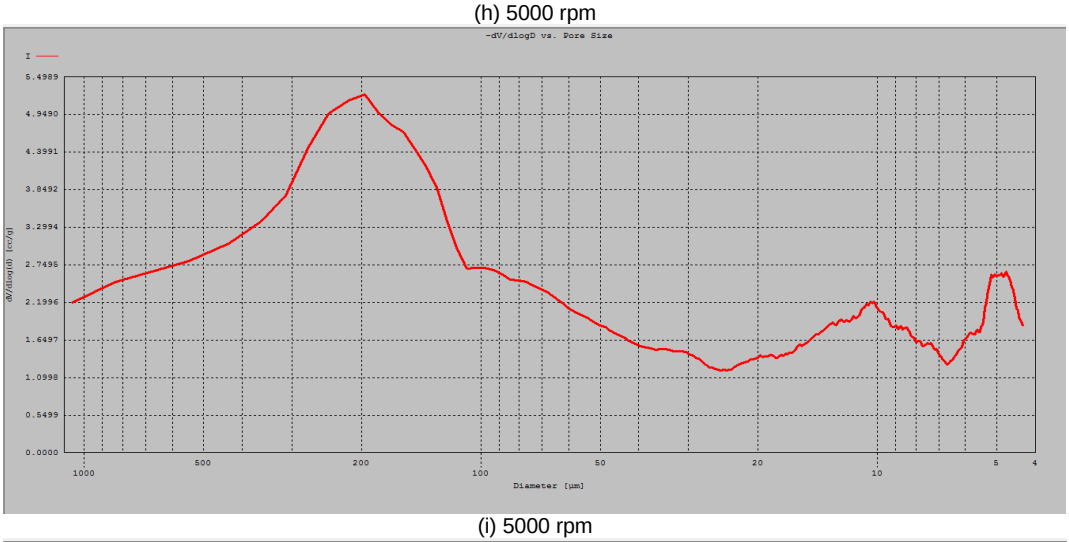

(i) 5000 rpm

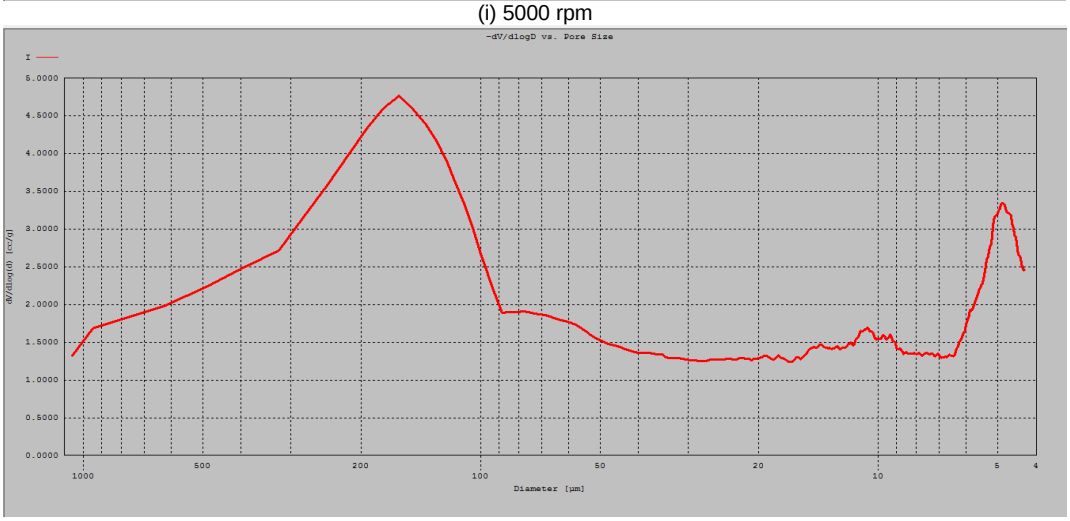

(j) 5000 rpm

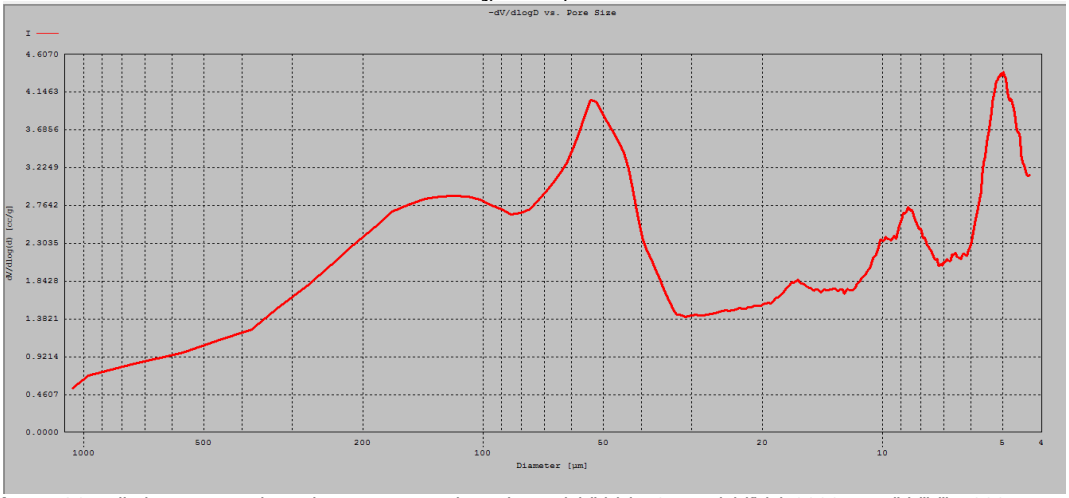

Figure C2 Full size mercury intrusion porometry data charts (a)(b)(c) 10 rpm (e)(f)(g) 3000 rpm (h)(i)(j) 5000 rpm

C-3 In Vivo Certificates

Certification of IACUC Approval

Principle investigator

Name	Dept	Status	Phone	Lab animal training number
Hae-Won Kim	NBM	Associate professor	+82-10-4156-7336	DKU-13-028

Protocol information

Proposal No		14-030
Project title	Korean	조직재생공학을 위한 소재-세포-인자 융합연구를 위해 자체 개발한 생체 적합성 고분자의 생적합성 평가
	English	Evaluation of Biocompatibility of Developed Biopolymer in Rat for Tissue Regeneration Engineering Interdisciplinary Research: Construction of Targeting Materials-Cells-Biofactors
Period		After approval ~ Oct 30 2015 (12 months)
Animal species and Number		SD Rat, ♂ 32
Classification		Grade D

Approval result

Revised date	Sep. 16. 2014
Approval date	Sep. 16. 2014
Approval number	DKU 14-030
Decision status	Approve as is

This protocol has been approved by the Dankook university IACUC.

September 16 2014

Chairperson of Dankook University IACUC

동물실험계획 승인서

1. 연구책임자

성 명	소속	직급	연락처	교육이수내용
김해원	나노바이오의과학과	부교수	010-4156-7336	DKU-13-028

2. 동물실험계획서

접 수 번 호	14-030
과 제 명	(국 문) 조직재생공학을 위한 소재-세포-인자 융합연구를 위해 자체 개발한 생체 적합성 고분자의 생적합성 평가 (영 문) Evaluation of Biocompatibility of Developed Biopolymer in Rat for Tissue Regeneration Engineering Interdisciplinary Research: Construction of Targeting Materials-Cells-Biofactors
실 험 기 간	위원회 승인 일 이후 ~ 2015년 10월 30일 (총 12개월)
사용 동물 종 및 마리 수	랫드 ♂: 32
동물이 경험하는 통증 및 스트레스의 정도	Grade D

3. 승인 사항

심 의 일 자	2014. 9. 16
승 인 일 자	2014. 9. 16
승 인 번 호	DKU-14-030
심 의 위 원 의 견	지적사항 없음

단국대학교 실험동물운영위원회에서는 상기의 동물실험계획을 승인합니다.

2014년 9월 16일

단국대학교 실험동물운영위원회 위원장